Recycled crustal material in the geochemical record of Pacific ocean island basalts from Pitcairn, Hawaii and Rurutu

Dissertation zur Erlangung des Grades
"Doktor der Naturwissenschaften"
am Fachbereich Geowissenschaften
der Johannes-Gutenberg-Universität, Mainz

Jürgen Eisele,
geb. 6. 8.1973 in Rheinfelden

Mainz, November 2001

Datum der mündlichen Prüfung: 2002

Ich versichere hiermit, die vorliegende Arbeit selbständig verfasst zu haben und alle benutzten Hilfsmittel und Quellen in der Arbeit angegeben zu haben. Diese Arbeit wurde an keiner anderen Fakultät als Dissertation eingereicht.

Zusammenfassung

Die Untersuchung der geochemischen Zusammensetzung von Ozeaninselbasalten (OIB) zielt darauf ab, Heterogenitäten im Erdmantel zu charakterisieren. Viele dieser Heterogenitäten können durch die Anwesenheit von "recyceltem" Material, das durch Subduktion in den Mantel eingebracht wurde, erklärt werden. Diese Doktorarbeit beschreibt die Zusammensetzungen von drei geochemisch sehr unterschiedlichen Vulkanen im Pazifischen Ozean: dem Pitcairn Hotspot (Südpazifik), dem Mauna Kea Vulkan (Hawaii) und der Insel Rurutu (Französisch Polynesien). Die Isotopenzusammensetzungen von Pitcairn und Rurutu repräsentieren zwei Endglieder der Mantelgeochemie, nämlich den "angereicherten Mantel 1" (EM1) und die HIMU Komponente. Die Signaturen radiogener Isotope von diesen Hotspots können als Indikatoren für recyceltes Material im Erdmantel benutzt werden. An den Proben von Pitcairn wurde die Os, Hf, Nd, Sr Isotopenzusammensetzung, sowie die Haupt- und Spurenelementzusammensetzung bestimmt. Der Schwerpunkt dieser Arbeit lag jedoch auf der Bleiisotopenzusammensetzung der Proben aller drei Lokalitäten, die mit Hilfe einer Dreiisotopenspiketechnik zur Korrektur der instrumentellen Massenfraktionierung gemessen wurde. Die Ziele der vorliegenden Studie waren (1) die Art von recyceltem Material in der EM1-Quelle in Pitcairn zu bestimmen, (2) die langzeitlichen Schwankungen der Bleiisotopie in Laven des Mauna Kea aus der HSDP-2 Bohrung zu beschreiben und (3) die HIMU-quelle in Rurutu zu charakterisieren und die Bleiisotopenentwicklung der OIB-quellen des Südpazifik zu untersuchen.

Die Ergebnisse dieser Arbeit weisen darauf hin, daß erstens die EM1-signatur des Pitcairn Hotspots am sinnvollsten durch eine pelagische Sedimentkomponente in der Magmenquelle erklärt werden kann. Zweitens treten die Bleiisotopenschwankungen der Mauna Kea Laven von HSDP-2 als rasche Oszillationen auf, die sich zu drei linearen Anordnungen im Bleiisotopenraum zusammensetzen. Diese linearen Anordnungen können durch Mischungen von heterogenen Materialien in der Mantelquelle entstehen. Das begrenzte zeitliche Auftreten einer bestimmten linearen Anordnung im Bleiisotopenraum in der HSDP-2 Bohrung zeigt, daß man sich dieses Mantelmaterial als Schlieren von mehreren zehner Kilometern Länge im aufsteigenden Mantelmaterial unter dem Vulkan vorstellen kann. Drittens zeigen auch die Isotopenzusammensetzungen der HIMU-laven von Rurutu lineare Anordnungen im Bleiisotopenraum. Wenn man diese Anordnungen mit Literaturdaten von anderen HIMU Hotspots vergleicht, unterstützen hochpräzise Bleiisotopendaten, daß die HIMU-quellen ähnliche Zusammensetzungen haben. Die linearen Anordnungen im Bleiisotopenraum scheinen jedoch keine identischen Mischendglieder zu besitzen. Das weist

darauf hin, daß die HIMU-quellen ähnliche recycelte Materialien darstellen könnten, daß diese jedoch nicht identisch sind und getrennte Einheiten im Mantel darstellen könnten. Ein Modell zur Bleiisotopenentwicklung legt nahe, daß die EM1-quelle und die HIMU-quellen im Südpazifik zu einem ähnlichen Zeitpunkt in der Erdgeschichte im Proterozoikum differenziert worden sein könnten.

Das auffälligste Merkmal der Bleiisotopensystematik der Pazifischen OIB, das die Dreiisotopenspiketechnik offen legt, ist die Linearität der Bleiisotopenzusammensetzungen der einzelnen Hotspots, was daraufhinweist, daß die Bleiisotopie eines jeweiligen Hotspots durch eine vorwiegend binäre Mischung erklärt werden kann. Weiterhin unterstützt ein Bleiisotopenentwicklungsmodell, daß die Differenzierung der OIB-quellen im Th-U-Pb Isotopensystem vor weniger als etwa zwei Milliarden Jahren geschah und im Fall des Mauna Kea relativ jung sein könnte. Außerdem scheinen keine der Hotspots, von denen hochpräzise Bleiisotopendaten vorliegen, identische Mischungsendglieder im Bleiisotopenraum zu besitzen, was darauf hinweist, daß jede der Heterogenitäten, die von Ozeaninselvulkanismus beprobt wird, einzigartig ist, und daß diese Heterogenitäten relativ kleinräumige Merkmale im Erdmantel sind.

Abstract

The study of the geochemistry of ocean island basalts (OIB) is aimed at characterizing heterogeneities in the Earth's mantle. It has been proposed that much of this heterogeneity can be explained by the presence of recycled materials introduced into the mantle by subduction. This thesis describes the geochemical composition lavas from three geochemically very different locations in the Pacific Ocean: the Pitcairn hotspot (South Pacific), Mauna Kea volcano (Hawaii) and Rurutu Island (French Polynesia). The isotopic compositions of Pitcairn and Rurutu represent two end members in mantle geochemistry, namely the enriched mantle 1 (EM1) and HIMU components. Radiogenic isotope signatures from these hotspots can be used as a tracer for recycled material in the mantle. For samples from Pitcairn, Os, Hf, Nd, Sr isotopic compositions as well as major and trace element compositions were determined. The main focus of this thesis, however, was on the Pb isotopic compositions of samples from all three locations measured using a triple spike technique to correct for instrumental mass fractionation. The aims of this study were (1) to identify the sort of recycled material in EM1 type lavas, of which Pitcairn is an extreme example, (2) to characterize the Pb isotopic fluctuations in Mauna Kea lavas from ~200 to ~500 ka in the HSDP-2 drill hole, and (3) to characterize the HIMU source in Rurutu and to investigate the Pb isotopic evolutions of the OIB sources in the South Pacific.

The results suggest first, that the EM1 signature in the Pitcairn hotspot is most reasonably explained by recycled pelagic sediment in the source. Second, the Pb isotopic fluctuations in Mauna Kea lavas of HSDP-2 occur as fast oscillations and form three linear arrays in Pb isotope space. These arrays may result from mixing of heterogeneous materials present in the mantle source of the lavas. The limited age range of the individual Pb isotope arrays in the HSDP-2 drill hole indicates that the arrays may originate from heterogeneities in the plume source that are tens of km in size. Third, the HIMU lavas from Rurutu also display linear arrays in Pb isotope space. When compared to literature data from other HIMU hotspots, the high-precision Pb isotope data show that HIMU sources have a similar isotopic composition. However, their Pb isotope arrays do not appear to share identical mixing end members in Pb isotope space. This suggests that HIMU sources may originate from similar types of recycled material, but that these recycled materials are discrete entities in the mantle. Modelling of the Pb isotope evolution suggests that the EM1 source and HIMU sources in the South Pacific may have differentiated at a similar time in Earth history in the Proterozoic.

The most striking feature of the Pb isotope systematics of the Pacific OIB revealed by the triple spike technique is the linearity of Pb isotope arrays from the individual hotspots,

indicating that the Pb isotopic composition of each hotspot may be explained by predominantly binary mixing. Further, a Pb isotope evolution model supports that the differentiation of the OIB sources in the U-Th-Pb isotope system occurred at times less than about two billion years ago and in the case of the Mauna Kea source may be quite young. None of the hotspots, for which high-precision Pb isotope data are available appear to share identical mixing end members of the arrays in Pb isotope space, indicating that each of the heterogeneities tapped by ocean island volcanism is unique, and that these heterogeneities represent relatively small-scale features in the mantle.

CHAPTER 1: INTRODUCTION

1.1 Oceanic intraplate magmatism

Linear chains of ocean islands and seamounts are a conspicuous feature of the Pacific ocean floor. Figure 1.1 shows the bathymetry of the Pacific Ocean with the locations of the three studied volcanic islands Hawaii, Pitcairn and Rurutu. All three islands are part of chains of oceanic intraplate volcanoes, namely the Hawaiian-Emperor chain, the Pitcairn-Gambier chain and the Austral-Cook chain. Magmatism along the Hawaiian-Emperor chain is age progressive. Active volcanoes exist on the Hawaiian Island, whereas the oldest seamounts at the NW end of the chain are ~80 Ma old (Clague and Dalrymple, 1989). On the Hawaiian Islands, the age-progressive line of volcanism can be subdivided into volcanoes belonging to the Loa-trend and to the Kea-trend (Fig. 1.2). Wilson (1963) proposed that Hawaiian volcanism may be explained by movement of the Pacific Plate over a stationary "hotspot" in the mantle. Morgan (1971) suggested the existence of plumes from the lower mantle to explain the origin of hotspots, because at least some hotspots, such as Hawaii, are relatively long-lived features.

In the South Pacific, migration in the site of magmatism was more complex. Different lines of simultaneous volcanism exist and are partly superimposed on one another (Fig. 1.3). In the Austral-Cook chain, age-progressive volcanism from MacDonald Seamount (0 Ma) to Mangaia Island (~20 Ma) is relatively well defined. However, volcanism on Rurutu Island occurred in two episodes. Although the older episode (8 – 14 Ma) fits to the age-progressive trend, the younger volcanic rocks (1 – 2 Ma) are too young to be related to the same trend. On other volcanic chains, there is poorer age-resolution (e. g. Pitcairn-Gambier chain), or no clear age-progression can be seen (e.g. Rarotonga Island). Additionally, there is volcanism occurring along fracture zones in the South Pacific ocean floor. This volcanicsm is not age progressive and is due to lithospheric extension (Janney et al., 2000). Thus, many intraplate seamount chains in the South Pacific are not easily explained by a single mantle plume as on

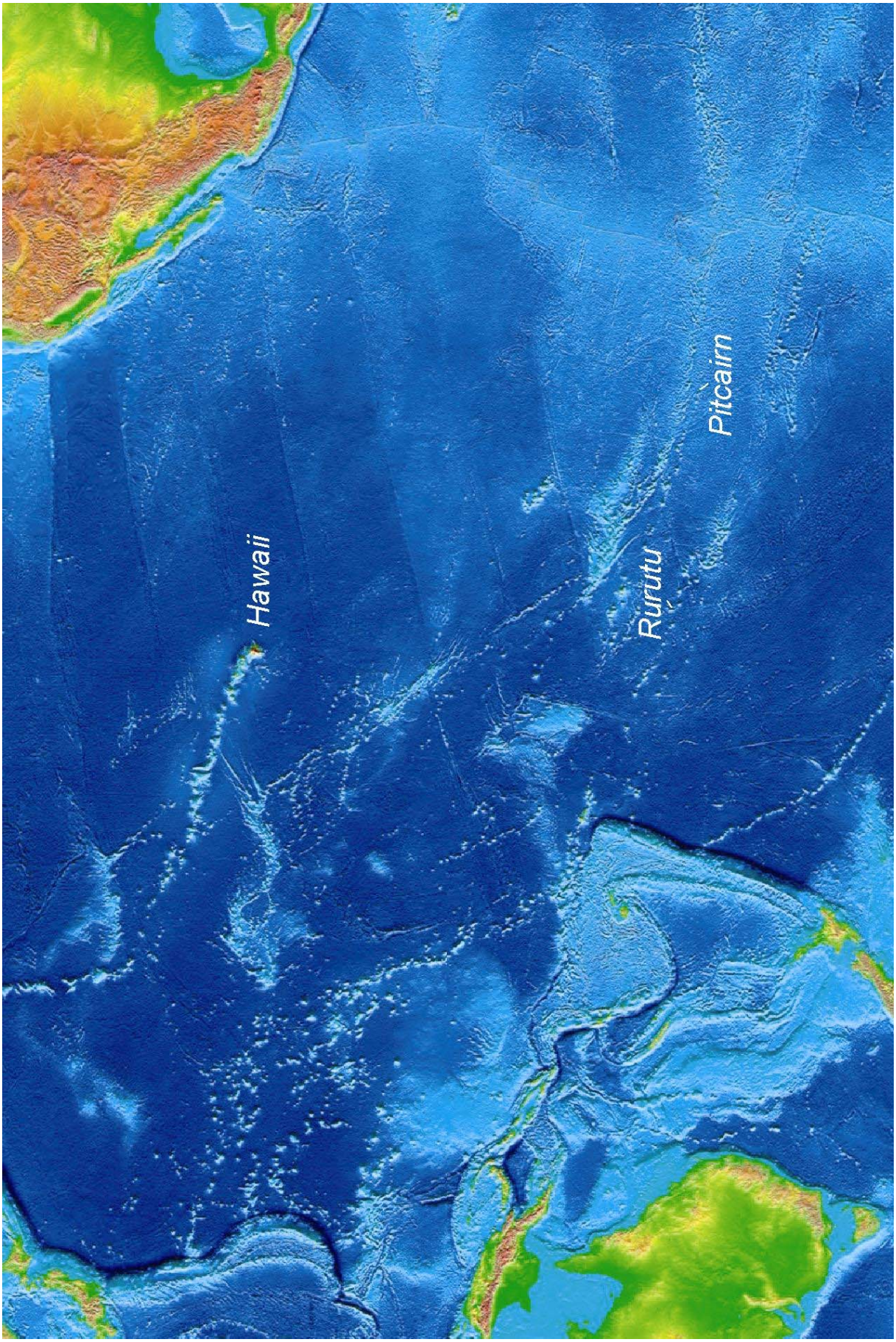

Fig. 1.1: Bathymetry of the Pacific ocean floor. Indicated are the locations of the volcanic islands Hawaii, Pitcairn and Rurutu.

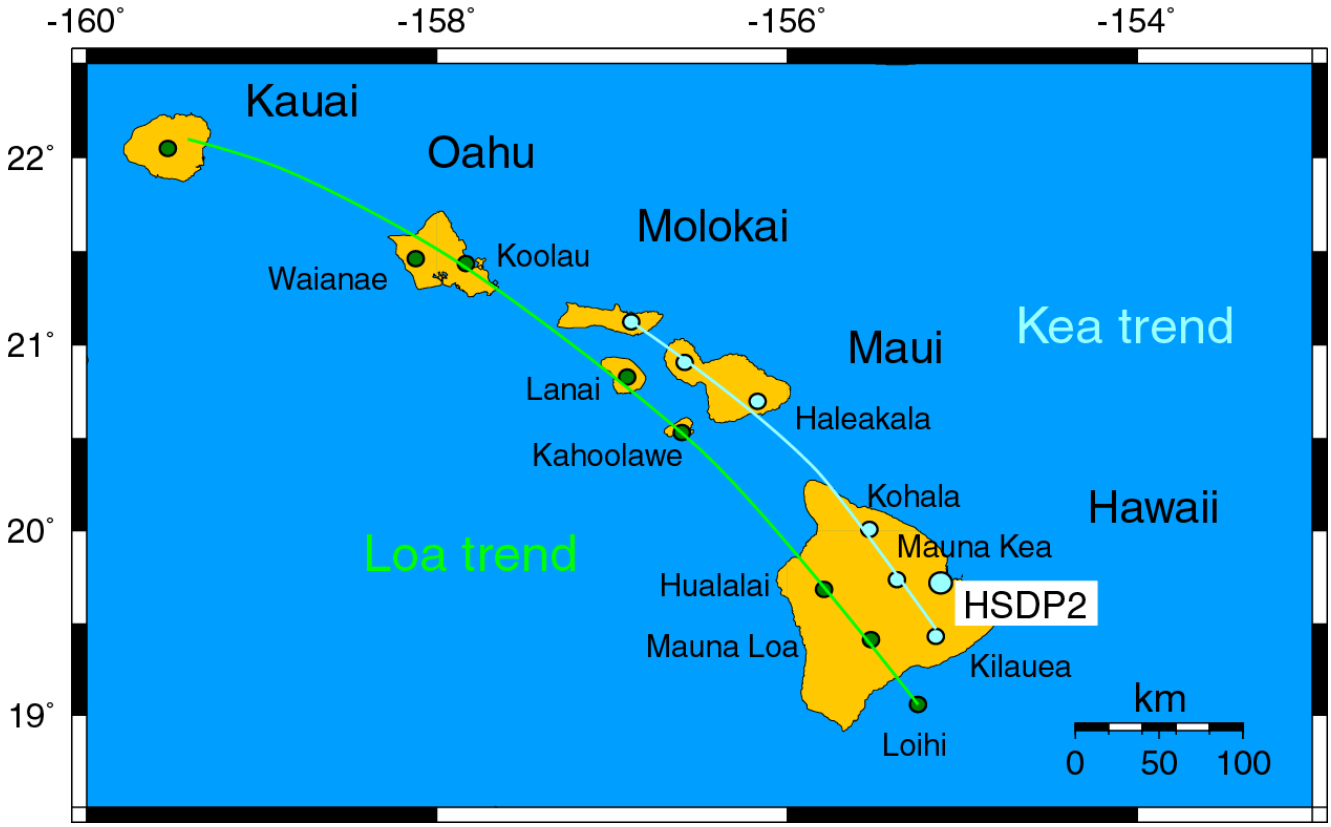

Fig. 1.2: Map of the Hawaiian Island chain with the locations of the volcanic centers and the location of the HSDP-2 drill hole. Also indicated are the two lines of age-progressive volcanism - the Loa and Kea trends. The map was created using the "Aquarius" server of the GEOMAR Institute, Kiel (http://www.aquarius.geomar.de/omc/make_map.html).

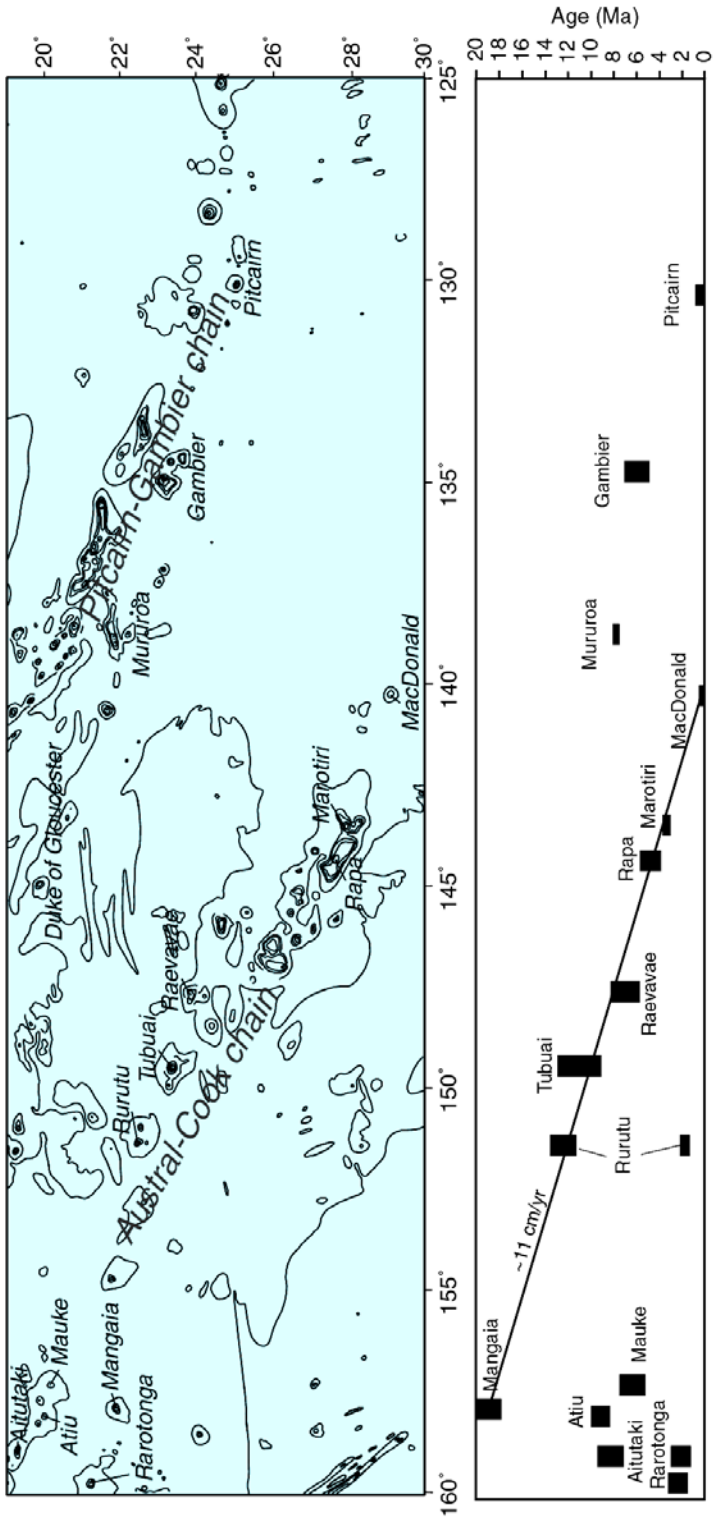

Fig. 1.3: Bathymetry of the South Pacific ocean surrounding the Austral-Cook and Pitcairn-Gambier volcanic chains and the age versus location relationships of the island and seamount chains. The bathymetry map was plotted using the PanMap software of the Alfred-Wegener-Institut für Polar- und Meeresforschung, Bremerhaven, (http://www.pangaea.de/Software/PanMap/index.html) which uses the General Bathymetric Chart of the Oceans (GEBCO) Digital Atlas, published by the International Hydrographic Organization (IHO) and the Intergovernmental Oceanographic Commission (UNESCO). The ages of the volcanic islands and the age-trend of ~11 cm/yr are from Chauvel et al. (1997) for the Austral-Cook chain. Ages for the Pitcairn-Gambier chain are from Duncan et al. (1974).

Hawaii. McNutt and Fischer (1987) observed that there may be a common origin of the diffuse volcanism in the Southern Pacific. They showed that there is an updoming of the South Pacific ocean floor, and they called this phenomenon the South Pacific Superswell. The Superswell was inferred to be located above a large-scale mantle upwelling (McNutt and Fisher, 1987). However, the interpretation of the origin of the Superswell varies, and explanations include large-scale convective flow in the lower mantle (Davies and Pribac, 1993), two distinct pulses of volcanism derived from a thermal anomaly in the upper mantle (McNutt, 1998) or a superplume from the core-mantle boundary (Larson and Kincaid, 1996).

1.2 The geochemical approach

The geochemical compositions of ocean island volcanoes are used as probes into the Earth's mantle. For this purpose, methods must be sought to "see through" the melting event that oceanic volcanics have undergone to decipher the signatures of mantle heterogeneity. An overview of the geochemical approach is given by Hofmann (1997). Isotope ratios and ratios of highly incompatible trace elements are not significantly fractionated during melting and fractional crystallization. Therefore, they can serve as tools to describe the sources of ocean island volcanoes. Oceanic intraplate volcanoes erupt on thin lithospheric covers, and their isotopic composition is therefore in many cases thought to record mantle heterogeneities.

1.3 Geochemistry of ocean island basalts

It was early recognized that hotspot volcanism is independent of the movement of oceanic plates (Fig. 1.4a, from Wilson, 1963), and that ocean island basalts may be derived from a different source region compared to mid-ocean ridge basalts (MORB). The geochemical signatures of MORB are thought to represent the Earth's upper mantle and have relatively uniform and "depleted" trace element compositions (Hofmann, 1997). In contrast, ocean island basalts (OIB) have much more variable but generally more enriched compositions.

a.

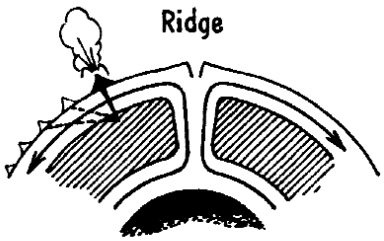

b.

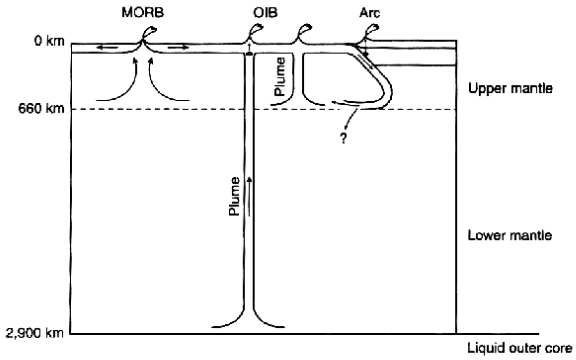

c.

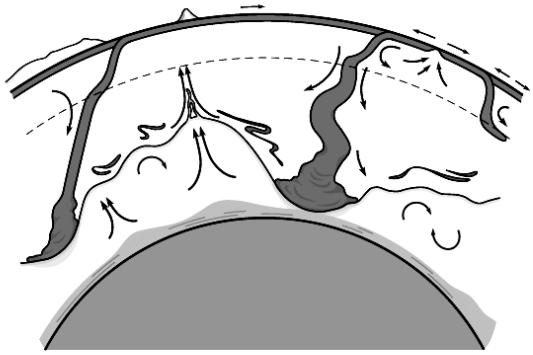

d.

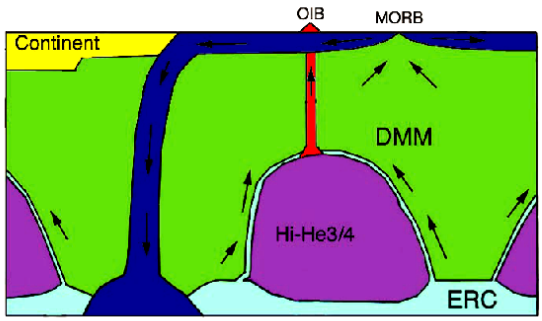

e.

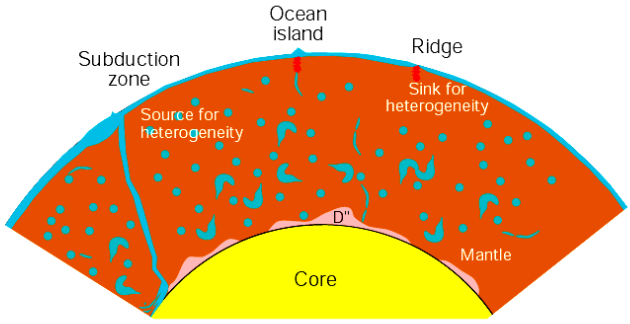

Fig. 1.4: Sections through the Earth's mantle describing its chemical and physical structure. Figure 1.4a is from Wilson (1963), b from Hofmann (1997), c from Kellogg et al. (1999), d from Tackley (2000), where DMM is depleted MORB mantle and ERC is enriched recycled crust, e from Helffrich and Wood (2001).

Hofmann and White (1982) argued, that subducted materials may be stored at the core-mantle boundary from where they rise as thermo-chemical plumes to form the intra-plate hotspot volcanoes (Fig. 1.4b). White (1985) and Zindler and Hart (1986) interpreted the isotopic compositions of ocean island basalts in Sr-Nd-Pb isotope space as reflecting mixing between four mantle components: the depleted MORB mantle (DMM), two types of enriched mantle (EM1 and EM2) and a component with high time-integrated $^{238}U/^{204}Pb$ ratio (HIMU). The compositions of these mantle components in $^{143}Nd/^{144}Nd$ versus $^{87}Sr/^{86}Sr$ isotope space are shown in Figure 1.5 (from Hofmann, 1997). The mantle components remain valid in that they represent end member compositions. The isotope and trace element character of the source of MORB (DMM) can be explained by the extraction of incompatible trace elements during formation of the continental crust (Hofmann, 1988). The heterogeneities in OIB may originate from different types of recycled materials in the sources of OIB. The interpretations of the mantle components are centered around the hypothesis that subducted material is incorporated into the sources of ocean island basalts proposed by Hofmann and White (1982). The OIB components can be interpreted in terms of (mainly oceanic) recycled material in their sources. For example HIMU is often attributed to recycled oceanic crust (see Chapter four for discussion), and the EM mantle sources may contain different types of ancient recycled sediment components (see Chapter 2).

1.4 Geochemical reservoirs

The study of the geochemical composition of the Earth's interior attempts to locate geochemical reservoirs within the mantle. These reservoirs may represent mantle regions that have a specific geochemical composition (e.g. the depleted mantle). The location and distribution of geochemical heterogeneities in the mantle is a debated subject and remains unclear. Many different attempts have been made to subdivide the Earth's mantle into reservoirs and to assign a location to these reservoirs. Figure 1.4 shows different versions of

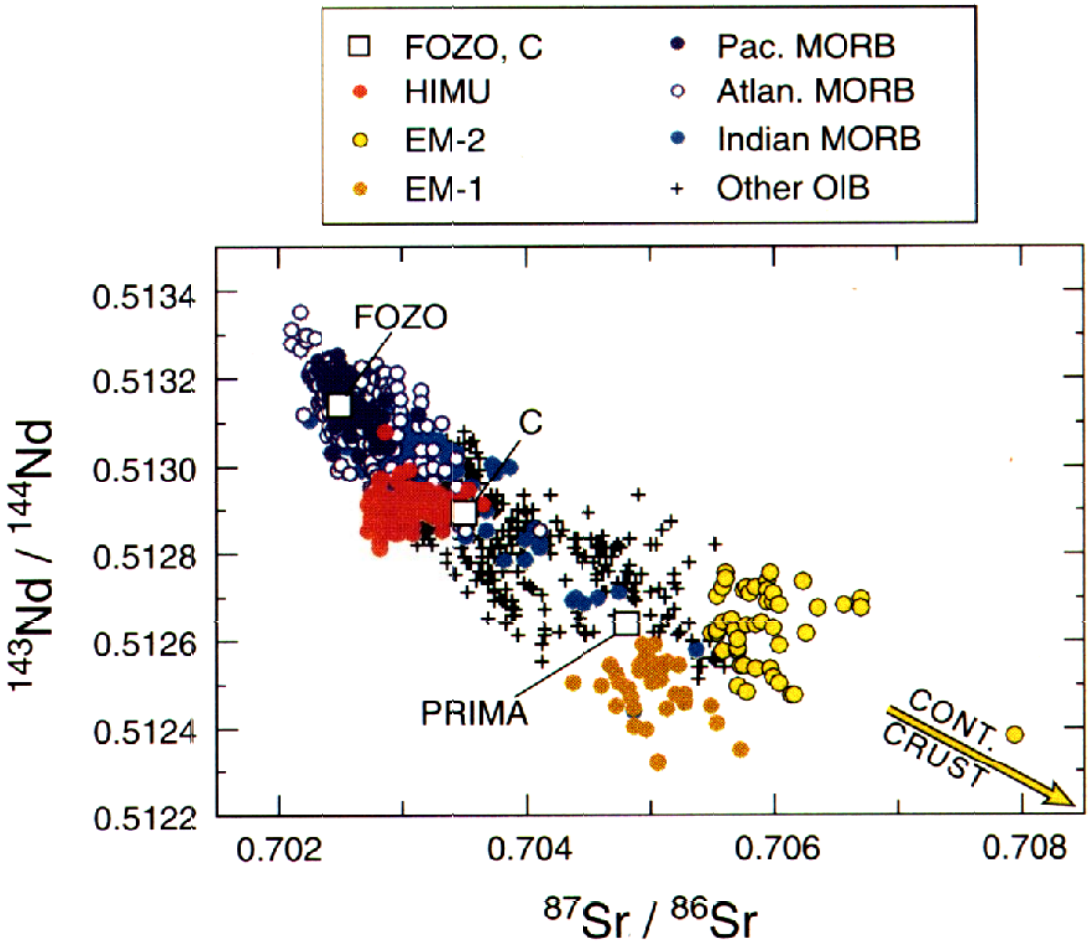

Fig. 1.5: Geochemical mantle components in $^{143}Nd/^{144}Nd$ versus $^{87}Sr/^{86}Sr$ isotope space (from Hofmann, 1997). Indicated are the isotopic compositions of MORB and OIB. OIB data were subdivided into samples belonging to the HIMU, EM-1 and EM-2 end members (Zindler and Hart, 1986). Also indicated are the approximate composition of continental crustal material, the composition of primitive mantle (PRIMA) and the proposed common mantle components FOZO (Hart et al., 1992) and C (Hanan and Graham, 1996).

sections through the Earth's mantle aiming to describe the geochemical reservoirs and their distribution within the Earth.

The composition of the MORB source, which is depleted in incompatible elements cannot not account for the composition of the whole mantle. Therefore, a chemically stratified mantle was proposed. The arguments for geochemical layering of the mantle are first, mass balances which estimate the mass fraction of the depleted mantle to be ~50% of the total mantle (for an overview, see Hofmann, 1997) and second, the budget of the heat-producing elements. The concentration of the heat-producing elements K, U and Th in the MORB source (Jochum et al., 1983) can only account for 2-6 Tera Watts (1 TW = $1 \cdot 10^{12}$ W) of the global heat flow, which is 44 TW (see Helffrich and Wood, 2001 for an overview). This suggests that a deeper layer exists, which is enriched in these elements. These arguments supported a model assuming a geochemical and convectional layering of the mantle (Fig. 1.4b). The boundary between the depleted upper mantle and the lower mantle reservoir was assumed to be the 660 km seismic discontinuity. However, seismic tomography contradicted the hypothesis of two isolated reservoirs in the upper and lower mantle. Seismic tomographic images indicated that subducted oceanic slabs can penetrate into the lower mantle (van der Hilst et al., 1997). Thus, there appears to be material exchange between the upper and lower mantle across the 660 km discontinuity (Fig. 1.4c). Therefore, it appeared unlikely that the 660 km discontinuity represented a chemical boundary in the mantle. Kellogg et al. (1999) suggested a chemical stratification deeper in the mantle and proposed the existence of a deep primitive layer in the Earth with an oscillating boundary (Fig. 1.4d). Some hotspot volcanoes yield high ratios of $^{3}He/^{4}He$, and the high proportion of the primordial isotope ^{3}He requires a relatively undegassed mantle source (e.g. Kurz et al., 1983; Farley et al., 1992; Hanan and Graham, 1996), which may be located in the deep mantle (Fig. 1.4c, d).

An alternative approach, advocating relatively small-scale heterogeneity in the mantle instead of large-scale stratification, is the marble-cake model of the mantle (Allègre and Turcotte, 1986), which proposes that subducted materials are stretched to long thin bands by mantle convection and are as such distributed in the mantle. Allègre and Turcotte (1986) show that most if not all of the mantle may have been processed by MORB formation and subduction if whole mantle convection is assumed. A graphical representation of an unstratified marble-cake mantle is shown in Fig. 1.4e. A similar mantle model advocating whole-mantle convection as well as small-scale heterogeneity throughout the mantle, is the plum-pudding model of Jason Phipps Morgan and W. Jason Morgan (1999).

1.5 Geophysical mantle models

Many Earth scientists would agree that "heterogeneity is ubiquitous in the mantle and that subduction is the key process producing it" (Helffrich and Wood, 2001). Seismology can be used to identify mineralogical, chemical and temperature variations in the mantle. Although the major seismic discontinuities within the mantle are likely to result from mineralogical phase changes rather than chemical layering, there is convincing seismic evidence for thermo-chemical heterogeneity in the mantle. The idea that heterogeneity in the mantle exists at small scales (Allègre and Turcotte, 1986) is supported by the discovery of seismic "scatterers" in the lower mantle (see Helffrich and Wood, 2001), which are interpreted to be heterogeneities smaller than 10 km in size. The hypothesis that subducted slabs may be stored at the core-mantle boundary (Hofmann and White, 1982) is supported by the seismic properties of the D" layer at the bottom of the mantle. The D" layer shows distinct seismic wave speeds compared to the overlying mantle and can be interpreted to represent a mineralogically and chemically distinct reservoir. Additionally, with seismic tomographic models, large-scale domains of anomalously fast or slow wave speed were recognized in the Earth's interior. These models have shown that subducting slabs may sink into the lower

mantle (van der Hilst, 1997). But they also show large-scale anomalies of slow seismic wave speed extending from the lower into the upper mantle (Tackley, 2000), for example under the South Pacific and under Africa (see Fig. 1.6). These features may be interpreted as upwelling "superplumes".

1.6 Lead isotope compositions of ocean island volcanics

Ratios of radiogenic nuclides over an unradiogenic isotope of the same element (e.g. $^{206}Pb/^{204}Pb$) in a long-lived radiogenic isotope system can be used as tracers to infer the nature of reservoirs in the mantle. From this knowledge, inferences on the location of a reservoir, and inferences on the exchange between several reservoirs can be made. In a radiogenic isotope ratio measured on an ocean island basalt two pieces of information are superimposed on one another: first, information on the time-integrated ratio of the parent nuclide to a stable nuclide of the daughter-element (e.g. $^{238}U/^{204}Pb$) of the source material. Second, there is information on the time period of decay, because of accumulation of the radiogenic nuclide over time. It is difficult to resolve the effects of these two variables from one another, because neither of the two parameters is known independently. However, different source materials can be expected to have distinct radiogenic isotope ratios at the present day, so that the isotope ratios can be used as tracers. The combination of isotope tracers, such as Pb isotopes with other isotopic systems and trace element data can place some constraints upon the age and origin of mantle heterogeneity.

Pb isotopic compositions of ocean island volcanoes are particularly interesting, because Pb isotope variations in OIB can form linear arrays in ^{208}Pb-^{207}Pb-^{206}Pb-^{204}Pb isotope space. These linear arrays imply an age if interpreted as isochrons or, alternatively, may yield end member compositions if interpreted in terms of binary mixing (Oversby and Gast, 1970). Pb isotopes have three radiogenic isotope ratios and are able to identify mixing end members in three-dimensional isotope space. Early analyses of OIB demonstrated that there is significant

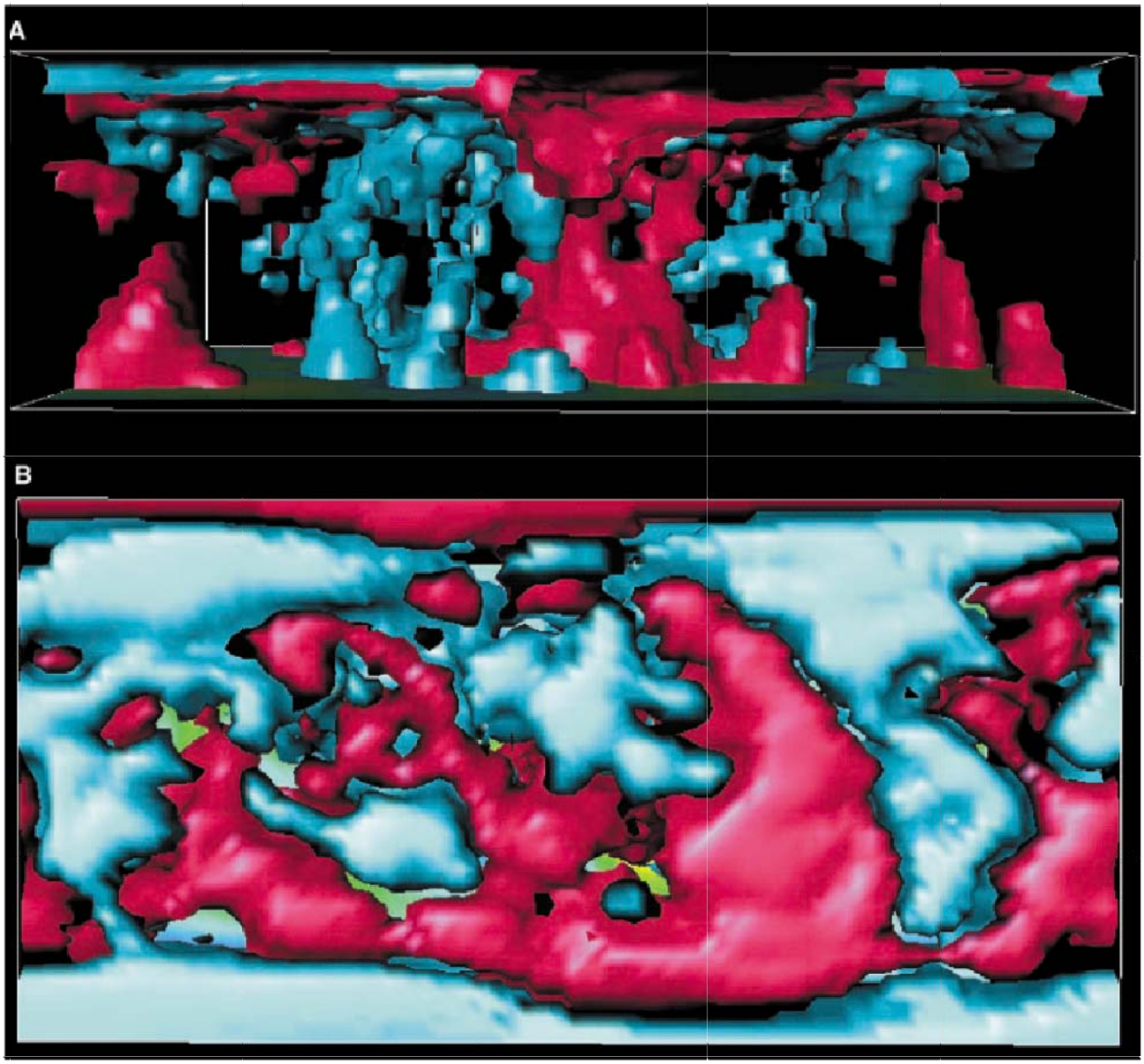

Fig. 1.6: Seismic tomographic model of the mantle structure from Tackley (2000). Blue areas have faster than average shear-wave velocities, while red areas have slower than average shear-wave velocities. a: section of the mantle down to the core-mantle boundary. Apparent are the blue zones of anomalously fast seismic wave speed, reaching from the upper into the lower mantle, which are related to circum-Pacific subduction zones. Red areas of slower-than-average wave-speed occur under the South Pacific and under Africa and may be interpreted as large plumes from the lower mantle. b: Looking from above the pattern of continents and oceans is visible.

Pb isotope heterogeneity in the mantle (Gast et al., 1964). Gast and coworkers also recognized that Pb isotopic compositions of OIB were displaced to the right of the geochron, and suggested that this feature implies an increase in the U/Pb ratio since the formation of the Earth (Fig. 1.7). Oversby and Gast (1970) outlined some principles of Pb isotope systematics of OIB on the basis of analyses of lavas from Tristan da Cunha, St. Helena and the few literature data available at that time (Fig. 1.7). They realized that the linear arrays formed by OIB may be interpreted as two component mixtures of end member compositions that differentiated between ~1 and 2 Ga ago, and that the component today called HIMU may have developed with a μ ~15 since ~2 Ga. They also postulated that the global OIB array forms an apparent isochron with an age of ~1.4 Ga (see Fig. 1.7a).

Many improvements have been made in the analytical techniques since the study of Oversby and Gast (1970), and numerous case studies on the Pb isotopic compositions of ocean island basalts exist. Figure 1.7b shows the data available from the Pacific ocean islands today and the Pb isotopic compositions of the three volcanoes Pitcairn, Rurutu and Mauna Kea. Pitcairn samples plot near the inferred end member EM1 (Zindler and Hart, 1986), Mauna Kea lavas have a relatively depleted composition, while Rurutu lavas are representative of the HIMU source (Fig. 1.7b).

I will not attempt to provide an overview on the studies of Pb isotopes in OIB, nor try to describe the development of the analytical techniques, but just to contrast the early studies of Oversby and Gast (1970) with the results available today. In spite of the improvement in analytical precision, the main findings of Oversby and Gast (1970) remain valid. However, the use of double and triple spike techniques to correct for instrumental mass fractionation (Dodson, 1963; Woodhead et al., 1995; Galer, 1999; Thirlwall, 2000) improves the analytical precision by a factor five to ten compared to conventional techniques. Therefore a higher resolution "image" of Pb isotope heterogeneities of the mantle may be drawn (Galer et al., 2001). It is important to determine the exact positions and slopes of linear arrays in Pb isotope

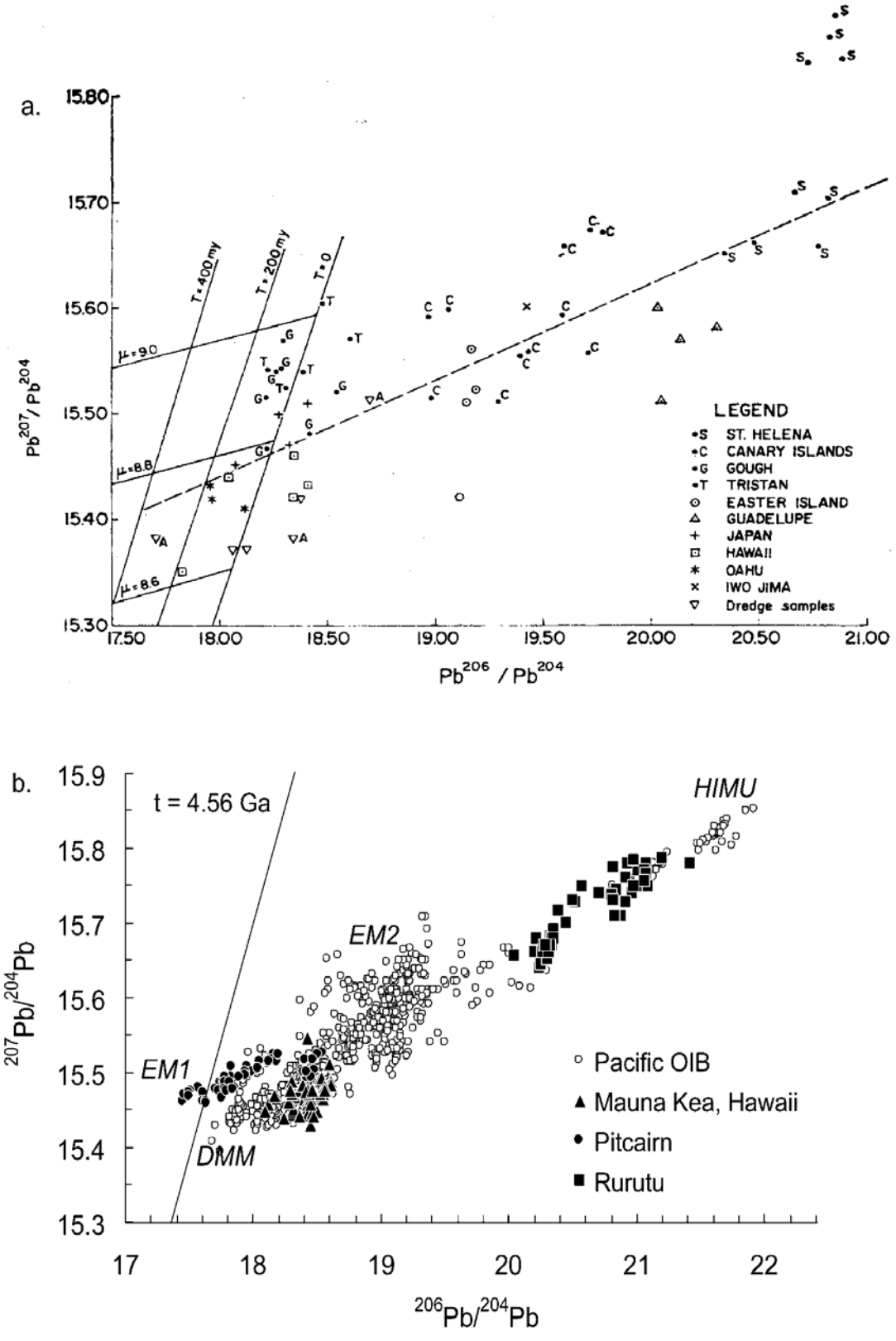

Fig. 1.7: a. Pb isotopic compositions of oceanic volcanics in a figure from Oversby and Gast (1970), showing the geochron and growth lines for μ = 8.6, 8.8 and 9.0. The dashed line is a fit through the global data available at that time, reflecting an apparent isochron with ~1.4 Ga age. b. Pb isotopic compositions of Pacific OIB, compiled using the GEOROC database (http://georoc.mpch-mainz.gwdg.de/). The Pb isotopic compositions of Pitcairn, lying near the EM1 end member, of Rurutu, near the HIMU end member, and of Mauna Kea are highlighted.

space. This is the case, because linear arrays in Pb isotope space can be used to determine an "age" of apparent isochrons. Alternatively, when interpreting the Pb isotope arrays as reflecting binary mixtures one can investigate the extensions of the arrays to find end member compositions.

From the published Pb isotope data using double or triple spike techniques on OIB lavas (Woodhead and Devey, 1993; Woodhead, 1996; Thirlwall, 2000; Abouchami et al., 2000a) the most striking feature is the existence of linear arrays in Pb isotope space defined by the lavas from a particular volcano. Abouchami et al. (2000a) showed that for Mauna Kea lavas, these linear arrays are most reasonably explained by mixing of end members lying along their radiogenic and unradiogenic extensions. Recent studies at the MPI using the triple spike technique revealed similar Pb isotope arrays for the lavas from other oceanic islands (Abouchami et al., 2000b; Galer et al., 2001, this study). The Pb isotope arrays themselves and their end members appear to be distinct for most ocean island volcanoes (Galer et al., 2001), which may be an indication that the mantle components do not represent homogeneous large-scale reservoirs within the Earth, but that there is relatively small-scale heterogeneity throughout the mantle, as was predicted by the marble-cake mantle model of Allègre and Turcotte (1986).

The central unresolved questions of ocean island geochemistry that remain are, which of the hotspot volcanoes may result from deep mantle plumes and which may not, and what type of recycled material a particular volcano may have incorporated.

1.7 Aims

This thesis describes the signature of three geochemically very different suites of ocean island basalts from the Pacific Ocean – lavas from the Pitcairn hotspot, Mauna Kea lavas from the main hole of the Hawaiian Scientific Drilling Project (HSDP-2) and lavas from Rurutu Island. The major goals of this work were to geochemically characterize the mantle

sources of the lavas and to investigate the role of recycling of subducted materials in creating isotope and trace element heterogeneities in the lavas.

The main emphasis in this thesis was the Pb isotopic composition of the lavas. The lavas from Pitcairn and Rurutu Islands cover the extremes of Pb isotopic variations in OIB, whereas Mauna Kea lavas have intermediate compositions in Pb isotope space (Fig. 1.7b). Although the Pb isotopic compositions of samples from all three volcanoes have been determined by previous workers (Pitcairn: e.g. Woodhead and McCulloch, 1989; Woodhead and Devey, 1993; Mauna Kea: e.g. Lassiter et al., 1996; Rurutu: e.g. Chauvel et al., 1997), the Pb isotope triple-spike technique (Galer, 1999) used in this study offered the opportunity to determine the Pb isotopic composition of the samples with an improved analytical precision. In the case of HSDP-2, this study was a follow-up of the work of Abouchami et al. (2000a), who had found linear arrays in Pb isotope space for Mauna Kea lavas of the HSDP-1 pilot hole using the triple spike technique. In addition to analysis of Pb isotopic compositions, a detailed study on Pitcairn lavas was undertaken, involving determination of trace element and Os, Hf, Nd and Sr isotopic compositions in order to investigate the origin of the EM1 source. The specific questions to be answered for the three OIB suites were:

1. What is the Os isotopic composition of EM1, and what sort of recycled material may the EM1 signature in Pitcairn represent? Three hypotheses for the origin of EM1 have previously been proposed: incorporation of recycled subcontinental lithospheric mantle (McKenzie and O'Nions, 1983), recycled pelagic sediments (Woodhead and McCulloch, 1989; Chauvel et al., 1992; Woodhead and Devey, 1993), and recycled oceanic plateaus (Gasperini et al., 2000). The different materials should be identifiable on the basis of their contrasting Os isotope, Hf-Nd isotope and trace element systematics.

2. What does the long-term Pb isotopic evolution of Mauna Kea lavas look like? Pb isotopic compositions of lavas from the HSDP-2 drill hole provided a ~300 ka record of the Pb isotopic fluctuations in a hotspot volcano and a high resolution of the Pb isotope arrays.

Mauna Kea represents one isotopic end member of Hawaiian magmatism and the origin of this signature was investigated using a Pb isotope evolution model. This study also focused on the reproducibility of Pb isotope measurements of lavas and the possible sources of analytical error.

3. The study of Rurutu lavas was aimed at characterizing the HIMU Pb isotope signature. Additionally, these data complemented those from the Pitcairn hotspot. Pitcairn and Rurutu are both situated in the South Pacific (Fig. 1.1), but span almost the entire range in Pb isotope compositions of all OIB. The possible age relationships of the sources were investigated.

1.8 Contributions to the following chapters

As already obvious from the introduction, this thesis is mainly based on the long-term research done and the ideas developed at the MPI. Al Hofmann provided me with the samples from Pitcairn Island and with the possibility to study Pb isotopes on the HSDP-2 core. He also proposed many of the hypotheses that were tested during this thesis. Without the years of preparation setting up the Pb triple spike technique this thesis would not exist. The main responsibles here are of course Wafa Abouchami and Steve Galer. The program to calculate the fractionation correction and error propagation of the Pb isotope triple-spike data used during this thesis was developed by Steve Galer. Samples from the Pitcairn seamounts were provided by Colin Devey, samples from Rurutu Island are from Catherine Chauvel. Additionally, the Hafnium isotope data presented in Chapter two were analyzed at the Ecole Normal Superieure de Lyon by Janne Blichert-Toft. Some trace element compositions of samples from the Pitcairn hotspot were commercially analyzed at the Memorial University, St. John's, Canada. Some trace element analyses from Pitcairn seamount samples were provided by Colin Devey, University of Bremen as described in Table 2.3 of Chapter two.

Chapter two is the revised version of a manuscript submitted to Earth and Planetary Science Letters.

1.9 References

Abouchami, W., Galer, S. J. G. and Hofmann, A. W. (2000a): High precision lead isotope systematics of lavas from the Hawaiian Scientific Drilling Project, Chemical Geology 169, 187-209

Abouchami, W., Hofmann, A. W., Eisele, J. and Galer, S. J. G. (2000b): Long-term Pb isotope record of sources within the Hawaiian plume, Eos Trans. AGU, 81 (48), Fall Meet. Suppl., Abstract V21D-03

Allègre, C. J. and Turcotte, D. L. (1986): Implications of a two-component marble-cake mantle, Nature 323, 123-127

Chauvel, C., Hofmann, A. W. and Vidal, P. (1992): HIMU-EM: the French Polynesian connection, Earth and Planetary Science Letters 110, 99-119

Chauvel, C., McDonough, W., Guille, G., Maury, R. and Duncan, R. (1997): Contrasting old and young volcanism in Rurutu Island, Austral chain, Chemical Geology 139, 125-143

Clague, D. A. and Dalrymple, G. B. (1989): Tectonics, geochronology and origin of the Hawaiian-Emperor volcanic chain, In: Winterer, E. L., Hussong, D. M. and Decker, R. W. (eds.): The geology of North America, Volume N, 188-217

Davies, G. F. and Pribac, F. (1993): Mesozoic seafloor subsidence and the Darwin Rise, past and present, in: The Mesozoic Pacific: Geology, Tectonics and Volcanism, Geophysical Monograph 77, 39-52

Dodson, M. H. (1963): A theoretical study of the use of internal standards for precise isotopic analysis by the surface ionization technique: Part I. General first-order algebraic solutions, Journal of Scientific Instruments 40, 289-295

Duncan, R. A., McDougall, I., Carter, R. M. and Coombs, D. S. (1974): Pitcairn Island - another Pacific hot spot?, Nature 251, 679-682

Farley, K. A., Natland, J. H. and Craig, H. (1992): Binary mixing of enriched and undegassed (primitive-questionable) mantle components (He, Sr, Nd, Pb) in Samoan lavas, Earth and Planetary Science Letters 111, 183-199

Galer, S. J. G. (1999): Optimal double and triple spiking for high precision lead isotopic measurement, Chemical Geology 157, 255-274

Galer, S. J. G., Abouchami, W., Eisele, J., Haase, K., Moeller, H., Regelous, M. and Hofmann, A. W. (2001): A New Pb Isotope Perspective on Oceanic Basalts: Reading Between the Lines, Eos Trans. AGU, Fall Meet. Suppl.

Gasperini, D., Blichert-Toft, J., Bosch, D., Del Moro, A., Macera, D., Télouk, P. and Albarède, F. (2000): Evidence from Sardinian basalt geochemistry for recycling of plume heads into the Earth's mantle, Nature 408, 701-704

Gast, P. W., Tilton, G. R. and Hedge, C. (1964): Isotopic composition of lead and strontium from Ascension and Gough Islands, Science 145, 1181-1185

Hanan, B. B. and Graham, D. W. (1996): Lead and Helium isotope evidence from oceanic basalts for a common deep source of mantle plumes, Science 272, 991-995

Hart, S. R., Hauri, E. H., Oschmann, L. A. and Whitehead, J. A. (1992): Mantle plumes and entrainment: isotopic evidence, Science 256, 517-520

Helffrich, G. R. and Wood, B. J. (2001): The Earth's mantle, Nature 412, 501-507

Hofmann, A. W. and White, W. M. (1982): Mantle plumes from ancient oceanic crust, Earth and Planetary Science Letters 57, 421-436

Hofmann, A. W. (1988): Chemical differentiation of the Earth: the relationship between mantle, continental crust and oceanic crust, Earth and Planetary Science Letters 90, 297-314

Hofmann, A. W. (1997): Mantle geochemistry: the message from oceanic volcanism, Nature 385, 219-228

Janney, P. E., MacDougall, J. D., Natland, J. H. and Lynch, M. A. (2000): Geochemical evidence from the Pukapuka volcanic ridge system for a shallow enriched mantle domain beneath the South Pacific Superswell, Earth and Planetary Science Letters 181, 47-60

Jochum, K. P., Hofmann, A. W., Ito, E., Seufert, H. M. and White, W. M. (1983): K, U and Th in mid-ocean ridge basalt glasses and heat production, K/U and K/Rb in the mantle, Nature 306, 431-436

Kellogg, L. H., Hager, B. H. and van der Hilst, R. D. (1999): Compositional stratification in the deep mantle, Science 283, 1881-1884

Kurz, M. D., Jenkins, W. J. Hart, S. R. and Clague, D. (1983): Helium isotopic variations in volcanic rocks from Loihi Seamount and the island of Hawaii, Earth and Planetary Science Letters 66, 388-406

Lassiter, J. C., DePaolo, D. J. and Tatsumoto, M. (1996): Isotopic evolution of Mauna Kea volcano: Results from the initial phase of the Hawaiian Scientific Drilling Project, Journal of Geophysical Research 101, 11769-11780

Larson, R. L. and Kincaid, C. (1996): Onset of mid-cretaceous volcanism by elevation of the 670 km thermal boundary layer, Geology 24, 551-554

McKenzie, D. and O'Nions, R. K. (1983): Mantle reservoirs and ocean island basalts, Nature 301, 229-231

McNutt, M. K. and Fischer, K. M. (1987): The South Pacific superswell, in: Seamounts, Islands and Atolls, Geophysical Monograph Series, vol. 43 B. H. Keating et al. (eds), 25-34

McNutt, M. K. (1998): Superswells, Reviews in Geophysics 36(2), 211-244

Morgan, J. P. and Morgan, W. J. (1999): Two-stage melting and the geochemical evolution of the mantle: a recipe for mantle plum-pudding, Earth and Planetary Science Letters 170, 215-239

Morgan, W. J. (1971): Convection plumes in the lower mantle, Nature 230, 42-43

Oversby, V. M. and Gast, P. W. (1970): Isotopic composition of lead from oceanic islands, Journal of Geophysical Research 75, 2097-2114

Tackley, P. J. (2000): Mantle convection and plate tectonics: toward an integrated physical and chemical theory, Science 288, 2002-2007

Thirlwall, M. F. (2000): Inter-laboratory and other errors in Pb isotope analyses investigated using a 207Pb-204Pb double spike, Chemical Geology 163, 299-322

van der Hilst, R. D., Widiyantoro, S. and Engdahl, E. R. (1997): Evidence for deep mantle circulation from global tomography, Nature 386, 578-584

White, W. M. (1985): Sources of oceanic basalts - radiogenic isotopic evidence, Geology 13(2), 115-118

Wilson, J. T. (1963): A possible origin of the Hawaiian Islands, Canadian Journal of Physics 41, 863-870

Woodhead, J. D. and McCulloch, M. T. (1989): Ancient seafloor signals in Pitcairn Island lavas and evidence for large amplitude, small length-scale mantle heterogeneities, Earth and Planetary Science Letters 94, 257-273

Woodhead, J. D. and Devey, C. W. (1993): Geochemistry of the Pitcairn Seamounts, I: source character and temporal trends, Earth and Planetary Science Letters 116, 81-99

Woodhead, J. D., Volker, F. and McCulloch, M. T. (1995): Routine Lead isotope determination using a Lead-207-Lead-204 double spike: a long-term assessment of analytical precision and accuracy, Analyst 120, 35-39

Woodhead, J. D. (1996): Extreme HIMU in an oceanic setting: the geochemistry of Mangaia Island (Polynesia) and temporal evolution of the Cook-Austral hotspot, Journal of Volcanology and Geothermal Research 72, 1-19

Zindler, A. and Hart, S. (1986): Chemical geodynamics, Annual Reviews in Earth and Planetary Sciences 14, 493-571

Chapter 2: The role of sediment recycling in EM-1 inferred from Os, Pb, Hf, Nd, Sr isotope and trace element systematics of the Pitcairn hotspot

Jürgen Eisele, Mukul Sharma, Stephen J. G. Galer, Janne Blichert-Toft,

Colin W. Devey and Albrecht W. Hofmann

Abstract

We present comprehensive radiogenic isotope (Os, Pb, Hf, Nd, Sr) and trace element data on basaltic lavas from Pitcairn Island and the Pitcairn seamounts and examine the origin of the enriched mantle isotopic signature (EM-1) found in these lavas. The $^{187}Os/^{188}Os$ ratios of the lavas range from 0.131 to 0.254, while those of the high-Os concentration samples (>50 pg/g) lie between 0.131 and 0.148. All $^{187}Os/^{188}Os$ ratios are higher than the bulk silicate Earth reference value of 0.127. Since ancient subcontinental lithospheric mantle (SCLM) is expected to have a $^{187}Os/^{188}Os$ ratio less than 0.127, it appears that recycled SCLM plays no role in the Pitcairn source. Variations in $^{187}Os/^{188}Os$ ratios appear to be unconnected with those of $^{206}Pb/^{204}Pb$ ratios in Pitcairn lavas, suggesting that Pb and Os isotopic variations are controlled by different factors. Modeling shows that variations in Pb isotopic compositions may mainly reflect the proportion of recycled sediment in the source, while those of $^{187}Os/^{188}Os$ ratios may reflect the proportion of peridotite mantle versus recycled oceanic crust.

The occurrence of negative Nb anomalies in some of the lavas, a correlation between Nb anomaly and $^{87}Sr/^{86}Sr$ ratios (0.7036-0.7051), and extremely unradiogenic and strongly correlated Nd and Hf isotopic compositions (ε_{Nd} of –5.9 to +1.1 and ε_{Hf} of –5.3 to +2.2) together suggest that the Pitcairn mantle source contains a recycled continental crustal component. The slope of the ε_{Hf} vs. ε_{Nd} correlation is shallower for Pitcairn Island than that of the Pitcairn seamounts or the global OIB array, and may be due to a variable ratio of recycled mud to sand in the Pitcairn source. A trace element mixing model also indicates the presence of small amounts of recycled pelagic and terrigenous sediment and permits variable amounts of depleted components such as recycled MORB, gabbro and depleted mantle.

The $^{206}Pb/^{204}Pb$ ratios of the Pitcairn lavas vary between 17.47 and 18.10 and are very unradiogenic compared to those of other ocean island basalts. By contrast, $^{208}Pb/^{204}Pb$ ratios are high and relatively homogeneous at values of ~39.0. This observation along with the

measured Th/U ratios of the lavas, which range up to 14.1, indicate a long-term history of U loss in the Pitcairn source. In $^{207}Pb/^{204}Pb$-$^{206}Pb/^{204}Pb$ space, the data form a linear array that can be interpreted in terms of mixing between a minor recycled sediment end member and more depleted material. Lead isotopic compositions suitable for the recycled end member were investigated using a three-stage evolution model by Monte Carlo methods and suggest ages between 0.7 and 1.9 Ga for the recycled sediment. The relationships between measured Th/U and radiogenic $^{208}Pb^*/^{206}Pb^*$ ratios suggest that the isotopic arrays displayed by the lavas were produced by mixing, probably occurring during magma genesis.

Keywords: Pitcairn; hotspot volcanism; EM-1; Os isotopes; Hf isotopes; Pb isotope evolution; recycling

2.1 Introduction

The involvement of recycled lithospheric material in producing the chemical and isotopic heterogeneities observed in ocean island basalts (OIB) [1,2] appears to be well established from numerous case studies [3-10]. However, the type of recycled material present in the Enriched Mantle 1 (EM-1) source and the processes leading to isotopic variability remain largely unresolved and are the subject of considerable debate.

The current models for the EM-1 signature invoke the presence of the following recycled material in the source: oceanic crust with pelagic sediment [4,8,11-14], delaminated subcontinental lithospheric mantle (SCLM) [5,15] and, more recently, subducted oceanic plateaus [10]. We present comprehensive radiogenic isotope (Os, Pb, Hf, Nd, Sr) and trace element data on basaltic lavas from Pitcairn Island and the Pitcairn seamounts in order to better understand the source material in the Pitcairn hotspot. The Pitcairn hotspot lavas were chosen for this study as they display some of the most extreme Sr, Nd and Pb isotopic compositions found in OIB [11,12], falling close to the inferred EM-1 end member [16,17].

Woodhead and coworkers [11, 12] presented Sr,- Nd-, Pb-isotope and trace element data from Pitcairn Island and seamounts and interpreted these data in terms of pelagic sediment recycling. However, it may not be possible to distinguish between models involving recycled sediments and SCLM on the basis of Sr- Nd- and Pb-isotope data alone. Therefore, a reassessment of the hypotheses for the Pitcairn EM-1 signature by combining Os and Hf isotope systematics with Sr-, Nd-, Pb-isotope and trace element systematics is undertaken here. Our results indicate that the Pitcairn recycled component carries the signature of continentally-derived material including a pelagic sediment component. Modeling of the Os-Pb isotope systematics suggests that in mixtures involving more than two components (e.g. sediment, oceanic crust and peridotite mantle) no correlations are expected in Os-Pb isotope space. The unique Th-U-Pb isotope systematics of the Pitcairn lavas demonstrate that the isotope variability was produced by mixing of the continentally-derived material with more depleted material. This process is best explained by mixing of melts from these components during magma genesis.

2.2 Results

The samples analyzed here were collected during a cruise of the German research vessel *Sonne* in 1989 [18]. Ten samples come from Pitcairn Island, eight of which are from the shield-building Tedside volcanics, and two are from the post-erosional Pulawana volcanics. Duncan et al. [19] obtained K-Ar ages for Tedside volcanism of 0.76-0.95 Ma and 0.62-0.67 Ma for the Pulawana series. The Pitcairn seamounts are the youngest expression of volcanism of the Pitcairn hotspot [12], and therefore the samples can be regarded as being essentially recent. The Pitcairn Island samples analyzed can be classified as tholeiites, potassic trachybasalts and hawaiites based upon the scheme of Le Maitre et al. [20]. Macroscopically, and in thin-section, all samples from Pitcairn Island are fresh except for Pit89-2 which has a chloritized groundmass. The samples from the Pitcairn seamounts are

unaltered and consist mainly of basalts, except for one basaltic trachyandesite (52DS-2) and one trachyandesite (57DS-6). The Os-, Pb-, Hf-, Nd- and Sr-isotope data for the Pitcairn lavas are given in Table 2.1. Trace element concentrations as well as analytical methods are reported in the Background Dataset. Pb isotopic compositions were measured at high precision using a triple-spike technique [21].

Figure 2.1 shows ε_{Nd} vs. $^{87}Sr/^{86}Sr$ of Pitcairn samples together with Pacific OIB data. In comparison with other OIB lavas, the Pitcairn samples possess intermediate $^{87}Sr/^{86}Sr$ and low ε_{Nd}, characteristic of EM-1, as previously shown by Woodhead and coworkers [11,12]. The isotopic compositions of samples range from $^{87}Sr/^{86}Sr = 0.7036$ to 0.7051 and $\varepsilon_{Nd} = -5.9$ to +1.1 (Table 2.1). The ε_{Nd} of –5.9 measured in sample Pit89-8 is the lowest value reported for samples from the Pitcairn hotspot and confirms the extreme, probably long-term, enrichment of Nd over Sm in the Pitcairn mantle source.

Osmium concentrations in the lavas vary by a factor of fifty, from 2 to 112 pg/g (Table 2.1), and are typical of those found in OIB [23]. The measured Os isotopic compositions of the lavas range from $^{187}Os/^{188}Os = 0.131$ to 0.255 and correspond closely to initial ratios (see Table 2.1). All measured $^{187}Os/^{188}Os$ ratios are higher than the present-day canonical bulk silicate Earth reference value of 0.127 [23]. In $^{187}Os/^{188}Os$ versus 1/[Os] space (Fig. 2.2a), the Tedside volcanics form a broad linear array that extends to low concentrations (4 to 72 pg/g) and high $^{187}Os/^{188}Os$ ratios (from 0.131 to 0.254). A subset of the samples from the Pitcairn seamounts also forms a linear array with higher Os concentrations (15 to 112 pg/g) and a more limited range of $^{187}Os/^{188}Os$ ratios (0.135 to 0.146). One sample from the Pitcairn seamounts (47DS-11) shows a highly radiogenic value (0.174) with an Os concentration of 43 pg/g. The two linear arrays of the Tedside and the Pitcairn seamount samples in $^{187}Os/^{188}Os$ vs. 1/[Os] space have intercepts at $^{187}Os/^{188}Os = 0.128$ and 0.137, respectively. These values put limits on the minimum Os isotopic composition of the Os-rich end member.

Table 2.1. Isotopic compositions of Pitcairn lavas.

Sample	$^{87}Sr/^{86}Sr$	2σ	$^{143}Nd/^{144}Nd$	2σ	ε_{Nd}	$^{176}Hf/^{177}Hf$	2σ	ε_{Hf}	$^{206}Pb/^{204}Pb$	2σ	$^{207}Pb/^{204}Pb$	2σ	$^{208}Pb/^{204}Pb$	2σ	$^{187}Os/^{188}Os$	2σ	Os (pg/g)	2σ	Re (pg/g)	$^{187}Re/^{188}Os$	$(^{187}Os/^{188}Os)_{initial}$
Pitcairn Island, Tedside volcanics (shield-building)																					
Pit89-1	0.704876	8	0.512456	5	-3.6	0.282667	4	-3.71	17.7346	9	15.4928	10	39.016	3	0.1484	11	71.64	26	39	3	0.1484
duplicate	0.704866	13																			
Pit89-2	0.704498	8	0.512526	6	-2.2	0.282727	5	-1.59	17.8072	11	15.4988	11	38.964	3	0.1308	14	60.11	28	37	3	0.1307
duplicate			0.512533	6	-2.0																
Pit89-4	0.704689	8	0.512496	5	-2.8	0.282708	3	-2.26	17.8024	8	15.4959	9	38.976	3	0.1717	8	15.80	4	41	13	0.1716
duplicate															0.1759	25	12.60	89			
Pit89-5	0.704691	10	0.512503	5	-2.6	0.282713	3	-2.09	17.8204	7	15.4985	9	38.992	3	0.1502	12	8.74	3			
duplicate	0.704695	8							17.8180	7	15.4954	8	38.982	3							
Pit89-6	0.704702	7	0.512497	5	-2.8	0.282714	3	-2.05	17.8210	11	15.4983	11	38.997	3							
duplicate									17.8234	7	15.5003	9	39.002	3							
Pit89-8	0.705105	8	0.512333	4	-5.9	0.282622	4	-5.30	17.6431	15	15.4861	20	39.018	7	0.2546	27	3.91	29	47	54	0.2539
duplicate			0.512341	4	-5.8				17.6443	10	15.4877	12	39.023	4							
Pit89-10	0.704646	9	0.512437	4	-3.9	0.282692	3	-2.83	17.7720	12	15.4934	14	39.002	4	0.1650	12	7.92	3	54	33	0.1646
duplicate			0.512423	6	-4.2																
Pit89-19	0.704677	7	0.512495	6	-2.8	0.282718	4	-1.91	17.8147	10	15.4971	11	39.026	4	0.1494	1	23.37	1			
duplicate									17.8153	12	15.4980	14	39.028	5	0.1495	8	21.04	5			
duplicate2															0.1425	2			80		
Pitcairn Island, Pulawana volcanics (post-erosional)																					
Pit89-20	0.703603	9	0.512674	4	0.7	0.282810	3	1.34	18.0199	13	15.4930	14	39.034	5	0.1688	10			147		
Pit89-21	0.703625	8	0.512673	8	0.7	0.282813	3	1.45							0.2149	113	1.90	9	209	512	0.2115
Pitcairn seamounts, volcano 2																					
46DS-2	*0.704228*		*0.512692*		*1.1*	0.282834	4	2.19	*18.037*		*15.502*		*38.939*		0.1398	6					
duplicate															0.1447	26	15.04	10			
46DS-10									18.0984	7	15.5198	7	38.983	2							
47DS-2									17.7171	9	15.4895	12	38.822	4	0.13502	1	106.06	1			
47DS-4									17.7214	8	15.4887	8	38.791	2	0.13853	2	59.99	1			
47DS-8	*0.704699*		*0.512525*		*-2.2*	0.282721	5	-1.80	17.7215	6	15.4879	8	38.796	2	0.1375	2	111.58	7			
47DS-11									17.7204	6	15.4873	7	38.790	2	0.17418	2	43.17	1			
duplicate									17.7216	6	15.4890	8	38.796	2							
48DS-6	*0.704251*		*0.512629*		*-0.2*	0.282799	3	0.95	*17.853*		*15.484*		*38.611*								
49DS-1	*0.705010*		*0.512501*		*-2.7*	0.282695	5	-2.72	17.6361	7	15.4814	8	38.850	3	0.1381	4	94.73	10			
51DS-1	*0.704431*		*0.512661*		*0.4*	0.282805	5	1.17	*17.948*		*15.499*		*38.809*		0.1459	15	31.03	7			
duplicate															0.1475	1					
51DS-2	*0.704431*		*0.512657*		*0.4*				17.9569	6	15.5079	7	38.834	2	0.14506	2	32.25	1			
52DS-2	*0.705200*		*0.512476*		*-3.2*	0.282674	3	-3.47	17.4665	6	15.4728	7	39.023	2							
duplicate									17.4687	6	15.4756	8	39.033	2							
55SLS-6	*0.704212*		*0.512676*		*0.7*	0.282833	3	2.16	*18.041*		*15.504*		*38.940*		0.1439	21	26.91	16			
Pitcairn seamounts, volcano 5																					
57DS-6	*0.705296*		*0.512478*		*-3.2*	0.282689	3	-2.94	*17.507*		*15.467*		*38.876*								

Sr, Nd and Pb duplicates are from the same dissolution, while Os duplicates are from duplicate dissolutions. Numbers in italics are from Woodhead and Devey [12]. Os concentrations for over- or underspiked analyses are not reported, only their isotopic composition. The ε_{Hf} values were calculated with $(^{176}Hf/^{177}Hf)_{CHUR(0)} = 0.282772$. The ε_{Nd} values were calculated with $(^{143}Nd/^{144}Nd)_{CHUR(0)} = 0.512638$.

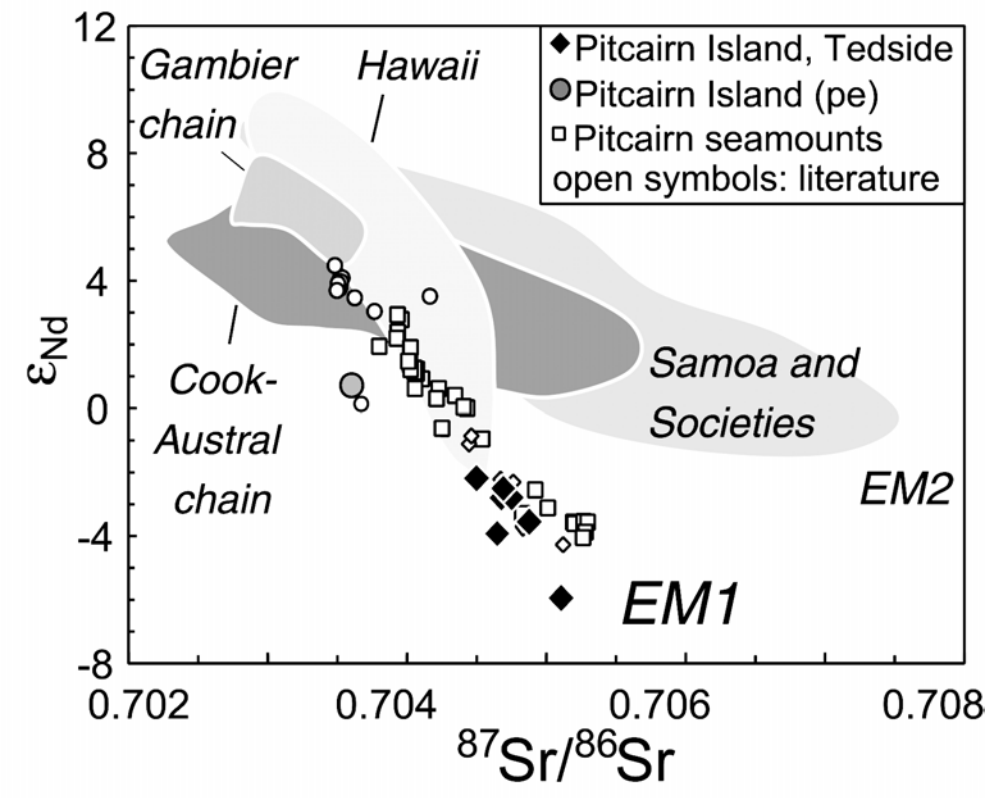

Fig. 2.1. εNd versus $^{87}Sr/^{86}Sr$ for samples from the Pitcairn hotspot (symbols) compared to shaded data fields for other oceanic island basalts from the Pacific Ocean. Filled symbols are from this study, open symbols are from Woodhead and coworkers [11,12]; the latter were renormalized to conform to our standard values. The post-erosional lavas are abbreviated with "pe". Pacific OIB data are from the compilation of Hofmann [22].

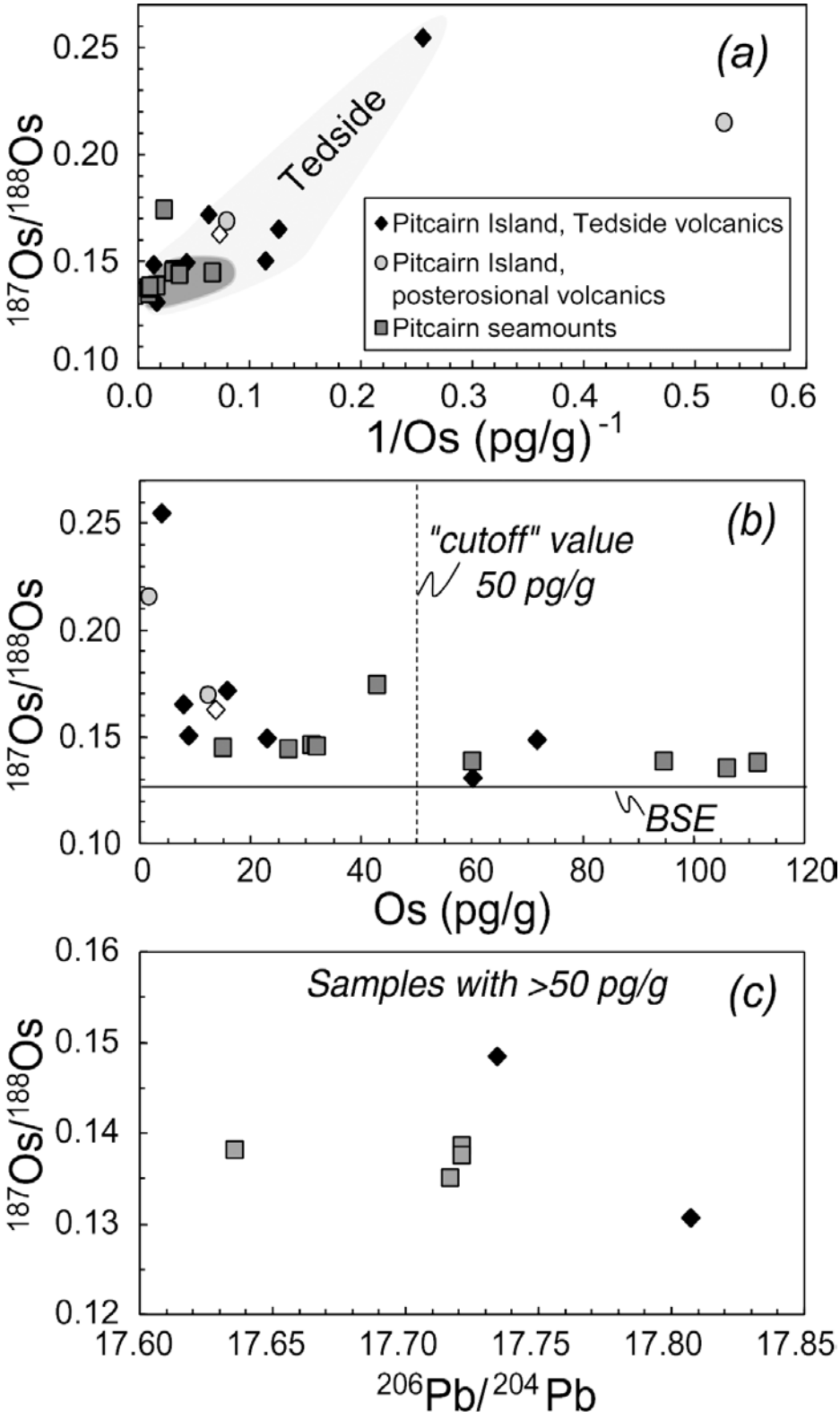

Fig. 2.2. (a) In $^{187}Os/^{188}Os$ versus 1/[Os] space, the Pitcairn samples display broad linear arrays. (b) Increasing $^{187}Os/^{188}Os$ ratios with decreasing Os concentration. Open symbol is a single sample from Reisberg et al. [6]. Pitcairn samples with Os >50 pg/g have $^{187}Os/^{188}Os$ ratios ranging from 0.131 to 0.148. BSE stands for Bulk Silicate Earth. (c) In $^{187}Os/^{188}Os$ versus $^{206}Pb/^{204}Pb$ space, Pitcairn volcanics with Os >50 pg/g show no correlation with Pb isotopes.

Samples with Os concentrations lower than 50 pg/g display variable and relatively radiogenic Os isotopic compositions ($^{187}Os/^{188}Os$ from 0.144 to 0.255), while samples with Os concentrations >50 pg/g show much less variation and less radiogenic ratios ($^{187}Os/^{188}Os$ from 0.131 to 0.148) (Fig. 2.2b). There is no straightforward relationship between $^{187}Os/^{188}Os$ and $^{206}Pb/^{204}Pb$ ratios for the Pitcairn samples. Similarly, even considering only those samples with Os concentrations >50 pg/g, there is no simple correlation between $^{187}Os/^{188}Os$ ratios and Pb isotopic compositions (Fig. 2.2c), nor with Sr, Nd and Hf isotopic compositions (not shown).

Hafnium isotopic compositions of the Pitcairn lavas range from $\varepsilon_{Hf} = -5.3$ to +2.2 and are strongly correlated with ε_{Nd} (Fig. 2.3). The Tedside volcanics from Pitcairn Island form a linear array, which can be described by the regression line $\varepsilon_{Hf} = 0.99\ (\pm 0.24)\ \varepsilon_{Nd} + 0.5\ (\pm 0.4)$ with a reduced chi-squared ($\chi^2_{red.}$) of 2.1. The Pitcairn seamount samples yield a linear array described by $\varepsilon_{Hf} = 1.31\ (\pm 0.11)\ \varepsilon_{Nd} + 1.5\ (\pm 0.3)$ with $\chi^2_{red.} = 0.98$. Both Pitcairn arrays lie close to the OIB array with $\varepsilon_{Hf} = 1.49\ (\pm 0.04)\ \varepsilon_{Nd} + 2.1\ (\pm 0.2)$ [9]. However, the Pitcairn Island array yields a somewhat shallower slope compared to other OIB (i.e. 1.0 versus 1.5). A shallower slope has also been noted for the Hawaiian isotope array in Hf-Nd isotope space [9], which lies parallel to the Pitcairn correlation but with the intercept offset to higher ε_{Hf} (Fig. 2.3).

In a multi-element plot (Fig. 2.4) the Pitcairn lavas show no apparent excesses in Ba or Pb and no strong Eu or Sr anomalies. The lavas have Ba/Nb ratios ranging from 3.5 to 8.9, and are in all cases lower than the primitive mantle value of 9.8 [26]. Sr/Nd ratios are quite variable (6.4 - 18.3) and only in some cases higher than the primitive mantle value of 15.1. Figure 2.4 also compares the Pitcairn trace element patterns to those of globally-averaged subducting sediment (GLOSS) [25]. In contrast to the Pitcairn lavas, GLOSS displays a negative Nb anomaly, a positive Pb anomaly and a relatively flat rare earth element pattern

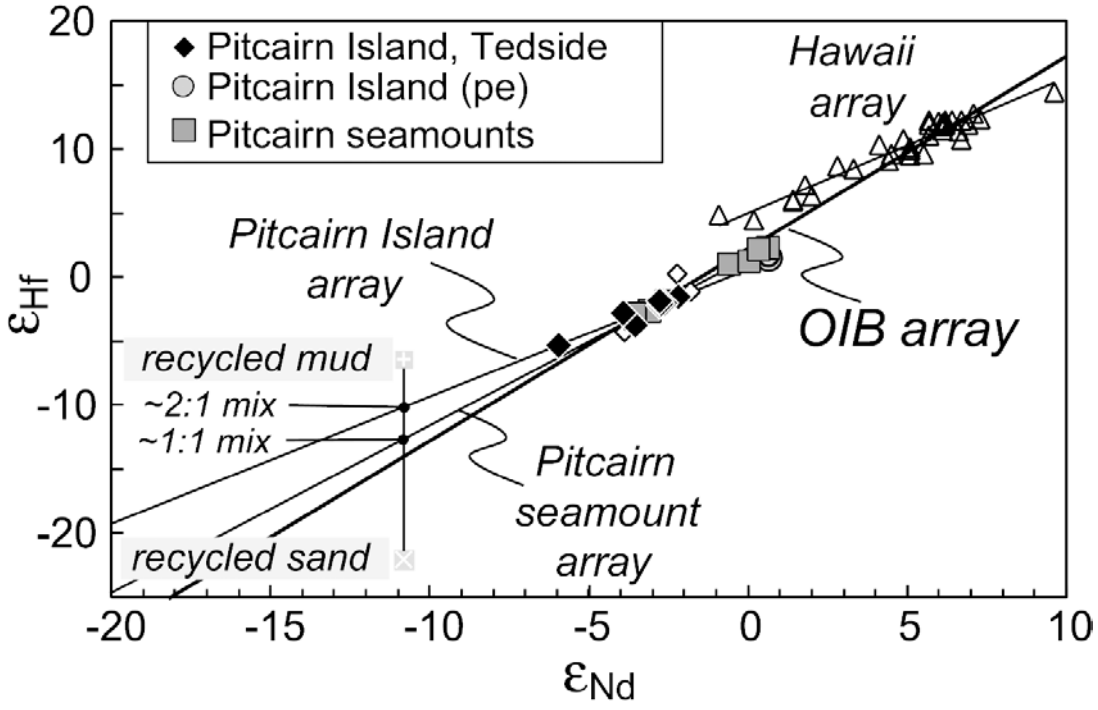

Fig. 2.3. ε_{Hf} versus ε_{Nd} of Pitcairn samples compared to Hawaii and the OIB array [9]. Pitcairn Island samples with open symbols are from Salters and White [24]. The Pitcairn samples extend to low values of ε_{Hf} and ε_{Nd}, and the slopes of the Pitcairn Island and seamount arrays can be explained by addition of ~2:1 and ~1:1 mixtures of recycled mud and sand to the OIB source.

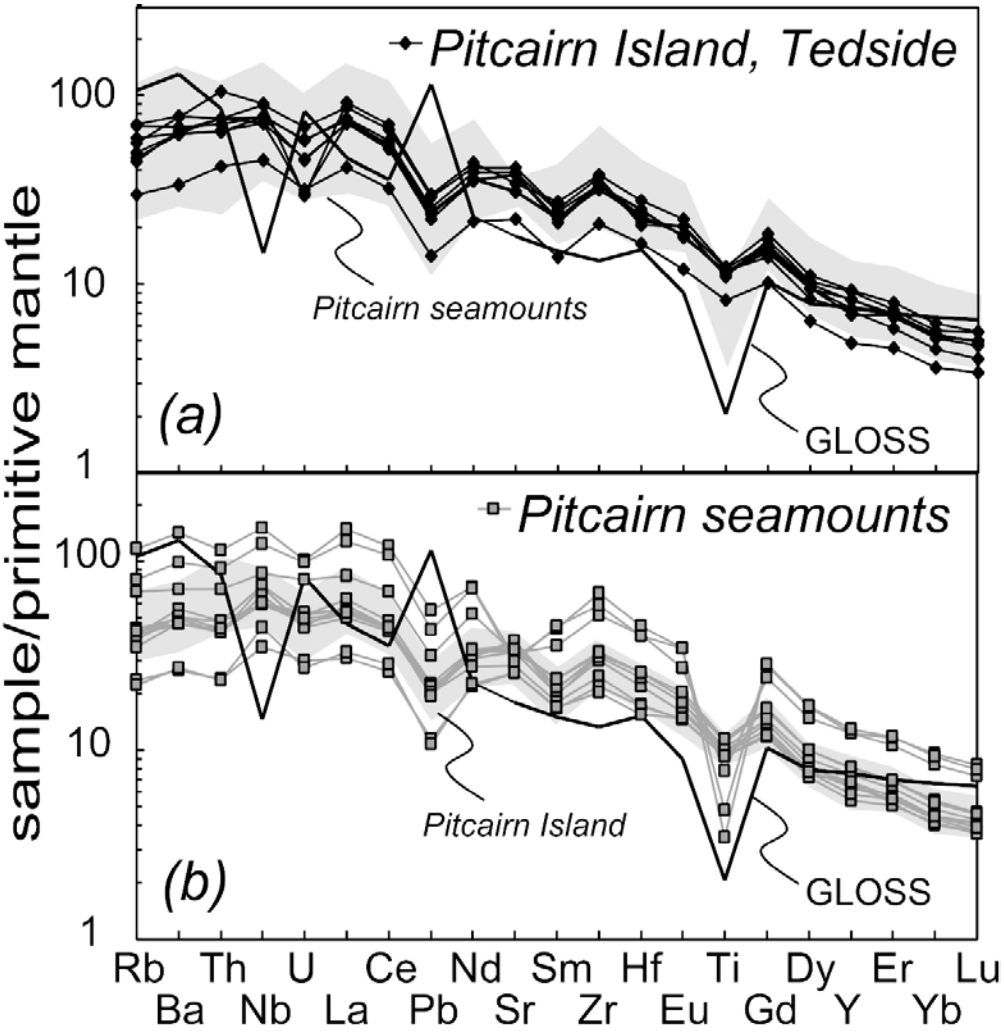

Fig. 2.4. Normalized multi-element patterns for the Pitcairn volcanics and the global subducting sediment (GLOSS) composition [25]. GLOSS has a similar composition as Pitcairn for most trace elements, but shows a strong negative Nb anomaly and a positive Pb anomaly. Trace elements are arranged in the order of decreasing incompatibility, normalized to primitive mantle [26].

Two Pitcairn Island samples (Pit89-1 and Pit89-8) have far higher Nb/U ratios (72 and 93) than the reference value for oceanic volcanics of 47±10 [27]. This indicates that some Pitcairn basalts, or their sources, lost U at some point in time, as was previously argued by Woodhead and coworkers [11, 12]. In addition to the high Nb/U ratios, the Pitcairn Island samples possess extraordinarily high Th/U ratios (from 4.4 to 14.1) relative to other OIB, and contrast with those measured on Pitcairn seamount samples, which range from 3.2 to 4.5 [12]. To assess whether the Th/U ratios and particularly the U concentrations of the samples were affected by recent surface alteration, we analyzed Th and U concentrations in weathered and fresh splits of rock chips from Pitcairn Island, as well as hand-picked, fresh glasses from the Pitcairn seamounts (see Background Dataset). Fresh and weathered rock chips reproduce the Th/U ratio to better than 7%, while the fresh glasses reproduce the Th/U ratios reported by Woodhead and Devey [12] within 2% and 15%, respectively. This demonstrates that the Th/U ratio is not influenced by subaerial weathering on Pitcairn Island, nor by seawater interaction for the Pitcairn seamount samples. Our data show, instead, a significant difference in primary Th/U ratios of lavas from Pitcairn Island (4.4 to 14.1) and the Pitcairn seamounts (3.2 to 4.5), consistent with the observations of Woodhead and Devey [12].

Pb isotopic compositions are reported in Table 2.1. In a plot of $^{207}Pb/^{204}Pb$ versus $^{206}Pb/^{204}Pb$ (Fig. 2.5a), the data from the Tedside volcanics form a well-defined linear array (slope = 0.064 ± 0.014, 2σ error, $\chi^2_{red.}$ = 1.2), and the Pitcairn seamount data also define an array with the same slope within analytical error (slope = 0.077 ± 0.010, 2σ error, $\chi^2_{red.}$ = 4.8). Two other features of the Pb isotope dataset are particularly striking (Fig. 2.5b): First, compared to other OIB lavas, $^{208}Pb/^{204}Pb$ ratios of the samples are extremely high (~39.0) given their low $^{206}Pb/^{204}Pb$ ratios (from 17.5 to 18.1), as was shown previously by Woodhead and coworkers [11,12]. Second, in a $^{208}Pb/^{204}Pb$-$^{206}Pb/^{204}Pb$ plot (Fig. 5b), the samples display a nearly horizontal extension. Thus, the data show variation in $^{206}Pb/^{204}Pb$ and $^{207}Pb/^{204}Pb$

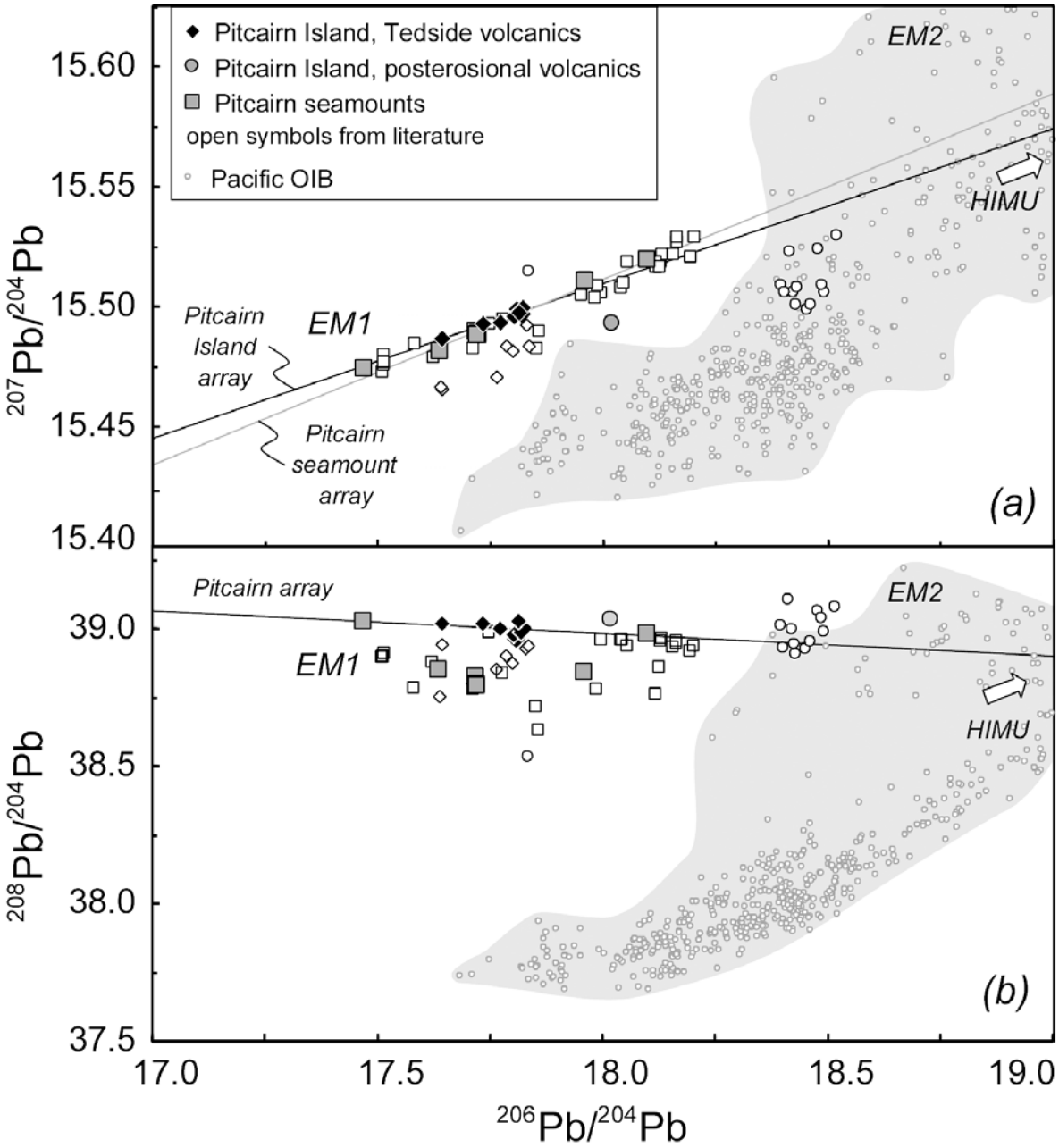

Fig. 2.5. Pb isotopic compositions for the Pitcairn hotspot show a tight linear array in $^{207}Pb/^{204}Pb$ versus $^{206}Pb/^{204}Pb$ space. The $^{208}Pb/^{204}Pb$ versus $^{206}Pb/^{204}Pb$ array has a roughly horizontal slope with considerably greater scatter, especially for the seamount samples. Open symbols are Pitcairn samples from Woodhead and coworkers [11,12], renormalized to conform to our standard values. Reference data for Pacific OIB data are from the compilation of Hofmann [22].

while $^{208}Pb/^{204}Pb$ remains relatively constant. This latter observation suggests that the Th/Pb ratio of the source is relatively homogeneous, and that the main control on the Pb isotopic evolution has been variation in the source U/Pb ratios, which are relatively low (see also [11, 12]).

2.3 Discussion

2.3.1 Os isotopic composition of EM-1

To date, there has only been a single published Os isotope analysis of EM-1 OIB by Reisberg et al. [6] - a Pitcairn sample with $^{187}Os/^{188}Os$ of 0.15. This composition has been widely used as an EM-1 mixing end member in models of OIB petrogenesis [23,28,29]. Our analyses show, first, that the composition of EM-1 material extends to $^{187}Os/^{188}Os$ ratios as low as 0.131, and second, that there is a considerable spread in measured Os isotopic compositions, ranging from 0.131 to 0.254 (Table 2.1).

The increase of $^{187}Os/^{188}Os$ ratios with decreasing Os concentration (Fig. 2.2) is a well-known phenomenon [23]. It may be caused by assimilation of a radiogenic component by a melt in the crust or lithosphere [6] or, alternatively, by mixing between radiogenic and unradiogenic mantle components having different Os concentrations. With the data set presented here it is not possible to argue conclusively for either one of the two hypotheses for the behavior of Os isotopes, but we favor an assimilation process in this case. A "cut-off" of greater than ~50 pg/g Os [6,29,30], albeit arbitrary, seems to separate samples with variable, radiogenic $^{187}Os/^{188}Os$ ratios, possibly influenced by shallow-level assimilation, from those more likely to reflect a primary, magmatic signature. Applying this "filter" to the data yields $^{187}Os/^{188}Os$ ratios of 0.131 and 0.148 for the two Pitcairn Island samples, and a range of 0.135 to 0.139 for the Pitcairn seamount samples (N = 4). Thus, these data do not support a $^{187}Os/^{188}Os$ ratio for EM-1 as high as ~0.15 [6,23,28,29].

2.3.2 An Os-Pb isotope mixing model

The overall range in $^{187}Os/^{188}Os$ ratios for the Pitcairn lavas is similar to that found in high Os concentration lavas from other ocean islands (Fig. 2.6). For example, shield-building lavas from Hawaii have $^{187}Os/^{188}Os$ ratios from 0.130 to 0.148 [8,29,32], while values for Azores lavas range from 0.128 to 0.137 [30]. This similarity in Os isotopic composition is striking given that the Sr, Nd and, in particular, Pb isotope systematics of Pitcairn, Hawaii and the Azores are quite different. This also means that the notion of defining an EM-1 end member in terms of Os isotopic composition should be abandoned. Previous authors [23,29] have invoked two-component mixing models in Os-Pb isotope space between an "enriched plume-type" mantle and recycled oceanic crust containing a pelagic sediment component. These models assume that the $^{187}Os/^{188}Os$ ratio of EM-1 is ~0.15, and predict a correlation between $^{187}Os/^{188}Os$ and $^{206}Pb/^{204}Pb$ ratios. The data from Pitcairn (Figs 2.2c and 2.6), however, show no hint of a simple hyperbolic mixing relationship. If the OIB source comprises “plume-type" mantle and a small component of recycled oceanic crust and/or pelagic sediment, mass balance dictates that the Os isotopic composition will largely be dominated by the peridotite mantle, while the incompatible elements Sr, Nd and Pb will primarily reside in the recycled material.

In order to assess quantitatively the relationships in Os-Pb isotope space, we performed five-component mixing calculations (see Background Dataset for details). These components are: recycled pelagic and terrigenous sediments, recycled oceanic crust, recycled subcontinental lithospheric mantle and peridotite mantle. Mixtures between these five components were sought that fitted the Os and Pb isotope compositions of the Pitcairn lavas ($^{187}Os/^{188}Os$ = 0.131 to 0.148, $^{206}Pb/^{204}Pb$ = 17.5 to 17.9). The results of the calculations are shown in Fig. 2.7; they indicate that (1) a small fraction of pelagic sediment is necessary to explain the composition of the Pitcairn source (Fig. 2.7a). This result is mainly required by the low $^{206}Pb/^{204}Pb$ ratio (17.1) assumed for ancient pelagic sediment. (2) The presence of

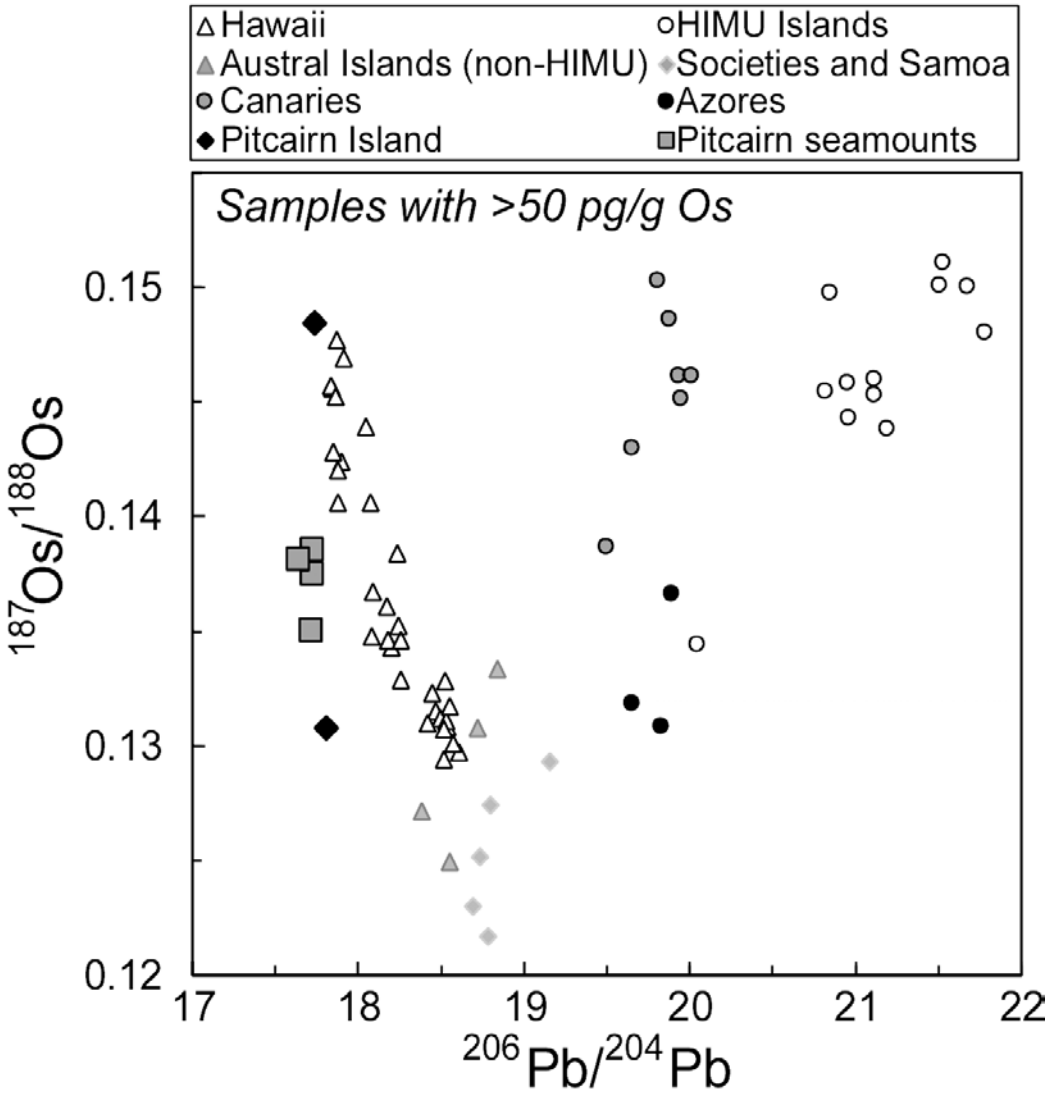

Fig. 2.6. $^{187}Os/^{188}Os$ versus $^{206}Pb/^{204}Pb$ ratios for OIB samples with Os >50 pg/g. The Pitcairn lavas show a similar range in $^{187}Os/^{188}Os$ ratios compared to other OIB and do not lie along a mixing array. Data sources: [5,6,8,29-32]. The Os concentrations of the samples reported by Schiano et al. [28] are all <50 pg/g and have not been plotted.

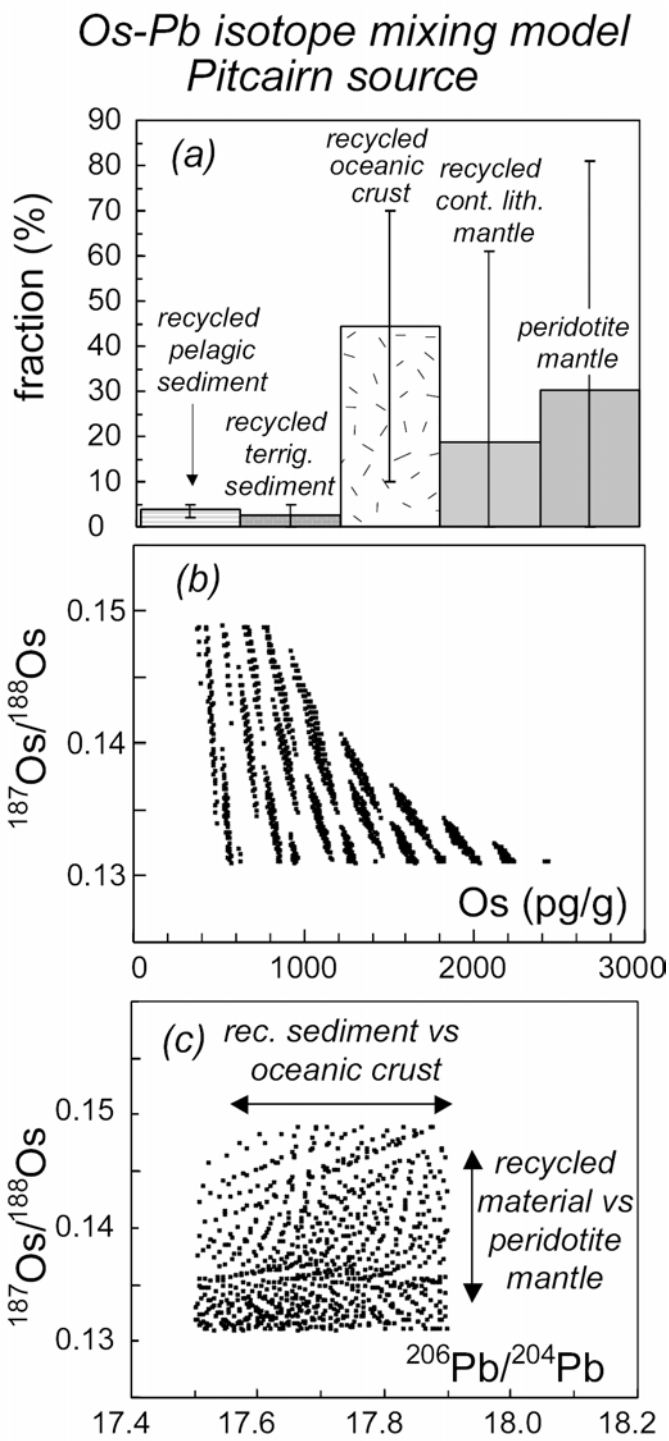

Fig. 2.7. Results of a Os-Pb isotope mixing model involving five components. (a) Mean fraction of materials in the Pitcairn source estimated by the model. The error bars represent the total ranges found in ~800 valid solutions. All solutions require some fraction of recycled pelagic sediment and recycled oceanic crust, while for all other components large ranges are possible (for details, see Background Dataset). (b) For $^{187}Os/^{188}Os$ ratios between 0.13 and 0.15, the Os concentrations in the model mixtures are higher than ~300 pg/g in the OIB source. (c) In $^{187}Os/^{188}Os$ vs. $^{206}Pb/^{204}Pb$ space, multi-component mixing calculations show that the $^{206}Pb/^{204}Pb$ ratio mainly varies with changing proportions of recycled sediment, whereas the $^{187}Os/^{188}Os$ ratio changes with the proportion of peridotite mantle versus other recycled material. Therefore, no correlations are expected in this plot.

subcontinental lithospheric mantle in the Pitcairn source is theoretically possible, but the Os isotopic composition of the Pitcairn source can also be explained by mixing between other components. (3) The expected Os concentrations in the mixtures present in the Pitcairn source range between ~300 and 2500 pg/g (Fig. 2.7b). (4) In $^{187}Os/^{188}Os$ versus $^{206}Pb/^{204}Pb$ space, mixing between more than two components in varying proportions does not yield hyperbolic arrays (Fig. 2.7c). The variation in $^{206}Pb/^{204}Pb$ ratio is mainly influenced by proportions of recycled oceanic crust versus recycled sediment, while the variation in $^{187}Os/^{188}Os$ is mainly influenced by the proportions of a peridotite mantle versus the overall amount of recycled material. Increase in $^{187}Os/^{188}Os$ ratios is mainly a result of larger fractions of recycled oceanic crust in the source.

2.3.3 Subcontinental lithospheric mantle in the source?

It has been suggested that the recycled material present in the source of EM-1-type OIB, such as Pitcairn, is delaminated subcontinental lithospheric mantle (SCLM) [2,5,15]. It has proven difficult to evaluate this hypothesis because of the extreme range in Sr, Nd and Pb isotope and trace element compositions found in continental ultramafic xenoliths and peridotite massifs. The available Os isotope data from these materials show a strong depletion of Re over Os. This Re depletion over time, leads to a signature of low, subchondritic $^{187}Os/^{188}Os$ ratios in SCLM [33], which is distinct from that of upper crustal rocks and sediments. Therefore, SCLM in the Pitcairn hotspot would be implied by $^{187}Os/^{188}Os$ ratios in the lavas lower than the present-day chondritic value of 0.127 [23]. The samples analyzed here all have $^{187}Os/^{188}Os$ ratios higher than the chondrite reference value. Similarly, the intercepts of the Pitcairn arrays in $^{187}Os/^{188}Os$ versus 1/[Os] space (Fig. 2.2a) indicate that the Os-rich end member has $^{187}Os/^{188}Os$ ratios higher than 0.127. Altogether, this builds a reasonably strong case against ancient SCLM being present in the Pitcairn source, and presumably EM-1 in general. With regard to other ocean islands, Schiano et al. [28] have

recently used Os isotope data on lavas from the Austral-Cook chain to argue for a SCLM component in the source of these hotspots. So, the discussion about SCLM recycling [2] does not appear to be resolved. However, on the basis of the data presented here, SCLM does not appear to be involved in the formation of the EM-1 signature.

2.3.4 A continentally-derived component in the Pitcairn source

The presence of sedimentary material in the Pitcairn source, in the form of ancient subducted pelagic sediment, was suggested Woodhead and coworkers [11,12]. Since sediments possess strong negative Nb anomalies while most oceanic basalts have positive Nb anomalies, the occurrence of a negative Nb anomaly in the trace element pattern of the lavas should be quite diagnostic of continentally-derived material in the source. However, calculating the Nb anomaly itself is not a straightforward exercise in this case.

Fig. 2.8a shows that the Nb/U ratios of EM-type basalts from the Southern Pacific are not constant [27], but rather depend on the U concentration to a significant degree. Overall, these observations suggest that the Nb/U ratios of these lavas are not good indicators of the presence of a Nb anomaly. Therefore, we calculated the Nb anomaly using Th and La as reference elements [13], which have similar incompatibilities to Nb. The Nb anomaly Nb/Nb* defined in this way is $Nb_N/\sqrt{(Th_N \times La_N)}$. The main advantage in using Th and La as reference elements is that in comparison with U or K, these elements are expected to be less mobile during subduction zone processing. The Pitcairn Island samples show a negative correlation between Nb/Nb* and $^{87}Sr/^{86}Sr$ (Fig. 2.8b), which coincides with the broader trend formed by Polynesian EM-2 OIB. This trend is consistent with variable addition of ancient continental material to a mantle source. The Nb/Nb* in the Pitcairn Island lavas range from 0.9 to 1.2 and are higher than that of average continental crust (~0.5, [37]), but significantly lower than the value of ~1.5 typical for the depleted mantle [26] and non-EM OIB. Thus, the intermediate Nb/Nb* found in Pitcairn Island lavas are best explained in terms of mixing between a

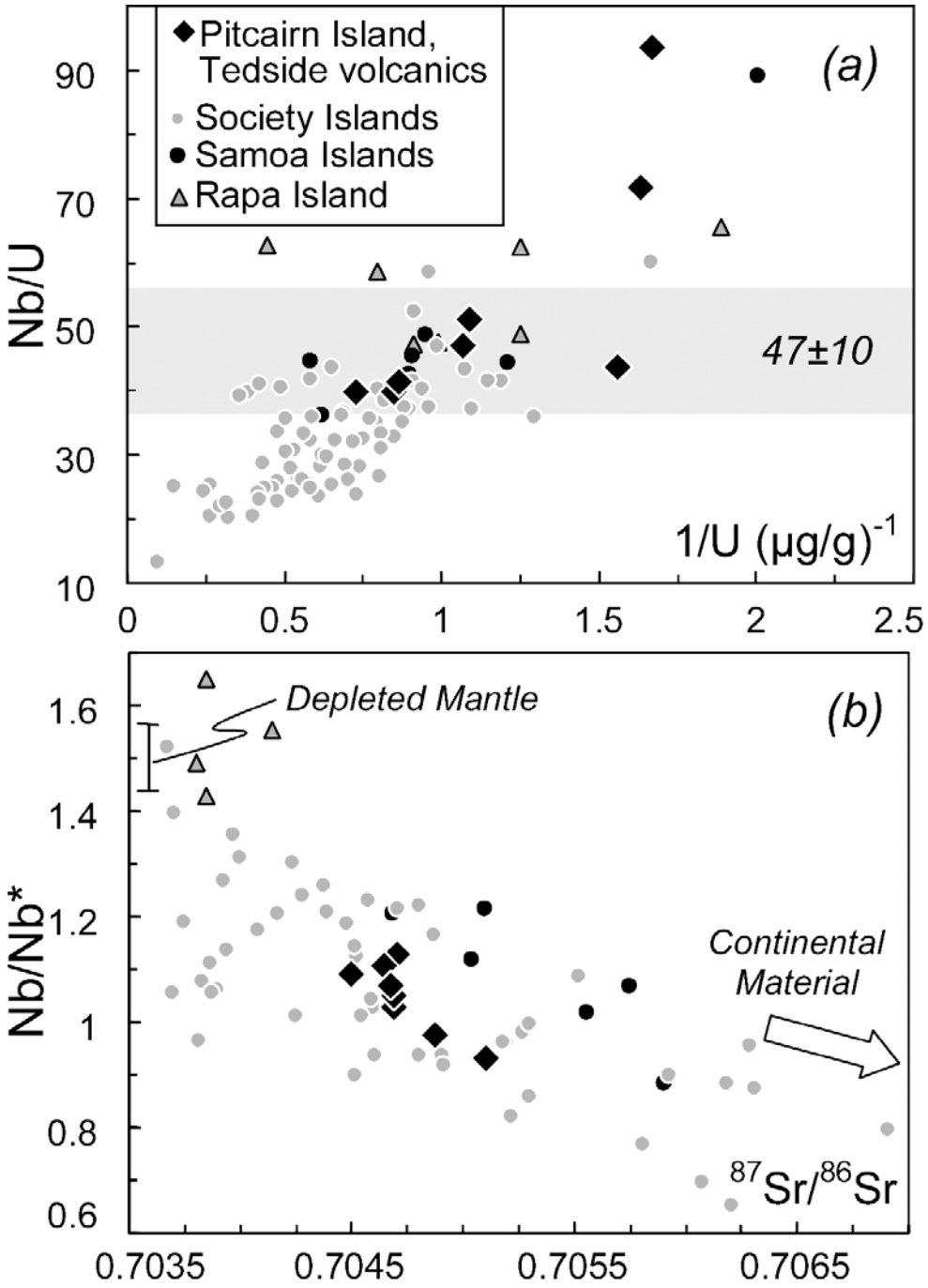

Fig. 2.8. (a) The Nb/U ratio of EM-type lavas from the Southern Pacific increases with decreasing U concentration, indicating that U has been fractionated from Nb at some stage in the evolution of these rocks. (b) The Nb anomaly, $Nb/Nb^* = Nb_N/\sqrt{(Th_N \times La_N)}$, correlates with $^{87}Sr/^{86}Sr$ and extends towards compositions typical for continental material. Data sources: [7,27,34-36].

depleted end member and continentally-derived components found in the source. Samples from other EM-type ocean Islands (Samoa, Societies and Rapa) show a correlation between Nb/Nb* and $^{87}Sr/^{86}Sr$, similar to that seen for Pitcairn Island. The data from the Pitcairn seamounts of Woodhead and Devey [12] and from this study, determined by ICP-MS, agree in general with the array found for Pitcairn Island (XRF measurements) but show a larger scatter. By comparison of the two analytical methods, Hémond et al. [35] showed that there may be analytical scatter introduced by the ICP-MS technique for Nb. For this reason, and for clarity, we have excluded the Pitcairn seamount data from Figure 2.8.

In order to be more specific about what sort of continental material might be present in the Pitcairn source, it is necessary to consider the isotope and trace element systematics further. The Pitcairn samples possess low ε_{Nd} values (-5.9 to +1.1), very unradiogenic $^{206}Pb/^{204}Pb$ ratios (17.5 to 18.1), together with high $^{208}Pb/^{204}Pb$ ratios (~39.0). These systematics imply a source with low time-integrated Sm/Nd and U/Pb, coupled with high Th/U ratios. Such elemental fractionations are quite characteristic of pelagic sediments. The mean of six pelagic sediment compositions reported by Plank and Langmuir [25] has Sm/Nd = 0.23, similar to typical crustal values [37], while U/Pb is low at 0.041 ($^{238}U/^{204}Pb$ ~3), and Th/U extremely high (8.9). The only other continental materials possessing elemental characteristics similar to those mentioned above are some felsic mid- and lower crustal granulites [38].

In principle, pelagic muds can be identified and distinguished from other crustal sources using Hf and Nd isotope systematics (Fig. 2.3). Hf and Nd isotopic compositions are highly correlated in crustal materials as a whole, with regression line slopes in $\varepsilon_{Hf} - \varepsilon_{Nd}$ space ranging between 1.3 and 1.9 [39]. Pelagic sediments, however, are an exception to this since they lack a zircon-hosted Hf component, and generally have higher Lu/Hf ratios as a consequence [39,40]. The slope of the Pitcairn Island array in ε_{Hf} versus ε_{Nd} is 1.0±0.2 (Fig. 2.3), a value significantly lower than the range of slopes found for other crustal materials (1.3

to 1.9). A shallow slope could indicate that the end member at the lower extension of the array had a higher time-integrated Lu/Hf for a given Sm/Nd compared to other crustal materials. Thus, the shallow slope can be interpreted as implying pelagic sediment recycling [9].

In order to characterize the sediment component in the Pitcairn source, we estimated the compositions of 1.5 Ga old mud and sand components in ε_{Hf} versus ε_{Nd} space (Fig. 3). We assume that the present-day ε_{Nd} of the sediment would be around -11 ($^{147}Sm/^{144}Nd \sim 0.11$ since 1.5 Ga, $(^{143}Nd/^{144}Nd)_{initial} = 0.511$). Using a $^{176}Lu/^{177}Hf$ ratio of 0.02 for the mud and a $^{176}Lu/^{177}Hf$ ratio of 0.005 for the sand ($(^{176}Hf/^{177}Hf)_{initial} = 0.282$), the present-day ε_{Hf} values would be -6 (mud) and -22 (sand). For these sediment compositions, a mixture of about two-to-one of recycled mud to sand could explain the lower end member of the Pitcairn Island array. The slope of the Pitcairn seamount array is almost identical to that of the general OIB array (Fig. 2.3). As was pointed out by Patchett et al. [40], the slope of this array can be produced by recycled mud and sand in the proportions of about one-to-one (Fig. 2.3).

2.3.5 A trace element mixing model

We performed six-component mixing calculations for the incompatible trace elements Sr, Ba, Nb, La, Ce, Nd, Pb, Th and U in order to assess the proportions of recycled pelagic and terrigenous sediments, recycled oceanic crust, recycled gabbroic material, depleted MORB mantle (DMM) and primitive mantle (PRIMA) present in the Pitcairn source (see Background Dataset). In the model, we used an estimate of a residue of the recycled materials after subduction. The calculated mixtures were accepted as reasonable for the Pitcairn source if they matched the averages of the Ba/Nb, Ba/La, Sr/Nd, Ce/Pb, Th/Nb and Th/U ratios measured in the Pitcairn lavas to within ±20%. Different models were calculated for the Tedside volcanics from Pitcairn Island and the Pitcairn seamount lavas, and the results are summarized in Fig. 2.9 and Table 2.2. The trace element mixing calculations indicate that the Pitcairn hotspot carries a significant, though volumetrically minor, amount of recycled

Table 2.2. Estimated fractions of recycled materials in the Pitcairn and EM1 sources

		sediments			depleted components			
		pelagic sediment (residue)*	**terrigenous sediment (residue)**	**total sediment (residue)**	**N-MORB (residue)**	**gabbro (residue)**	**DMM**	**PRIMA**
Location	Ref.	mean (total range in brackets)						
Pitcairn Island, Tedside volcanics	trace element model,	2%	2%	4%	57%	18%	2%	19%
	this study	(0.5 - 3 %)	(0 - 5 %)	(2.5 - 6.5 %)	(45 - 65 %)	(9 - 24 %)	(0 - 16 %)	(14 - 24 %)
Pitcairn seamounts	trace element model,	1%	2%	3%	48%	17%	9%	24%
	this study	(0 - 2 %)	(0 - 4.5 %)	(1.5 - 4.5 %)	(35 - 60 %)	(10 - 23 %)	(4 - 20 %)	(18 - 30 %)
Pitcairn seamounts	Woodhead et al. [41]			max. 9%				
Pitcairn Island, Tedside volcanics	Eiler et al. [42]			< 1.5 %				
EM1 source	Weaver [13]	< 5%						
EM sources	Chauvel et al. [4]			< 1%				
Sardinian basalts and EM1 in general	Gasperini et al. [10]	"free of sedimentary material"			dominated by rec. gabbro			
OIB array	Patchett et al. [40]	turbidite sand / pel. sed. ~ 1:1		max. 2.2 %				

*this study uses an estimate for subduction residues, whereas other studies use pure compositions for the recycled materials.
Therefore the estimates for recycled material of this study are slightly higher than those of most previous work (except for Woodhead et al. [41]).
See Background Dataset for end member compositions used and details of mixing calculations

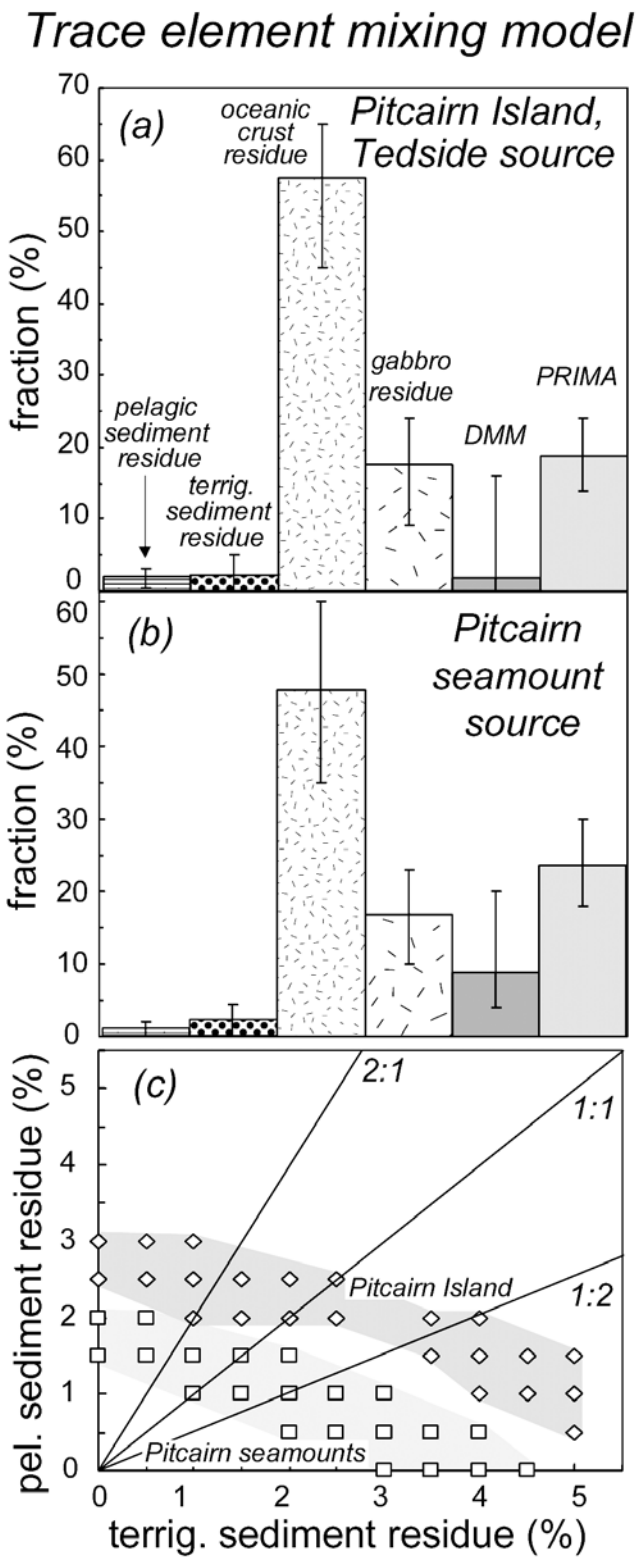

Fig. 2.9. Results of a multi-component trace element mixing model (see Background Dataset). For the model, mixing was assumed to take place between residues of materials after subduction with depleted MORB mantle (DMM) and primitive mantle (PRIMA). (a) Fraction of mantle materials in the source of the Tedside volcanics inferred from the model. The error bars are the total range of a particular material in ~60 successful model solutions. (b) Fraction of mantle materials in the Pitcairn seamount source. (c) Fractions of pelagic versus terrigenous sediment residue. The Pitcairn Island source generally requires a larger fraction of sediments. The lines indicate possible proportions of recycled mud versus sand.

sediment in the source. The amount and compositions of the recycled sediment appears to be slightly different between Pitcairn Island and the seamounts. Volumetrically, the largest part of the Pitcairn source is composed of depleted material, which may consist of a mixture of recycled MORB with gabbro, depleted mantle and PRIMA (Fig. 2.9 and Table 2.2). The inferences derived from the trace element modeling are consistent with the Hf-Nd isotope systematics, which suggest that the differences in isotope and trace element systematics between Pitcairn Island and seamounts are caused by a lower overall proportion of recycled sediment and a lower ratio of pelagic versus terrigenous sediment in the seamount source (Fig. 2.3, 2.9c).

It has been suggested that gabbroic sections of recycled oceanic plateaus play a role in the source of EM-1-like Sardinian basalts [10]. Recycled gabbroic crust in the Pitcairn source should be evident from its characteristic trace element signature, and especially the presence of strong positive Sr and Eu anomalies or Ba and Pb excesses. Such anomalies are not observed in the Pitcairn lavas. The trace element modeling for the Pitcairn source suggests that gabbro can only comprise about 10-20 % of the source (Fig. 2.9; Table 2.2).

2.3.6 Pb isotope systematics

Because the trace element systematics of the Pitcairn hotspot strongly implicate mixing between a recycled sediment and more depleted material, the linear array in $^{207}Pb/^{204}Pb$ versus $^{206}Pb/^{204}Pb$ space most probably reflects mixing rather than a "mantle isochron". The Pb isotopic composition in such a mixture will be dominated by the volumetrically minor sediments which have the highest Pb concentrations [4]. Although the Os-Pb isotope and trace element systematics of the Pitcairn hotspot suggest mixing between more than two components, the Pb isotope systematics in $^{207}Pb/^{204}Pb$-$^{206}Pb/^{204}Pb$ space strongly conform to a binary mixing line (Fig. 2.5a). This could be the case, because the contribution of Pb from depleted sources (e.g. DMM and gabbros) would be so low that it

would not significantly influence the mixture between recycled sediment and oceanic crust; alternatively the proportions of some components (e.g. recycled oceanic crust/PRIMA) may remain relatively constant in the mixture. In $^{208}Pb/^{204}Pb$-$^{206}Pb/^{204}Pb$ space, there is more scatter among the Pitcairn samples, lending support to the presence of more than two compositional end members in the Pitcairn source (Fig. 2.5b).

The Pitcairn samples are unique among OIB in that the $^{208}Pb/^{204}Pb$ ratios are high and nearly constant, while the $^{206}Pb/^{204}Pb$ ratios are extraordinarily low (Fig. 2.5). The only reasonable explanation for these characteristics is that the Pitcairn mantle source has lost U and, further, that the Th/Pb ratio was nearly constant in the source, as inferred by Woodhead and McCulloch [11]. In order to put constraints on the elemental fractionations in the Th-U-Pb system and the age of the recycled sediment component we performed Monte Carlo simulations of a three-stage Pb isotope evolution model, and then selected the subset of solutions resulting in present-day Pb isotopic compositions suitable for the recycled Pitcairn end member. The details of the model are described in the Background Dataset and the results are summarized in Fig. 2.10. The ranges of parameters for the successful simulations yield a low μ (<6.7) and a high κ (>5.7) during the final stage of Pb isotope evolution. Significant U loss in the Pitcairn source is required at the beginning of the final stage. The time of U loss is most easily interpreted as the original time of sediment deposition and/or subduction, and therefore represents the age of the recycled material. This age (t_2) ranges between 0.7 and 1.9 Ga (Fig. 2.10d), consistent with the age estimates of Woodhead and McCulloch [11], which were based on a similar Pb isotope evolution model.

2.3.7 Evidence for recent mixing

The measured Th/U ratios of some samples are extraordinarily high, ranging up to a value of 14.1. Given time, such high ratios will produce anomalously high $^{208}Pb/^{206}Pb$ ratios. One way to express this is by using the "radiogenic $^{208}Pb/^{206}Pb$ ratio" originally defined by

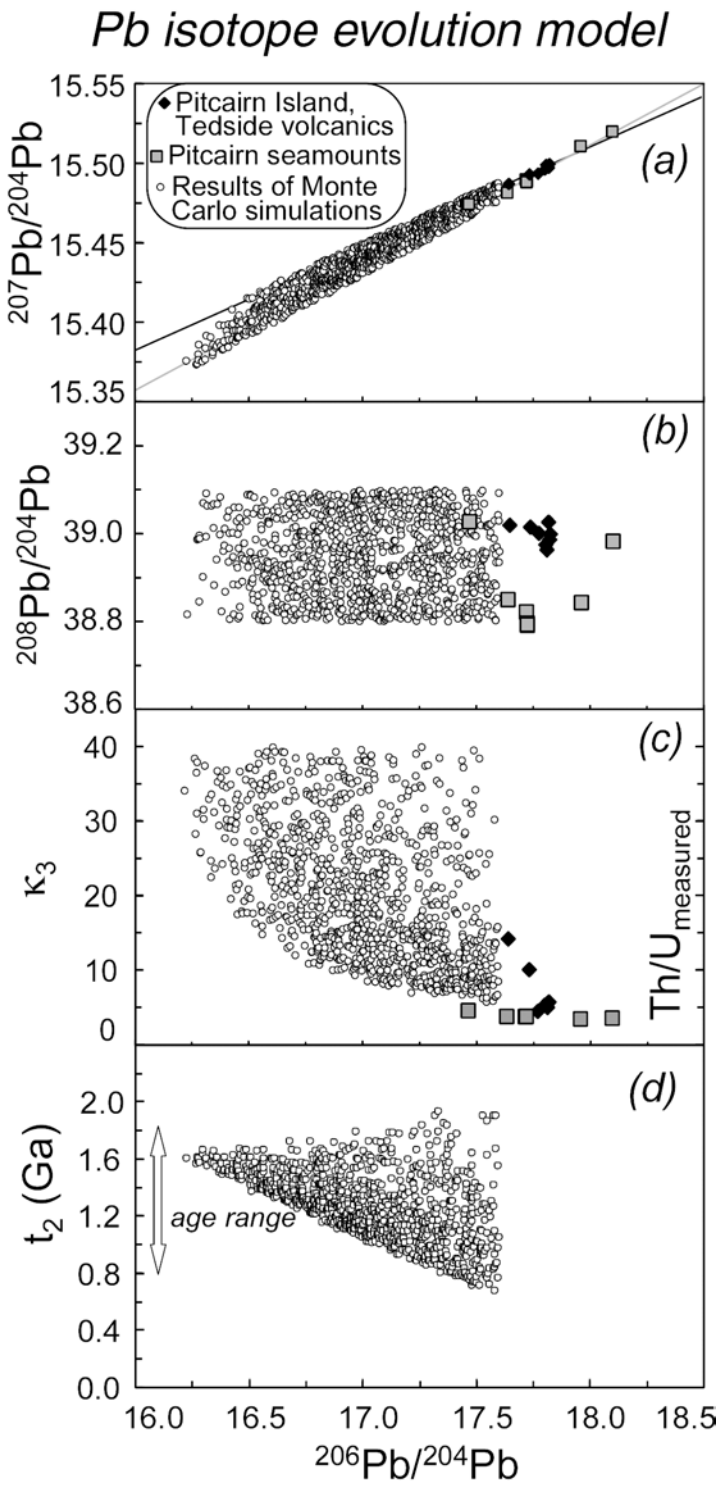

Fig. 2.10. Results of Monte Carlo simulations for a three-stage Pb model evolution of the recycled component in Pitcairn (see Background Dataset). (a, b) Results of the simulations in $^{207}Pb/^{204}Pb$-$^{206}Pb/^{204}Pb$ and $^{208}Pb/^{204}Pb$-$^{206}Pb/^{204}Pb$ space together with the Pitcairn samples. The results lie on the lower extension of the Pitcairn array to model a recycled sediment end member (c) The calculated κ_3 (κ values during the third evolutionary stage) of the recycled sediment in the model are >5.7. These ratios are higher than most measured Th/U ratios of the Pitcairn lavas. (d) A range of ages between 0.7 and 1.9 Ga by the recycled sediment component is implied by the model calculations (see text and Background Dataset for further explanation).

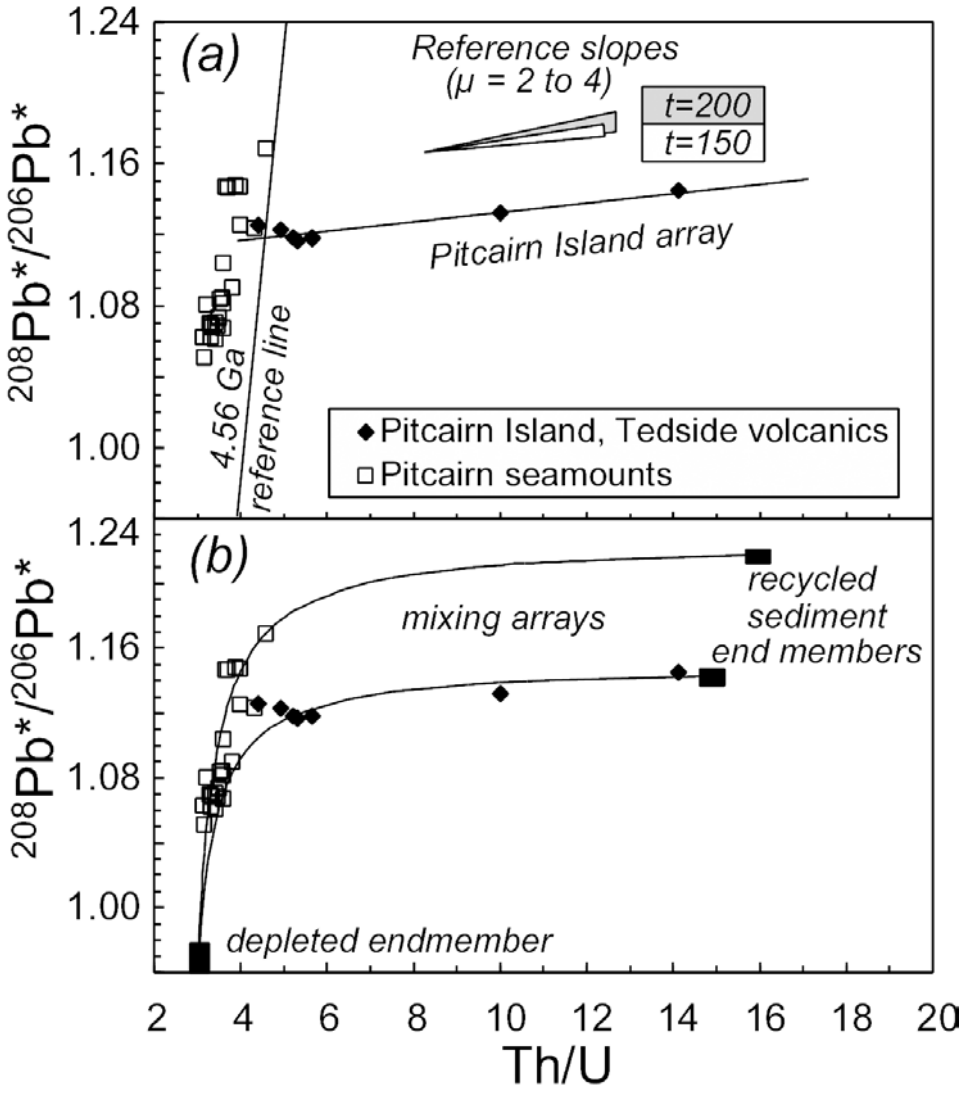

Fig. 2.11. Measured Th/U ratio versus radiogenic $^{208}Pb^*/^{206}Pb^*$ ratio. (a) Pitcairn seamount samples have low measured Th/U ratios relative to their high $^{208}Pb^*/^{206}Pb^*$ ratios and plot to the left of a 4.56 Ga reference line. Pitcairn Island samples show a linear array with a shallow slope and a large range of Th/U ratios. If interpreted as isochron, this array yields an approximate age of 150 to 200 Ma (μ = 2 to 4, $(^{206}Pb/^{204}Pb)i$ = 17.6, $(^{208}Pb/^{204}Pb)i$ = 39). (b) Alternatively, the arrays of Pitcairn Island and seamounts can be produced by mixing between a recycled sediment and a depleted end member. The calculation of the mixing hyperbolas assumes mixing of two parental melts with concentrations of Pb = 0.1 μg/g, Th = 0.3 μg/g and U = 0.1 μg/g for the depleted end member, Pb = 40 μg/g, Th = 20 μg/g, U = 1 μg/g for the enriched end members of Pitcairn Island and seamounts. Open symbols are from Woodhead and Devey [12].

Galer and O'Nions [43] as $^{208}Pb^*/^{206}Pb^* = [(^{208}Pb/^{204}Pb)_{sample} - 29.475] / [(^{206}Pb/^{204}Pb)_{sample} - 9.307]$. Figure 2.11 shows this parameter plotted against the measured Th/U ratio. This plot yields two approximately linear arrays with rather different slopes. The data for the Pitcairn Island samples have a rather shallow slope, which could, in principle, be interpreted as an isochron, if one assumed a uniform initial isotopic composition for all samples as well as uniform μ values. The equation of such an isochron is given by:

$$\frac{^{208}Pb^*}{^{206}Pb^*} = \frac{(\frac{^{208}Pb}{^{204}Pb})_i - (\frac{^{208}Pb}{^{204}Pb})_I + \frac{^{232}Th}{^{204}Pb} \times (e^{\lambda" t} - 1)}{(\frac{^{206}Pb}{^{204}Pb})_i - (\frac{^{206}Pb}{^{204}Pb})_I + \frac{^{238}U}{^{204}Pb} \times (e^{\lambda t} - 1)}$$

where $(^{208}Pb/^{204}Pb)_i$ and $(^{206}Pb/^{204}Pb)_i$ are the isotope ratios at time *t*, $(^{208}Pb/^{204}Pb)_I$, $(^{206}Pb/^{204}Pb)_I$ are initial ratios for the Earth 4.56 Ga ago [44], and λ" and λ are the decay constants of ^{232}Th and ^{238}U, respectively. Assuming μ values of 2 and 4, one obtains apparent ages of about 200 and 150 Ma, respectively. In contrast, the seamount samples would yield a very high age similar the age of the Earth. Given the overall isotopic similarity of the island and seamount samples, such discrepant age interpretations appear to be rather unreasonable. It is therefore more plausible to explain these apparently linear arrays as the nearly linear "arms" of mixing hyperbolas between recycled subducted sediments as modeled in the previous section and a depleted end member (Fig. 2.11b). The most reasonable way of explaining these systematics is that they result from mixing associated with generating the Pitcairn magmas themselves. As was pointed out by Woodhead and Devey [12], the mixing appears to occur between asthenospheric melts and does not involve Pacific lithosphere.

2.4 Conclusions

The Os, Pb, Hf, Nd and Sr isotope and trace element data for Pitcairn hotspot lavas presented here imply the presence of an enriched, volumetrically minor component in the mantle source. This component is unlikely to be dominated by recycled subcontinental lithospheric mantle. Rather, the enriched component most likely represents continentally-

derived material and contains varying proportions of recycled pelagic sediment. The overall compositions of the Pitcairn lavas reflect mixing between this enriched end member and several other end members, such as recycled MORB and gabbro, DMM and PRIMA. Such a scenario may be relevant for other EM-1-type ocean islands, such as Tristan da Cunha and Gough Island as well. In such cases where more than two components are involved, no correlations are expected in Os-Pb isotope space, while linear arrays in $^{207}Pb/^{204}Pb$ versus $^{206}Pb/^{204}Pb$ space will predominantly reflect the varying proportions of recycled sediment in the source. The unique systematics of Th/U vs. radiogenic $^{208}Pb^*/^{206}Pb^*$ ratios in Pitcairn underscore mixing - probably occurring during magma genesis - as an important process for generating radiogenic isotope arrays in ocean island basalts.

Acknowledgements

We thank K.-P. Jochum, B. Stoll, W. Abouchami, J. Lassiter, E. Macsenaere-Riester and H. Feldmann for their help during acquisition of these data at MPI. D. Garbe-Schönberg is acknowledged for technical assistance with the ICP-MS at University of Kiel. P. Stoffers (Geosciences Institute, University of Kiel) is thanked for provision of the Pitcairn Island and Seamount samples collected during the Sonne 65 cruise funded by the German Research Ministry (BMBF). P. Télouk is acknowledged for his assistance with the Plasma 54 in Lyon. W. Abouchami is thanked for helpful comments, and J. Woodhead, P. Schiano and V. Salters for their helpful reviews.

2.5 References

[1] A.W. Hofmann, W.M. White, Mantle plumes from ancient oceanic crust, Earth Planet. Sci. Lett. 57 (1982) 421-436.

[2] D. McKenzie, R.K. O'Nions, Mantle reservoirs and ocean island basalts, Nature 301 (1983) 229-231.

[3] C.W. Devey, F. Albarède, J.-L. Cheminée, A. Michard, R.K. Mühe, P. Stoffers, Active submarine volcanism on the Society hotspot swell (west Pacific): a geochemical study, J. Geophys. Res. B95 (1990) 5049-5066.

[4] C. Chauvel, A.W. Hofmann, P. Vidal, HIMU-EM: the French Polynesian connection, Earth Planet. Sci. Lett. 110 (1992) 99-119.

[5] E.H. Hauri, S.R. Hart, Re-Os isotope systematics of HIMU and EMII oceanic island basalts from the south Pacific Ocean, Earth Planet. Sci. Lett. 114 (1993) 353-371.

[6] L. Reisberg, A. Zindler, F. Marcantonio, W. White, D. Wyman, B. Weaver, Os isotope systematics in ocean island basalts, Earth Planet. Sci. Lett. 120 (1993) 149-167.

[7] W.M. White, R.A. Duncan, Geochemistry and Geochronology of the Society Islands: New evidence for deep mantle recycling, in: A. Basu, S.R. Hart (Eds), Earth Processes: Reading the Isotopic Code, American Geophysical Union, Washington DC 95, 1996, pp. 183-206.

[8] J.C. Lassiter, E.H. Hauri, Osmium-isotope variations in Hawaiian lavas: evidence for recycled oceanic lithosphere in the Hawaiian plume, Earth Planet. Sci. Lett. 164 (1998) 483-496.

[9] J. Blichert-Toft, F.A. Frey, F. Albarède, Hf isotope evidence for pelagic sediments in the source of Hawaiian basalts, Science 285 (1999) 879-882.

[10] D. Gasperini, J. Blichert-Toft, D. Bosch, A. Del Moro, D. Macera, P. Télouk, F. Albarède, Evidence from Sardinian basalt geochemistry for recycling of plume heads into the Earth's mantle, Nature 408 (2000) 701-704.

[11] J.D. Woodhead, M.T. McCulloch, Ancient seafloor signals in Pitcairn Island lavas and evidence for large amplitude, small length-scale mantle heterogeneities, Earth Planet. Sci. Lett. 94 (1989) 257-273.

[12] J.D. Woodhead, C.W. Devey, Geochemistry of the Pitcairn Seamounts, I: source character and temporal trends, Earth Planet. Sci. Lett. 116 (1993) 81-99.

[13] B.L. Weaver, The origin of ocean island basalt end-member composition: trace element and isotopic constraints, Earth Planet. Sci. Lett. 104 (1991) 381-397.

[14] M. Rehkämper, A.W. Hofmann, Recycled ocean crust and sediment in Indian Ocean MORB, Earth Planet. Sci. Lett. 147 (1997) 93-106.

[15] J. Mahoney, C. Nicollet, C. Dupuy, Madagascar basalts - tracking oceanic and continental sources, Earth Planet. Sci. Lett. 104 (1991) 350-363.

[16] W.M. White, Sources of oceanic basalts - radiogenic isotopic evidence, Geology 13(2) (1985) 115-118.

[17] A. Zindler, S. Hart, Chemical geodynamics, Ann. Rev. Earth Planet. Sci. 14 (1986) 493-571.

[18] P. Stoffers et al., Cruise Report Sonne 65 - Midplate II: Hotspot volcanism in the central South Pacific, Geol. Paläont. Inst., Kiel, 1990

[19] R.A. Duncan, I. McDougall, R.M. Carter, D. S. Coombs, Pitcairn Island - another Pacific hot spot?, Nature 251 (1974) 679-682.

[20] R.W. Le Maitre, P. Bateman, et al., A classification of igneous rocks and a glossary of terms, International Union of Geosciences, Oxford, 1989, 172 pp.

[21] S.J.G. Galer, Optimal double and triple spiking for high precision lead isotopic measurement, Chem. Geol. 157 (1999) 255-274.

[22] A.W. Hofmann, Mantle geochemistry: the message from oceanic volcanism, Nature 385 (1997) 219-228.

[23] S.B. Shirey, R.J. Walker, The Re-Os isotope system in cosmochemistry and high-temperature geochemistry, Annual Reviews in Earth and Planetary Science 26 (1998) 423-500.

[24] V.J.M. Salters, W.M. White, Hf isotope constraints on mantle evolution, Chem. Geol. 145 (1998) 447-460.

[25] T. Plank, C.H. Langmuir, The chemical composition of subducting sediment and its consequences for the

crust and mantle, Chem. Geol. 145 (1998) 325-394.

[26] A.W. Hofmann, Chemical differentiation of the Earth: the relationship between mantle, continental crust and oceanic crust, Earth Planet. Sci. Lett. 90 (1988) 297-314.

[27] A.W. Hofmann, K.P. Jochum, M. Seufert, W.M. White, Nb and Pb in oceanic basalts: new constraints on mantle evolution, Earth Planet. Sci. Lett. 79 (1986) 33-45.

[28] P. Schiano, K.W. Burton, B. Dupré, J.-L. Birck, G. Guille, C.J. Allègre, Correlated Os-Pb-Nd-Sr isotopes in the Austral-Cook chain basalts: the nature of mantle components in plume sources, Earth Planet. Sci. Lett. 186 (2001) 527-537.

[29] E.H. Hauri, J.C. Lassiter, D.J. DePaolo, Osmium isotope systematics of drilled lavas from Mauna Loa, Hawaii, Journal of Geophysical Research B 101 (1996) 11793-11806.

[30] E. Widom, S.B. Shirey, Os isotope systematics in the Azores: implications for mantle plume sources, Earth Planet. Sci. Lett. 142 (1996) 451-465.

[31] F. Marcantonio, A. Zindler, T.R. Elliott, H. Staudigel, Os isotope systematics of La Palma, Canary Islands: Evidence for recycled crust in the mantle source of HIMU ocean island, Earth Planet. Sci. Lett. 133 (1995) 397-410.

[32] V.C. Bennett, T.M. Esat, M. D. Norman, Two mantle-plume components in Hawaiian picrites inferred from correlated Os-Pb isotopes, Nature 381 (1996) 221-224.

[33] D.G. Pearson, The age of continental roots, Lithos 48 (1999) 171-194.

[34] Z.A. Palacz, A.D. Saunders, Coupled trace element and isotope enrichment in the Cook-Austral-Samoa Islands, southwest Pacific, Earth Planet. Sci. Lett. 79 (1986) 270-280.

[35] C. Hémond, C.W. Devey, C. Chauvel, Source compositions and melting processes in the Society and Austral plumes (South Pacific Ocean); element and isotope (Sr, Nd, Pb, Th) geochemistry, Chem. Geol. 115 (1994) 7-45.

[36] J. Dostal, B.L. Cousens, C. Dupuy, The incompatible element characteristics of an ancient subducted sedimentary component in ocean island basalts from French Polynesia, J. Petrol. 39 (1998) 937-952.

[37] S.R. Taylor, S.M. McLennan, The continental crust: its composition and evolution, Blackwell, London, 1985, 312 pp.

[38] R.L. Rudnick, D.M. Fountain, Nature and composition of the continental crust -- a lower crustal perspective, Rev. in Geophys. 33 (1995) 267-309

[39] J.D. Vervoort, P.J. Patchett, J. Blichert-Toft, F. Albarède, Relationships between Lu-Hf and Sm-Nd isotopic systems in the global sedimentary system, Earth Planet. Sci. Lett. 168 (1999) 79-99.

[40] P.J. Patchett, W.M. White, H. Feldmann, S. Kielinczuk, A.W. Hofmann, Hafnium Rare-Earth element fractionation in the sedimentary system and crustal recycling into the Earths mantle, Earth Planet. Sci. Lett. 69 (1984) 365-378.

[41] J.D. Woodhead, P. Greenwood, R.S. Harmon, P. Stoffers, Oxygen isotope evidence for recycled crust in the source of EM-type ocean island basalts, Nature 362 (1993) 809-813.

[42] J.M. Eiler, K.A. Farley, J.M. Valley, E.M. Stolper, E.H. Hauri, H. Craig, Oxygen isotope evidence against bulk recycled sediment in the mantle sources of Pitcairn Island lavas, Nature 377 (1995) 138-141.

[43] S.J.G. Galer, R.K. O'Nions, Residence time of thorium, uranium and lead in the mantle with implications for mantle convection, Nature 316 (1985) 778-782

[44] M. Tatsumoto, R.J. Knight, C.J. Allègre, Time difference in the formation of meteorites as determined from the ratio of lead-207 to lead-206, Science 180 (1973) 1279-1283.

Table 2.3, Background Dataset
Major and trace element composition of Pitcairn lavas

	Pitcairn Island, Tedside volcanics (shield-building)							Pulawana[#]		
Sample	Pit89-1	Pit89-2	Pit89-4	Pit89-5	Pit89-6	Pit89-8	Pit89-10	Pit89-19	Pit89-20	Pit89-21
Major elements (wt.%)										
SiO2	47.73	46.24	48.34	46.69	48.39	50.91	49.53	48.11	49.96	49.24
TiO2	3.55	2.47	3.50	3.41	3.50	3.72	3.64	3.31	2.94	2.94
Al2O3	14.23	13.24	15.07	14.64	15.18	15.06	15.79	14.89	15.67	15.71
Fe2O3	11.92	12.42	11.63	11.54	11.61	11.13	10.76	11.30	12.34	12.45
MnO	0.15	0.15	0.15	0.15	0.15	0.15	0.14	0.14	0.20	0.19
MgO	8.98	11.85	6.42	6.56	6.46	4.11	4.89	5.63	3.71	3.60
CaO	8.02	7.51	8.38	8.46	8.58	7.98	8.77	8.57	7.34	7.27
Na2O	2.96	2.42	3.47	3.38	3.46	3.96	3.59	3.39	4.58	4.15
K2O	1.51	0.90	1.58	1.53	1.57	1.82	1.76	1.55	1.97	1.98
P2O5	0.56	0.35	0.59	0.54	0.56	0.67	0.70	0.57	1.11	1.12
LOI (%)	0.0	2.0	0.0	0.0	0.0	0.0	0.1	0.0	0.0	0.0
Total	99.37	99.63	98.99	96.44	98.89	99.12	99.71	97.11	99.20	98.65
Trace elements (µg/g)										
Sc	19	15	23	21	22	22	25	22	15	17
V	230	185	246	237	251	241	230	254	122	138
Cr	209	349	167	165	158	27	80	166	1	1
Co	49	57	43	37	38	28	32	43	22	23
Ni	197	307	125	117	118	31	72	103	6	7
Cu	20	34	42	34	37	26	42	34	9	4
Zn	112	104	112	111	115	115	109	118	145	159
Ga	22	21	25	24	26	27	24	24	30	29
Rb	24	16	27	25	32	30	38	37	47	46
Sr	694	404	566	561	688	618	756	713	608	629
Y	28	19	29	27	33	37	33	36	52	49
Zr	320	201	325	307	326	365	359	327	520	534
Nb	44	28	47	44	47	56	55	48	74	76
Mo	1.2	1.5	2.4	2.3	2.3	2.1	2.8	2.9	4.7	4.5
Cs	0.08	0.08	0.12	0.17	0.15	0.06	0.12	0.17	0.28	0.18
Ba	391	204	382	377	381	463	473	411	261	266
La	43	25	45	43	44	56	53	46	62	65
Ce	83	51	88	86	89	111	105	93	126	131
Pr	10.6	6.4	11.0	10.7	10.7	13.2	12.5	11.5	15.8	16.4
Nd	41	25	43	42	42	52	49	46	63	67
Sm	8.1	5.4	8.6	8.6	8.6	10.6	9.6	9.4	13.1	13.8
Eu	2.6	1.8	2.7	2.7	2.6	3.2	3.0	2.9	3.7	3.9
Gd	7.1	5.2	8.0	7.9	7.6	9.4	8.3	8.8	12.3	12.9
Tb	0.95	0.68	1.04	1.04	1.06	1.27	1.13	1.13	1.57	1.66
Dy	5.4	4.1	6.1	6.1	6.0	7.1	6.3	6.5	8.9	9.5
Ho	0.97	0.73	1.10	1.09	1.09	1.28	1.11	1.16	1.60	1.69
Er	2.4	1.9	2.9	2.8	2.8	3.3	2.9	3.0	4.2	4.4
Tm	0.33	0.25	0.40	0.41	0.36	0.42	0.39	0.40	0.54	0.59
Yb	1.9	1.5	2.2	2.2	2.1	2.6	2.2	2.3	3.3	3.4
Lu	0.26	0.22	0.32	0.32	0.30	0.36	0.31	0.35	0.50	0.51
Hf	6.7	4.4	6.2	6.1	6.5	7.4	5.5	5.8	9.3	10.7
Ta	3.2	2.0	2.9	2.9	3.0	3.2	3.0	2.8	4.4	5.0
Pb	3.8	2.5	4.1	4.2	4.1	5.2	5.1	4.4	5.8	5.5
Th	6.1	3.4	6.2	5.3	5.2	8.5	6.1	5.7	8.4	8.6
U	0.61	0.64	1.18	0.94	0.92	0.60	1.38	1.16	1.80	1.70
Nb/U	72	44	40	47	51	93	40	41	41	45
Nb/Nb*	0.97	1.08	1.02	1.04	1.12	0.92	1.10	1.06	1.16	1.15
Th/U	10.0	5.3	5.2	5.6	5.7	14.1	4.4	4.9	4.6	5.1

Numbers in italics are from Woodhead and Devey [12]. Major elements and Sc, V, Cr, Co, Ni, Cu, Zn, Ga, Nb on Pitcairn Island samples: XRF, Mainz. Hf, Ta, Th, U on Pitcairn Island samples: SSMS, Mainz. Rb, Sr, Y, Zr, Mo, Ba, REE, Pb on Pitcairn Island and all trace elements on samples 47DS-2, 47DS-4: ICPMS, St. John's, Newfoundland. Major and trace elements on Pitcairn seamount samples: XRF and ICPMS, University of Kiel,

Table 2.3 (continued), Background Dataset

	Pitcairn seamounts, volcano 2															
Sample	46DS-2	Dupl.	46DS-10	Dupl.	47DS-2	47DS-4	47DS-8	Dupl.	47DS-11	48DS-6	Dupl.	49DS-1	Dupl.	51DS-1	Dupl.	51DS-2	52DS-2
Major elements (wt.%)																	
SiO2	48.41	48.62	50.39		47.13	47.04	47.19	47.39	47.67	49.01		*46.73*		49.77	49.65	50.01	*53.23*
TiO2	3.35	3.35	2.35		3.00	2.99	2.88	2.87	3.10	3.13		*2.80*		2.82	2.82	2.81	*1.44*
Al2O3	14.93	14.95	14.47		13.16	13.42	13.09	13.27	13.87	16.25		*12.38*		14.15	14.22	14.11	*16.53*
Fe2O3	11.82	11.93	11.41		12.29	11.99	12.29	12.19	11.77	10.74		*12.68*		11.78	11.66	11.87	*10.04*
MnO	0.14	0.15	0.19		0.15	0.15	0.15	0.15	0.15	0.14		*0.15*		0.15	0.14	0.15	
MgO	7.37	7.89	7.16		12.07	11.27	12.37	12.67	10.32	5.74		*14.80*		9.14	9.16	9.50	*1.72*
CaO	8.43	8.53	10.02		7.17	7.36	7.06	7.07	7.55	9.25		*6.81*		8.24	8.26	8.19	*4.40*
Na2O	3.35	3.26	2.76		3.04	3.06	3.04	3.28	3.33	3.59		*2.90*		2.96	3.07	2.95	*5.34*
K2O	1.28	1.19	0.94		1.42	1.49	1.43	1.44	1.51	1.48		*1.30*		0.80	0.807	0.82	*3.37*
P2O5	0.66	0.62	0.44		0.54	0.62	0.54	0.50	0.66	0.64		*0.45*		0.47	0.449	0.43	*0.77*
LOI (%)																	
Total	99.74	100.50	100.13		99.97	99.39	100.04	100.80	99.93	99.97		*101.00*		100.28	100.236	100.84	*96.84*
Trace elements (µg/g)																	
Sc	21		16	16			20			23	22	*19*	20	22		20	*14*
V	288		216	219			262			308	309	*254*	268	306		244	*45*
Cr	238		11	12			553			166	163	*769*	731	366		395	*2*
Co	46		21	21			64			37	35	*85*	78	49		58	*8*
Ni	159		13	14			378			97	95	*528*	512	236		251	*1*
Cu	47		28	29			54			39	40	*59*	57	44		50	*8*
Zn	115		128	136			111			107	102	*123*	144	108		105	*231*
Ga																	
Rb	22		37	37	24	22	22			20	21	*19*	20	13		12	*62*
Sr	603		594	591	675	646	606			694	692	*513*	551	468		465	*559*
Y	31		48	49	26	25	25			29	30	*21*	22	27		23	*49*
Zr	310		505	503	308	314	290			301	300	*239*	238	212		198	*656*
Nb	37		53	53	45	45	37			37	39	*40*	37	22		28	*92*
Mo					3.0	3.0											
Cs	0.24		0.45	0.45	0.20	0.23	0.31			0.27	0	*0.17*	0.21	0.25		0.10	*0.47*
Ba	282		427	430	300	339	303			309	307	*284*	304	160		164	*859*
La	32		51	51	36	39	34			34	33	*31*	33	19		20	*91*
Ce	70		111	111	72	77	72			71	71	*68*	70	42		45	*192*
Pr	9.3		14.6	14.7	9.1	10.0	9.1			9.2	9	*8.4*	8.64	5.8		5.9	*22.6*
Nd	40		63	62	37	40	37			38	38	*33*	34	26		27	*87*
Sm	9.2		13.8	13.7	7.6	8.2	7.7			8.3	8	*6.9*	7.1	6.4		6.5	*17.0*
Eu	2.8		4.0	4.1	2.4	2.6	2.3			2.6	3	*2.1*	2.2	2.1		2.2	*5.1*
Gd	8.3		12.4	12.8	6.6	7.1	6.7			7.4	8	*6.1*	6.3	6.2		6.1	*14.4*
Tb	1.18		1.75	1.75	0.85	0.93	0.93			1.03	1.06	*0.79*	0.87	0.88		0.83	*1.84*
Dy	6.3		9.4	9.52	4.8	5.3	4.9			5.7	5.72	*4.6*	4.7	5.1		4.9	*10.7*
Ho	1.11		1.67	1.71	0.85	0.94	0.87			1.01	1.04	*0.82*	0.84	0.89		0.87	*1.87*
Er	2.9		4.4	4.33	2.2	2.4	2.3			2.6	2.65	*2.1*	2.1	2.4		2.3	*4.8*
Tm	0.36		0.55	0.56	0.27	0.33	0.29			0.32	0.34	*0.27*	0.28	0.31		0.29	*0.64*
Yb	2.2		3.4	3.37	1.7	1.8	1.8			2.0	2.15	*1.7*	1.7	1.9		1.8	*4.0*
Lu	0.30		0.47	0.45	0.24	0.26	0.24			0.27	0.28	*0.23*	0.24	0.27		0.25	*0.53*
Hf	6.9		10.9	10.58			5.8			6.4	6.63	*4.7*	5.2	4.6		4.1	*12.2*
Ta	2.4		3.2	3.17	2.4	2.8	2.4			2.3	3.14	*2.3*	2.3	1.6		1.7	*4.1*
Pb	3.6		5.5	5.51	3.5	3.9	3.8			3.5	3.70	*3.5*	3.6	2.0		1.9	*9.6*
Th	3.4		5.7	5.80	3.4	3.9	3.9			3.6	3.70	*3.4*	3.6	1.9		1.9	*9.3*
U	0.96		1.63	1.63	0.92	1.05	1.05			1.08	1.11	*0.91*	0.92	0.61		0.56	*2.06*
Nb/U	38		32		49	43	35			34		*45*		36		50	*45*
Nb/Nb*	1.25		1.11		1.46	1.32	1.13			1.21		*1.41*		1.29		1.59	*1.14*
Th/U	3.6		3.5		3.7	3.7	3.7			3.3		*3.7*		3.2		3.4	*4.5*

Table 2.4, Background Dataset
Multiple analyses of Th and U concentrations on selected samples

Sample	comment	method	Th (µg/g)	U (µg/g)	Th/U
Pit89-1	fresh chips	SSMS	6.13	0.613	10.0
	fresh chips	SSMS	6.13	0.594	10.3
	altered chips	SSMS	6.89	0.673	10.2
	fresh chips	ICPMS	6.17	0.613	10.1
Pit89-2	fresh chips	SSMS	3.41	0.642	5.31
	altered chips	SSMS	3.47	0.664	5.23
	fresh chips	ICPMS	3.35	0.593	5.65
Pit89-8	fresh chips	SSMS	8.46	0.599	14.1
	fresh chips	ICPMS	7.84	0.568	13.8
	fresh chips	ICPMS	8.17	0.588	13.9
49DS-1	fresh glass*	SSMS	3.47	0.910	3.81
	whole rock	ICPMS	*3.4*	*0.91*	*3.75*
52DS-2	fresh glass*	SSMS	8.4	2.18	3.85
	whole rock	ICPMS	*9.3*	*2.06*	*4.51*

SSMS analyses from MPI, Mainz, and ICPMS analyses from St. John's
*glasses were cleaned with ultrapure H_2O and a 1:1 mixture
of 10% H_2O_2 and 0.25N HCl for 10 min at 20°C.
Numbers in italics are from Woodhead and Devey [12]

2.6 Background Dataset

Appendix 2.A: Analytical methods

Osmium, rhenium concentrations and Os isotopic compositions were determined on dissolutions of 0.5 to 3 g of whole-rock powder to which a mixed ^{190}Os-^{185}Re spike was added. Dissolution was effected using the Carius tube method [A1]. Osmium was extracted into liquid bromine and purified through microdistillation [A2] using a distillation apparatus which permits high and reproducible Os yields. Rhenium was separated using ion exchange extraction. Isotopic compositions were measured at MPI in Mainz using a Finnigan MAT-262 operating in negative ion mode (N-TIMS). Osmium was loaded onto Pt filaments as hexabromoosmate, dried and then mixed with Na(OH) - $Ba(OH)_2$ emitter, while Re was loaded on Ni filaments with $BaSO_4$ emitter. Eight procedural blanks for Os ranged from 24 fg to 178 fg ($^{187}Os/^{188}Os$ between 0.30 and 0.48), with one outlier of 892 fg ($^{187}Os/^{188}Os$ = 0.21). Blank corrections on $^{187}Os/^{188}Os$ were smaller than 1% in most cases, between 1 and 2 % for five analyses, and 5 % for Pit89-21. Blank corrections to Os concentrations were smaller than 1%, except in four cases where corrections ranged from 2 % to 8 %. Measured Re procedural blanks were 1.5 pg, 5 pg and 37 pg Re, resulting in corrections to Re concentrations between 1% and 28%. The Mainz in-house Os standard yielded $^{187}Os/^{188}Os$ of 0.10693 ± 18 (N = 7, errors are 2σ). The reproducibility of $^{187}Os/^{188}Os$ ratios, based upon four duplicate dissolutions, ranged from 0.5 % to 3.1 %, while that of Os concentrations is 5 % and 11 % for two duplicates, respectively.

Rock chips (~100-200 mg) were used for Pb isotope analysis. The chips were thoroughly cleaned in H_2O, leached with hot 6N HCl for one hour, and then rinsed with water prior to dissolution. Following dissolution, lead was separated by anion exchange in mixed HBr-HNO_3 media [A3]. The Pb isotopic composition was corrected for instrumental mass bias using a triple-spike technique [21]. The NIST NBS-981 standard yielded $^{206}Pb/^{204}Pb$ = 16.9407 ± 18, $^{207}Pb/^{204}Pb$ = 15.4978 ± 24 and $^{208}Pb/^{204}Pb$ = 36.7267 ± 65 (2σ errors) based on

25 runs during the period of measurement. Six duplicate measurements of sample aliquots from the same dissolution deviated from their respective means by 18-67 ppm in $^{206}Pb/^{204}Pb$, 26-99 ppm in $^{207}Pb/^{204}Pb$, and 35-132 ppm in $^{208}Pb/^{204}Pb$. Procedural Pb blanks analyzed alongside the samples varied between 10 and 35 pg Pb and are negligible.

Strontium and Nd isotope analyses were performed on ~50 mg of rock chips, leached for 1 hour with 6N HCl and then rinsed with ultrapure water prior to dissolution. Separation of Sr and Nd followed standard cation exchange column techniques. Isotopic compositions were measured on a Finnigan MAT-261 mass spectrometer operating in static multi-collection mode. The NIST NBS-987 standard yielded a $^{87}Sr/^{86}Sr$ of 0.710212 ± 24 (2σ; N = 8), while the La Jolla Nd standard gave a value of $^{143}Nd/^{144}Nd$ = 0.511850 ± 15 (2σ; N = 8). Hf isotopic compositions were measured at the Ecole Normale Supérieure in Lyon using the VG Plasma 54 MC-ICPMS following methods described by Blichert-Toft et al. [A4]. The JMC-475 Hf standard gave $^{176}Hf/^{177}Hf$ of 0.28216 ± 1 during this study, with the standard run every two to three samples. Major and trace elements were analyzed by XRF, spark source mass spectrometry (SSMS) and by ICP-MS, as described in Table 2.4. For the trace element analyses by ICP-MS at the Department of Earth Science, Memorial University of Newfoundland, St. John's, Canada, the precision of the method (1 r.s.d.), determined from multiple analyses of several international reference standards, is 3-7 %. For the ICP-MS analyses performed at University of Kiel, Germany, sample duplicates and standard values are given in Table 2.3.

Appendix 2.B: Os-Pb isotope mixing model

For a quantitative assessment of the Os-Pb isotope systematics of the EM-1 source, we have used a five component mixing model. The compositions of the five components, recycled pelagic and terrigenous sediments, recycled oceanic crust, recycled subcontinental

Table 2.5, Background Dataset. Compositions of recycled material for Os-Pb mixing model

	pelagic sediment	terrigenous sediment	N-MORB	continental lithospheric mantle	peridotite mantle
$^{187}Os/^{188}Os$	0.78	2	1.78	0.11	0.127
Os (pg/g)	200	20	10	1000	3000
$^{206}Pb/^{204}Pb$	17.1	18.9	22.5	18.5	18.5
Pb (μg/g)	11.6	3.03	0.073	0.1	0.049

The Os input compositons are similar to the estimates of recycled material from Shirey and Walker [23]. The Pb concentrations are taken from the trace element modeling of this study.

lithospheric mantle and peridotite mantle are shown in Table 2.5. The fraction of pelagic and terrigenous sediment residues in the mixtures were varied from 0 to 5 % in 0.5 % increments. The fraction of MORB residue in the mixture was varied from 0 to 90 % in 10 % steps. For each combination of sediments and oceanic crust, the rest was filled with continental lithospheric mantle in 10 steps. The remaining fraction after addition of these four components was filled with peridotite mantle. For these five component mixtures, 20000 combinations were tested. In order to explain the Os-Pb isotopic composition of the Pitcairn source, solutions were filtered out that had $^{187}Os/^{188}Os$ ratios from 0.131 to 0.149 and $^{206}Pb/^{204}Pb$ ratios ranging from 17.5 and 17.9. Fig. 2.7 shows about 800 solutions from these mixing calculations that fulfill these criteria. The Os concentrations in these solutions lie between 300 and 2500 pg/g Os.

Appendix 2.C: Trace element mixing model

In order to quantitatively evaluate the trace element systematics of the Pitcairn hotspot and to test for involvement of different recycled materials in the Pitcairn source, we have performed mixing calculations for the trace element compositions. These calculations used the incompatible elements Sr, Ba, Nb, La, Ce, Nd, Pb, Th and U. The possible involvement of the following components was tested: recycled pelagic and terrigenous sediment, recycled MORB, recycled gabbro, DMM, PRIMA. The input compositions were estimated using literature data for the trace element concentrations in these components and then applying an "element mobility factor" to estimate the composition of a residue after subduction (see Table 2.6). A large factor implies that the trace element concentration in the starting material is preserved, while small factors imply a large degree of mobility for an element. These factors were taken from the estimates of element mobility in oceanic crust and in sediments during subduction experimentally determined by Kogiso et al. [A7] for oceanic crust and Johnson and Plank [A6] for sediments. The fraction of pelagic and terrigenous sediment residues in the

Table 2.6, Background Dataset: Input compositions used for the mixing calculations.

	pelagic sediment	element mobility factor sediment	pelagic sediment residue	terrigenous sediment	element mobility factor sediment	terrigenous sediment residue
Sr	204	0.68	**139**	246	0.68	**167**
Nb	12.8	0.9	**11.5**	11.9	0.9	**10.7**
Ba	821	0.75	**616**	353	0.75	**265**
La	75.7	1	**75.7**	20.0	1	**20.0**
Ce	140	0.9	**126**	41.4	0.9	**37.3**
Nd	82.2	0.92	**75.6**	19.9	0.92	**18.3**
Pb	38.6	0.3	**11.6**	10.1	0.3	**3.03**
Th	11.6	0.8	**9.28**	4.48	0.8	**3.58**
U	1.43	0.75	**1.07**	1.29	0.75	**0.97**

	N-MORB	element mobility factor oceanic crust	N-MORB residue	gabbro	element mobility factor oceanic crust	gabbro residue	DMM	PRIMA
Sr	113	0.59	**66.7**	453	0.59	**267**	**11.3**	**18.2**
Nb	3.51	0.96	**3.37**	2.89	0.96	**2.77**	**0.351**	**0.618**
Ba	13.9	0.48	**6.67**	50.8	0.48	**24.4**	**1.39**	**6.05**
La	3.9	0.44	**1.72**	1.43	0.44	**0.629**	**0.39**	**0.614**
Ce	12	0.49	**5.88**	4.09	0.49	**2.00**	**1.2**	**1.6**
Nd	11.2	0.69	**7.73**	2.75	0.69	**1.90**	**1.12**	**1.19**
Pb	0.489	0.15	**0.073**	0.31	0.15	**0.047**	**0.0489**	**0.175**
Th	0.187	0.62	**0.116**	0.046	0.62	**0.029**	**0.0187**	**0.0813**
U	0.071	0.71	**0.050**	0.027	0.71	**0.019**	**0.0071**	**0.0203**

For the calculations the residues after subduction were used. No solutions were found for the pure recycled materials.The compositions of pelagic and terrigenous sediments are means of analyses reported by Plank and Langmuir [25]. N-MORB and PRIMA are from Hofmann [26] and DMM is 1/10 N-MORB. Gabbro composition is the mean of the Gabal Gerf gabbros from Zimmer et al. [A5]. The composition of the subduction residues was estimated using the element mobility estimates of Johnson and Plank [A6] for the sediments and those of Kogiso et al. [A7] for the oceanic crust. The factor for Pb of Kogiso et al. (0.5) was lowered to 0.3.

mixtures were varied from 0 to 5 % in 0.5 % increments. The fraction of MORB residue in the mixtures was varied from 0 to 90 % in 10 % steps. For each combination of sediments and oceanic crust, the remaining fraction was filled with gabbro in 10 steps. The remaining fraction after addition of these four components was either filled with pure DMM, a 1:1 mix of DMM and PRIMA or pure PRIMA. In order to find solutions for these six component mixtures, 40000 combinations were tested. Successful models were selected when they matched incompatible trace element ratios of the Pitcairn lavas. The mean values of the trace element ratios Ba/Nb, Ba/La, Sr/Nd, Ce/Pb, Th/Nb and Th/U were calculated for the Tedside volcanics and the Pitcairn seamount samples. A model mixture was accepted if it matched all these trace element ratios by ± 20 %. Because the model calculations are thought to reflect the trace element composition of the Pitcairn source, models were only accepted if they had absolute trace element concentrations lower than those measured in the Pitcairn lavas. From the 40000 combinations of the six components in the mixture, ~60 solutions were found that matched the trace element composition of the Tedside volcanics, and about the same number of solutions was found for the Pitcairn seamount source. The mean and total variation of these solutions is shown in Fig. 2.9. No solutions for the mixing calculations were found using the pure recycled components, which indicates that alteration of the original composition of the recycled materials is necessary to explain the trace element composition of the Pitcairn source.

Appendix 2.D: A three-stage Pb isotope evolution model for the recycled sediment component

We examined a three-stage Pb isotope evolution model, similar to that of Rehkämper and Hofmann [14], in order to better understand the origin of the "recycled" Pitcairn end member. The aims are, first, to arrive at models consistent with the present-day Pb isotopic composition needed for this end member, and second, to examine the ranges in source U/Pb

and Th/U ratios implied by these models. The results place significant constraints on the "age" of this recycled end member.

We start by considering Pb isotope evolution models evolving from the initial isotopic composition of the solar system 4.56 Ga ago [44]. Since many of the Pitcairn Pb isotopic compositions lie to the left of the geochron in $^{207}Pb/^{204}Pb$-$^{206}Pb/^{204}Pb$ space, it is immediately clear that a single-stage model is inadequate. A simple two-stage model will not work either, because any Pb isotope evolution with first and second stage μ-values typical of crustal material of around 9.5 would result in present-day $^{206}Pb/^{204}Pb$ and $^{207}Pb/^{204}Pb$ ratios far higher than those seen in Pitcairn. In order to model the composition of the "recycled" Pitcairn end member, a Pb isotope evolution model with a minimum of three stages is required, with retarded ingrowth of radiogenic ^{206}Pb in the final stage.

We used a Pb isotope evolution model with three stages [A8], which can be described in terms of:

$$\frac{^{206}Pb}{^{204}Pb} = \left(\frac{^{206}Pb}{^{204}Pb}\right)_I + \mu_1(e^{\lambda t_0} - e^{\lambda t_1}) + \mu_2(e^{\lambda t_1} - e^{\lambda t_2}) + \mu_3(e^{\lambda t_2} - 1)$$

where t_0 is the age of the Earth, $(^{206}Pb/^{204}Pb)_I$ is the initial isotopic composition at t_0, μ_i is the (present-day effective) $^{238}U/^{204}Pb$ ratio during stage i, ages t_1 and t_2 mark the start of the second and third stages, respectively, and λ is the decay constant of ^{238}U. The corresponding isotopic evolution of $^{207}Pb/^{204}Pb$ and $^{208}Pb/^{204}Pb$ can be calculated in a similar manner.

In the three-stage model, the purpose of the first stage is largely to provide time for the Pb isotope ratios to evolve from the initial isotopic composition 4.56 Ga ago to a suitable composition for the silicate Earth following accretion [A9,A10]. In practice, the isotopic composition at the end of the first stage is best constrained by the compositions of Archean ore leads. For a crustal reservoir at ~3.7 Ga, estimates of μ_1 and κ_1 and the Pb isotopic composition at the start of the second stage are relatively similar [A9-A11].

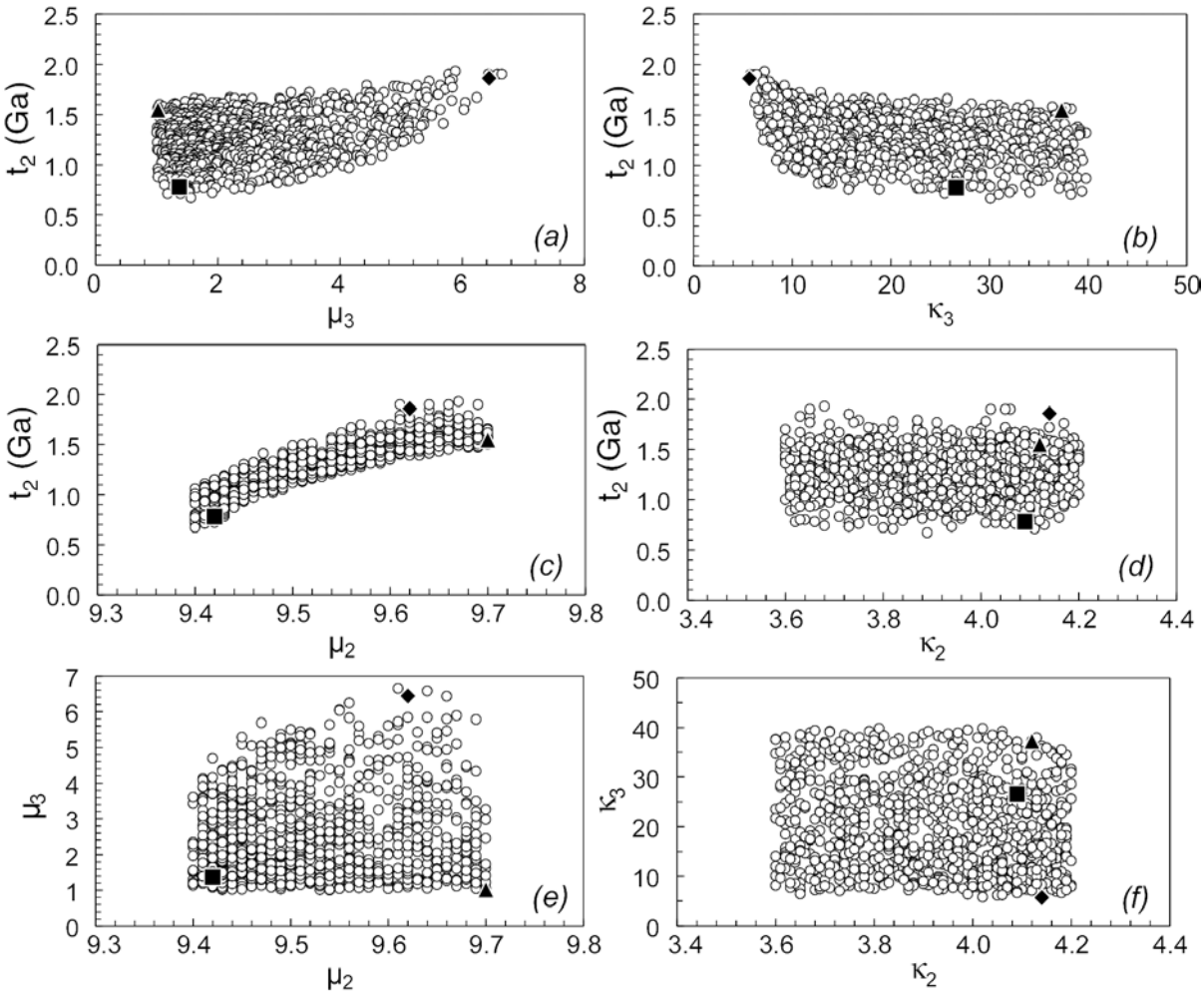

Fig. 2.12. Interdependence of the evolution parameters in the three-stage Pb isotope evolution model for the Pitcairn source. The age is dependent on the μ-values chosen for the second and the third stages, while it is relatively independent of k. Three example evolutions for the Pitcairn source are shown:

$\mu_2 = 9.62$, $\mu_3 = 6.44$, $\kappa_2 = 4.14$, $\kappa_3 = 5.7$, $t_2 = 1.86$ and $^{206}Pb/^{204}Pb = 17.55$ (diamond);

$\mu 2 = 9.42$, $\mu_3 = 1.37$, $\kappa_2 = 4.09$, $\kappa_3 = 26.6$, $t_2 = 0.78$ and $^{206}Pb/^{204}Pb = 17.42$ (square);

$\mu 2 = 9.70$, $\mu_3 = 1.02$, $\kappa_2 = 4.12$, $\kappa_3 = 37.3$, $t_2 = 1.55$ and $^{206}Pb/^{204}Pb = 16.31$ (triangle).

We performed Monte Carlo simulations of the three-stage model, and then selected a subset of solutions resulting in present-day Pb isotopic compositions suitable for the recycled Pitcairn end member (Fig. 2.10). In order to make meaningful statements on the possible age of the Pitcairn source, the evolution parameters of the first and second stages have to be kept relatively constant. When larger ranges for μ_1 and μ_2 are assumed, a larger range of t_2 ages can be obtained. In the simulations, the first stage parameters were fixed, while those of the second and third stages were allowed to vary slightly. Below, we show results for a first-stage $\mu_1 = 7.19$, $\kappa_1 = 4.48$ and $t_1 = 3.7$ Ga [A11]. The parameters that were allowed to vary randomly during the simulations are as follows: (1) μ_2-values ranged between 9.4 and 9.7 (Fig. 2.12), similar to values for the continental crust and conformable ore Pb [A9,A11]. (2) μ_3 varied freely between 1 and 8. (3) $^{232}Th/^{204}Pb$ ratios varied from 35 to 40 and were taken to be the same in both the second and third stages, resulting in $\kappa_2 = 3.6$ to 4.2 and κ_3 up to 40. From the simulations, 1000 "successful" models based upon the filtering criteria are plotted (Fig. 2.10). These successful models were selected using the criterion that the calculated present-day Pb isotopic composition lies on, or close to, the lower extension of the Pitcairn arrays in $^{207}Pb/^{204}Pb$-$^{206}Pb/^{204}Pb$ and $^{208}Pb/^{204}Pb$-$^{206}Pb/^{204}Pb$ spaces. These filtering criteria were that the $^{206}Pb/^{204}Pb$ ratio was lower than 17.6, the $^{207}Pb/^{204}Pb$ ratio deviated no more than 0.005 from the Pb isotope arrays of Pitcairn Island and seamounts, and that $38.8 < {}^{208}Pb/^{204}Pb < 39.1$. The ranges of parameters for the successful simulations yield a low μ_3 (<6.7) and a high κ_3 (>5.7). The time of the beginning of the third stage (t_2) ranged between 0.7 and 1.9 Ga (Fig. 2.10d). The interdependence of the μ_2, μ_3, κ_2, κ_3 and t_2 parameters is shown in Fig. 2.12 of the Background Dataset.

Background Data References

[A1] S.B. Shirey, R.J. Walker, Carius Tube digestion for low-blank Rhenium-Osmium analysis, Analytical Chemistry 67 (1995) 2136-2141.

[A2] J.L. Birck, M. Roy-Barman, F. Capmas, Re-Os isotopic measurements at the femtomole level in natural samples, Geostandard Newsletters 20 (1997) 19-27.

[A3] W. Abouchami, S.J.G. Galer, A.W. Hofmann, High precision lead isotope systematics of lavas from the Hawaiian Scientific Drilling Project, Chem. Geol. 169 (2000) 187-209.

[A4] J. Blichert-Toft, C. Chauvel, F. Albarède, Separation of Hf and Lu for high-precision isotope analysis of rock samples by magnetic sector-multiple collector ICP-MS, Contrib. Min. Petrol. 127 (1997) 248-260.

[A5] M. Zimmer, A. Kröner, K.P. Jochum, T. Reischmann, W. Todt, The Gabal Gerf complex: A Precambrian N-MORB ophiolite in the Nubian shield, NE Africa, Chem. Geol. 123 (1995) 29-51.

[A6] M.C. Johnson, T. Plank, Dehydration and melting experiments constrain the fate of subducted sediments, Geochemistry, Geophysics, Geosystems 1 (1999) Paper number 1999GC000014.

[A7] T. Kogiso, Y. Tatsumi, S. Nakano, Trace element transport during dehydration processes in the subducted oceanic crust: 1. Experiments and implications for the origin of ocean island basalts, Earth Planet. Sci. Lett. 148 (1997) 193-205.

[A8] N.H. Gale, A.E. Mussett, Episodic uranium-lead models and the interpretation of variations in the isotopic composition of lead in rocks, Reviews of Geophysics and Space Physics 11 (1974) 37-86.

[A9] S.J.G. Galer, S.L. Goldstein, Influence of accretion on lead in the Earth, in: A. Basu, S.R. Hart (Eds), Earth Processes: Reading the Isotopic Code, American Geophysical Union, Washington DC 95, 1996, pp. 75-98.

[A10] J.D. Kramers, I.N. Tolstikhin, Two terrestrial lead isotope paradoxes, forward transport modeling, core formation and the history of the continental crust, Chem. Geol. 139 (1997) 75-110.

[A11] J.S. Stacey, J.D. Kramers, Approximation of terrestrial lead isotope evolution by a two-stage model, Earth Planet. Sci. Lett. 26 (1975) 207-221.

[A12] K. Govindaraju, 1989 Compilation of working values and sample description for 272 Geostandards, Geostandard Newsletters 13 Special Issue (1989) 1-113.

Chapter 3: The long-term Pb isotope record of Mauna Kea: Results from HSDP-2

Jürgen Eisele, Wafa Abouchami, Stephen J. G. Galer and Albrecht W. Hofmann

Abstract

We analyzed Pb isotopes, using the triple-spike technique, on fifty samples from the HSDP-2 drill hole with the aim of searching for and characterizing the Pb isotope arrays contained in the stratigraphic record of Mauna Kea from 180 to 550 ka. The Pb isotopic compositions of the lavas range from 18.41 to 18.63, 15.47 to 15.49 and 37.97 to 38.22 in the $^{206}Pb/^{204}Pb$, $^{207}Pb/^{204}Pb$ and $^{208}Pb/^{204}Pb$ ratios, respectively. The samples display a linear array in $^{207}Pb/^{204}Pb$-$^{206}Pb/^{204}Pb$ space, while three different arrays are found in $^{208}Pb/^{204}Pb$-$^{206}Pb/^{204}Pb$ space. The $^{206}Pb/^{204}Pb$ stratigraphy in the drill core exhibits rapid shifts by ~0.2 over 100 m depth intervals, and jumps from one Pb isotope array to another and back in less than ~100 m depth. Despite the presence of these Pb isotope fluctuations, a particular Pb isotope array appears to dominate over certain periods, representing several tens to hundreds of ka.

We interpret the Pb isotope arrays found in HSDP-2 in terms of mixing of end members lying along the radiogenic and unradiogenic extensions of the arrays. At the radiogenic extension, the three HSDP-2 arrays appear to converge to a common end member in Pb isotope space. The lower extensions of the arrays diverge in three directions, each with different $^{208}Pb/^{204}Pb$ ratios. This geometry suggests that the HSDP-2 arrays were produced by mixing of four end members. Model calculations of a three-stage Pb isotope evolution model using Monte Carlo methods suggest that the common end member at the upper extension of the Pb isotope arrays may contain young HIMU material. This Pb isotopic signature may be interpreted as a contribution from recycled oceanic crust. The three lower end members could represent mantle material that contains little or no recycled material. Model calculations suggest that the Pb isotope heterogeneities may have length scales of several tens of km within the Hawaiian plume. The youngest Pb isotope array (180 to 370 ka) may be derived from the peripheral part of the plume, while the older HSDP-2 arrays (370 to 550 ka) may represent a more central part of the plume. It appears that young HIMU material is a mixing

end member throughout the cross-section of the plume sampled by HSDP-2, while the three other mixing end members may represent entrained mantle material from heterogeneous source regions.

3.1 Introduction

Volcanism in the Hawaiian Island and Emperor seamount chain is time-progressive and has been explained by the movement of the Pacific plate over a localized mantle plume formed of thermally and/or compositionally buoyant material (Morgan, 1971). Geochemical studies showed that temporal isotope fluctuations occur at time-scales of millions of years along the Hawaiian-Emperor chain (Keller et al., 2000; Regelous et al., submitted). Similarly, isotopic variability has been documented at smaller timescales during the lifetime of single volcanoes from the Hawaiian Islands (Kurz and Kammer, 1991; Kurz et al., 1995; Rhodes and Hart, 1995; Chen et al., 1996; Lassiter et al., 1996; Pietruszka and Garcia, 1999). Such fluctuations carry important information about the chemical structure of the Hawaiian plume.

Pb isotopic compositions of Hawaiian volcanoes are particularly interesting, because the Pb isotope variations in Hawaii form linear arrays in ^{208}Pb-^{207}Pb-^{206}Pb-^{204}Pb isotope space (e.g. Tatsumoto, 1978). The exact positions and slopes of linear arrays in ^{207}Pb/^{204}Pb-^{206}Pb/^{204}Pb space carry an age information if interpreted as isochrons (Tatsumoto, 1978; Chase, 1981) or, alternatively, may yield end member compositions if interpreted in terms of binary mixing (Abouchami et al., 2000a). Pb isotopes have three radiogenic isotope ratios and thus in themselves are able to identify mixing end members in three-dimensional isotope space. The Pb isotope compositions of Mauna Kea lavas from the pilot hole of the Hawaiian Scientific Drilling Project (HSDP-1) (Abouchami et al., 2000a) as well as Pb isotope studies of other Hawaiian volcanoes (Abouchami et al., 2000b) measured using a triple-spike for correction of instrumental mass fractionation, demonstrate the existence of linear arrays in Pb isotope space for individual volcanoes.

The record of the HSDP-2 drill hole may help to answer what the long-term Pb isotopic fluctuations of Mauna Kea lavas look like, and what image of the Hawaiian plume source may be drawn from the temporal isotopic variations. We report Pb isotope data on 50 samples from HSDP-2 obtained with a triple-spike technique (Galer, 1999) and show that different Pb isotope arrays exist in the long-term record of Mauna Kea lavas. We interpret the arrays in terms of mixing and investigate the significance of the mixing end members with a three-stage Pb isotope evolution model using Monte Carlo methods. Moreover, the possible lengthscales and distribution of the Pb isotope heterogeneities in the Hawaiian plume are examined.

3.2 Results

The Pb isotopic compositions were determined on 50 Mauna Kea lavas and one Mauna Loa sample from HSDP-2. These samples cover a depth range from 125 to 3068 meters below sea level (mbsl). Fourteen analyses were duplicated, six of which were replicate runs on the same dissolution, while eight were duplicate dissolutions. Analytical methods are described in Appendix 3.A, and the Pb isotopic data are summarized in Table 3.1. The external reproducibility of the Pb isotopic measurements is discussed in Appendix 3.B. The deviations of the duplicate analyses from a mean value is shown in Figure 3.1. We assume that the deviation of the 14 duplicates from HSDP-2 is a measure of the standard error for the analyses (see Appendix 3.B). The 2σ deviation from a mean for these fourteen analyses was 0.0019 (100 ppm) for the $^{206}Pb/^{204}Pb$ ratio, 0.0020 (130 ppm) for the $^{207}Pb/^{204}Pb$ ratio and 0.0060 (160 ppm) for the $^{208}Pb/^{204}Pb$ ratio (Fig. 3.1, Table 3.1).

3.2.1 The Pb isotope composition of HSDP-2 samples

The Pb isotope ratios of HSDP-2 Mauna Kea samples ranged from $^{206}Pb/^{204}Pb = 18.41$ to 18.63, $^{207}Pb/^{204}Pb = 15.47$ to 15.49 and $^{208}Pb/^{204}Pb = 37.97$ to 38.23 (Table 3.1, Fig.

Table 3.1: Pb isotopic composition of HSDP samples

		depth	age model	^{206}Pb		^{207}Pb		^{208}Pb		$^{208}Pb^*$
	Pb-array	(mbsl)	(ka)	^{204}Pb	2σ	^{204}Pb	2σ	^{204}Pb	2σ	$^{206}Pb^*$
Mauna Loa										
SR0080-1.23		-125		18.2191	12	15.4641	12	37.9562	37	0.9516
Mauna Kea										
SR0133-8.20	Kea-lo8	-281	232	18.4219	11	15.4746	11	37.9794	30	0.9330
SR0137-5.98	Kea-lo8	-293	244	18.4285	12	15.4753	12	37.9718	35	0.9315
SR0141-7.90	Kea-lo8	-306	255	18.4367	7	15.4768	7	37.9997	22	0.9337
SR0184-2.80	Kea-lo8	-421	313	18.4798	6	15.4810	8	38.0253	24	0.9321
SR0222-2.00	Kea-lo8	-516	342	18.5646	12	15.4865	12	38.1415	36	0.9361
SR0222-2.00.diss2	Kea-lo8	-516	342	18.5678	6	15.4911	7	38.1525	22	0.9370
SR0232-8.50	Kea-lo8	-542	349	18.5426	21	15.4758	17	38.0747	47	0.9311
SR0267-6.85	Kea-lo8	-616	366	18.5396	40	15.4773	33	38.0941	86	0.9336
SR0276-10.00	Kea-lo8	-636	369	18.5257	7	15.4758	8	38.0827	24	0.9337
SR0328-3.10	Kea-mid8	-760	392	18.5184	8	15.4783	9	38.1015	27	0.9365
SR0346-5.60	Kea-mid8	-813	400	18.5264	7	15.4808	7	38.1138	23	0.9370
SR0354-7.75	Kea-mid8	-834	404	18.4090	10	15.4711	10	38.0695	31	0.9443
SR0379-5.15	Kea-mid8	-888	411	18.4490	7	15.4765	8	38.0682	22	0.9400
SR0413-3.10	Kea-mid8	-984	425	18.4728	12	15.4764	12	38.0991	34	0.9409
SR0413-3.10.run2	Kea-mid8	-984	425	18.4707	17	15.4739	18	38.0909	58	0.9402
SR0423-4.35	Kea-mid8	-1012	429	18.5790	9	15.4862	10	38.1496	31	0.9356
SR0450-3.55	Kea-mid8	-1083	442	18.5552	22	15.4860	23	38.1433	70	0.9373
SR0490-1.50	Kea-mid8	-1229	452	18.4891	9	15.4803	9	38.1004	25	0.9394
SR0502-4.85residue	Kea-mid8	-1265	454	18.5664	10	15.4865	10	38.1517	29	0.9371
SR0502-4.85leach				18.5936	17	15.4935	17	38.1735	47	
SR0545-8.35	Kea-mid8	-1395	462	18.4396	8	15.4738	8	38.1102	26	0.9455
SR0545-8.35.run2	Kea-mid8	-1395	462	18.4401	9	15.4743	11	38.1145	32	0.9459
SR0574-1.90	Kea-mid8	-1474	467	18.6212	10	15.4881	9	38.1933	27	0.9360
SR0574-1.90.run2	Kea-mid8	-1474	467	18.6199	15	15.4867	14	38.1890	38	0.9357
SR0583-0.0	Kea-mid8	-1497	468	18.6195	7	15.4862	7	38.1838	23	0.9352
SR0604-2.50	Kea-mid8	-1549	471	18.5110	9	15.4791	9	38.1053	25	0.9377
SR0655-4.00	Kea-mid8	-1678	479	18.5420	17	15.4836	16	38.1173	48	0.9358
SR0683-5.75	Kea-mid8	-1763	484	18.4885	10	15.4773	10	38.0916	28	0.9385
SR0683-5.75.diss2	Kea-mid8	-1763	484	18.4858	21	15.4768	18	38.0940	46	0.9390
SR0709-13.35	Kea-mid8	-1851	489	18.5888	23	15.4881	20	38.1837	51	0.9383
SR0723-13.70	Kea-mid8	-1933	494	18.5129	12	15.4856	11	38.1314	29	0.9403
SR0732-1.10	Kea-hi8	-1973	496	18.4422	8	15.4700	8	38.1703	23	0.9518
SR0741-7.90	Kea-hi8	-2009	498	18.4417	11	15.4715	12	38.1770	38	0.9526
SR0750-12.45	Kea-hi8	-2062	501	18.4401	13	15.4701	12	38.1687	32	0.9519
SR0756-13.25	Kea-hi8	-2098	503	18.4348	16	15.4718	14	38.1704	41	0.9526
SR0756-13.25.run2	Kea-hi8	-2098	503	18.4359	17	15.4722	15	38.1728	41	0.9528
SR0756-13.25.diss2	Kea-hi8	-2098	503	18.4366	11	15.4727	10	38.1756	31	0.9530
SR0762-4.60	Kea-hi8	-2123	505	18.4335	13	15.4697	13	38.1638	33	0.9520
SR0776-17.70	Kea-mid8	-2209	509	18.5092	13	15.4823	13	38.1273	35	0.9402
SR0778-3.20	Kea-mid8	-2218	510	18.5330	16	15.4834	15	38.1286	40	0.9380
SR0800-13.20	Kea-hi8	-2321	515	18.4931	14	15.4721	12	38.1794	41	0.9476
SR0800-13.20.diss2	Kea-hi8	-2321	515	18.4935	10	15.4743	10	38.1854	29	0.9482
SR0826-20.60	Kea-hi8	-2413	520	18.4953	25	15.4744	24	38.1928	64	0.9488
SR0836-5.80	Kea-hi8	-2467	523	18.4974	8	15.4758	9	38.1911	27	0.9484
SR0842-2.35	Kea-hi8	-2503	525	18.4959	11	15.4741	10	38.1860	31	0.9480
SR0846-2.80	Kea-mid8	-2525	526	18.5566	13	15.4827	12	38.1460	35	0.9374
SR0855-0.10	Kea-hi8	-2581	529	18.6354	10	15.4905	10	38.2278	29	0.9383
SR0855-0.10.run2	Kea-hi8	-2581	529	18.6324	10	15.4886	10	38.2217	27	0.9379
SR0855-0.10.diss2	Kea-hi8	-2581	529	18.6347	10	15.4896	10	38.2214	28	0.9377
SR0860-8.10	Kea-mid8	-2614	530	18.4894	8	15.4733	9	38.1230	27	0.9418
SR0860-8.10.diss2	Kea-mid8	-2614	530	18.4882	8	15.4721	8	38.1197	24	0.9416
SR0871-13.00	Kea-hi8	-2653	532	18.4404	17	15.4704	16	38.1728	48	0.9523
SR0871-13.00.run2	Kea-hi8	-2653	532	18.4434	26	15.4730	23	38.1799	62	0.9528
SR0891-15.10	Kea-mid8	-2730	536	18.5638	12	15.4830	12	38.1621	34	0.9385
SR0896-2.40	Kea-mid8	-2759	538	18.4987	14	15.4813	14	38.1313	42	0.9418
SR0899-4.40	Kea-mid8	-2770	538	18.4927	20	15.4746	17	38.1089	45	0.9399
SR0913-2.40	Kea-hi8	-2825	541	18.5486	16	15.4876	15	38.1901	39	0.9430
SR0916-1.15	Kea-mid8	-2837	541	18.6095	15	15.4850	14	38.1792	41	0.9357
SR0930-15.85	Kea-mid8	-2919	545	18.4979	22	15.4765	21	38.1136	52	0.9399
SR0939-18.10	Kea-mid8	-2960	547	18.6074	11	15.4862	12	38.1717	37	0.9351
SR0954-8.00	Kea-mid8	-3008	550	18.6095	10	15.4870	11	38.1763	32	0.9354
SR0956-18.35	Kea-mid8	-3018	550	18.4858	7	15.4724	7	38.1179	21	0.9416
SR0956-18.35.diss2	Kea-mid8	-3018	550	18.4858	10	15.4742	9	38.1212	26	0.9420
SR0967-2.75	Kea-mid8	-3068	552	18.4920	13	15.4824	14	38.1196	39	0.9412
SR0967-2.75.diss2	Kea-mid8	-3068	552	18.4934	6	15.4802	7	38.1119	21	0.9402
HSDP1 duplicates										
R160-mean				*18.4218*		*15.4764*		*37.9956*		*0.9348*
R160dup				18.4224	14	15.4802	13	37.9997	36	0.9352
R166				*18.4095*	*32*	*15.4753*	*38*	*37.9809*	*122*	*0.9345*
R166dup				18.4101	8	15.4781	8	37.9913	25	0.9355
R212-powder				*18.4289*	*47*	*15.4815*	*58*	*38.0207*	*188*	*0.9368*
R212dup				18.4207	16	15.4685	14	37.9802	39	0.9332
R229-mean				*18.4866*		*15.4878*		*38.0613*		*0.9354*
R229dup				18.4830	7	15.4814	7	38.0390	23	0.9333
R243				*18.5529*	*14*	*15.4953*	*13*	*38.1364*	*36*	*0.9368*
R243dup				18.5484	7	15.4869	13	38.1086	21	0.9342
R286				*18.5239*	*11*	*15.4892*	*11*	*38.1054*	*33*	*0.9364*
R286dup				18.5166	6	15.4785	7	38.0681	22	0.9331
R395				*18.5360*	*43*	*15.4929*	*47*	*38.1611*	*144*	*0.9412*
R395dup				18.5248	7	15.4813	7	38.1143	21	0.9372

Pb isotope ratios in italics are from Abouchami et al., 2000a.
The age model is from DePaolo and Sharp (unpublished).

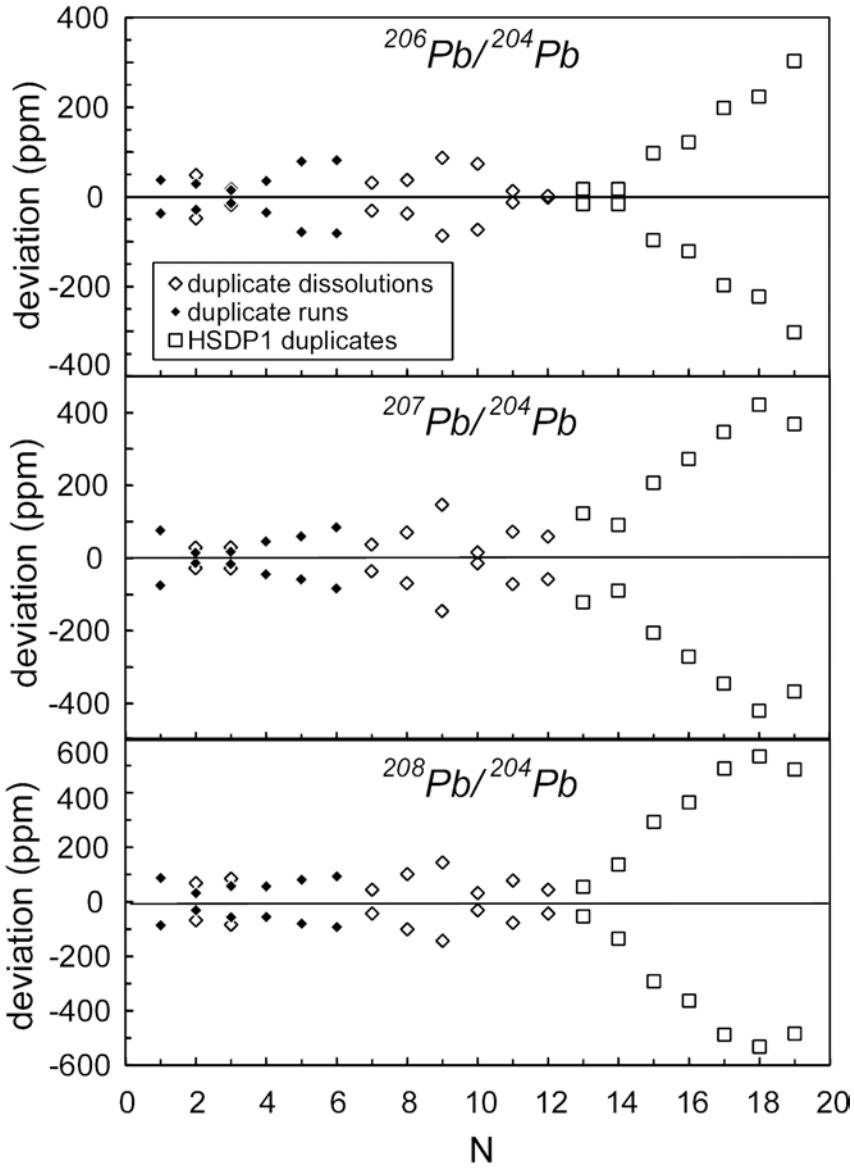

Fig. 3.1: Duplicate analyses of HSDP-2 samples and duplication of HSDP-1 samples analyzed by Abouchami et al. (2000a), which were reanalyzed here. Shown are the deviations from a mean in ppm of the duplicate dissolutions and duplicate runs of samples.

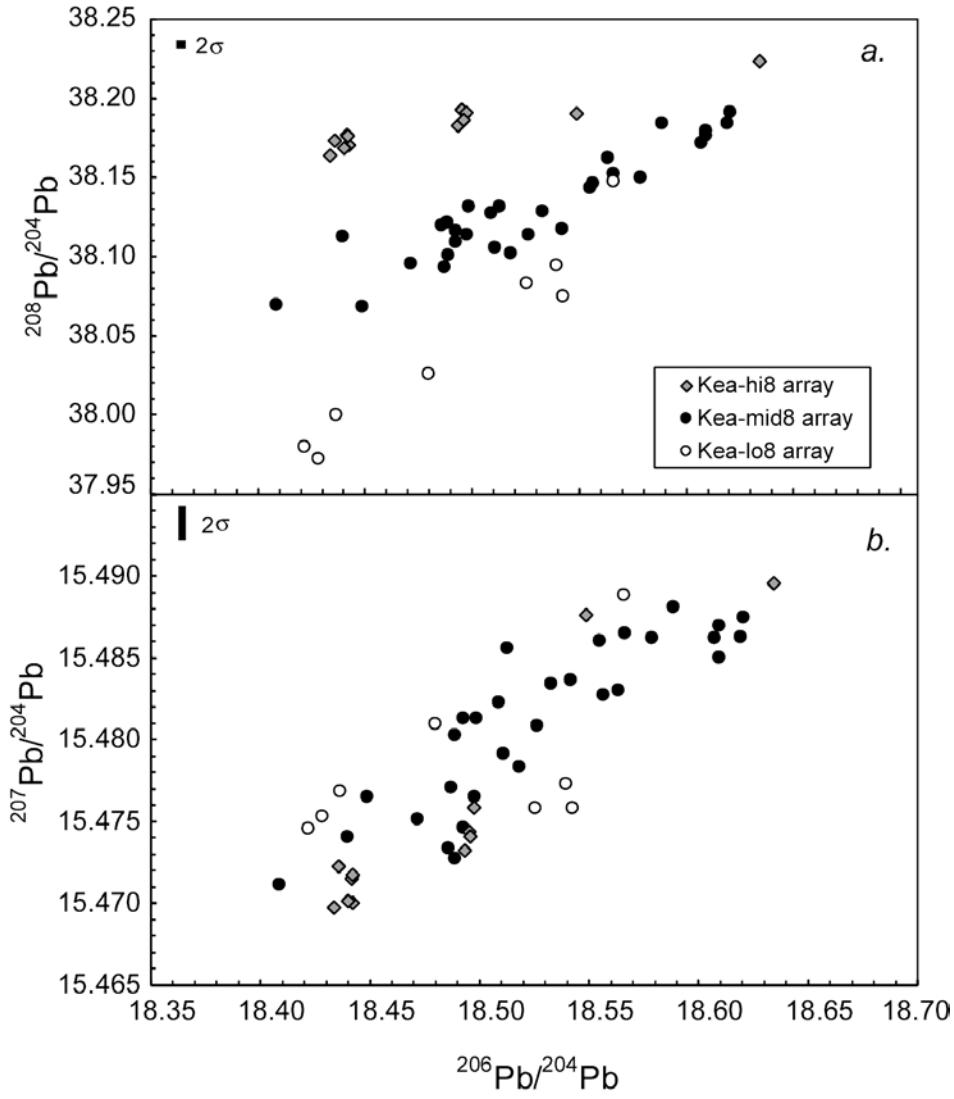

Fig. 3.2: Pb isotopic composition of HSDP-2 samples. The samples were subdivided into three different groups called Kea-lo8, Kea-mid8 and Kea-hi8 arrays on the basis of their difference in $^{208}Pb/^{204}Pb$ ratio.

3.2a,b). One Mauna Loa sample had $^{206}Pb/^{204}Pb$ = 18.22, $^{207}Pb/^{204}Pb$ = 15.46 and $^{208}Pb/^{204}Pb$ = 37.96. These ranges of Pb isotope compositions of Mauna Loa and Mauna Kea lavas are similar to those found for HSDP-1 samples (Abouchami et al., 2000a). The Pb isotope variations of HSDP-2 Mauna Kea lavas represent about 120, 10 and 40 times the analytical precision determined by the analysis of duplicates in $^{206}Pb/^{204}Pb$, $^{207}Pb/^{204}Pb$ and $^{208}Pb/^{204}Pb$, respectively, and are therefore significant. The variations of the $^{208}Pb/^{204}Pb$ ratios for a given $^{206}Pb/^{204}Pb$ ratio are up to 30 times the reproducibility. In $^{207}Pb/^{204}Pb$-$^{206}Pb/^{204}Pb$ space (Fig. 3.2b), the samples appear to form a coherent array, but on the basis of their differences in $^{208}Pb/^{204}Pb$-$^{206}Pb/^{204}Pb$ space (Fig. 3.2a), we subdivided the samples into three groups. The first group are the samples with the lowest $^{208}Pb/^{204}Pb$ ratios (Fig. 3.2a), which we call Kea-lo8 array samples. The majority of the samples belongs to the second group, which we call Kea-mid8 array samples. These samples have $^{208}Pb/^{204}Pb$ ratios intermediate compared to the two other arrays (Fig. 3.2a). The third group consists of samples with the highest $^{208}Pb/^{204}Pb$ ratios, which we call Kea-hi8 array samples.

3.2.2 Arrays and Regression lines

In $^{207}Pb/^{204}Pb$-$^{206}Pb/^{204}Pb$ space, there does not appear to be a consistent difference between the three groups of samples (Fig. 3.2b), but rather they form a broad band of data points. However, in $^{208}Pb/^{204}Pb$-$^{206}Pb/^{204}Pb$ space, the three groups of samples each form separate linear arrays (Fig. 3.2a) with different slopes. In order to quantify this further, we performed a linear regression on the three different groups of data points. The regression parameters for the three groups of samples in $^{207}Pb/^{204}Pb$-$^{206}Pb/^{204}Pb$ and $^{208}Pb/^{204}Pb$-$^{206}Pb/^{204}Pb$ spaces are summarized in Table 3.2.

The regression lines of the Kea-mid8 and Kea-hi8 arrays in $^{207}Pb/^{204}Pb$-$^{206}Pb/^{204}Pb$ space are relatively shallow with slopes of 0.079±17 and 0.104±24, respectively (Table 3.2). The regression lines have reduced chi-squared values greater than 1 (see Table 3.2) indicating that

Table 3.2 Regression parameters for HSDP-2 Mauna Kea Pb isotope arrays

	n	$^{207}Pb/^{206}Pb$ slope	2σ	$\chi^2_{red.}$	residuals ($^{207}Pb/^{204}Pb$)	age (Ga)	$^{208}Pb/^{206}Pb$ slope	2σ	$\chi^2_{red.}$	residuals ($^{208}Pb/^{204}Pb$)	κ
Kea-lo8	8	0.044	56	15.9	-0.0045 to +0.0074	0.27(±0.34)	1.044	201	22.5	-0.023 to +0.024	3.3
Kea-mid8	30	0.079	17	6.1	-0.0053 to +0.0057	0.49(±0.10)	0.554	86	17.8	-0.024 to +0.031	1.8
Kea-hi8	12	0.104	24	5.4	-0.0028 to +0.0058	0.64(±0.14)	0.253	52	2.7	-0.009 to +0.007	0.82

the deviation of the samples from a linear regression model is greater than the analytical precision. The y-axis residuals of the samples range between -0.005 and +0.007 in $^{207}Pb/^{204}Pb$-$^{206}Pb/^{204}Pb$ space (see Table 3.2) and -0.024 and +0.031 in $^{208}Pb/^{204}Pb$-$^{206}Pb/^{204}Pb$ space. The residuals are up to six times the 2σ error inferred from the analyses of duplicates (see Appendix 3.B, Fig. 3.1). These observations suggest that the arrays in Pb isotope space are not strictly linear within analytical precision, but rather need an additional process to explain the residual scatter.

3.2.3 Comparison to HSDP-1 samples

The Kea-lo8 array samples are similar to those of HSDP-1 (Abouchami et al., 2000a), because both groups of samples have relatively low $^{208}Pb/^{204}Pb$ ratios and form an array with identical slope within error in $^{208}Pb/^{204}Pb$-$^{206}Pb/^{204}Pb$ space (Fig. 3.3a). However, the Kea-lo8 samples yield less radiogenic $^{207}Pb/^{204}Pb$ and $^{208}Pb/^{204}Pb$ ratios than the "normal Kea" array of HSDP-1 (Abouchami et al., 2000a). The variations in the $^{207}Pb/^{204}Pb$ ratios recorded by HSDP-2 lavas are about half of the variation recorded in HSDP-1 lavas and lie between the "normal" and "anomalous" Kea arrays of Abouchami et al. (2000a) (Fig. 3.3b). To explore the possible reasons for this discrepancy, we reanalyzed samples from HSDP-1 (Fig. 3.3). Some HSDP-1 samples reanalyzed here show an offset similar to that between HSDP-1 and HSDP-2. The possible reasons for this observation are discussed in detail in Appendix 3.B. It appears that this offset may be attributed to variable subaerial contamination of the samples on the Hawaiian Island. For clarity and internal consistency in this paper, we only show the samples analyzed from the main hole of HSDP (HSDP-2) when discussing the $^{207}Pb/^{204}Pb$-$^{206}Pb/^{204}Pb$ and $^{208}Pb/^{204}Pb$-$^{206}Pb/^{204}Pb$ relationships of the Mauna Kea lavas in detail (e.g. Fig. 3.5).

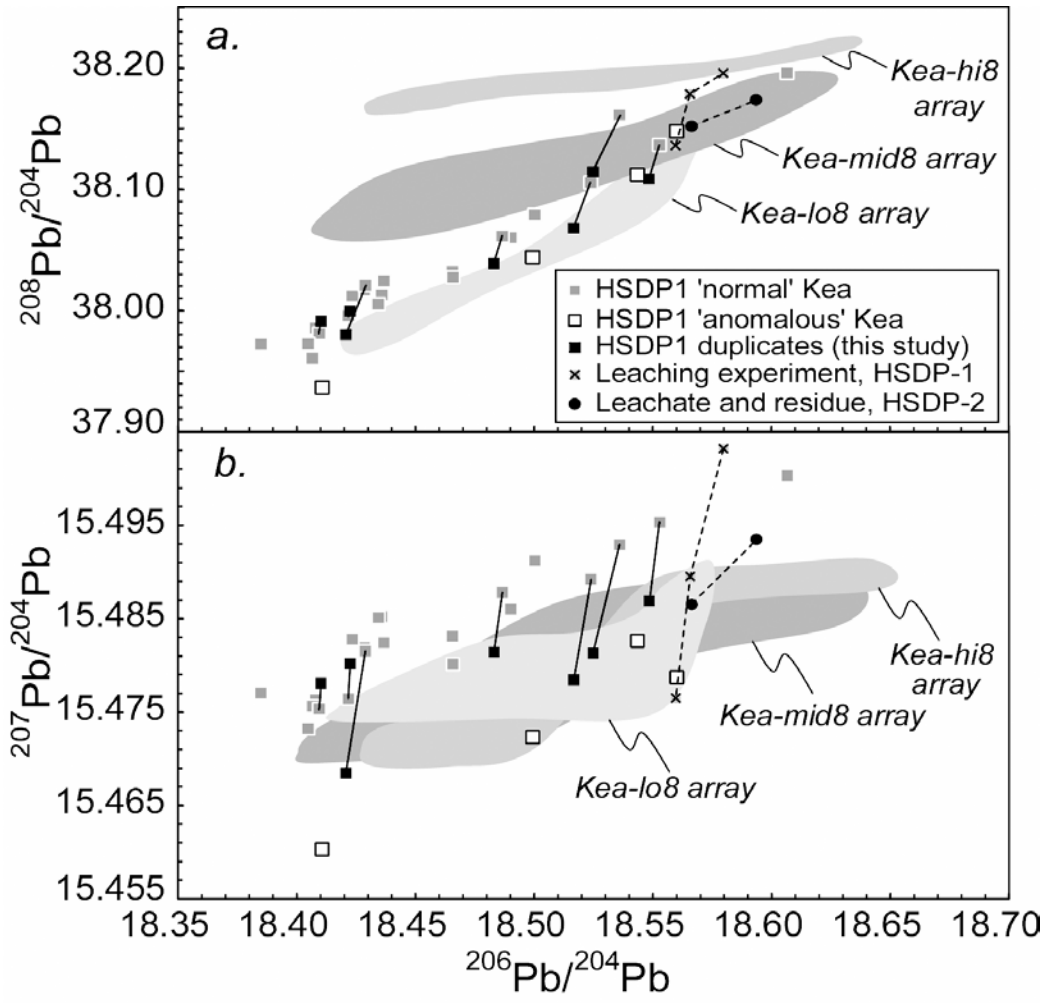

Fig. 3.3: HSDP-1 analyses (Abouchami et al., 2000a) compared to HSDP-2 samples. HSDP-1 samples which were reanalyzed in this study are also plotted. The offset between Abouchami et al. (2000a) and this study is indicated by the black lines. The dashed lines show the leaching experiment of Abouchami et al. (2000a) and analyses of leachate and residue from a HSDP-2 sample. The offset between HSDP-1 and HSDP-2 samples is thought to be a result of variable subaerial contamination on the Hawaiian Island.

3.2.4 Pb isotope stratigraphy

The Pb isotope stratigraphy of HSDP-2 (Fig. 3.4a, b) displays (1) a relatively small overall isotopic variability of the $^{206}Pb/^{204}Pb$ ratio of ~0.25, (2) rapid shifts in $^{206}Pb/^{204}Pb$ ratio by ~0.2 within 100 m depth intervals (e.g. at ~1400 mbsl and at ~2600 mbsl), (3) no unidirectional isotopic trend towards higher or lower Pb isotope ratios and (4) jumps from one Pb isotope array to another and back in less than ~100 m depth intervals.

Lavas belonging to the Kea-lo8 Pb isotope array occur at depths less than 750 mbsl. Samples of the Kea-mid8 array occur within the whole range of depths from >750 mbsl to 3068 mbsl of the HSDP-2 core. Kea-hi8 array samples mainly occur as two clusters within the drill core at 1973 to 2123 mbsl and at 2321 to 2503 mbsl and as several intercalated lavas at >2500 mbsl depth (see Fig. 3.4). The different Pb isotope arrays of Mauna Kea can be distinguished by their different radiogenic $^{208}Pb^*/^{206}Pb^*$ ratios (Fig. 3.4b). The radiogenic $^{208}Pb^*/^{206}Pb^*$ ratio represents the time-integrated $^{232}Th/^{238}U$ ratio since formation of the Earth and is calculated as $([^{208}Pb/^{204}Pb]_{sample} - 29.475) / ([^{206}Pb/^{204}Pb]_{sample} - 9.307)$ (Galer and O'Nions, 1985). Although there is some overlap between the different sample groups in $^{208}Pb^*/^{206}Pb^*$ ratio, Kea-hi8 array samples clearly display the highest $^{208}Pb^*/^{206}Pb^*$ ratios, and Kea-mid8 array samples are intermediate between the $^{208}Pb^*/^{206}Pb^*$ ratios of the Kea-hi8 and Kea-lo8 array samples.

To a depth of 750 mbsl, the HSDP-1 and HSDP-2 cores reveal a similar Pb isotope stratigraphy (Fig. 3.4c, d) and similar compositions in Pb-Pb isotope space (Fig. 3.3), because the Kea-lo8 array is similar to lavas of HSDP-2. At depths greater than 750 mbsl, some HSDP-2 samples yield lower $^{206}Pb/^{204}Pb$ ratios (at 800-900 mbsl) (Fig. 3c). In Pb-Pb space, it remains unclear, if the two HSDP cores have different Pb isotopic compositions at greater than 750 mbsl depth, because there are mainly conventional Pb isotope data (Lassiter et al., 1996) but only three triple spike analyses available (Abouchami et al., 2000a) from that depth. These three analyses lie at the intersection of the Kea-lo8 and the Kea-mid8 arrays (Fig. 3.3)

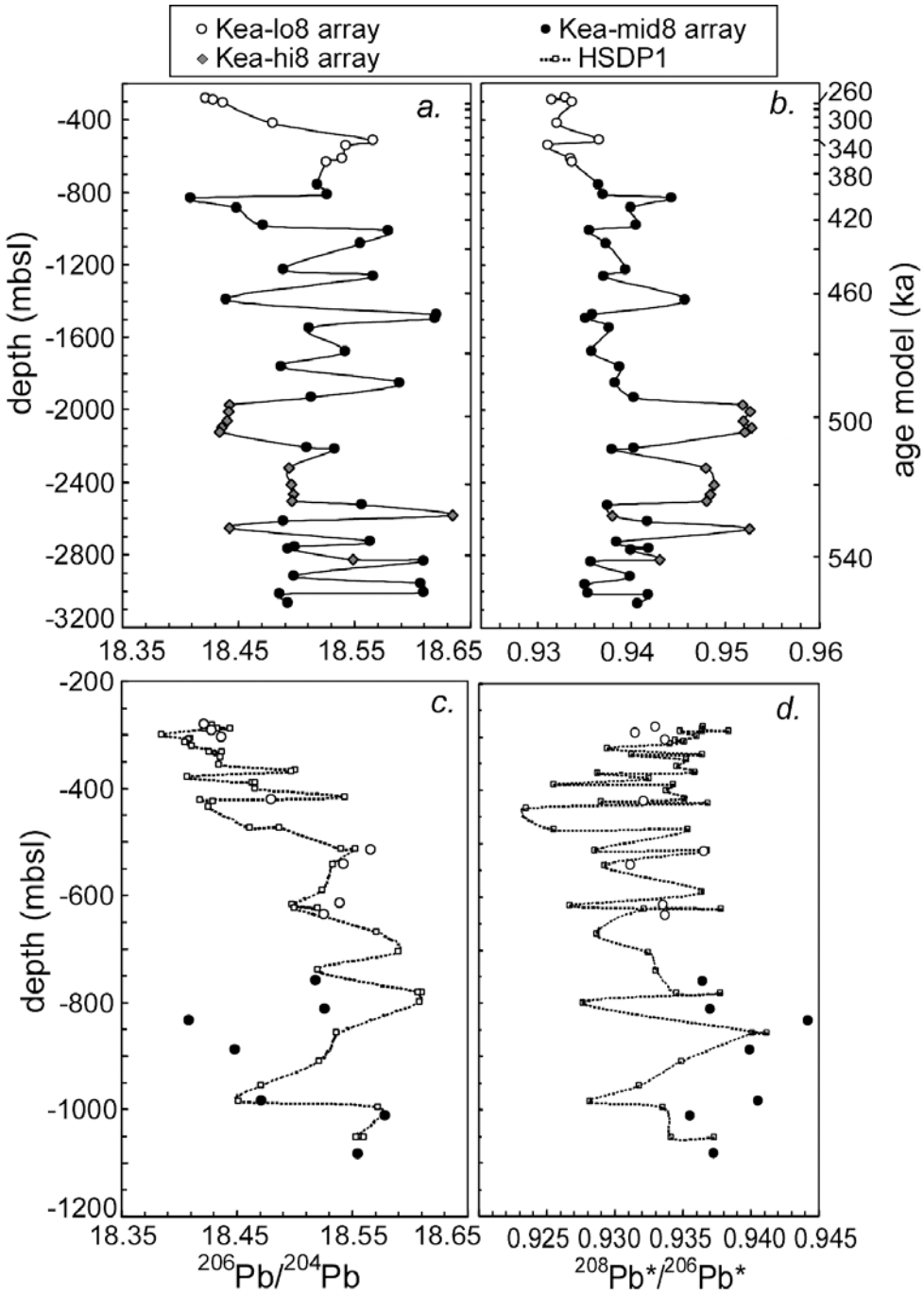

Fig. 3.4: Pb isotope stratigraphy. (a) Fluctuations of $^{206}Pb/^{204}Pb$ ratio with statigraphic depth in the HSDP-2 drill hole. (b) Fluctuations of $^{208}Pb^*/^{206}Pb^*$ ratios (=($[^{208}Pb/^{204}Pb]_{sample}$- $[^{208}Pb/^{204}Pb]_{primordial}$) / ($[^{206}Pb/^{204}Pb]_{sample}$-$[^{208}Pb/^{204}Pb]_{primordial}$)) in the HSDP-2 core. The Pb isotope arrays of HSDP-2 can be distinguished by their different $^{208}Pb^*/^{206}Pb^*$ ratios. (c) The $^{206}Pb/^{204}Pb$ isotope stratigraphy of HSDP-1 (data from Lassiter et al., 1996; Lassiter and Hauri, 1998; Abouchami et al., 2000a) and HSDP-2 samples from the same depth. HSDP-2 and HSDP-1 samples are very similar at the same depth, except for three samples between 800 and 900 mbsl depth. (d) The $^{208}Pb^*/^{206}Pb^*$ isotope stratigraphy of HSDP-1 and HSDP-2 to 1200 mbsl.

and do not determine whether Kea-mid8 array lavas are present in the HSDP-1 core, as well. However, given the overall similarity of the HSDP-1 and HSDP-2 samples from the same depth (Fig. 3.4c, d), the two cores appear to match each other stratigraphically, and only a few lava flows may not be present in both cores at a similar depth. We therefore regard it unlikely that an offset exists between the two HSDP cores as was proposed by Blichert-Toft and Albarède (2000).

3.3 Discussion

3.3.1 Interpretation of the Pb isotope arrays

The Pb isotopic compositions of basalts are susceptible to contamination either after eruption by geological processes such as dust contamination, sea-water alteration, subaerial weathering or to contamination during sampling and sample processing (McDonough and Chauvel, 1991). Especially with an improved analytical precision, contamination influences can never be excluded for the measured Pb isotopic compositions and probably represent the limiting factor for the accuracy of the analyses (Appendix 3.B). This also applies to the HSDP-2 samples. However, two observations suggest that the Pb isotope variations between Kea-lo8, Kea-mid8 and Kea-hi8 array samples represent variations in the Mauna Kea lavas themselves and not variations in the degree of contamination. First, the absolute variation in the measured $^{207}Pb/^{204}Pb$ ratios is very small (~0.02), while there is a larger difference in slopes and positions of the arrays in $^{208}Pb/^{204}Pb$-$^{206}Pb/^{204}Pb$ space (Fig. 3.2). Variable contamination should influence the $^{207}Pb/^{204}Pb$ ratios of the samples as much as, or even more than the $^{208}Pb/^{204}Pb$ ratios. Second, eight duplicate dissolutions of HSDP-2 samples reproduced the Pb isotopic composition very well (Fig. 3.1). This, however, does not preclude that contamination may have influenced the compositions of the duplicated samples to a similar degree. While we are aware about the analytical error that contamination may

introduce, the above indications lead us to treat the three different Pb isotope arrays as significant signatures of Mauna Kea basalts.

The three groups of samples of HSDP-2 lavas do not form strictly linear arrays within analytical precision in $^{207}Pb/^{204}Pb$-$^{206}Pb/^{204}Pb$ and $^{208}Pb/^{204}Pb$-$^{206}Pb/^{204}Pb$ spaces. Therefore, the arrays do not represent pure binary mixtures, and an additional process is necessary to explain the residual scatter. The deviations of the Pb isotopic composition from a linear regression model could be explained by a variation in the degree of contamination or by interaction between more than two compositional end members either in the asthenospheric mantle or in the lithosphere en route to the surface. However, the fact that the different linear arrays are still recognizable (Fig. 3.2a) indicates that mixing between two end members is the dominant process and that a third end member material – either a contaminant or a mantle material – is only added in minor amounts.

Abouchami et al. (2000a) showed an approach to distinguish linear arrays in Pb isotope space reflecting binary mixing arrays from those reflecting mantle isochrons. Their argument was based on the comparison of the κ ($\equiv(^{232}Th/^{238}U)_{today}$)as calculated from the Pb isotope regression lines to the measured element ratio κ^* of the lavas. If the κ^* is not similar to the κ required from the Pb isotope arrays, then these arrays most probably do not represent true isochrons but resulted from mixing of materials with independent Pb isotope evolutions. Abouchami et al. (2000a) also showed that the κ calculated from the slopes of the Pb isotope arrays $^{208}Pb/^{204}Pb$-$^{206}Pb/^{204}Pb$ space is relatively insensitive to the "age" inferred from the slope in $^{207}Pb/^{204}Pb$-$^{206}Pb/^{204}Pb$ space. In the HSDP-2 lavas, the κ values for the Kea-mid8 and Kea-hi8 arrays are 1.8 and 0.82 (Table 3.2), respectively. These values are lower than the Th/U element ratios measured in the HSDP-2 lavas (from 1.9 to 3.4, Jochum et al., 2000). This makes an interpretation of the HSDP-2 arrays as mantle isochrons unlikely.

3.3.2. Mauna Kea end members and their differentiation in the Th-U-Pb isotope system

3.3.2.1 Mauna Kea Pb isotope end members

The Pb isotope signatures may be interpreted in terms of mixing between end members lying along the radiogenic and unradiogenic extensions of the arrays (Fig. 3.5a, b). In order to assess the number and composition of the end members involved in the formation of the Pb isotope arrays in Mauna Kea lavas from HSDP-2, we investigated the extensions of the arrays to look for possible end member compositions. The 95% confidence intervals of the regression lines are shown in Figure 3.5a, b.

The "radiogenic extensions" of the HSDP-2 regression lines converge towards a single end member. The intersection field of the 95% confidence intervals of the regressions yields a $^{206}Pb/^{204}Pb$ ratio between 18.60 and 18.75 and a $^{208}Pb/^{204}Pb$ ratio between 38.20 and 38.26 (Fig. 3.5a). The $^{207}Pb/^{204}Pb$ ratios of a common intersection lie between 15.48 to 15.50 (Fig. 3.5b). This Pb isotope array intersection may mean that the lavas share similar radiogenic mantle material with this composition. The intersection field is similar to the Kea mixing end member proposed by Eiler et al. (1996), but slightly more radiogenic in $^{207}Pb/^{204}Pb$ and $^{208}Pb/^{204}Pb$ ratio (Fig. 3.5).

If we assume that the three groups of HSDP-2 samples represent predominantly binary mixing, then as a minimum the common end member is needed and three more independent end members at the lower extensions of the arrays in $^{208}Pb/^{204}Pb$-$^{206}Pb/^{204}Pb$ space to explain the Pb isotope heterogeneities of Mauna Kea. In principle, it is possible to explain multiple linear arrays by mixing of only three end members (Douglass and Schilling, 2000). This scenario, however, would require the rather special circumstance of premixing of two end members. Regardless of the exact number of end members involved, it remains clear, that there is considerable heterogeneity in Mauna Kea lavas, requiring not one or two, but several end member materials appearing and disappearing in the Hawaiian plume. The Pb isotope end members of HSDP-2 were compared to the Pb isotope arrays found for other Hawaiian

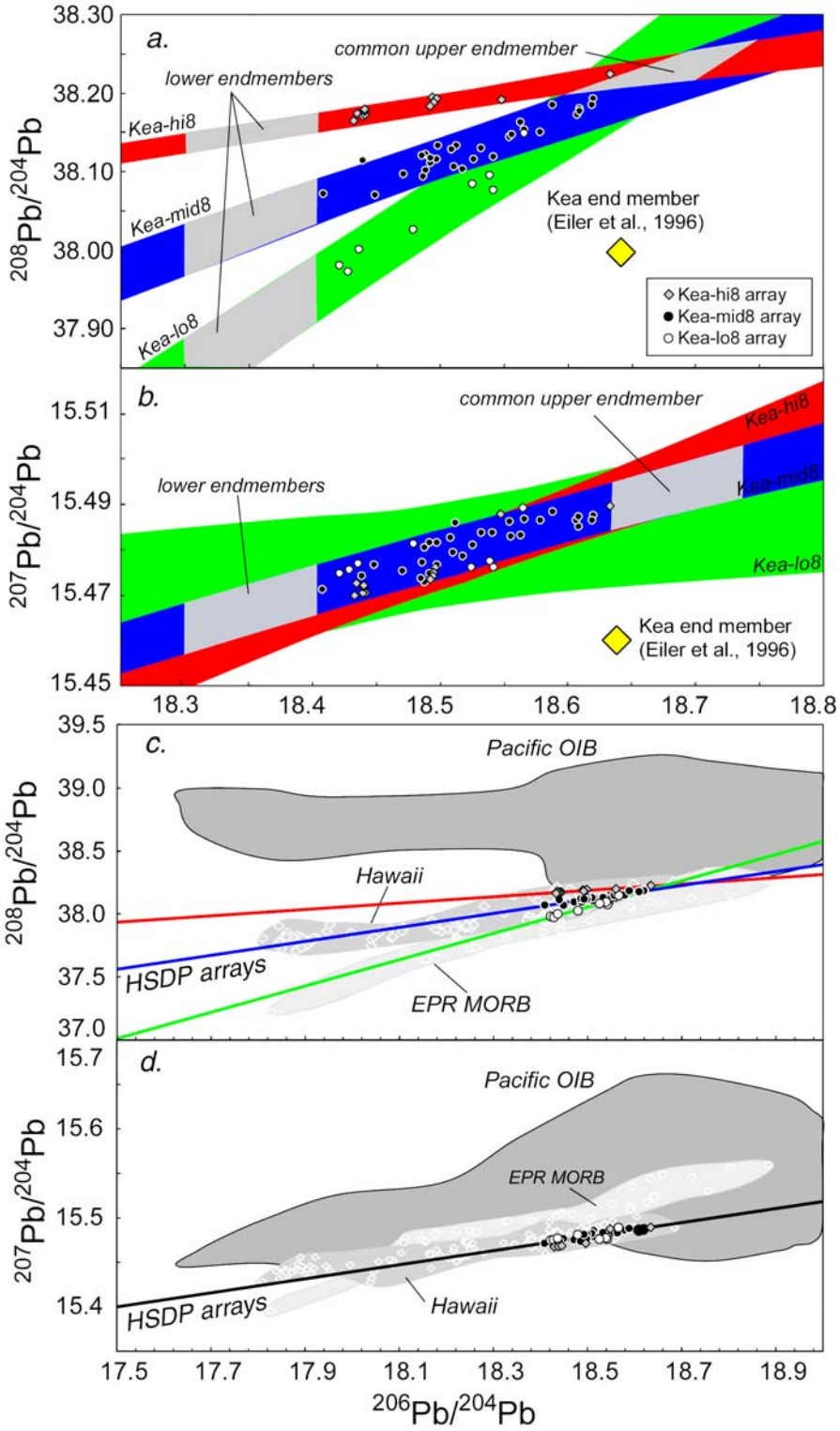

Fig. 3.5: (a, b) 95% confidence intervals of the HSDP-2 Pb isotope arrays (in color) and the composition of the inferred end members (dark gray). Also indicated is the Kea end member proposed by Eiler et al. (1996), which is similar to the common end member found for HSDP-2 lavas, but slightly less radiogenic in $^{208}Pb/^{204}Pb$ and $^{207}Pb/^{204}Pb$ ratios. (c, d) HSDP samples and regression lines compared to Hawaiian basalts (unpublished triple spike Pb isotope data, Abouchami and Galer), East Pacific Rise MORB (unpublished triple spike Pb isotope data, Galer and Abouchami) and Pacific OIB (compilation of Hofmann, 1997).

volcanoes by Abouchami et al. (2000b). The end member on the lower extension of the Kea-hi8 array has similarities with Loihi lavas, while the Kea-mid8 array as a whole is similar to Kilauea lavas.

3.3.2.2 Pb isotopic character and evolution of the Mauna Kea end members

Mauna Kea lavas represent one compositional end member of Hawaiian volcanism (e.g. Stille et al., 1986, Lassiter and Hauri, 1998) (Fig. 3.5c, d). The Mauna Kea lavas generally show a "depleted character", which is illustrated in their Sr, Nd and Hf isotopic composition (Lassiter et al., 1996; Lassiter and Hauri, 1998; Blichert-Toft and Albarède, 2000; Bryce and DePaolo, 2000). The distinction between several types of depleted material in the source of Mauna Kea lavas, i.e. depleted mantle (Lassiter et al., 1996), recycled lower oceanic crust or lithospheric mantle (Lassiter and Hauri, 1998), or assimilated Pacific lithosphere (Stille et al., 1986; Eiler et al., 1996) has been subject of some discussion. A distinction between these materials on the basis of their isotopic signature is difficult, because different types of depleted material may have similar Pb, Sr and Nd isotope characteristics. The question what sort of material the Kea end members may represent is therefore unlikely to be answered from a single isotopic system, such as Pb isotopes, alone. However, we can give some constraints on the significance of the end members that come from the Pb isotopic system.

In Pb isotope space, the depleted character of the Mauna Kea lavas is manifested by the relatively low $^{207}Pb/^{204}Pb$ ratios and low $^{208}Pb/^{204}Pb$ ratios at a given $^{206}Pb/^{204}Pb$ ratio compared to other OIB (Fig. 3.5c, d) (Thirlwall, 1997). This suggests relatively low μ ($\equiv(^{238}U/^{204}Pb)_{today}$) values in the early history of the Mauna Kea source and relatively low Th/U ratios. The fundamental characteristic of the HSDP-2 Pb isotope arrays is, that there is variation in the $^{208}Pb/^{204}Pb$ ratios of the end members, while there is very little variation in their $^{207}Pb/^{204}Pb$ ratios (Fig. 3.5). If the end members had variable Th/U ratios as well as

variable U/Pb ratios in the past, the uniform $^{207}Pb/^{204}Pb$ but variable $^{208}Pb/^{204}Pb$ ratios of the Mauna Kea source could argue for a relatively recent differentiation. This is the case, because ^{235}U has a much shorter half-live compared to ^{232}Th and is almost extinct at the present-day. Therefore, a recent differentiation of the U/Pb ratios will cause only subtle differences in the present-day $^{207}Pb/^{204}Pb$ ratios, while different Th/U ratios will result in contrasting ratios of $^{208}Pb/^{204}Pb$.

3.3.2.3. Modeling the Pb isotope evolution of the Pb array end members

In order to quantitatively evaluate the possible ranges of U/Pb and Th/U ratios in the history of the Mauna Kea source, we investigate a three-stage Pb isotope evolution model by Monte Carlo methods (see Appendix 3.C for details of the calculations). The main points raised in this discussion were also emphasized by Thirlwall (1997), and our model supports his argument for young HIMU mantle in the Mauna Kea source. The constraints on the Pb isotope evolution of the Mauna Kea source revealed by relationship of μ ($\equiv(^{238}U/^{204}Pb)_{today}$) and κ ($\equiv(^{232}Th/^{204}Pb)_{today}$) values with the beginning of the final Pb isotope evolution stage (t_2) (Fig. 3.6) are: (1) For young t_2-ages, μ_2 converges to a single value (~9.1), and for old t_2-ages, μ_3 approaches a similar value. The κ value approaches ~3.8 in a similar fashion (Appendix 3.C). These μ and κ values represent the parameters with which the source would have developed in a single-stage evolution since 3.7 Ga. (2) The μ values in the early evolution were relatively low ($\mu_2 < 9.3$ for t_2 between 3.5 and 2 Ga). (Fig. 3.6), underscoring the depleted character of the Mauna Kea lavas. (3) For the upper end member of the Mauna Kea arrays, an increase in U/Pb ratio with time is necessary (Fig. 3.6). If differentiation occurred at 2 Ga, μ_3 was moderately high (between 9.9 and 12.5). For a differentiation at 1 Ga, the μ_3 could have been more extreme, ranging between 10 and 16. The latter interpretation corresponds well with the measured μ values of the lavas ranging between 10 and 33 (F. Frey, unpublished data). (4) For the lower end member, a relatively recent

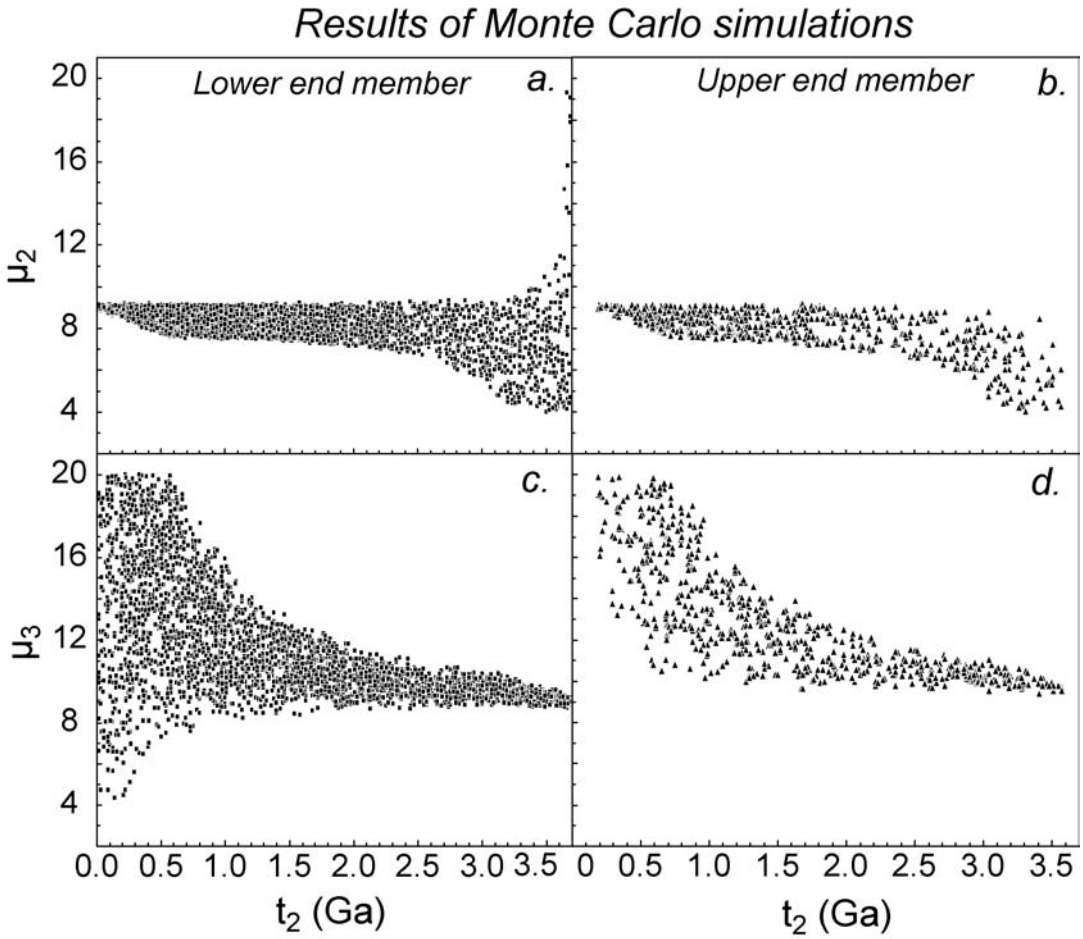

Fig. 3.6: Results of Monte Carlo simulations of a three-stage Pb isotope model for the HSDP-2 Pb array end members. Shown are variations of μ2 and μ3 values with the beginning of the third stage (t2). Parameters for the lower end members are shown in a, b and parameters for the upper end member in c and d. The μ3 values for the upper end member indicate that an increase in U/Pb ratio is necessary to explain this end member, which is interpreted as a young HIMU signature.

differentiation at e.g. 1 Ga would allow for a range in μ between 8.1 and 14.6. Consequently, for differentiation ages of ~1 Ga, materials with drastically different U/Pb ratios can explain the "single component" observed in $^{207}Pb/^{204}Pb$-$^{206}Pb/^{204}Pb$ space (Fig. 3.5b). (5) For the upper end member there are no solutions possible with $t_2 < 0.2$ Ga.

The ranges of μ_3 with the beginning of the final evolutionary stage (Fig. 3.6) may be explained by two alternative scenarios. If differentiation of the end members took place relatively early (at ~3.5 to 2 Ga), then μ_3 was relatively homogeneous. In this case, not much can be said from the Pb isotopic composition about the Kea array end members at all. Alternatively, if differentiation took place more recently (2 Ga to 0.5 Ga), then a large range in μ-values was possible for the lower end member, whereas the upper end member of the Pb array contained material with elevated μ values. Since there is a difference in $^{208}Pb/^{204}Pb$ ratios but not in $^{207}Pb/^{204}Pb$ ratios for the Mauna Kea end members, which is likely to be explained by a differentiation at <1.5 Ga, we consider the latter scenario more likely. This is consistent with models of mantle differentiation assuming that materials of ~1.5 Ga age or less are recorded in the OIB Pb isotope arrays (Christensen and Hofmann, 1994).

3.3.2.4 Significance of the Mauna Kea Pb array end members

3.3.2.4.1 The common radiogenic end member

It has already been argued by Thirlwall (1997) that the Mauna Kea source contained "young HIMU mantle". From our model results, it also appears that the common end member differentiated at <1.5 Ga and contains HIMU material (μ_3 = 10 - 20). Most explanations of the HIMU signature invoke Pb loss in the source, occurring by hydrothermal alteration of oceanic crust (Chauvel et al., 1992, 1995; Woodhead, 1996). The Pb isotope evolution model presented above indicates that the upper end member of the Pb isotope arrays is unlikely to be younger than 0.2 Ga and is therefore probably not derived from the oceanic crust underlying Hawaii (~100 Ma old). This supports the finding of Abouchami et al. (2000a), that the Pacific

lithosphere does not appear to be involved in the formation of the Pb isotope heterogeneities of the Mauna Kea lavas. Therefore, it seems plausible that the common end member of the Pb isotope arrays could contain recycled oceanic crust which may be <1.5 Ga old.

3.3.2.4.2 The unradiogenic end members

The lower end members of the Pb isotope arrays appear to change during the eruptive history of Mauna Kea and have different Pb isotope compositions in $^{208}Pb/^{204}Pb$-$^{206}Pb/^{204}Pb$ space (Fig. 3.5a). If we draw a line from the Pb isotope model composition 3.7 Ga ago to this end member in $^{207}Pb/^{204}Pb$-$^{206}Pb/^{204}Pb$ space, the age given by the slope is almost identical to that of a 3.7 Ga isochron. For that reason, the lower end members of the HSDP-2 arrays could be explained by a closed system, single stage evolution in the U-Pb system since 3.7 Ga. The μ and κ values of this single stage evolution are given by the values of convergence of the μ and κ values in the Monte Carlo simulations (Fig. 3.7, 3.9). These are μ = 8.9 to 9.2 and κ = 3.6 to 3.9. These values lie between those inferred for the bulk silicate Earth (κ = 3.9, μ = 8.7; Galer and Goldstein, 1996) and those inferred for a depleted mantle reservoir (κ = 3.75, Galer and O'Nions, 1985; μ = 9.3, Hofmann, 2001). The difference between the HSDP-2 arrays is expressed in their different radiogenic $^{208}Pb^*/^{206}Pb^*$ ratios (Fig. 3.4b). The Kea-lo8 array yields $^{208}Pb^*/^{206}Pb^*$ ratios of 0.933±3, the Kea-mid8 has $^{208}Pb^*/^{206}Pb^*$ ratios of 0.939±5, while the Kea-hi8 array yields $^{208}Pb^*/^{206}Pb^*$ of 0.949±9 (means and 2σ variation). Comparing the radiogenic $^{208}Pb^*/^{206}Pb^*$ ratios of the HSDP-2 arrays to those of typical mantle reservoirs, the HSDP-2 ratios lie between estimates for average MORB ($^{208}Pb^*/^{206}Pb^* \sim 0.92$) and primitive mantle ($^{208}Pb^*/^{206}Pb^* \sim 0.96$) (Galer and O'Nions, 1985), as well.

The possible closed-system evolution of the lower end members of the HSDP-2 arrays and their $^{208}Pb^*/^{206}Pb^*$ ratios suggest that the end members may represent variably depleted mantle material – the degree of depletion being strongest for the Kea-lo8 array and relatively weak for the Kea-hi8 array end member. These end members would appear to contain little or

no recycled material. This is, however, not the sole explanation what the lower end members may represent, because many different combinations of μ values could mimic a "closed system" behavior since 3.7 Ga (see Fig. 3.6). So our findings by no means exclude the presence of recycled lower oceanic crust in the Mauna Kea source (Hofmann and Jochum, 1996; Lassiter and Hauri, 1998). What remains clear though, is that the elevated $^{3}He/^{4}He$ isotope ratios (Kurz and Curtice, 2000) and the Pb isotopic signatures of the Kea-hi8 and the Kea-mid8 array samples indicate, that these materials carry at least some portion derived from a relatively undepleted and undegassed source. This suggests that the lower end members are contained within the rising plume itself and are not likely to be derived from the Pacific lithosphere underlying the Hawaiian hotspot (see also Abouchami et al., 2000a).

3.3.3 Temporal isotope fluctuations in the HSDP-2 core

In Hawaii, relationships between stratigraphic position and isotope signatures of the lavas were first described for Mauna Loa by Kurz and coworkers (Kurz and Kammer, 1991; Kurz et al., 1995). More recent studies illustrated rapidly oscillating Pb isotope fluctuations in Hawaiian volcanoes (Abouchami et al., 2000a) and dramatic shifts within very short time intervals (Pietruszka and Garcia, 1999). Pietruszka and Garcia (1999) documented a shift in the $^{206}Pb/^{204}Pb$ ratio by 0.25 occurring in about 100 years in historical Kilauea lavas. Compared to these findings, the rapid fluctuations in Pb isotopic composition observed in the HSDP-2 drill core (Fig. 3.4) do not appear surprising. The sampling intervals for our Pb isotope analyses range between 10 and 150 m, with a mean of ~60 m. Using the age model of DePaolo and Sharp (unpublished data, 2001) for the HSDP-2 drill hole, depth intervals of 60 m would correspond to age intervals of >2800 yr. The shifts in $^{206}Pb/^{204}Pb$ ratio by ~0.2 at ~1400 mbsl and ~2600 mbsl in the HSDP-2 drill core (Fig. 3.4) consequently occur in several thousand years and are less dramatic than those documented for Kilauea (Pietruszka and Garcia, 1999). The inference that may be drawn from the presence of rapid $^{206}Pb/^{204}Pb$

fluctuations in the HSDP-2 core (Fig. 3.5a, b) is that the Pb isotope heterogeneities are not homogenized in a magma chamber or in a deep molten zone under Mauna Kea (Fig. 3.8c). Moreover, residence times of Pb in a magma chamber must be sufficiently short to preserve rapid isotope fluctuations in the erupting lavas. The variations in $^{206}Pb/^{204}Pb$ ratios most likely represent changing proportions of mixing end members of a Pb isotope array. The observation that the mixing proportions of the end members appear to fluctuate rapidly may provide little information on the chemical structure of the Hawaiian mantle plume. Rather, the change from one Pb isotope array to another is interpreted here to represent the transition between different chemical zones in the source material.

3.3.4 HSDP-2 Pb isotope arrays and the model of the Hawaiian mantle plume

One of the aims of HSDP was to integrate the geochemical information into a geophysical model of mantle upwelling and melting in the Hawaiian plume. Recently, DePaolo et al. (2001) put constraints on the chemical structure of the Hawaiian plume from the Nd and He isotopic signature of Hawaiian volcanism. We used an approach similar to that of DePaolo et al. (2001) to determine the location of Mauna Kea relative to the assumed position of the Hawaiian plume (Fig. 3.7b). The HSDP-2 drill hole records the displacement of Mauna Kea from 17 km to 40 km away from the plume center (Fig. 3.7c) (details of the calculations are described in Appendix 3.D).

From the time spans in which a particular Pb isotope array is present in Mauna Kea lavas (Fig. 3.7a, b), inferences on the lengthscale and distribution of Pb isotope heterogeneities in the Hawaiian plume may be drawn. The Kea-hi8 and Kea-mid8 arrays are not strictly confined to a depth interval (Fig. 3.4). However, a particular Pb isotope array appears to dominate for a given time span ranging between 30 and 190 ka (Fig. 3.7a). These time intervals were calculated applying the age-model of DePaolo and Stolper (1996) and DePaolo and Sharp (unpublished data). Such a duration of an isotopic signature can be converted into

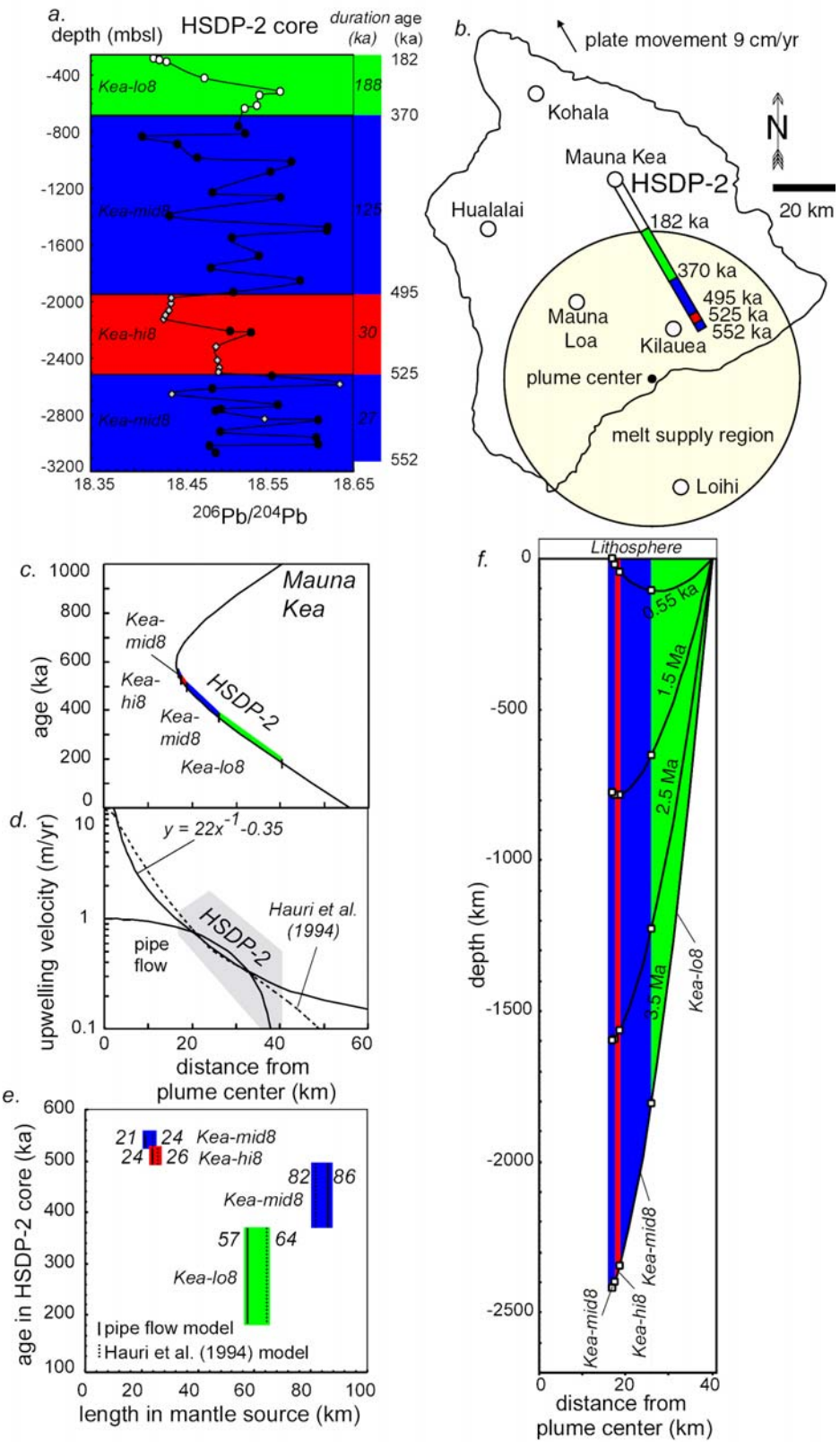

Fig. 3.7: HSDP-2 Pb isotope arrays and the model of the Hawaiian plume. (a) Pb isotope stratigraphy, (b) The HSDP-2 record relative to the Hawaiian plume center. (c) Distance of Mauna Kea from the plume center with time. (d) Two models for the mantle upwelling velocity structure in the Hawaiian plume. Also indicated is the position of HSDP-2. (e) Lengthscale of Pb isotope heterogeneities in the HSDP-2 mantle source. (f) Possible location of the HSDP-2 material in the mantle source in the past. The lines can be thought of as front of passive tracer material that is moved backwards in time. Shown are snapshots of the HSDP-2 source material at 0.55, 1.5, 2.5 and 3.5 Ma in the past.

lengthscales in the upwelling mantle source. For this calculation assumptions have to be made regarding the position of the volcano relative to the plume center, the radius of the mantle plume and its upwelling velocity structure. Constraints on these parameters come from geophysical models (Hauri et al., 1994; DePaolo and Stolper, 1996; Ribe and Christensen, 1999). We estimated the lengthscales in the mantle source represented by the HSDP-2 Pb isotope arrays using two models for the upwelling velocity structure in the Hawaiian mantle plume, namely a pipe flow velocity structure, and an approximation to the model of Hauri et al. (1994) (Fig. 3.7d). Details of the calculations are described in Appendix 3.D. The model calculations indicate that the lengthscales of the materials in the mantle source represented by the HSDP-2 Pb isotope arrays range between 21 and 86 km (Fig. 3.7e). These lengthscales, however, do not go straight down in the plume.

Assuming a radius of 40 km for the Hawaiian mantle plume (Hauri et al., 1994) and a pipe flow upwelling velocity structure, the location of the material sampled by HSDP-2 can be inferred for the past (Fig. 3.7f). This is done by "turning time backwards" and calculating the position of the material in the past. Figure 3.7f shows snapshots of the location of the HSDP-2 material in an upwelling mantle plume 0.55, 1.5, 2.5 and 3.5 Ma ago. The lines in Fig. 3.7f can be regarded as a front of a passive tracers in the mantle plume moved backwards in time. The Kea-hi8 and Kea-mid8 source materials are positioned in the more central part of the plume, while the Kea-lo8 material is located in the peripheral part of the plume. The velocity structure in the upwelling mantle is such that the material in the plume center will move faster (see Fig. 3.7d). This material could have risen from the deep mantle in 3.5 Ma (Fig. 3.7f), while material from the plume periphery may only have risen from the middle or upper mantle in the same time-interval. In this way, completely unrelated types of mantle material may be juxtaposed against each other.

The common radiogenic end member of the HSDP-2 Pb isotope arrays appears to be a mixing end member in the whole cross section of the plume sampled by HSDP-2. This mixing

end member may consist of recycled oceanic crust. The end members at the lower extensions of the HSDP-2 Pb arrays vary during the passage of Mauna Kea over the plume cross section. The lower end members may represent mantle material containing less recycled material. This material could be entrained mantle derived from heterogeneous source regions. Whether these source regions are all located in the deep mantle or if material is derived from the middle or upper mantle, as well, is open to question.

3.4 Conclusions

We consider it likely that the Pb isotope arrays recorded in Mauna Kea lavas from HSDP-2 were produced by mixing of a common end member with three independent end member materials contained in the Hawaiian plume. The common end member appears to possess a contribution from a relatively young (<1.5 Ga) HIMU mantle source. We interpret the possible HIMU characteristics as an indication for recycled oceanic crust in the Mauna Kea source. The other end members of the Pb isotopic arrays may be derived from a variably depleted mantle source, containing little or no recycled material.

The HSDP-2 lavas record the displacement of Mauna Kea away from the Hawaiian plume center and record heterogeneities derived from initially more central and later peripheral material of the Hawaiian plume. The Pb isotope systematics of the HSDP-2 lavas suggest that recycled oceanic crust may be a mixing end member throughout the section of the plume sampled by the drill core. This recycled oceanic crust may mix with heterogeneous entrained mantle sources to produce the three Pb isotope arrays observed in HSDP-2.

3.5 Appendices

Appendix 3.A: Analytical methods

The analytical methods followed the procedures outlined by Abouchami et al. (2000a). Rock chips (~100-200 mg) were used for the Pb isotope analysis. To remove contaminants and render the basalts as clean as possible, the rock chips were thoroughly cleaned in H_2O, leached with hot 6N HCl for one hour, and then rinsed with water prior to dissolution. Following dissolution, lead was separated by anion exchange in mixed HBr-HNO_3 media. The Pb isotopic composition was measured on a Finnigan MAT 261 mass spectrometer in static multi-collector mode and corrected for instrumental mass bias using a triple-spike technique (Galer, 1999). The long term variations of the Pb isotope ratios of NIST NBS-981 standard over a 10 month period yielded $^{206}Pb/^{204}Pb = 16.9409 \pm 19$, $^{207}Pb/^{204}Pb = 15.4976 \pm 24$ and $^{208}Pb/^{204}Pb = 36.7262 \pm 86$ (2σ errors) based on 60 runs. Procedural Pb blanks analyzed alongside the samples varied between 5 and 65 pg Pb and are negligible. The isotopic ratios of the standard are within error of the values reported for HSDP-1 analyses, and the procedural blanks are similar. The isotopic ratios for the NIST NBS-981 reported by Abouchami et al. (2000a) for HSDP-1 were $^{206}Pb/^{204}Pb = 16.9405 \pm 15$, $^{207}Pb/^{204}Pb = 15.4963 \pm 16$ and $^{208}Pb/^{204}Pb = 36.7219 \pm 44$ and procedural blanks ranged between 15 and 50 pg.

Appendix 3.B: Reproducibility of Pb isotopic composition

The 2σ deviation from a mean of fourteen HSDP-2 sample duplicates was 0.0019 (100 ppm) for $^{206}Pb/^{204}Pb$, 0.0020 (130 ppm) for $^{207}Pb/^{204}Pb$ and 0.0060 (160 ppm) for $^{208}Pb/^{204}Pb$ (Fig. 3.1, Table 3.1). Six of the replicate analyses were multiple runs on the same dissolution and eight were duplicate dissolutions of rock chips. The reproducibility of duplicate runs and duplicate dissolutions is similar, indicating that a variation of procedural blanks during the chemical separation did not contribute significantly to the analytical error. Additionally, the degree, to which the samples are affected by the leaching procedure (see Appendix 3.A)

seems to be reproducible in the HSDP-2 lavas. The reproducibility of the samples was similar, but slightly better than the long-term reproducibility of the standard (see Appendix 3.A), indicating that the main source of error was the precision of the mass-spectrometric measurement and not variation in blanks or variation of the effects of the leaching procedure for HSDP-2. Whether the absolute Pb isotope ratios of the HSDP-2 samples, in particular the $^{207}Pb/^{204}Pb$ ratios, that we measured represent the true composition of the lava erupted is more open to question. It may be, that even when duplicating samples that we can only reproduce a certain degree of residual contamination, which we are not able to remove completely by the leaching procedure.

Deviations of HSDP-1 samples measured in this study from the Pb isotopic ratios reported by Abouchami et al. (2000a) were more variable and larger in some cases. The deviations from a mean value range from 20 ppm in $^{206}Pb/^{204}Pb$ ratio to 530 ppm in $^{208}Pb/^{204}Pb$ ratio (see Fig. 3.1, Table 3.1). Samples R160, R166 remeasured in this study yield higher Pb isotopic ratios but within analytical error of the ratios reported by Abouchami et al. (2000a). However, on the samples R212, R229, R243, R286 and R395 lower Pb isotopic ratios were found, significantly outside the reproducibility of the NIST NBS-981 standard or the HSDP-2 duplicates.

The offset between HSDP-1 samples and the Kea-lo8 array of HSDP-2 is similar to the offset between some HSDP-1 samples (Abouchami et al., 2000a) and duplicates reanalyzed in this study (Fig. 3.3). This could potentially be explained by an interoperator bias or by different degrees of sample contamination. An interoperator bias could theoretically be produced by different blank concentrations, a different leaching procedure, or a mass spectrometer bias. However, neither the blank concentrations, nor the leaching procedure, nor the measured isotope ratios of the NIST NBS-981 standard (see Appendix 3.A) changed appreciably between the measurement of HSDP-1 and HSDP-2 samples. Not all, but only five out of seven of the HSDP-1 duplicates show an offset (Fig. 3.2). Moreover, the offset

observed for HSDP-1 duplicates is parallel to the offset between leached and unleached rock powder analyzed for one HSDP-1 sample (Abouchami et al., 2000a) (see Fig. 3.2). We therefore consider it likely that the offset was produced by variable contamination of the samples.

To test the hypothesis that the discrepancy between multiple analyses of HSDP-1 samples could have been caused by contamination with dust on the Hawaiian Island during lava emplacement, we magnified the offset between the samples by factors of fifteen to thirty (Fig. 3.8). The resulting Pb isotopic composition lies along mixing arrays formed by leachate, residue and bulk analyses of Chinese Loess (Abouchami, unpublished data; Jones et al., 2000) in both Pb isotope spaces (Fig. 3.8). Such an observation is unlikely to be coincidence, and magnification of fractionation effects would produce an array with a shallower slope in $^{208}Pb/^{204}Pb$-$^{206}Pb/^{204}Pb$ space. These observations could point to the influence of dust contamination which is not removed completely and in a reproducible way by the sample leaching. The large deviation between the duplicates was not observed on those HSDP-2 samples that were erupted in a submarine environment.

Although we cannot exclude an interoperator bias, it seems likely that subaerial contamination has altered the Pb isotope composition of the samples, and that it is not possible to remove contamination effects in a reproducible way by the leaching procedure. The contamination effect may be smaller for submarine samples, which in this study reproduced relatively well. Limitations for the reproducibility of subaerial basalt samples due to weathering and contamination were already encountered for HSDP-1 samples from Mauna Loa (Abouchami et al., 2000a), and this represents one of the limitations of the high-precision Pb isotope measurements in basaltic rocks. However, the observed offset between HSDP-1 and HSDP-2 samples does not obliterate the differences between the three groups of samples observed in HSDP-2 nor the similarity of HSDP-1 samples in $^{208}Pb/^{204}Pb$-$^{206}Pb/^{204}Pb$ space to the Kea-lo8 array.

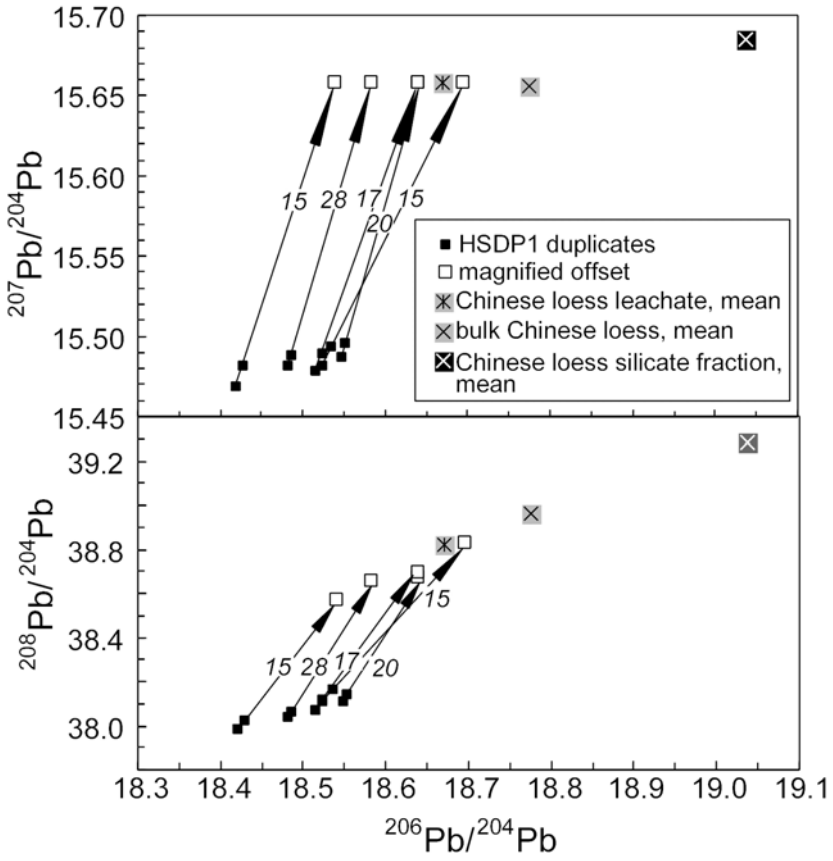

Fig. 3.8: HSDP-1 samples (Abouchami et al., 2000a) and their duplicates analyzed in this study. The offset between these analyses was magnified by factors of 15 to 28 as indicated by the black arrows. The resulting Pb isotopic compositions lie along the extension of mixing arrays in both Pb isotope spaces formed by different fractions of Chinese loess samples (from Jones et al., 2000). This observation is most easily explained by the variable incorporation of minor amounts of dust as a contaminant in the subaerial Hawaiian basalt samples.

Appendix 3.C: Monte Carlo simulations of a three-stage Pb isotope evolution model

In order to quantitatively evaluate the possible ranges of U/Pb and Th/U ratios in the history of the Mauna Kea source materials, we used a Pb isotope evolution model. Pb isotope evolution models involving more than one stage generally have many degrees of freedom, and such models with many unknown or ill-constrained parameters are best evaluated using Monte Carlo simulations. In principle, Pb isotope compositions of oceanic volcanics can be modeled using two or more evolution stages. While models with two or three evolutionary stages assume an episodic change of the U/Pb and Th/Pb ratios at a given time, multistage models can mimic step-wise differentiation processes. Here, we have chosen the approach that the isotopic evolution of the Mauna Kea lavas can be modeled by two abrupt changes in the element ratios. We used a Pb isotope evolution model with three stages (Gale and Mussett, 1974) which can be described in terms of:

$$\frac{^{206}Pb}{^{204}Pb} = \left(\frac{^{206}Pb}{^{204}Pb}\right)_I + \mu_1(e^{\lambda t_0} - e^{\lambda t_1}) + \mu_2(e^{\lambda t_1} - e^{\lambda t_2}) + \mu_3(e^{\lambda t_2} - 1)$$

where t_0 is the age of the Earth, $(^{206}Pb/^{204}Pb)_I$ is the initial isotopic composition at t_0, μ_i is the (present-day effective) $^{238}U/^{204}Pb$ ratio during stage i, ages t_1 and t_2 mark the start of the second and third stages, respectively, and λ is the decay constant of ^{238}U. The corresponding isotopic evolution of $^{207}Pb/^{204}Pb$ and $^{208}Pb/^{204}Pb$ can be calculated in a similar manner. We realize that the evolution parameters in a three stage model can only provide estimates for a particular time interval. It is however expected that the Monte Carlo simulations of a three stage model evolution can provide estimates for possible parameters in more complex evolution models.

The aims of the modeling were first to find estimates of the U/Pb and Th/U elemental fractionations in the history of the Mauna Kea end members and second to estimate the possible differentiation times of the Kea end members. In a three stage model of terrestrial Pb isotope evolution, the composition during the first stage from the formation of the solar

system to the beginning of the geologic record is difficult to evaluate. Questions about the Pb isotopic composition during this stage are complicated by uncertainties about the age of the Earth and the duration of the Earth accretion interval (Galer and Goldstein, 1996). Therefore, instead of using a fixed age, μ and k for the first stage, we used a range of Pb isotopic compositions at t_1 = 3.7 Ga as starting point for the second stage. In the model, this range of compositions is constrained by the measured range in Pb isotopic compositions of galenas from the Isua volcanics (Appel et al., 1978) and is also consistent with models of terrestrial Pb isotope evolution (Stacey and Kramers, 1975; Galer and Goldstein, 1996; Kramers and Tolstikhin, 1997). We therefore defined a "box" in Pb isotope space encompassing possible compositions at 3.7 Ga. For this "Archean box", we use $^{206}Pb/^{204}Pb$ ratios varying randomly between 11.151 and 11.434, $^{207}Pb/^{204}Pb$ = 12.998 to 13.345 and $^{208}Pb/^{204}Pb$ = 30.978 to 31.424. The Pb isotope evolution parameters for the second and third stage were allowed to vary freely within broad limits (μ between 4 and 20, κ between 2 and 5, t_2 between 0.01 and 3.69 Ga). From the Monte Carlo simulations, results that lay on the extensions of the Mauna Kea Pb isotope arrays as illustrated in Fig. 3.5a, b were selected to estimate the Pb isotope evolution of the Mauna Kea end member materials (Fig. 3.6, 3.9). Shown are 3000 models for the end members at the lower extension of the Pb isotope arrays and ~600 models for the upper end member. The evolution parameters (μ_2, μ_3, κ_2, κ_3 and t_2) of these models are used to estimate the Pb isotopic development of the Mauna Kea source. The possible μ-values during the evolution of the Mauna Kea source materials are shown in Fig. 3.6 and two example evolutions are shown in Fig. 3.9. The interdependence of the Pb isotope evolution parameters is shown in Fig. 3.9, as well.

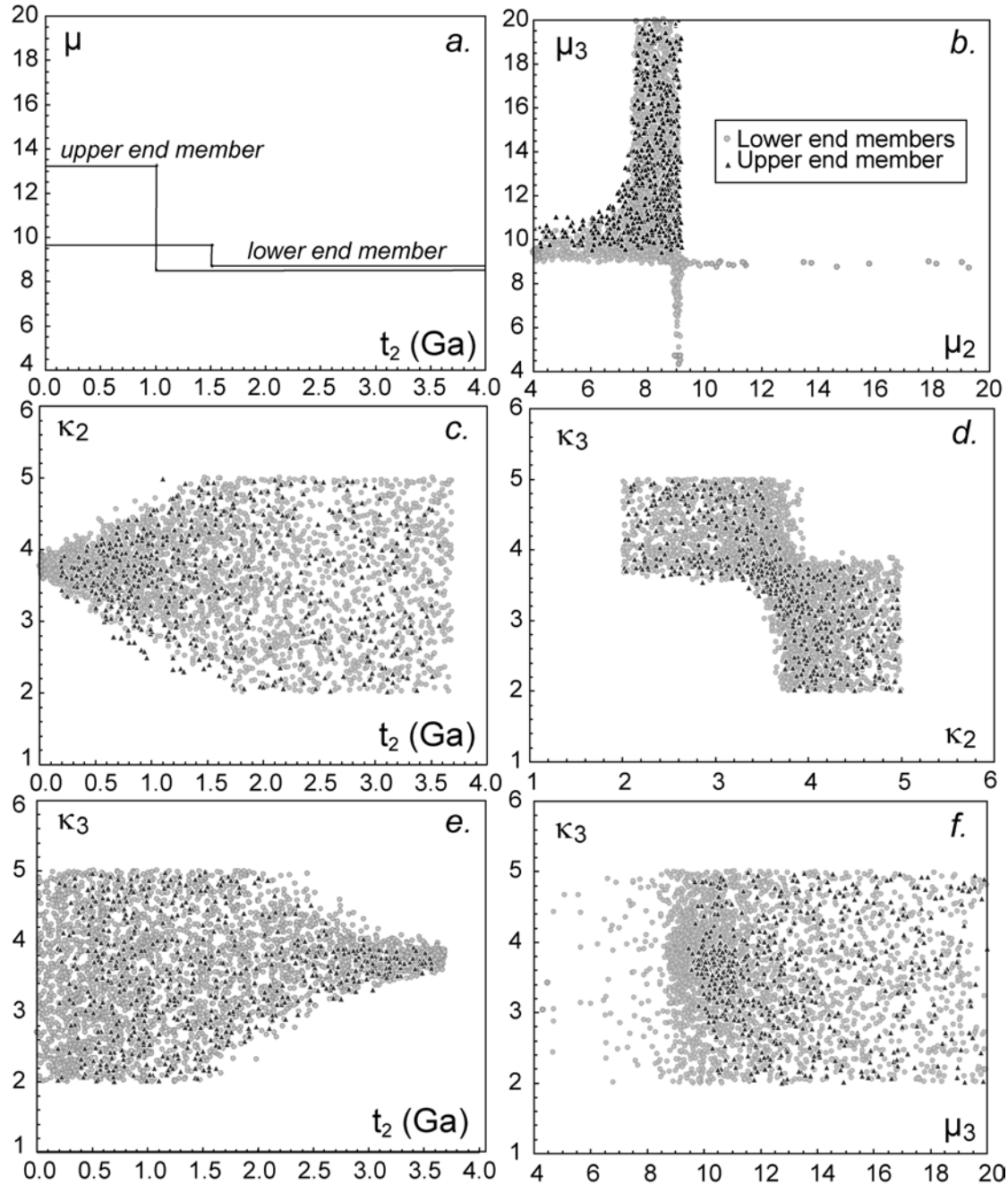

Fig. 3.9: The interdependence of evolution parameters in the Monte Carlo simulations of a three-stage Pb isotope evolution model. a. shows an example evolution for the lower and upper end member.

Appendix 3.D: Calculation of lengthscales of materials in the mantle source

In order to determine the position of Mauna Kea relative to a hypothetical plume center, we adopt the approach used by DePaolo et al. (2001). Figure 3.7b illustrates the path of movement of the Mauna Kea summit relative to the plume, as recorded in the HSDP-2 drill core. The x and y-coordinates of the volcano summit can be calculated as a function of time as

$$\begin{aligned} x(t) &= x_0 + \sin\alpha \cdot w \cdot t \\ y(t) &= y_0 - \cos\alpha \cdot w \cdot t \end{aligned} \tag{1}$$

where x_0 = -12330 m and y_0 = 54200 m is the present day position of Mauna Kea relative to the plume center. The plume center is chosen as the origin at (0|0). The angle of plate motion is $\alpha = 30°$. The plate velocity is w = 9 cm/yr, and t is age. The radial distance from the plume center can be calculated as function of time using

$$d(t) = \sqrt{(x_0 + \sin\alpha \cdot w \cdot t)^2 + (y_0 - \cos\alpha \cdot w \cdot t)^2} \tag{2}$$

The upwelling velocity structure in the mantle plume is described using two models, first flow similar to that through a pipe (constant viscosity, parabolic velocity structure approaching zero at the outer boundary) and second using an approximation to the model of Hauri et al. (1994) (temperature-dependent viscosity) (see Fig. 3.7d). We will first describe the pipe flow model. The equation describing the velocity of flow through a pipe as function of the radius (Kuchling, 1995) is

$$v(r) = -\frac{\Delta p}{4\mu}(R^2 - r^2) \tag{3}$$

where Δp is the pressure gradient in the pipe, μ is the viscosity and R is the radius of the pipe. This equation can be scaled to the maximum velocity at the center of the pipe v_{max}. When v_{max} is known, the pressure gradient becomes

$$\Delta p = -\frac{v_{\max} 4\mu}{R^2} \tag{4}$$

and substitution into equation (3) yields

$$v(r) = v_{\max} - \frac{v_{\max}}{R^2} r^2 \tag{5}$$

For the Hawaiian plume, we scaled this equation to fit the model of Hauri et al. (1994) for a distance between ~15 to 40 km radial distance from the plume center (see Fig. 3.7d), using v_{max} = 1m/yr and R = 40 km. For the Mauna Kea source sampled by HSDP-2, the radial distance from the plume center will be a function of time (equation (2)) and consequently, the upwelling velocity in the mantle source will be a function of distance and time as follows

$$v(d(t)) = v_{\max} - \frac{v_{\max}}{R^2}((x_0 + \sin\alpha \cdot w \cdot t)^2 + (y_0 - \cos\alpha \cdot w \cdot t)^2) \tag{6}$$

The lengthscale of an Pb isotope array in the Mauna Kea mantle source can then be calculated by integrating over a time-interval *l*

$$l = \int_{t_1}^{t_2} v_{\max} - \frac{v_{\max}}{R^2}((x_0 + \sin\alpha \cdot w \cdot t)^2 + (y_0 - \cos\alpha \cdot w \cdot t)^2)dt \tag{7}$$

This integral becomes

$$L = \int_{t_1}^{t_2} \left[\tfrac{1}{3} \cdot \left(-\frac{v_{\max}}{R^2}\sin^2\alpha w^2 - \frac{v_{\max}}{R^2}\cos^2\alpha w^2 \right) \cdot t^3 + \tfrac{1}{2} \cdot \left(-\frac{v_{\max}}{R^2} 2x_0 \sin\alpha w + \frac{v_{\max}}{R^2} 2x_0 \cos\alpha w \right) \cdot t^2 + \left(-\frac{v_{\max}}{R^2} x_0^2 - \frac{v_{\max}}{R^2} y_0^2 - v_{\max} \right) \cdot t \right] \tag{8}$$

The integral was solved for the time-intervals of the HSDP-2 Pb isotope arrays to yield the lengthscales of the material in the mantle source (Fig. 3.7e).

For a velocity structure in the mantle source assuming temperature-dependent viscosity, we used an approximation to the model of Hauri et al. (1994) (see Fig. 3.7d), which can be described by the equation

$$v(r) = 22 \cdot r^{-1} - 0.35 \tag{9}$$

For an estimation of the lengthscales in the mantle source with equation (9), we used a linear interpolation

$$l = \frac{v(t_1) + v(t_2)}{2} \Delta t \tag{10}$$

Finally, to determine the position of the HSDP-2 material in the past (Fig. 3.7f), the depth in the mantle source was calculated using

$$z = v(d(t)) \cdot (T - t) \tag{11}$$

where z is depth, *v(d(t))* is the mantle upwelling velocity, *t* is the age of a lava in the HSDP-2 core and *T* is the age at which the material was at depth *z* in the mantle.

3.6 References:

Abouchami, W., Galer, S. J. G. and Hofmann, A. W. (2000a): High precision lead isotope systematics of lavas from the Hawaiian Scientific Drilling Project, Chemical Geology 169, 187-209

Abouchami, W., Hofmann, A. W., Eisele, J. and Galer, S. J. G. (2000b): Long-term Pb isotope record of sources within the Hawaiian plume, Eos Trans. AGU, 81 (48), Fall Meet. Suppl., Abstract V21D-03

Appel, P. W. U., Moorbath, S. and Taylor, P. N. (1978): Least radiogenic terrestrial lead from Isua, West Greenland, Nature 272, 524-526

Blichert-Toft, J. and Albarède, F. (2000): High-Resolution Hf Isotope Stratigraphy of Mauna Kea Lavas From the Second Hawaii Scientific Drilling Project Core, Eos Trans. AGU, 81 (48), Fall Meet. Suppl., Abstract V12C-02

Bryce, J. G. and DePaolo, D. J. (2000): Sr and Nd variations in Mauna Kea lavas: Preliminary results from analyses from the 1999 Hawaii Scientific Drilling Project, Eos Trans. AGU, 81 (48), Fall Meet. Suppl., Abstract V12C-01

Chase, C. G. (1981): Oceanic island Pb: two-stage histories and mantle evolution, Earth and Planetary Science Letters 52, 277-284

Chauvel, C., Hofmann, A. W. and Vidal, P. (1992): HIMU-EM: the French Polynesian connection, Earth and Planetary Science Letters 110, 99-119

Chauvel, C., Goldstein, S. L. and Hofmann, A. W. (1995): Hydration and dehydration of oceanic crust controls Pb evolution in the mantle, Chemical Geology 126, 65-75

Chen, C.-Y., Frey, F. A., Rhodes, J. M. and Easton, R. M. (1996): Temporal geochemical evolution of Kilauea volcano: comparison of Hilina and Puna basalt, in: Earth Processes: Reading the Isotopic Code (eds Basu, A. and Hart, S. R.), Geophysical Monograph 95, American Geophysical Union, Washington DC , 161-181

Christensen, U. R. and Hofmann, A. W. (1994): Segregation of subducted oceanic crust in the

convecting mantle, Journal of Geophysical Research 99, 19867-19884

DePaolo, D. J. and Stolper, E. M. (1996): Models of Hawaiian volcano growth and plume structure: implications of results from the Hawaiian Scientific Drilling Project, Journal of Geophysical Research 101, 11643-11654

DePaolo, D. J., Bryce, J. G., Dodson, A., Shuster, D. L. and Kennedy, B. M. (2001): Isotopic evolution of Mauna Loa and the chemical structure of the Hawaiian plume, Geochemistry, Geophysics, Geosystems , Paper number 2000GC000139

Douglass, J. and Schilling, J.-G. (2000): Systematics of three-component, pseudo-binary mixing lines in 2D isotope ratio space representations and implications for mantle plume-ridge interaction, Chemical Geology 163, 1-23

Eiler, J. M., Farley, K. A., Valley, J. W., Hofmann, A. W. and Stolper, E. M. (1996): Oxygen isotope constraints on the sources of Hawaiian volcanism, Earth and Planetary Science Letters 144, 453-468

Gale, N. H. and Mussett, A. E. (1974): Episodic uranium-lead models and the interpretation of variations in the isotopic composition of lead in rocks, Reviews of Geophysics and Space Physics 11, 37-86

Galer, S. J. G. and O'Nions, R. K. (1985): Residence time of thorium, uranium and lead in the mantle with implications for mantle convection, Nature 316, 778-782

Galer, S. J. G. and Goldstein, S. L. (1996): Influence of accretion on lead in the Earth, in: Earth Processes: Reading the Isotopic Code (eds Basu, A. and Hart, S. R.), American Geophysical Union, Washington DC 95, 75-98

Galer, S. J. G. (1999): Optimal double and triple spiking for high precision lead isotopic measurement, Chemical Geology 157, 255-274

Hauri, E. H., Whitehead, J. A. and Hart, S. R. (1994): Fluid dynamic and geochemical aspects of entrainment in mantle plumes, Journal of Geophysical Research 99, 24275-24300

Hofmann, A. W. and Jochum, K. P. (1996): Source characteristics derived from very incompatible trace elements in Mauna Loa and Mauna Kea basalts, Hawaiian Scientific Drilling Project, Journal of Geophysical Research 101, 11831-11839

Hofmann, A. W. (1997): Mantle geochemistry: the message from oceanic volcanism, Nature 385, 219-228

Hofmann, A. W. (2001): Lead isotopes and the age of the Earth - a geochemical accident, in: Lewis, C. L. and Knell, S. J., (eds), The Age of the Earth: from 4004 BC to AD 2002, Geological Society, London, Special Publications, 190, 223-236 ,

Jochum, K. P., Hofmann, A. W. and Stoll, B. (2000): Trace Element Ratios from the Hawaii Scientific Drilling Project: Constraints on the Evolution of the Mauna Kea Volcano, Eos Trans. AGU, 81 (48), Fall Meet. Suppl., Abstract V11D-05 ,

Jones, C. E., Halliday, A. N., Rea, D. K. and Owen, R. M. (2000): Eolian inputs of lead to the

North Pacific, Geochimica et Cosmochimica Acta 64, 1405-1416

Keller, R. A., Fisk, M. R. and White, M. W. (2000): Isotopic evidence for Late Cretaceous plume-ridge interaction at the Hawaiian hotspot, Nature 405, 673-676

Kramers, J. D. and Tolstikhin, I. N. (1997): Two terrestrial lead isotope paradoxes, forward transport modelling, core formation and the history of the continental crust, Chemical Geology 139, 75-110

Kuchling, H. (1995): Taschenbuch der Physik, Fachbuchverlag Leipzig-Köln, 711 pp.

Kurz, M. D. and Kammer, D. P. (1991): Isotopic evolution of Mauna Loa volcano, Earth and Planetary Science Letters 103, 257-269

Kurz, M. D., Kenna, T. C., Kammer, D. P., Rhodes, M. J. and Garcia, M. O. (1995): Isotopic evolution of Mauna Loa volcano: a view from the submarine southwest rift zone, in: Mauna Loa Revealed: Structure, Composition, History and Hazards (eds Rhodes, J. M. and Lockwood, J. P.), Geophysical Monograph 92, American Geophysical Union, Washington DC, 289-306

Kurz, M. D. and Curtice, J. M. (2000): Helium Isotopic Evolution of Mauna Kea Volcano: New Results From the 3 km Drill Core, Eos Trans. AGU, 81 (48), Fall Meet. Suppl., Abstract V11D-09

Lassiter, J. C., DePaolo, D. J. and Tatsumoto, M. (1996): Isotopic evolution of Mauna Kea volcano: Results from the initial phase of the Hawaiian Scientific Drilling Project, Journal of Geophysical Research 101, 11769-11780

Lassiter, J. C. and Hauri, E. H. (1998): Osmium-isotope variations in Hawaiian lavas: evidence for recycled oceanic lithosphere in the Hawaiian plume, Earth and Planetary Science Letters 164, 483-496

McDonough, W. F. and Chauvel, C. (1991): Sample contamination explains the Pb isotopic composition of some Rurutu island and Sasha seamount basalt, Earth and Planetary Science Letters 105, 397-404

Morgan, W. J. (1971): Convection plumes in the lower mantle, Nature 230, 42-43

Pietruszka, A. J. and Garcia, M. O. (1999): A rapid fluctuation in the mantle source and melting history of Kilauea volcano inferred from the geochemistry of its historical summit lavas, Journal of Petrology 40, 1321-1342

Regelous, M., Hofmann, A. W., Abouchami, W. and Galer, S. J. G. (submitted): Geochemistry of lavas from the Emperor seamounts and the geochemical evolution of Hawaiian magmatism 85-42 Ma, Journal of Petrology

Rhodes, J. M. and Hart, S. R. (1995): Episodic trace element and isotopic variations in historical Mauna Loa lavas: implications for magma and plume dynamics, in: Mauna Loa Revealed: Structure, Composition, History and Hazards (eds Rhodes, J. M. and Lockwood, J. P.), Geophysical Monograph 92, American Geophysical Union, Washington DC, 263-288

Ribe, N. M. and Chistensen, U. R. (1999): The dynamical origin of Hawaiian volcanism, Earth and Planetary Science Letters 171, 517-531

Stacey, J. S. and Kramers, J. D. (1975): Approximation of terrestrial lead isotope evolution by a two-stage model, Earth and Planetary Science Letters 26, 207-221

Stille, P., Unruh, D. M. and Tatsumoto, M. (1986): Pb, Sr, Nd and Hf isotopic constraints on the origin of Hawaiian basalts and evidence for a unique mantle source, Geochimica et Cosmochimica Acta 50, 2303-2319

Tatsumoto, M. (1978): Isotopic composition of lead in oceanic basalt and its implication to mantle evolution, Earth and Planetary Science Letters 38, 63-78

Thirlwall, M. F. (1997): Pb isotopic evidence for OIB derivation from young HIMU mantle, Chemical Geology 139, 51-74

Woodhead, J. D. (1996): Extreme HIMU in an oceanic setting: the geochemistry of Mangaia Island (Polynesia) and temporal evolution of the Cook-Austral hotspot, Journal of Volcanology and Geothermal Research 72, 1-19

Chapter 4: A new look at South Pacific OIB sources in Pb isotope space

Jürgen Eisele, Catherine Chauvel, Stephen J. G. Galer and Albrecht W. Hofmann

Abstract

We report Pb isotope data of HIMU-type ocean island basalts (OIB) from Rurutu Island (French Polynesia), obtained using a triple-spike technique for correction of instrumental mass fractionation. The Rurutu lavas yield $^{206}Pb/^{204}Pb$ ratios of 20.29 to 21.39 and show linear arrays in $^{207}Pb/^{204}Pb$-$^{206}Pb/^{204}Pb$ and $^{208}Pb/^{204}Pb$-$^{206}Pb/^{204}Pb$ spaces, which we interpret as mixing arrays.

Rurutu Island is located in the Austral chain, which is superimposed on the bathymetric anomaly called the South Pacific Superswell. We compare the data from Rurutu with other high-precision Pb isotope analyses from islands of the South Pacific Superswell (Mangaia in the Austral chain and Pitcairn in the Pitcairn-Gambier chain) and with analyses from the HIMU island St. Helena, located in the South Atlantic. The data from these four volcanoes all show linear arrays in Pb isotope space. The HIMU arrays defined by Rurutu, Mangaia and St. Helena are similar, but do not share identical end members in 3D Pb isotope space. As previously suggested (Chauvel et al., 1992 among others), the isotopic signature of the HIMU source is best interpreted in terms of old recycled oceanic crust, while the EM-1 source sampled by Pitcairn is likely to be strongly influenced by recycled pelagic sediment. We show that the recycled materials in the source of Rurutu and Pitcairn may have a similar age lying between 1 and 2 Ga. The hotspot volcanoes of the South Pacific Superswell may therefore not only result from one large geophysical anomaly, but they might also originate from a single but geochemically heterogeneous source. The recycled oceanic crust and sediments may have been subducted in a similar time and place in Earth history and may have aggregated in the lower mantle now reappearing as the largest isotope heterogeneities in OIB.

While one end member of each mixing array defined at Rurutu, Mangaia and Pitcairn is likely to be recycled material, the end member that is generally located in the middle of the OIB field is not identical for the three islands. This argues against the concept of a common

component for OIB (such as FOZO or C), and suggests that the mantle is heterogeneous throughout.

4.1 Introduction

In the Austral-Cook, Pitcairn-Gambier volcanic chains and in the Society Islands in the South Pacific, the whole range of isotopic variability observed in ocean island basalts occurs in an area that represents less than 1% of the total ocean floor. After the introduction of the concept of plate tectonics, the three volcanic chains (Fig. 4.1) were viewed as hotspot tracks of independent mantle diapirs (Wilson, 1963; Duncan et al., 1974). When the anomalously shallow bathymetry of the southwestern Pacific seafloor was recognized (Fig. 4.1), a link between the different hotspots was proposed and this lead to the concept of a South Pacific "Superswell" located above a large-scale mantle upwelling (McNutt and Fisher, 1987). A genetic link between the bathymetric signal and the isotopic anomalies was proposed by Staudigel et al. (1991) and called South Pacific Thermal and Isotopic Anomaly (SOPITA). However, the question remains open: if the Polynesian volcanic chains are related to the same geophysical signal – the Superswell – why are they geochemically so heterogeneous?

Chauvel et al. (1992) first suggested that the OIB sources in the French-Polynesian region represented subducted oceanic crust and sediments and that a genetic link existed between these sources. Here we present new triple-spike Pb isotopic data for Rurutu lavas, and we compare them with high-precision Pb isotopic data from Pitcairn (Woodhead and Devey, 1993; Eisele et al., submitted), Mangaia (Woodhead, 1996) and further with data from St. Helena (Thirlwall, 2000), located in the South Atlantic. These new data should provide tight constraints on the nature of the mantle sources and their potential relationships.

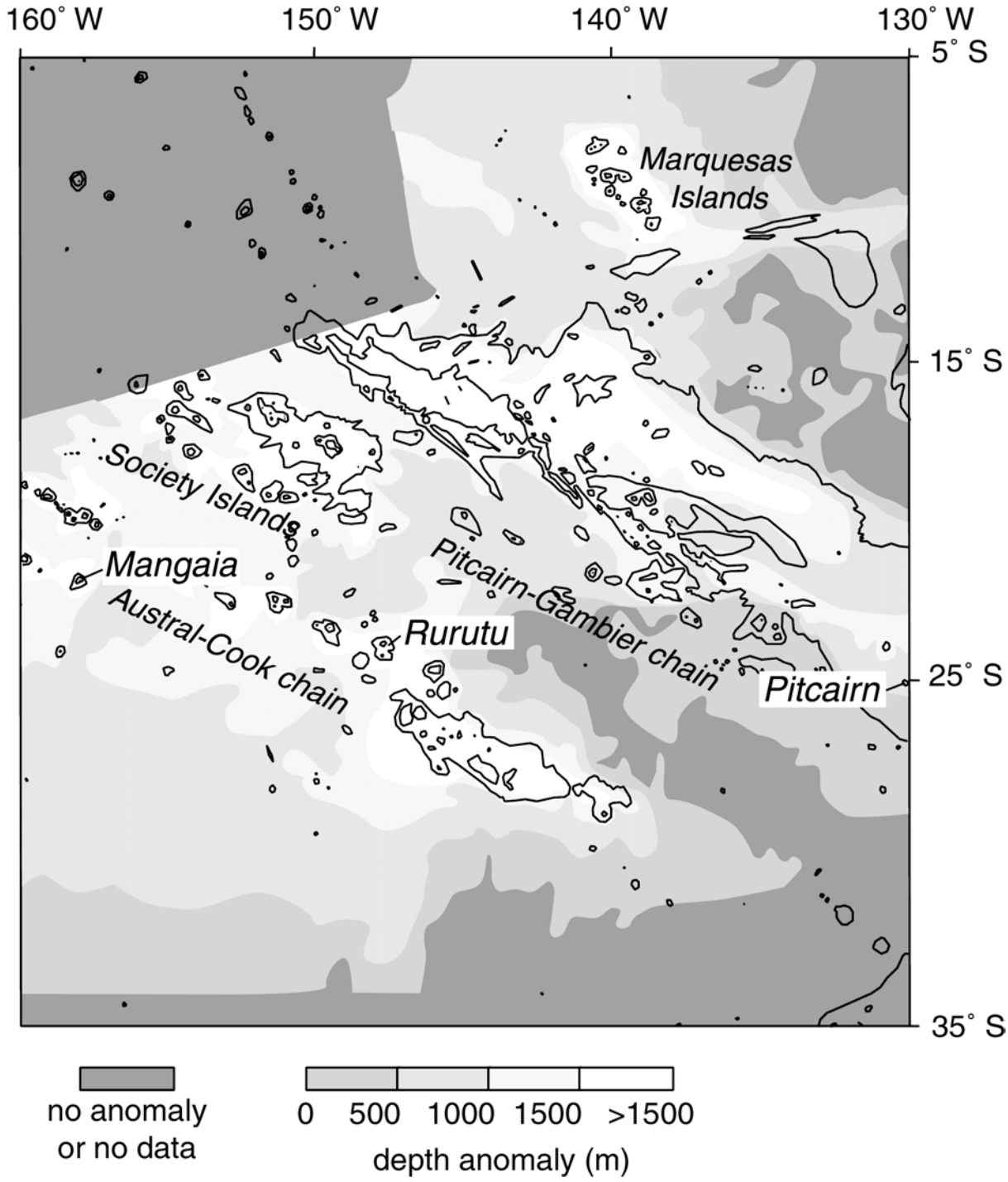

Fig. 4.1: Bathymetry of the South Pacific ocean floor (0, 2000, 4000 m contours) showing the depth anomalies of the South Pacific Superswell reported by Sichoix et al. (1998). Locations of Rurutu and Mangaia islands in the Austral chain and of Pitcairn island in the Pitcairn-Gambier chain are also shown.

4.2 Pb isotopic composition of the Rurutu lavas

The lavas analyzed in this study come from both old and young volcanic activities recorded on Rurutu Island. The older volcanics have an age of 8-14 Ma, while the younger volcanics erupted 1-2 Ma ago (Chauvel et al., 1997). Major and trace elements as well as Sr, Nd and conventionally-obtained Pb isotopic compositions of the Rurutu lavas were previously analyzed (Chauvel et al., 1997). We here present triple-spike Pb isotope analyses of hand-picked rock chips that were strongly leached before dissolution. Analytical methods followed the procedures described by Abouchami et al. (2000). Pb isotopic compositions were corrected for instrumental mass bias using a triple-spike technique (Galer, 1999), which greatly improves the external reproducibility. We performed an age-correction for in-growth of radiogenic Pb since eruption on the measured Pb isotopic ratios of the samples (see Appendix 4.A) using the U, Th and Pb concentrations and ages reported by Chauvel et al. (1997) (see Table 4.1). The age correction reduces the $^{206}Pb/^{204}Pb$ ratios of the old Rurutu volcanics by about 0.04, the $^{208}Pb/^{204}Pb$ ratios by about 0.06, while there is little change in the $^{207}Pb/^{204}Pb$ ratios. There may be some uncertainty on the measured Th, U and Pb abundances, translating into an uncertainty of the age correction. However, this uncertainty is supposedly only a fraction of the correction (e.g. much smaller than 0.04 for the $^{206}Pb/^{204}Pb$ ratios) and therefore close to the precision of the Pb isotopic measurement. The age correction is small, but necessary e.g. when comparing the high-precision arrays of Mangaia and Rurutu (see below).

As was described by Chauvel et al. (1997), the old Rurutu lavas yield very radiogenic initial Pb isotopic compositions. The triple-spike analyses yield ratios of $^{206}Pb/^{204}Pb$ = 20.86 to 21.39, while the young Rurutu lavas are less extreme ($^{206}Pb/^{204}Pb$ = 20.29 to 20.36) (Table 4.1). There is an offset between the conventional data and the triple-spike data which is indicated by the lines in Fig. 4.2. This offset results from the fractionation correction using the triple-spike technique. While the overall ranges of the Pb isotope ratios is almost identical for

Table 4.1: Pb isotopic compositions of Rurutu samples

Sample	Age (Ma)	$^{206}Pb/^{204}Pb$	2σ	$^{207}Pb/^{204}Pb$	2σ	$^{208}Pb/^{204}Pb$	2σ	μ	ω	κ*	$(^{206}Pb/^{204}Pb)_i$	$(^{207}Pb/^{204}Pb)_i$	$(^{208}Pb/^{204}Pb)_i$	$^{208}Pb^*/^{206}Pb^*$
Old volcanics														
74-386	8.4	21.0316	8	15.7621	8	40.2626	26	29	97	3.4	20.9941	15.7603	40.2222	0.9196
74-390	12	21.0982	7	15.7710	7	40.3271	23	30	132	4.4	21.0425	15.7684	40.2484	0.9180
74-396	12	21.4326	8	15.8033	9	40.5185	28	25	84	3.3	21.3859	15.8011	40.4688	0.9102
RR 03	12.42	20.9921	9	15.7578	9	40.2249	28	32	119	3.7	20.9308	15.7550	40.1520	0.9186
RR 67	*11*	20.9750	14	15.7529	13	40.1965	40	*26*	*95*	*3.7*	20.9306	15.7508	40.1448	0.9179
RRT-32	14.2	21.0654	10	15.7773	18	40.3095	29	28	101	3.6	21.0032	15.7745	40.2383	0.9202
RRT-37	11.3	20.9129	8	15.7491	8	40.1931	25	30	106	3.6	20.8609	15.7467	40.1338	0.9225
Young volcanics														
120D	*1.5*	20.3001	8	15.6764	8	39.7772	27	40	147	3.7	20.2908	15.6760	39.7664	0.9370
122M	*1.5*	20.3036	9	15.6786	9	39.7815	28	36	144	4.0	20.2952	15.6782	39.7707	0.9370
74-388	1.07	20.3701	11	15.6876	12	39.8411	37	36	117	3.2	20.3641	15.6873	39.8349	0.9369
74-393	2.1	20.3392	13	15.6896	12	39.8375	35	41	154	3.8	20.3260	15.6890	39.8214	0.9390
RRT-60	1.16	20.3362	10	15.6838	9	39.8193	27	40	147	3.7	20.3290	15.6835	39.8109	0.9377

Regression parameters for the Rurutu Pb isotope array

n	$^{207}Pb/^{206}Pb$ slope	$\chi^2_{red.}$	age (Ga)	$^{208}Pb/^{206}Pb$ slope	$\chi^2_{red.}$	κ
12	0.117±7	19	1.91±0.11	0.619±28	32	2.15

μ, ω and κ* values, initial Pb isotopic ratios and Th/U ratios are calculated from trace element concentrations and ages reported by Chauvel et al. (1997). Numbers in italics are assumed values for age, μ, ω and κ* where no data exist. The isotopic ratios of the NIST NBS-981 measured with the samples were $^{206}Pb/^{204}Pb$ = 16.9417±12, $^{207}Pb/^{204}Pb$ = 15.4980±15 and $^{208}Pb/^{204}Pb$ = 36.7265±25 (N = 5), within error of the values reported by Galer and Abouchami (1998) and Eisele et al. (submitted). The procedural blank contained ~10 pg Pb and is negligible relative to the amount of Pb present in the samples.

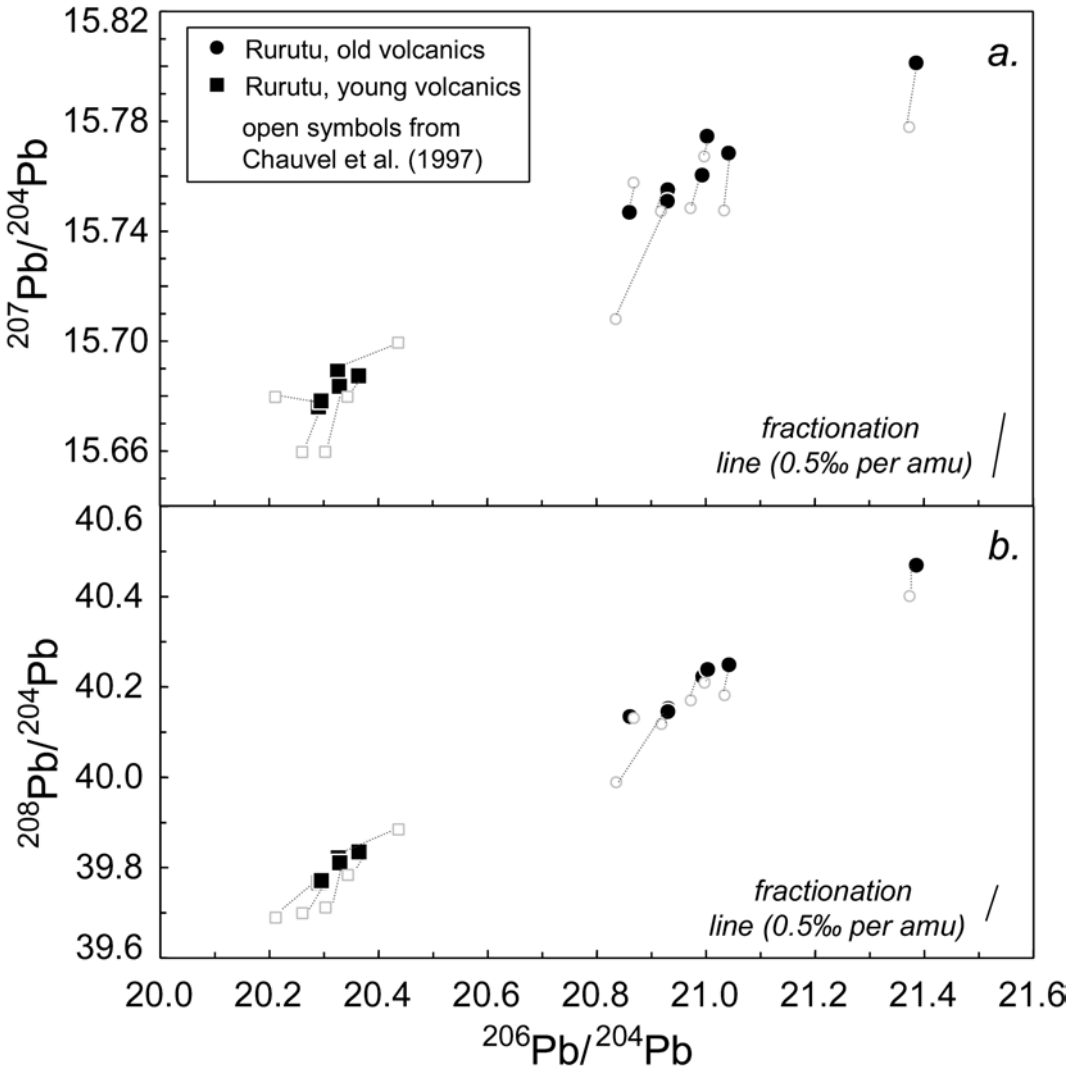

Fig. 4.2: Pb isotopic composition of old and young Rurutu lavas measured using a triple-spike technique. The new data are compared to the published conventional data (Chauvel et al., 1997). Both datasets were corrected for radiogenic ingrowth of Pb since eruption. Also indicated is a fractionation offset in Pb isotope space by 0.5 ‰ per amu. Many of the samples analyzed with the triple-spike technique move along fractionation trends. The scatter of the data is reduced to form a linear array.

the conventional and triple-spike data, many samples move along fractionation trends when corrected by the triple-spike technique (Fig. 4.2), and the scatter of the data Pb-Pb isotope space is reduced to a linear array. The Rurutu lavas define linear arrays in both $^{207}Pb/^{204}Pb$-$^{206}Pb/^{204}Pb$ and $^{208}Pb/^{204}Pb$-$^{206}Pb/^{204}Pb$ spaces (Fig. 4.2). Linear regressions of the triple-spike Pb isotope data yields a slope of 0.117±7 in $^{207}Pb/^{204}Pb$-$^{206}Pb/^{204}Pb$ space and a slope of 0.619±28 in $^{208}Pb/^{204}Pb$-$^{206}Pb/^{204}Pb$ space (see Table 4.1). The regression lines in Pb isotope space can theoretically yield ages. Also, the κ-value ($\equiv(^{232}Th/^{238}U)_{today}$) can be calculated when an age and the slope of the array in $^{208}Pb/^{204}Pb$-$^{206}Pb/^{204}Pb$ space is known (see Appendix 4.B for details).

4.3 Discussion

4.3.1 Linear arrays: mixing or isochrons?

For some OIB sources, it has recently been proposed that the Pb isotope arrays result from melting of complete sections of recycled oceanic lithosphere (Chauvel and Hémond, 2000), and that the slopes of the Pb isotopic arrays therefore may record the age of the recycled material (Geldmacher and Hoernle, 2000). For the Pb isotopic arrays defined by the Rurutu lavas, this hypothesis can be tested by comparing the κ implied by the slope of the $^{208}Pb/^{204}Pb$-$^{206}Pb/^{204}Pb$ array to the measured Th/U ratio (see Table 4.1), as was described by Abouchami et al. (2000). If the values for κ and κ* (relating to the measured Th/U ratio) are similar, then the Pb isotopic array may represent an isochron (see Appendix 4.B for explanation). The hypothesis that the Pb isotopic array represents an internal isochron of the recycled material unfortunately fails in the case of the Rurutu lavas, because the κ implied by the $^{208}Pb/^{204}Pb$-$^{206}Pb/^{204}Pb$ slope is 2.15, and the measured κ*-values range between 3.2 and 4.4 (see Table 4.1). This interpretation is of course dependent on the assumption that the measured Th/U ratios in the Rurutu lavas represent primary values and were not strongly influenced by weathering. However, in order to match κ and κ*, *all* the samples would have

to have lost an appreciable amount of U, which appears unlikely. The Pb isotope arrays of Rurutu lavas are therefore interpreted to represent mixing lines.

The old and young Rurutu lavas show almost identical regression lines in Pb isotope space. If young and old Rurutu lavas share the same mixing arrays, then they sample similar end members in Pb isotope space (Fig. 4.2). It is difficult to evaluate, whether the end members are identical or only very similar even with the triple-spike technique. Subtle differences might exist between the mixing end members for the old and young lavas, but we will treat them as defining a single Pb isotope array, although there are differences in $^{206}Pb/^{204}Pb$ ratios between old and recent lavas.

4.3.2 Are all HIMU sources alike?

When comparing high-precision Pb isotope data reported on three HIMU islands - Rurutu (this study), Mangaia (Woodhead, 1996) and St. Helena (Thirlwall, 2000) - it is immediately obvious that all three datasets define linear arrays in Pb isotope space (Fig. 4.3). However, in 3D Pb isotope space, the three arrays are not identical. St. Helena lavas yield higher $^{207}Pb/^{204}Pb$ ratios any given $^{206}Pb/^{204}Pb$ ratio than Rurutu and Mangaia basalts (Fig. 4.3a). The St. Helena Pb isotope array (Thirlwall, 2000) is offset from the Rurutu array by 0.02 in $^{207}Pb/^{204}Pb$ ratio and by 0.3 in $^{206}Pb/^{204}Pb$ ratio. Such differences may be explained by relatively small variations in the μ value ($(\equiv^{238}U/^{204}Pb)_{today}$) in the past. Assuming that the difference between the arrays was created in the last 1 Ga, a 20 % lower μ value for the St. Helena source would have been sufficient (e.g. $[^{206}Pb/^{204}Pb]_{initial}$ = 17.2, $[^{207}Pb/^{204}Pb]_{initial}$ = 15.5, $\mu_{St.Helena}$= 20, μ_{Rurutu} = 24) to result in different $^{206}Pb/^{204}Pb$ ratios of 20.6 and 21.2, and corresponding $^{207}Pb/^{204}Pb$ ratios of 15.74 and 15.79 at the present day.

Mangaia lavas have lower $^{208}Pb/^{204}Pb$ ratios at a given $^{206}Pb/^{204}Pb$ ratio than Rurutu and St. Helena lavas (Fig. 4.3b). The offset in $^{206}Pb/^{204}Pb$ ratio between the two arrays is about 0.2, while the difference in $^{208}Pb/^{204}Pb$ ratios is about 0.1. Such a difference can be

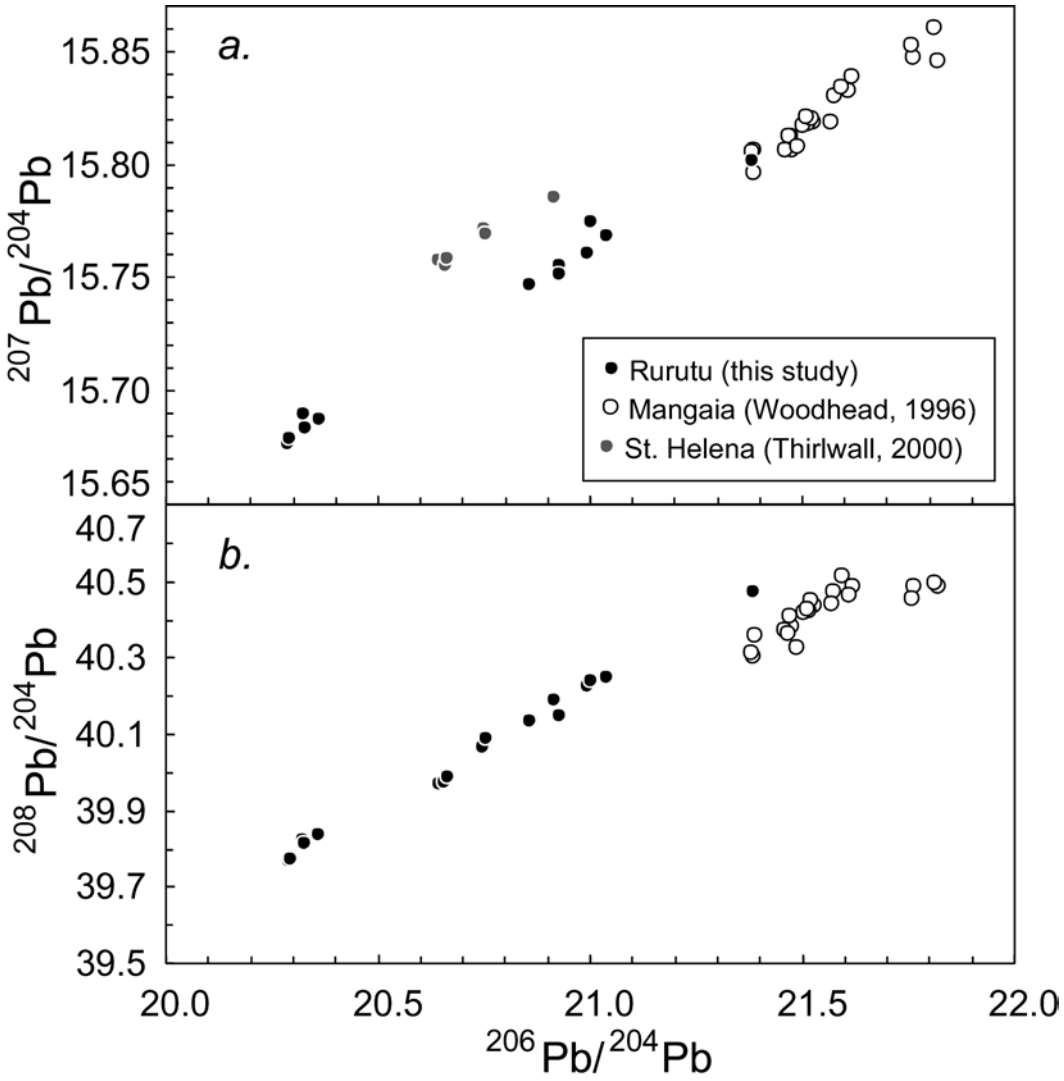

Fig. 4.3: Comparison of high-precision Pb isotope data from HIMU ocean island basalts. Mangaia data (Woodhead, 1996) were corrected for radiogenic ingrowth of Pb since eruption and corrected for offset of the NBS-981 standard between Woodhead (1996) ($^{206}Pb/^{204}Pb$ = 16.937, $^{207}Pb/^{204}Pb$ = 15.492 and $^{208}Pb/^{204}Pb$ = 36.708) and this study (see Table 4.1 for Standard values). St. Helena data from (Thirlwall, 2000) are not age-corrected because no U/Pb ratios were reported. The offset between Rurutu/Mangaia and St. Helena data in $^{207}Pb/^{204}Pb$-$^{206}Pb/^{204}Pb$ space may be greater than shown, because age-correction would lower the $^{206}Pb/^{204}Pb$ ratios of the samples, while $^{207}Pb/^{204}Pb$ ratios would remain relatively constant. All three sample suites form linear arrays in Pb isotope space, that are similar but not identical.

explained by slightly lower κ values for the Mangaia source. Assuming that the offset between the Rurutu and Mangaia sources was produced in the last 1 Ga, a homogeneous μ for both sources, but a 3 % lower Th/U ratio for the Mangaia source could explain the offset. For example, an evolution with $[^{206}Pb/^{204}Pb]_{initial} = 18$, $[^{207}Pb/^{204}Pb]_{initial} = 15.57$, $[^{208}Pb/^{204}Pb]_{initial} = 37$, $\mu = 20$, $\kappa_{Mangaia} = 3.35$, $\kappa_{Rurutu} = 3.45$ since 1 Ga would result in the same $^{206}Pb/^{204}Pb$ and $^{207}Pb/^{204}Pb$ ratios of 21.4 and 15.8 for both sources, but in different $^{208}Pb/^{204}Pb$ ratios of 40.4 and 40.5.

It is striking that the Pb isotope arrays formed by the HIMU islands yield linear arrays with similar slopes. Even though we do not interpret the Pb isotope arrays as representing isochrons, their similarity implies that the mixing end members at the extensions of the arrays had similar (though not identical) U/Pb and Th/Pb ratios in the past and differentiated at a similar time.

4.3.3 South Pacific Pb isotope arrays

Rurutu samples have $^{206}Pb/^{204}Pb$ ratios varying from 20.29 to 21.39, whereas samples from Pitcairn have much lower $^{206}Pb/^{204}Pb$ ratios ranging from 17.5 to 18.5 (Woodhead and McCulloch, 1989; Woodhead and Devey, 1993; Eisele et al., submitted). These two islands are characteristic of the HIMU and EM-1 end members (White, 1985; Zindler and Hart, 1986) and represent the most extreme of Pb isotopic compositions known in ocean island basalts (Fig. 4.4). Pb isotope analyses for Mangaia Island yield the most radiogenic isotope signature in the Austral chain (Woodhead, 1996). All three volcanic islands produce linear arrays in $^{207}Pb/^{204}Pb$-$^{206}Pb/^{204}Pb$ space (Fig. 4.4a). In $^{208}Pb/^{204}Pb$-$^{206}Pb/^{204}Pb$ space, Rurutu and Mangaia samples show linear arrays with a positive slope and Pitcairn samples have a roughly horizontal extension (Fig 4b). The linear arrays are best interpreted as mixing arrays, implying that the Pb isotope signature of each island is produced by mixing of two end members with different U-Th-Pb ratios. Recently, Saal et al. (1998) documented large Pb isotope variations

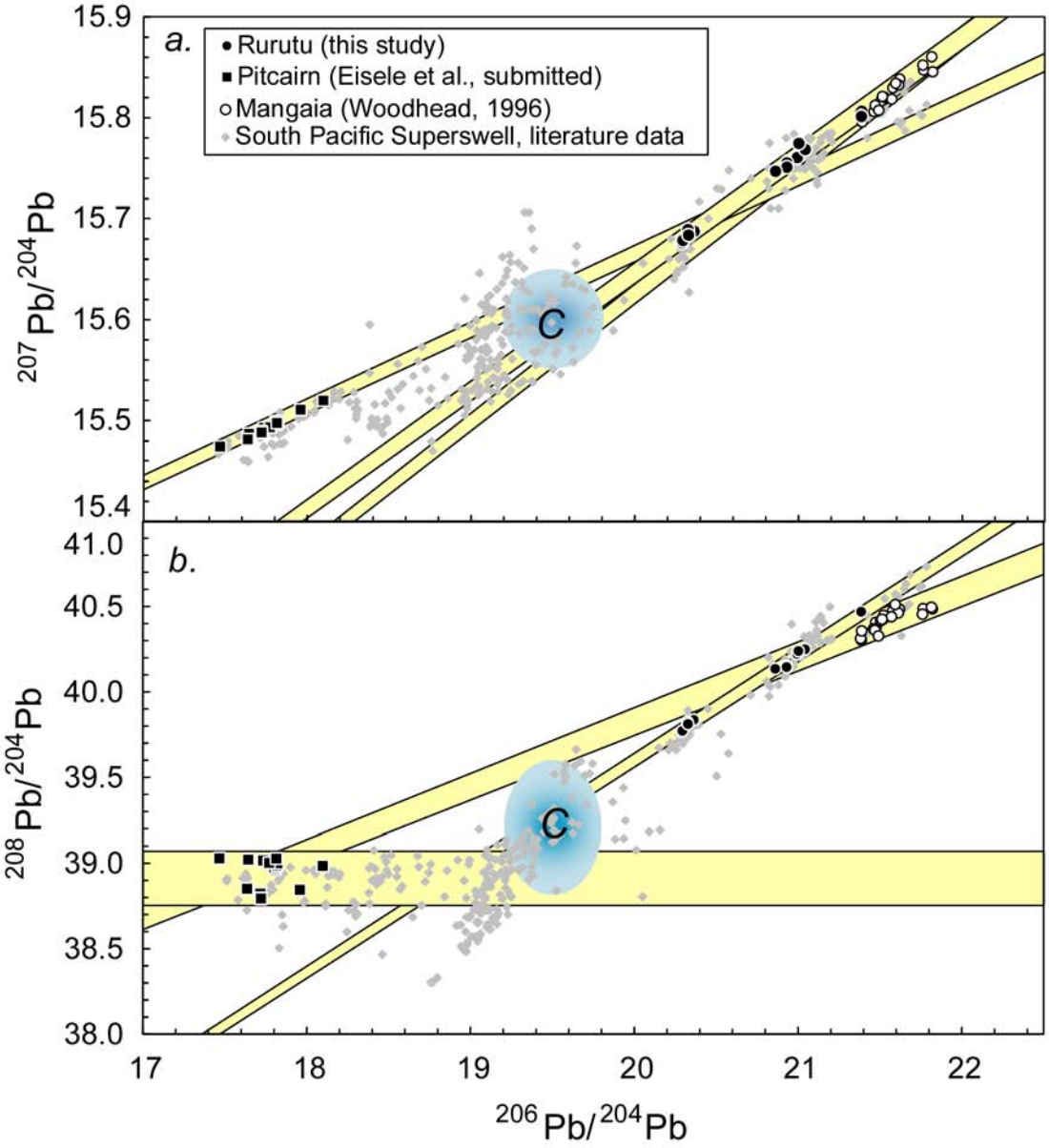

Fig. 4.4: (a) $^{207}Pb/^{204}Pb$ versus $^{206}Pb/^{204}Pb$ and (b) $^{208}Pb/^{204}Pb$ versus $^{206}Pb/^{204}Pb$ diagrams for Polynesian islands. Regression lines and their confidence intervals for the Pb isotope arrays for Rurutu, Pitcairn (Eisele et al., submitted) and Mangaia (Woodhead, 1996) are shown. The Pb isotope arrays do not intersect at a single point in both parts of the figure, and they intersect at different values in the two diagrams. Also shown are Pb isotope data for the entire South Pacific Superswell (Chauvel et al., 1992; Devey et al., 1990; Dupuy et al., 1993; Hémond et al., 1994; Kogiso et al., 1997a; Nakamura and Tatsumoto,1988; Palacz and Saunders, 1986; Schiano et al., 2001; Vidal et al., 1984; White and Duncan, 1996; Woodhead and McCulloch 1989; Woodhead and Devey, 1993; Woodhead, 1996;) together with the C component of Hanan and Graham (1996).

in melt inclusions in two samples from Mangaia island and Tahaa (Society Islands), spanning the entire range of Pb isotope variations between the EM-2 and HIMU end members. Saal et al. interpreted the Pb isotopic variations as essentially binary mixing arrays for both islands. The higher resolution of the triple-spike technique may put constraints on the exact position of the end members required. In the following, we will discuss the possible origin of the most extreme compositions that define the HIMU and EM1 end members. We will then evaluate the origin of the other end member for each Pb isotope array and discuss the possibility that this end member is shared by different arrays.

4.3.3.1 The HIMU and EM-1 end members

As previously suggested (Chauvel et al., 1992, 1995; Woodhead, 1996), the HIMU Pb isotopic signature is best explained by a process in which the mantle source lost Pb in the distant past but kept a relatively unmodified Th/U ratio. This process is interpreted to occur during alteration, subduction and recycling of oceanic crust (Chauvel et al., 1992; Hémond et al., 1994; Woodhead, 1996; Kogiso et al., 1997a; Schiano et al., 2001). Experimental and geochemical data (Kogiso et al., 1997b; Mühe et al., 1997) indeed show that Pb is lost from the oceanic crust during hydrothermal alteration and/or subduction, and that this loss can produce the high time-integrated U/Pb ratios of the HIMU source.

The element fractionation required to produce the Pb isotope signature of the EM-1 source of Pitcairn (low recent μ of ~1 to 7) is best interpreted as an U loss associated with an unchanged Th/Pb ratio (Woodhead and McCulloch, 1989; Eisele et al., submitted). These features are found in materials with a continental origin, and involvement of continentally-derived material in the EM sources is widely accepted (e.g. Hémond et al., 1994; White and Duncan, 1996). The isotopic and trace element characteristics of Pitcairn lavas have therefore been explained by the presence of recycled pelagic sediments in the source (Woodhead and McCulloch, 1989; Woodhead and Devey, 1993; Eisele et al., submitted).

4.3.3.2 The unknown "other" end member

For each of the Pb isotope arrays defined by Rurutu, Pitcairn and Mangaia, the existence of an end member internal to the OIB field could be argued (Fig. 4.4). But if one end member of the Pb isotopic arrays of Rurutu, Pitcairn and Mangaia is recycled material, what is the end member that is internal to the OIB field? Chauvel et al. (1997) suggested that the young Rurutu lavas with lower $^{206}Pb/^{204}Pb$ ratios (Fig. 4.2) incorporated new plume-derived material with isotopic characteristics similar to "Atiu-trend" lavas ($^{206}Pb/^{204}Pb$ ~19 to 20). This component could have mixed with remnants of the old volcanic activity stored as carbonatites in the oceanic lithosphere, which were remobilized by the arising melts. This model provides an explanation for the similarity of the radiogenic Pb isotope end members of the young and old Rurutu lavas. However, the meaning of the lower end member of the arrays or the meaning of the Atiu-trend Pb isotopic signature is still unresolved. Using combined isotopic constraints, Schiano et al. (2001) argued that this end member, most purely represented by Rarotonga lavas, could contain recycled subcontinental lithospheric mantle. On the basis of the Pb isotope data presented here it is not possible to evaluate, what exactly the meaning of the unradiogenic end member of the HIMU arrays may be. However, it appears that this end member may represent mantle material that contains less recycled oceanic crust compared to the extreme HIMU composition.

4.3.4 Evidence for a common end member in Pb isotope space?

Besides the four mantle components for OIB – EM1, EM2, HIMU and DMM (Zindler and Hart, 1986) – Hart et al. (1992) argued for a fifth mantle species that can be recognized in multi-isotope space. This mantle species was called a Focus Zone (FOZO), because many OIB suites appear to converge towards it. Similarly, Hanan and Graham (1996) argued that the Pb isotope systematics of MORB and OIB show a "common component" ("C") towards which many volcanic suites converge in Pb isotope space. This common component is

thought to be derived from the middle or deep mantle. Because the Pb isotopic arrays of Rurutu, Pitcairn and Mangaia form well-defined linear arrays, we can evaluate whether these arrays converge to a single point in Pb isotope space (Fig. 4.4). This would be a hint that at least at a more limited scale (the South Pacific Superswell) there is evidence for homogeneous material incorporated in the sources of Rurutu, Mangaia and Pitcairn.

The regression lines of the three volcanic islands are shown in Figure 4.4. We determined confidence intervals for the regression lines, taking into account the error on the intercept, but not on the slope of the regression line. If the error on the slope would be taken into account, as well, the confidence intervals would fan out, especially in $^{208}Pb/^{204}Pb$-$^{206}Pb/^{204}Pb$ space, when extrapolated over more than two $^{206}Pb/^{204}Pb$ units. The lines are well defined in $^{207}Pb/^{204}Pb$-$^{206}Pb/^{204}Pb$ space and the confidence intervals of the regressions are relatively narrow (Fig. 4.4a). While the arrays for Rurutu and Mangaia are almost identical in $^{207}Pb/^{204}Pb$-$^{206}Pb/^{204}Pb$ space, the Pitcairn array intersects the two HIMU arrays at $^{206}Pb/^{204}Pb$ of about 20.5. This value is relatively close to the proposed FOZO or C component ($^{206}Pb/^{204}Pb$ ratio ~19.6 and $^{207}Pb/^{204}Pb$ ratio ~15.6 (Fig. 4.4)). It is however not identical and none of the Pb isotopic arrays pierces the exact location of FOZO in $^{207}Pb/^{204}Pb$-$^{206}Pb/^{204}Pb$ space.

In $^{208}Pb/^{204}Pb$-$^{206}Pb/^{204}Pb$ space the Rurutu array is quite well defined. However, this is not the case for the Mangaia array because two samples (Woodhead, 1996) with the highest $^{206}Pb/^{204}Pb$ ratios have lower $^{208}Pb/^{204}Pb$ ratios and do not lie on the same array as the other Mangaia samples (Fig 4b). Similarly, some samples from the Pitcairn seamounts have lower $^{208}Pb/^{204}Pb$ ratios than the other Pitcairn samples (Woodhead and Devey, 1993; Eisele et al., submitted), and not all the data form a coherent array. Therefore, the regressions of the Mangaia and Pitcairn arrays form broad bands in $^{208}Pb/^{204}Pb$-$^{206}Pb/^{204}Pb$ space. However, even with the uncertainty of the exact slopes of the arrays in $^{208}Pb/^{204}Pb$-$^{206}Pb/^{204}Pb$ space, it appears to remain that the Pitcairn array intersects with the Rurutu and Tubuai arrays at

$^{206}Pb/^{204}Pb$ ratios significantly lower than 20.5, the intersection point defined in $^{207}Pb/^{204}Pb$-$^{206}Pb/^{204}Pb$ space.

The three arrays converge at values close to the proposed FOZO end member in Pb-Pb isotope space, but do not match it exactly, nor do the three arrays intersect at a single point. Also, none of the arrays intersect at the same $^{206}Pb/^{204}Pb$ ratio in both $^{207}Pb/^{204}Pb$-$^{206}Pb/^{204}Pb$ and $^{208}Pb/^{204}Pb$-$^{206}Pb/^{204}Pb$ spaces. We therefore regard the existence of a homogenous "common component" with a physical meaning in the mantle source of the South Pacific Superswell OIB unlikely. Rather, the HIMU end members as well as the end members internal to the OIB field appear to differ for each volcanic island.

4.3.5 Age model for Rurutu and Pitcairn recycled end members

Age estimates for OIB sources range between 3 Ga for a recycled sedimentary material in Hawaii (Blichert-Toft et al., 1999) to essentially recent formation of the Pb isotopic signature in the underlying oceanic lithosphere in some Atlantic OIB sources (Halliday et al., 1992). To estimate the age of OIB sources, most authors either use the age implied by the slopes of Pb isotopic arrays (Tatsumoto, 1978; Chase, 1981; Hofmann and White, 1982) or alternatively Pb isotope evolution models (Woodhead and McCulloch, 1989; Chauvel et al., 1992; Thirlwall, 1997). The interpretation of the Pb isotopic arrays as isochrons has proven to be inconsistent with the Pb isotopic data for Rurutu as well as Pitcairn (Eisele et al., submitted). We therefore use a Pb isotope evolution model to estimate the age of the OIB sources of the South Pacific Superswell. The model calculations are described in Appendix 4.C.

The main difficulty in constraining the age of an OIB source with a Pb isotope evolution model is that there are many unknown variables. The main inferences come from the trade-offs between three parameters: μ or κ and the age (Fig. 4.5, 4.6). One of these parameters must be fixed to calculate the others. The usual way of estimating ages for OIB

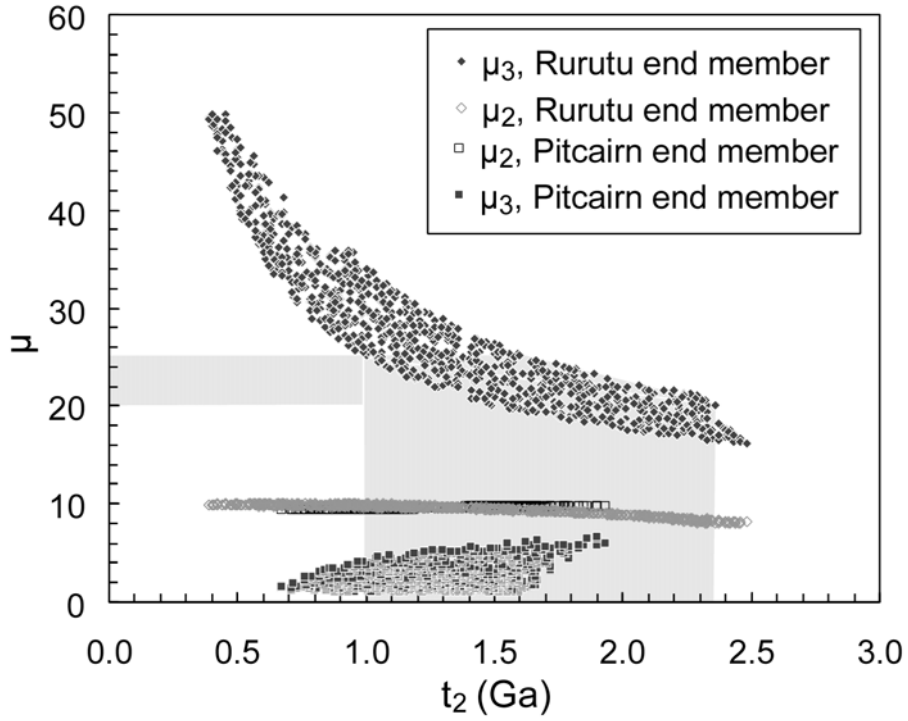

Fig. 4.5: Possible solutions of μ_2 and μ_3 versus the beginning of the third stage (t_2) for the Rurutu and Pitcairn end members in a three-stage Pb isotope evolution model. The time t_2 can be interpreted to represent the age of the recycled material. Also indicated is the age range for the Rurutu end member (1.0 to 2.4 Ga) assuming a μ_3 between 20 and 25 (see text and Appendix 4.C for details) .

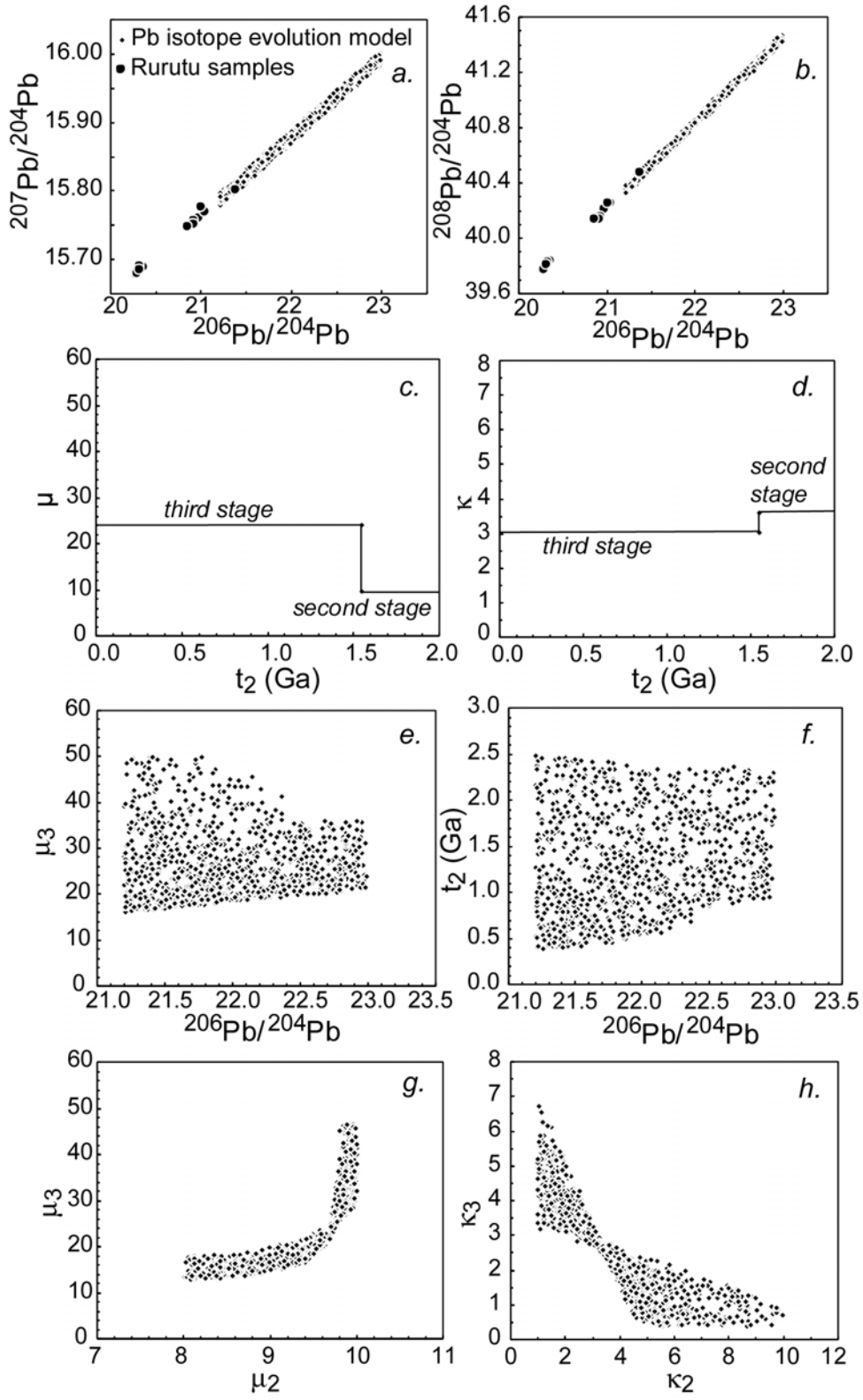

Fig. 4.6: Results of the Pb isotope evolution model (for details of the calculations, see Appendix 4.C). a, b show the results in Pb-Pb space. c, d show an example evolution with $\mu_1 = 9.49$, $\mu_2 = 24.08$, $\kappa_1 = 3.59$, $\kappa_2 = 3.03$ and $t_2 = 1.55$, resulting in a $^{206}Pb/^{204}Pb$ ratio of 22.47. e, f illustrate that the $^{206}Pb/^{204}Pb$ ratio in the model results is relatively independent of μ_3 or age. g, h show the interdependence of the μ and κ values of the second and third stages.

sources is to make a reasonable estimate on μ and κ in a Pb isotope evolution model and then try to determine the age (Chauvel et al., 1992; Thirlwall, 1997; Kogiso et al., 1997a). For the HIMU source, estimates for μ range between ~20 (Chauvel et al., 1992; Thirlwall, 1997) and 50 (Kogiso et al., 1997a).

We estimated the time of the U-Pb fractionation using a three-stage Pb isotope evolution model for the end members of the Rurutu and Pitcairn arrays (see Fig. 4.5). The model calculations use Monte Carlo methods and are described in Appendix 4.C. The model paramters for the Pitcairn end member were described by Eisele et al. (submitted). When letting all parameters (e.g. μ_1, μ_2 and μ_3) in a simulation vary over a wide range, solutions that can explain the Pb isotopic of Rurutu and Pitcairn can have t_2 ages from Archean time to relatively recent. When we however fix the starting composition at 3.7 Ga and restrict the μ_2 to typical crust or mantle values (between 8 and 10), then the recent extreme fractionation of the U/Pb ratio recorded by μ_3 can only occur in a relatively limited time-interval for the Pitcairn and Rurutu recycled end members (Fig. 4.5). The model solutions for the HIMU end member cover $^{206}Pb/^{204}Pb$ ratios between 21.2 and 23 (Fig. 4.6). The possible solutions for t_2 – interpreted to represent the age of the recycled material – range between 2.5 Ga and 0.4 Ga (see Fig. 4.5) for the Rurutu recycled end member. Consequently, an age greater than 1 Ga is possible for the HIMU source, but ages of ~1 Ga are just as reasonable.

If we assume that the U/Pb ratio measured for the most primitive Rurutu lavas records a rough upper estimate for the U/Pb ratio of the source (μ ~25, see Table 4.1), then the age range for μ_3 ~20 to 25 is between 1.0 and 2.4 Ga for the Rurutu source. The overall age range of the HIMU source corresponds to the age solutions for the Pitcairn recycled end member (range from 0.7 to 1.9 Ga). These age estimates have very broad limits and are dependent on the model parameters, namely initial Pb isotopic composition at 3.7 Ga, the range of μ_2 and the value chosen for μ_3. However, it is intriguing, that the possible age ranges for Pitcairn and

Rurutu recycled end members are similar (Fig. 4.5b), although their Pb isotopic compositions are so different (Fig. 4.5a).

4.3.6 A link between HIMU and EM in the South Pacific?

Chauvel et al., (1992) first proposed a link between the EM and HIMU signatures found in South Pacific OIB. Our calculations indicate that HIMU and EM-1 source materials sampled at Rurutu and Pitcairn may have similar ages. This finding together with the inference that the two volcanic islands originate from a common geophysical anomaly that forms the South Pacific Superswell leads us to speculate that the recycled materials in the South Pacific Superswell volcanoes may be derived from subduction at a similar time and place in Earth history and not have completely unrelated origins.

The geophysical evidence for a common origin of the hotspot volcanism in the southern Pacific was first based on the observation of a relatively shallow bathymetry, inconsistent with thermal subsidence similar to that in a cooling half-space model (McNutt and Fisher, 1987; McNutt et al., 1996). The hotspots or hotspot tracks of the Cook-Austral, Pitcairn-Gambier and Society Islands were regarded as smaller anomalies that are superimposed on a broadscale mantle upwelling (McNutt et al., 1997; Sichoix et al., 1998). The interpretation of the origin of the Superswell varies, and explanations include large-scale convective flow in the lower mantle (Davies and Pribac, 1993), two distinct pulses of volcanism derived from a thermal anomaly in the upper mantle (McNutt, 1998) or a superplume from the core-mantle boundary (Larson and Kincaid, 1996). An upper mantle thermal anomaly in the South Pacific seems to be well established from seismic evidence (Romanovicz, 1995; Niu et al. 2000; Suetsugu, 2001). But there is also mounting geophysical evidence that the Superswell may be rooted in the lower mantle. Vinnik et al. (1997) argue that the seismic signal of the 660 km discontinuity under the Superswell is disturbed by a thermo-chemical plume. Global tomographic images show an anomaly under the South

Pacific that extends to at least 2000 km depth that may be chemical as well as thermal (van der Hilst et al., 1997; Tackley, 2000).

The hypothesis that the isotope heterogeneities in the Austral-Cook, Pitcairn-Gambier and Society Islands may have a common geochemical origin is more speculative than the geophysical evidence. However, combining geophysical and geochemical evidence into a single model appears reasonable. The age model for the OIB sources in the South Pacific presented above appears to argue that the ages of the isotope heterogeneities of Rurutu and Pitcairn are confined to Proterozoic time. It seems possible that the origin of the isotopic heterogeneities in the South Pacific is related to recycled oceanic crust and sediments subducted during the Proterozoic. These subducted materials may have aggregated in the lower mantle, and if they stayed coherent for >1 Ga, then these materials may have risen to form the source of the hotspot volcanoes in the South Pacific Superswell erupting for ~100 Ma (Staudigel et al. 1991; Janney and Castillo, 1999). This model is of course very speculative, but seems a solution to integrate the geophysical and geochemical observations that very heterogeneous OIB occur in close proximity and are derived from a large-scale geophysical anomaly possibly extending into the lower mantle.

4.4 Conclusions

Linear arrays in Pb isotope space can be resolved for some volcanic islands in the South Pacific Superswell. We interpret these arrays as mixing arrays; each volcano has a source composed of two distinct end members, and the various volcanic islands do not share a common end member. Consequently, there is no evidence for the existence of a homogeneous common component in the South Pacific mantle sources. It rather appears that the mantle sources are heterogeneous for all the South Pacific OIB.

The materials with the most extreme Pb isotopic compositions in the South Pacific Superswell – the HIMU and EM-1 end members – may be interpreted as recycled oceanic

crust and sediment. They might have similar ages. These materials might have risen as a large thermo-chemical plume, to create the large-scale bathymetric and geochemical anomaly in the South Pacific.

4.5 Appendices

Appendix 4.A Correction for radiogenic in-growth of Pb

The correction for radiogenic in-growth of Pb since eruption on the Rurutu lavas was done using the U, Th and Pb concentrations measured by Chauvel et al. (1997). The μ value ($\equiv(^{238}U/^{204}Pb)_{today}$) was calculated using

$$\mu = \frac{[U]}{\frac{^{235}U}{^{238}U}+1} \cdot \frac{\frac{^{206}Pb}{^{204}Pb}+\frac{^{207}Pb}{^{204}Pb}+\frac{^{208}Pb}{^{204}Pb}+1}{[Pb]}$$

where [U] and [Pb] are the measured concentrations of U and Pb, respectively. Pb isotopic ratios are the measured ratios, and the $^{235}U/^{238}U$ ratio is 1/137.88. The ω value ($\equiv(^{232}Th/^{204}Pb)_{today}$) was calculated in a similar manner. The measured κ* ($\equiv(^{232}Th/^{238}U)_{today}$) can be calculated by dividing ω/μ. The measured isotope ratios were corrected for radiogenic in-growth of Pb since eruption. For example, the $^{206}Pb/^{204}Pb$ ratio was corrected with

$$\left(\frac{^{206}Pb}{^{204}Pb}\right)_{initial} = \left(\frac{^{206}Pb}{^{204}Pb}\right)_{measured} - \mu \cdot \left(e^{\lambda_{238}t} - 1\right)$$

where λ is the decay constant of ^{238}U, and *t* is age.

Appendix 4.B Regression lines in Pb isotope space

For a slope of a regression line in $^{207}Pb/^{204}Pb$-$^{206}Pb/^{204}Pb$ space, an age relating to this slope can be found by comparison of the slope *m* with tabulated values or by an iterative solution applying the equation

$$m = \frac{\left(\frac{^{207}Pb}{^{204}Pb}\right)_{sample} - \left(\frac{^{207}Pb}{^{204}Pb}\right)_{initial}}{\left(\frac{^{206}Pb}{^{204}Pb}\right)_{sample} - \left(\frac{^{206}Pb}{^{204}Pb}\right)_{initial}} = \frac{1}{137.88} \cdot \frac{\left(e^{\lambda_{235}t} - 1\right)}{\left(e^{\lambda_{238}t} - 1\right)}$$

where λ are the decay constants of the U isotopes and *t* is age. This equation is independent on the U/Pb ratio or initial Pb isotopic composition of the samples. The interpretation of a linear array in $^{207}Pb/^{204}Pb$-$^{206}Pb/^{204}Pb$ space as an isochron is, however, only applicable if the samples had the same Pb isotope initial ratios and had undisturbed U/Pb ratios since time *t*. Using an age inferred from the $^{207}Pb/^{204}Pb$-$^{206}Pb/^{204}Pb$ regression line interpreted as isochron, the κ ($\equiv(^{232}Th/^{238}U)_{today}$) implied by the slope of a linear array in $^{208}Pb/^{204}Pb$-$^{206}Pb/^{204}Pb$ space can be calculated as

$$\kappa = m_{86} \cdot \frac{e^{\lambda_{238}t} - 1}{e^{\lambda_{232}t} - 1}$$

with m_{86} being the slope in $^{208}Pb/^{204}Pb$-$^{206}Pb/^{204}Pb$ space and λ_{232} the decay constant of ^{232}Th. Because the elemental ratio Th/U is not fractionated appreciably during melting (Beattie, 1993), the measured κ* should yield a value similar to the calculated κ, if the line in Pb-Pb isotope space represents an isochron (see Abouchami et al., 2000). The alternative to the interpretation of the linear arrays in Pb isotope space as an isochron is the interpretation as a mixing line, in which case the slope does not have an age implication (see Abouchami et al., 2000).

Appendix 4.C A three-stage Pb isotope evolution model for the recycled component of the Rurutu source

We examined a three-stage Pb isotope evolution model in order to better understand the origin of the recycled Rurutu end member. The aims are, first, to arrive at models consistent with the present-day Pb isotopic composition needed for this end member, and

second, to examine the ranges in source U/Pb and Th/U ratios implied by these models. The results place significant constraints on the age of this recycled end member.

Since the Pb isotopic compositions of the HIMU source lie far to the right of the geochron in $^{207}Pb/^{204}Pb$-$^{206}Pb/^{204}Pb$ space, it is immediately clear that a single-stage model is inadequate. A two-stage model is possible (Chauvel et al., 1992), however, we here chose a three-stage model described by the equation (Gale and Mussett, 1974)

$$\frac{^{206}Pb}{^{204}Pb} = \left(\frac{^{206}Pb}{^{204}Pb}\right)_I + \mu_1(e^{\lambda t_0} - e^{\lambda t_1}) + \mu_2(e^{\lambda t_1} - e^{\lambda t_2}) + \mu_3(e^{\lambda t_2} - 1)$$

where t_0 is the age of the Earth, $(^{206}Pb/^{204}Pb)_I$ is the initial isotopic composition at t_0, μ_i is the (present-day effective) $^{238}U/^{204}Pb$ ratio during stage i, ages t_1 and t_2 mark the start of the second and third stages, respectively, and λ is the decay constant of ^{238}U. The corresponding isotopic evolution of $^{207}Pb/^{204}Pb$ and $^{208}Pb/^{204}Pb$ can be calculated in a similar manner. The purpose of the first stage is to simulate a Pb isotope evolution evolving from the initial isotopic composition 4.56 Ga ago (Tatsumoto et al., 1973) to a suitable composition for the silicate Earth following accretion (Galer and Goldstein, 1996; Kramers and Tolstikhin, 1997). The second stage is thought to represent a depleted mantle evolution, and the third stage is the HIMU evolution. In practice, the isotopic composition at the end of the first stage is best constrained by the compositions of Archean ore leads. For a crustal reservoir at ~3.7 Ga, estimates of μ_1 and κ_1 and the Pb isotopic composition at the start of the second stage are relatively similar (Galer and Goldstein, 1996; Kramers and Tolstikhin, 1997; Stacey and Kramers, 1975). We chose fixed values at the start of the second stage 3.7 Ga ago, using the values of Stacey and Kramers (1975) of $^{206}Pb/^{204}Pb$ = 11.151, $^{207}Pb/^{204}Pb$ = 12.998 and $^{208}Pb/^{204}Pb$ = 31.180. We performed Monte Carlo simulations of the second and the third stages of Pb isotope evolution, and then selected a subset of solutions resulting in present-day Pb isotopic compositions suitable for the recycled Rurutu end member (Fig. 4.6). In order to make meaningful statements on the possible age of the Rurutu source, the evolution

parameters of the first and second stages have to be kept relatively constant. When larger ranges for μ_1 and μ_2 are assumed, a larger range of t_2 ages can be obtained. In the simulations, the first stage parameters were fixed, while those of the second and third stages were allowed to vary slightly. The parameters that were allowed to vary randomly during the simulations are as follows: (1) μ_2-values ranged between 8 and 10 (Fig. 4.6), thought to simulate a depleted mantle evolution in the second stage. (2) μ_3 varied freely between 8 and 50, representing the HIMU evolution. (3) The κ values in both the second and third stages varied freely between 1 and 10. From the simulations, 1000 "successful" models based upon the filtering criteria are plotted (Fig. 4.6). These successful models were selected using the criterion that the calculated present-day Pb isotopic composition lies on, or close to, the upper extension of the Rurutu arrays in $^{207}Pb/^{204}Pb$-$^{206}Pb/^{204}Pb$ and $^{208}Pb/^{204}Pb$-$^{206}Pb/^{204}Pb$ spaces (Fig. 4.6). These filtering criteria were that the $^{206}Pb/^{204}Pb$ ratio ranged between 21.2 and 23, the $^{207}Pb/^{204}Pb$ ratio deviated no more than ±0.01 from the Pb isotope arrays of Rurutu and no more than ±0.035 from the array in $^{208}Pb/^{204}Pb$-$^{206}Pb/^{204}Pb$ space. The interdependence of the parameters in the Pb isotope evolution model and an example evolution are shown in Fig. 4.6.

4.5 References:

Abouchami, W., Galer, S. J. G. and Hofmann, A. W. (2000): High precision lead isotope systematics of lavas from the Hawaiian Scientific Drilling Project, Chemical Geology 169, 187-209

Beattie, P. (1993): Uranium-thorium disequilibria and partitioning on melting of garnet peridotite, Nature 363, 63-65

Blichert-Toft, J., Frey, F. A. and Albarède, F. (1999): Hf isotope evidence for pelagic sediments in the source of Hawaiian basalts, Science 285, 879-882

Chase, C. G. (1981): Oceanic island Pb: two-stage histories and mantle evolution, Earth and Planetary Science Letters 52, 277-284

Chauvel, C., Hofmann, A. W. and Vidal, P. (1992): HIMU-EM: the French Polynesian connection, Earth and Planetary Science Letters 110, 99-119

Chauvel, C., Goldstein, S. L. and Hofmann, A. W. (1995): Hydration and dehydration of oceanic crust controls Pb evolution in the mantle, Chemical Geology 126, 65-75

Chauvel, C., McDonough, W., Guille, G., Maury, R. and Duncan, R. (1997): Contrasting old and young volcanism in Rurutu Island, Austral chain, Chemical Geology 139, 125-143

Chauvel, C. and Hémond, C. (2000): Melting of a complete section of recycled oceanic crust: Trace element and Pb isotopic evidence from Iceland, Geochemistry, Geophysics, Geosystems , Paper number 1999GC000002

Davies, G. F. and Pribac, F. (1993): Mesozoic seafloor subsidence and the Darwin Rise, past and present, in: The Mesozoic Pacific: Geology, Tectonics and Volcanism, Geophysical Monograph 77, 39-52

Devey, C. W., Albarède, F., Cheminée, J.-L., Michard, A., Mühe, R. K. and Stoffers, P. (1990): Active submarine volcanism on the Society hotspot swell (west Pacific): a geochemical study, Journal of Geophysical Research B95, 5049-5066

Duncan, R. A., McDougall, I., Carter, R. M. and Coombs, D. S. (1974): Pitcairn Island - another Pacific hot spot?, Nature 251, 679-682

Dupuy, C., Vidal, P., Maury, R. C. and Guille, G. (1993): Basalts from Mururoa, Fangataufa and Gambier Islands (French Polynesia); Geochemical dependence on the age of the lithosphere, Earth and Planetary Science Letters 117, 89-100

Eisele, J., Sharma, M., Galer, S. J. G., Blichert-Toft, J., Devey, C. and Hofmann, A. W. (submitted): The role of sediment recycling in EM-1 inferred from Os. Pb, Hf, Nd, Sr isotope and trace element systematics of the Pitcairn hotspot, Earth and Planetary Science Letters

Gale, N. H. and Mussett, A. E. (1974): Episodic uranium-lead models and the interpretation of variations in the isotopic composition of lead in rocks, Reviews of Geophysics and Space Physics 11, 37-86

Galer, S. J. G. and Goldstein, S. L. (1996): Influence of accretion on lead in the Earth, in: Earth Processes: Reading the Isotopic Code (eds Basu, A. and Hart, S. R.), American Geophysical Union, Washington DC 95, 75-98

Galer, S. J. G. and Abouchami, W. (1998): Practical application of lead triple spiking for correction of instrumental mass discrimination, 8th Goldschmidt Conf Mineral. Mag. 62A, 491-492

Galer, S. J. G. (1999): Optimal double and triple spiking for high precision lead isotopic measurement, Chemical Geology 157, 255-274

Geldmacher, J. and Hörnle, K. (2000): The 72 Ma geochemical evolution of the Madeira hotspot (eastern North Atlantic): recycling of Palaeozoic (< 500 Ma) oceanic lithosphere, Earth and Planetary Science Letters 183, 73-92

Halliday, A. N., Davies, G. R., Lee, D.-C., Tommasini, S., Paslick, C. R., Fitton, J. G. and James, D. E. (1992): Lead isotope evidence for young trace element enrichment in the

oceanic upper mantle, Nature 359, 623-627

Hanan, B. B. and Graham, D. W. (1996): Lead and Helium isotope evidence from oceanic basalts for a common deep source of mantle plumes, Science 272, 991-995

Hart, S. R., Hauri, E. H., Oschmann, L. A. and Whitehead, J. A. (1992): Mantle plumes and entrainment: isotopic evidence, Science 256, 517-520

Hémond, C., Devey, C. W. and Chauvel, C. (1994): Source compositions and melting processes in the Society and Austral plumes (South Pacific Ocean); element and isotope (Sr, Nd, Pb, Th) geochemistry, Chemical Geology 115, 7-45

Hofmann, A. W. and White, W. M. (1982): Mantle plumes from ancient oceanic crust, Earth and Planetary Science Letters 57, 421-436

Janney, P. E. and Castillo, P. R. (1999): Isotope geochemistry of the Darwin Rise seamounts and the nature of long-term mantle dynamics beneath the south central Pacific, Journal of Geophysical Research 104, 10571-10589

Kogiso, T., Tatsumi, Y., Shimoda, G. and Barsczus, H. G. (1997a): High μ (HIMU) ocean island basalts in southern Polynesia: New evidence for whole mantle scale recycling of subducted oceanic crust, Journal of Geophysical Research 102, 8085-8103

Kogiso, T., Tatsumi, Y. and Nakano, S. (1997b): Trace element transport during dehydration processes in the subducted oceanic crust: 1. Experiments and implications for the origin of ocean island basalts, Earth and Planetary Science Letters 148, 193-205

Kramers, J. D. and Tolstikhin, I. N. (1997): Two terrestrial lead isotope paradoxes, forward transport modelling, core formation and the history of the continental crust, Chemical Geology 139, 75-110

Larson, R. L. and Kincaid, C. (1996): Onset of mid-cretaceous volcanism by elevation of the 670 km thermal boundary layer, Geology 24, 551-554

McNutt, M. K. and Fischer, K. M. (1987): The South Pacific superswell, in: Seamounts, Islands and Atolls, Geophysical Monograph Series, vol. 43, B. H. Keating et al. (eds), 25-34

McNutt, M. K., Sichoix, L. and Bonneville, A. (1996): Modal depths from shipboard bathymetry: There IS a South Pacific Superswell, Geophysical Research Letters 23, 3397-3400

McNutt, M. K., Caress, D. W., Reynolds, J., Jordahl, K. A. and Duncan, R. A. (1997): Failure of plume theory to explain midplate volcanism in the southern Austral islands, Nature 389, 479-482

McNutt, M. K. (1998): Superswells, Reviews in Geophysics 36(2), 211-244

Mühe, R., Peucker-Ehrenbrink, B., Devey, C. W. and Garbe-Schönberg, D. (1997): On the redistribution of Pb in the oceanic crust during hydrothermal alteration, Chemical Geology 137, 67-77

Nakamura, Y. and Tatsumoto, M. (1988): Pb, Nd and Sr isotopic evidence for a multicomponent source for rocks of Cook-Austral islands and heterogeneities of mantle plumes, Geochimica et cosmochimica Acta 52, 2909-2924

Niu, F., Inoue, H., Suetsugu, D. and Kanjo, K. (2000): Seismic evidence for a thinner mantle transition zone beneath the South Pacific Superswell, Geophysical Research Letters 27, 1981-1984

Palacz, Z. A. and Saunders, A. D. (1986): Coupled trace element and isotope enrichment in the Cook-Austral-Samoa Islands, southwest Pacific, Earth and Planetary Science Letters 79, 270-280

Romanowicz, B. (1995): A global tomographic model of shear attenuation in the upper mantle, Journal of Geophysical Research 100, 12375-12394

Saal, A. E., Hart, S. R., Shimizu, N., Hauri, E. H. and Layne, G. D. (1998): Pb isotopic variability in melt inclusions from oceanic island basalts, Polynesia, Science 282, 1481-1484

Schiano, P., Burton, K. W., Dupré, B., Birck, J.-L., Guille, G. and Allègre, C. J. (2001): Correlated Os-Pb-Nd-Sr isotopes in the Austral-Cook chain basalts: the nature of mantle components in plume sources, Earth and Planetary Science Letters 186, 527-537

Sichoix, L., Bonneville, A. and McNutt, M. K. (1998): The seafloor swells and Superswell in French Polynesia, Journal of Geophysical Research 103, 27123-27133

Stacey, J. S. and Kramers, J. D. (1975): Approximation of terrestrial lead isotope evolution by a two-stage model, Earth and Planetary Science Letters 26, 207-221

Staudigel, H., Park, K.-H., Pringle, M., Rubenstone, J. L., Smith, W. H. F. and Zindler, A. (1991): The longevity of the South Pacific isotopic and thermal anomaly, Earth and Planetary Science Letters 102, 22-44

Suetsugu, D. (2001): A low Q_{ScS} anomaly near the South Pacific Superswell, Geophysical Research Letters 28, 391-394

Tackley, P. J. (2000): Mantle convection and plate tectonics: toward an integrated physical and chemical theory, Science 288, 2002-2007

Tatsumoto, M., Knight, R. J. and Allègre, C. J. (1973): Time difference in the formation of meteorites as determined from the ratio of lead-207 to lead-206, Science 180, 1279-1283

Tatsumoto, M. (1978): Isotopic composition of lead in oceanic basalt and its implication to mantle evolution, Earth and Planetary Science Letters 38, 63-78

Thirlwall, M. F. (1997): Pb isotopic evidence for OIB derivation from young HIMU mantle, Chemical Geology 139, 51-74

Thirlwall, M. F. (2000): Inter-laboratory and other errors in Pb isotope analyses investigated using a ^{207}Pb-^{204}Pb double spike, Chemical Geology 163, 299-322

van der Hilst, R. D., Widiyantoro, S. and Engdahl, E. R. (1997): Evidence for deep mantle circulation from global tomography, Nature 386, 578-584

Vidal, P., Chauvel, C. and Brousse, R. (1984): Large mantle heterogeneity beneath French Polynesia, Nature 307, 536-538

Vinnik, L., Chevrot, S. and Montagner, J.-P. (1997): Evidence for a stagnant plume in the transition zone?, Geophysical Research Letters 24, 107-1010

White, W. M. (1985): Sources of oceanic basalts - radiogenic isotopic evidence, Geology 13(2), 115-118

White, W. M. and Duncan, R. A. (1996): Geochemistry and Geochronology of the Society Islands: New evidence for deep mantle recycling, in: Earth Processes: Reading the Isotopic Code (eds Basu, A. and Hart, S. R.), American Geophysical Union, Washington DC, 183-206

Wilson, J. T. (1963): A possible origin of the Hawaiian Islands, Canadian Journal of Physics 41, 863-870

Woodhead, J. D. and McCulloch, M. T. (1989): Ancient seafloor signals in Pitcairn Island lavas and evidence for large amplitude, small length-scale mantle heterogeneities, Earth and Planetary Science Letters 94, 257-273

Woodhead, J. D. and Devey, C. W. (1993): Geochemistry of the Pitcairn Seamounts, I: source character and temporal trends, Earth and Planetary Science Letters 116, 81-99

Woodhead, J. D. (1996): Extreme HIMU in an oceanic setting: the geochemistry of Mangaia Island (Polynesia) and temporal evolution of the Cook-Austral hotspot, Journal of Volcanology and Geothermal Research 72, 1-19

Zindler, A. and Hart, S. (1986): Chemical geodynamics, Annual Reviews in Earth and Planetary Sciences 14, 493-571

Chapter 5: Appendices

Appendix 5.A: Lithologic column of the HSDP-2 drill hole

The HSDP-2 drill hole is located at the NE coast of the Hawaiian Island between the Puna and Hilo volcanic ridges. It is drilled into the NE flank of Mauna Loa and Mauna Kea but mainly samples Mauna Kea lavas. Figure 5.1 shows a contour map and a wire-frame model of Big Island and the surrounding ocean floor.

Figure 5.2 shows the lithologic log of the HSDP-2 drill hole compiled by the HSDP-2 working group. Also indicated are the positions of the samples measured for Pb isotopic composition (Chapter 3). In the first ~260 m of the drill hole lavas from Mauna Loa were recovered. The transition to Mauna Kea lavas is a chemical boundary, because e.g. $^{206}Pb/^{204}Pb$ ratios (Abouchami et al., 2000) or Zr/Nb ratios (Rhodes, 1996) are distinct for the two volcanoes. It is, however, not a lithologic boundary (see Fig. 5.2). The subaerial lavas of the volcanoes are aphyric or olivine-phyric basalts with some intercalations of ash and soil. The change from the Kea-lo8 to the Kea-mid8 Pb isotopic composition of the lavas (see Chapter 3) occurs within the subaerial section of Mauna Kea at ~750 m. The transition to the submarine section of Mauna Kea occurs deeper, at 1090 m depth and is indicated by the first occurrence of hyaloclastites and basalt glass (Fig. 5.2). The submarine section of the drill core is dominated by hyaloclastite with minor intercalations of sediments to ~2000 m depth. Small intrusives occur at 1900 m and 1930 m depth. Pillow basalts only appear at >2000 m. The first interval of pillow lavas is accompanied by a change in Pb isotopic composition from the Kea-mid8 to the Kea-hi8 Pb isotope array samples. Kea-hi8 array samples are often related to the occurrence of pillow basalts (at 2000 - 2150 m, 2300 - 2500 m), there are, however, several exceptions where Kea-hi8 array samples are hyaloclastite. Pillow basalts and submarine flows intercalated with some hyloclastite prevail between 2000 m and the final depth of the HSDP-2 drill hole at 3110 m. Overall, only little intrusives are present in the fundament of the volcanic edifice and the drill core is dominated by effusive rocks.

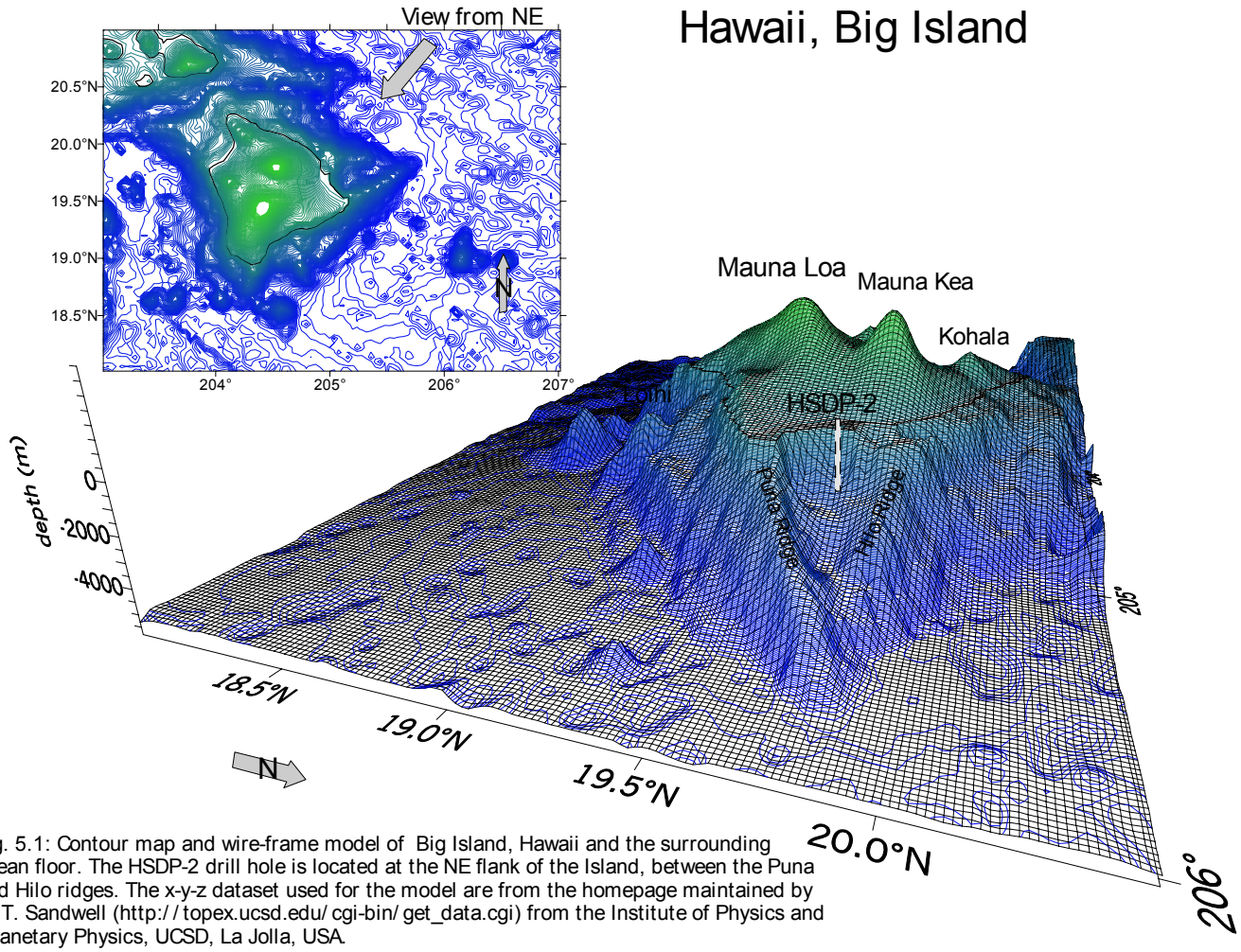

Fig. 5.1: Contour map and wire-frame model of Big Island, Hawaii and the surrounding ocean floor. The HSDP-2 drill hole is located at the NE flank of the Island, between the Puna and Hilo ridges. The x-y-z dataset used for the model are from the homepage maintained by D. T. Sandwell (http://topex.ucsd.edu/cgi-bin/get_data.cgi) from the Institute of Physics and Planetary Physics, UCSD, La Jolla, USA.

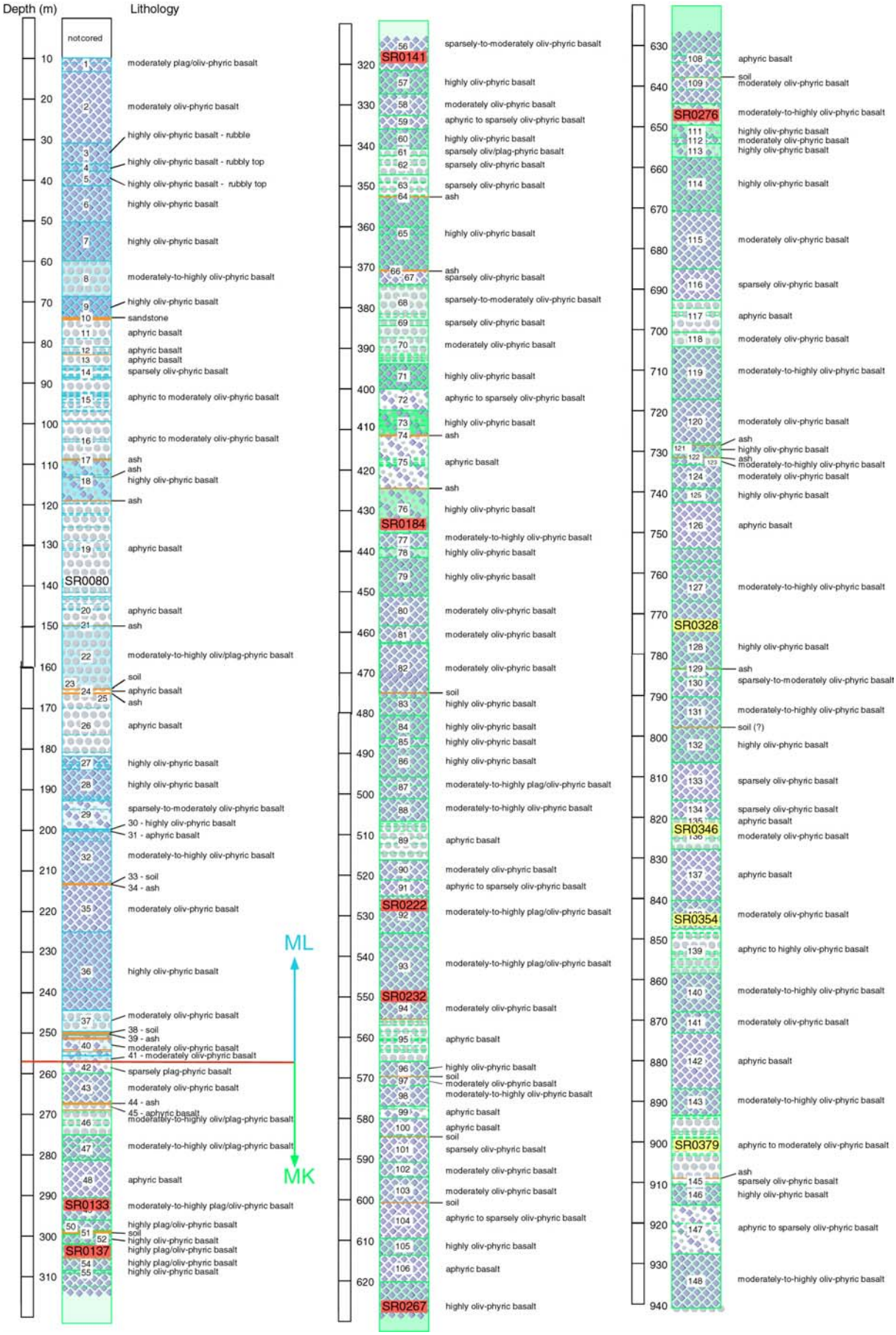
Depth (m)
Lithology
notcored
moderately plag/oliv-phyric basalt
moderately oliv-phyric basalt
highly oliv-phyric basalt - rubble
highly oliv-phyric basalt - rubbly top
highly oliv-phyric basalt - rubbly top
highly oliv-phyric basalt
highly oliv-phyric basalt
moderately-to-highly oliv-phyric basalt
highly oliv-phyric basalt
sandstone
aphyric basalt
aphyric basalt
aphyric basalt
sparsely oliv-phyric basalt
aphyric to moderately oliv-phyric basalt
aphyric to moderately oliv-phyric basalt
ash
ash
highly oliv-phyric basalt
ash
aphyric basalt
SR0080
aphyric basalt
ash
moderately-to-highly oliv/plag-phyric basalt
soil
aphyric basalt
ash
aphyric basalt
highly oliv-phyric basalt
highly oliv-phyric basalt
sparsely-to-moderately oliv-phyric basalt
30 - highly oliv-phyric basalt
31 - aphyric basalt
moderately-to-highly oliv-phyric basalt
33 - soil
34 - ash
moderately oliv-phyric basalt
highly oliv-phyric basalt
moderately oliv-phyric basalt
38 - soil
39 - ash
moderately oliv-phyric basalt
41 - moderately oliv-phyric basalt
sparsely plag-phyric basalt
moderately oliv-phyric basalt
44 - ash
45 - aphyric basalt
moderately-to-highly oliv/plag-phyric basalt
moderately-to-highly oliv/plag-phyric basalt
aphyric basalt
SR0133
moderately-to-highly plag/oliv-phyric basalt
highly plag/oliv-phyric basalt
soil
highly oliv-phyric basalt
SR0137
highly plag/oliv-phyric basalt
highly plag/oliv-phyric basalt
highly oliv-phyric basalt
ML
MK
sparsely-to-moderately oliv-phyric basalt
SR0141
highly oliv-phyric basalt
moderately oliv-phyric basalt
aphyric to sparsely oliv-phyric basalt
highly oliv-phyric basalt
sparsely oliv/plag-phyric basalt
sparsely oliv-phyric basalt
sparsely oliv-phyric basalt
ash
highly oliv-phyric basalt
ash
sparsely oliv-phyric basalt
sparsely-to-moderately oliv-phyric basalt
sparsely oliv-phyric basalt
moderately oliv-phyric basalt
highly oliv-phyric basalt
aphyric to sparsely oliv-phyric basalt
highly oliv-phyric basalt
ash
aphyric basalt
ash
highly oliv-phyric basalt
SR0184
moderately-to-highly oliv-phyric basalt
highly oliv-phyric basalt
highly oliv-phyric basalt
moderately oliv-phyric basalt
moderately oliv-phyric basalt
moderately oliv-phyric basalt
soil
highly oliv-phyric basalt
highly oliv-phyric basalt
highly oliv-phyric basalt
highly oliv-phyric basalt
moderately-to-highly plag/oliv-phyric basalt
moderately-to-highly oliv-phyric basalt
aphyric basalt
moderately oliv-phyric basalt
aphyric to sparsely oliv-phyric basalt
SR0222
moderately-to-highly plag/oliv-phyric basalt
moderately-to-highly plag/oliv-phyric basalt
SR0232
moderately oliv-phyric basalt
aphyric basalt
highly oliv-phyric basalt
soil
moderately oliv-phyric basalt
moderately-to-highly oliv-phyric basalt
aphyric basalt
soil
sparsely oliv-phyric basalt
moderately oliv-phyric basalt
moderately oliv-phyric basalt
soil
aphyric to sparsely oliv-phyric basalt
highly oliv-phyric basalt
aphyric basalt
SR0267
highly oliv-phyric basalt
aphyric basalt
soil
moderately oliv-phyric basalt
SR0276
moderately-to-highly oliv-phyric basalt
highly oliv-phyric basalt
moderately oliv-phyric basalt
highly oliv-phyric basalt
highly oliv-phyric basalt
moderately oliv-phyric basalt
moderately-to-highly oliv-phyric basalt
moderately oliv-phyric basalt
aphyric basalt
moderately oliv-phyric basalt
sparsely oliv-phyric basalt
aphyric basalt
moderately oliv-phyric basalt
moderately-to-highly oliv-phyric basalt
moderately oliv-phyric basalt
ash
highly oliv-phyric basalt
ash
moderately-to-highly oliv-phyric basalt
moderately oliv-phyric basalt
highly oliv-phyric basalt
aphyric basalt
moderately-to-highly oliv-phyric basalt
SR0328
highly oliv-phyric basalt
ash
sparsely-to-moderately oliv-phyric basalt
moderately-to-highly oliv-phyric basalt
soil (?)
highly oliv-phyric basalt
sparsely oliv-phyric basalt
sparsely oliv-phyric basalt
aphyric basalt
SR0346
moderately oliv-phyric basalt
aphyric basalt
moderately oliv-phyric basalt
SR0354
aphyric to highly oliv-phyric basalt
moderately-to-highly oliv-phyric basalt
moderately oliv-phyric basalt
aphyric basalt
moderately-to-highly oliv-phyric basalt
SR0379
aphyric to moderately oliv-phyric basalt
ash
sparsely oliv-phyric basalt
highly oliv-phyric basalt
aphyric to sparsely oliv-phyric basalt
moderately-to-highly oliv-phyric basalt

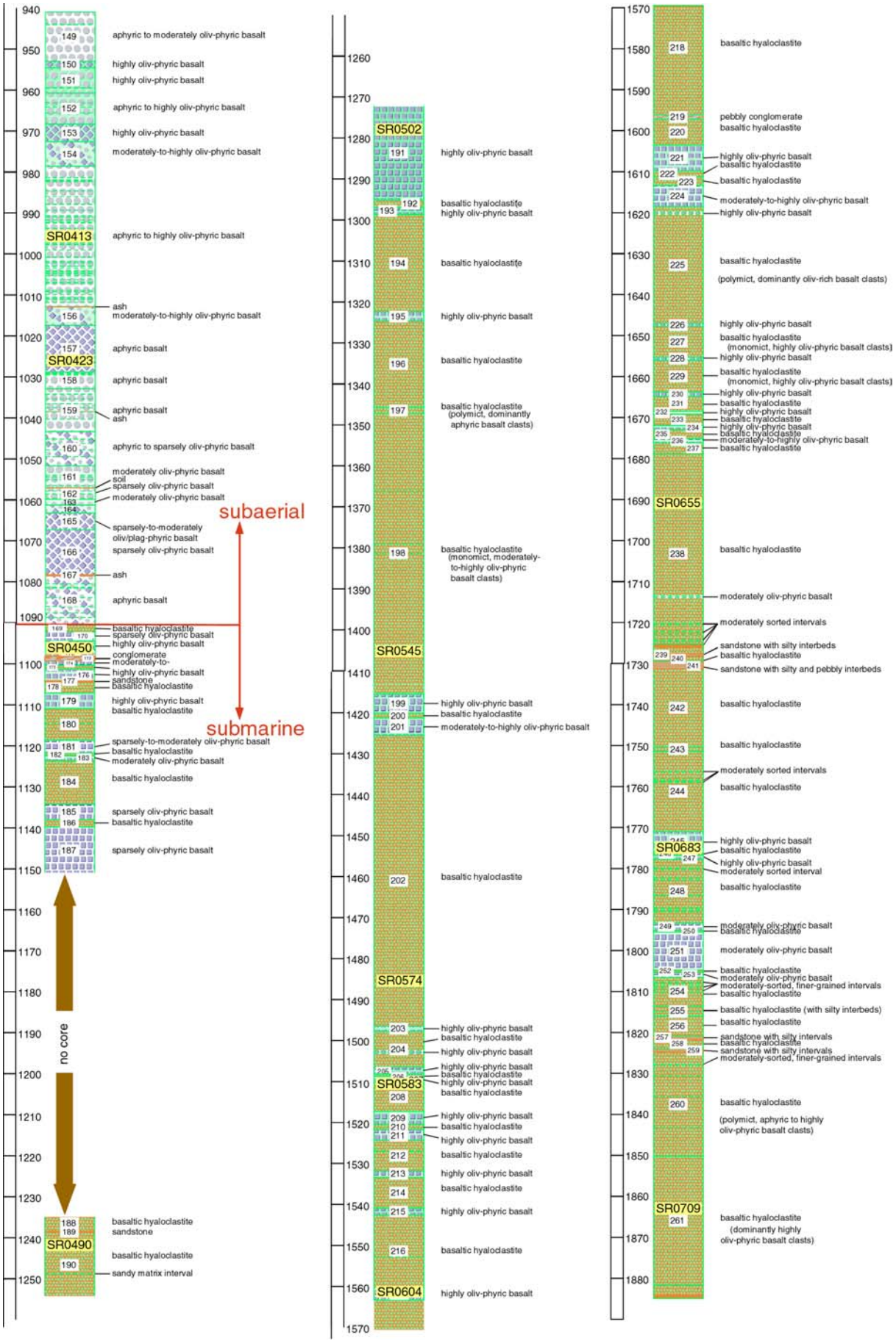
940
950
960
970
980
990
1000
1010
1020
1030
1040
1050
1060
1070
1080
1090
1100
1110
1120
1130
1140
1150
1160
1170
1180
1190
1200
1210
1220
1230
1240
1250
149
aphyric to moderately oliv-phyric basalt
150
highly oliv-phyric basalt
151
highly oliv-phyric basalt
152
aphyric to highly oliv-phyric basalt
153
highly oliv-phyric basalt
154
moderately-to-highly oliv-phyric basalt
SR0413
aphyric to highly oliv-phyric basalt
ash
156
moderately-to-highly oliv-phyric basalt
157
aphyric basalt
SR0423
158
aphyric basalt
159
aphyric basalt
ash
160
aphyric to sparsely oliv-phyric basalt
161
moderately oliv-phyric basalt
soil
162
sparsely oliv-phyric basalt
163
moderately oliv-phyric basalt
164
165
sparsely-to-moderately oliv/plag-phyric basalt
166
sparsely oliv-phyric basalt
167
ash
168
aphyric basalt
subaerial
169
basaltic hyaloclastite
170
sparsely oliv-phyric basalt
SR0450
highly oliv-phyric basalt
conglomerate
172
moderately-to-
173
174
highly oliv-phyric basalt
176
sandstone
177
178
basaltic hyaloclastite
179
highly oliv-phyric basalt
basaltic hyaloclastite
180
submarine
181
sparsely-to-moderately oliv-phyric basalt
182
basaltic hyaloclastite
183
moderately oliv-phyric basalt
184
basaltic hyaloclastite
185
sparsely oliv-phyric basalt
186
basaltic hyaloclastite
187
sparsely oliv-phyric basalt
no core
188
basaltic hyaloclastite
189
sandstone
SR0490
basaltic hyaloclastite
190
sandy matrix interval
1260
1270
1280
1290
1300
1310
1320
1330
1340
1350
1360
1370
1380
1390
1400
1410
1420
1430
1440
1450
1460
1470
1480
1490
1500
1510
1520
1530
1540
1550
1560
1570
SR0502
191
highly oliv-phyric basalt
192
basaltic hyaloclastite
193
highly oliv-phyric basalt
194
basaltic hyaloclastite
195
highly oliv-phyric basalt
196
basaltic hyaloclastite
197
basaltic hyaloclastite
(polymict, dominantly aphyric basalt clasts)
198
basaltic hyaloclastite
(monomict, moderately-to-highly oliv-phyric basalt clasts)
SR0545
199
highly oliv-phyric basalt
200
basaltic hyaloclastite
201
moderately-to-highly oliv-phyric basalt
202
basaltic hyaloclastite
SR0574
203
highly oliv-phyric basalt
basaltic hyaloclastite
204
highly oliv-phyric basalt
205
highly oliv-phyric basalt
206
basaltic hyaloclastite
SR0583
highly oliv-phyric basalt
basaltic hyaloclastite
208
209
highly oliv-phyric basalt
210
basaltic hyaloclastite
211
highly oliv-phyric basalt
212
basaltic hyaloclastite
213
highly oliv-phyric basalt
basaltic hyaloclastite
214
215
highly oliv-phyric basalt
216
basaltic hyaloclastite
SR0604
highly oliv-phyric basalt
1570
1580
1590
1600
1610
1620
1630
1640
1650
1660
1670
1680
1690
1700
1710
1720
1730
1740
1750
1760
1770
1780
1790
1800
1810
1820
1830
1840
1850
1860
1870
1880
218
basaltic hyaloclastite
219
pebbly conglomerate
220
basaltic hyaloclastite
221
highly oliv-phyric basalt
basaltic hyaloclastite
222
223
basaltic hyaloclastite
224
moderately-to-highly oliv-phyric basalt
highly oliv-phyric basalt
225
basaltic hyaloclastite
(polymict, dominantly oliv-rich basalt clasts)
226
highly oliv-phyric basalt
227
basaltic hyaloclastite
(monomict, highly oliv-phyric basalt clasts)
228
highly oliv-phyric basalt
229
basaltic hyaloclastite
(monomict, highly oliv-phyric basalt clasts)
230
highly oliv-phyric basalt
231
basaltic hyaloclastite
232
highly oliv-phyric basalt
233
basaltic hyaloclastite
234
highly oliv-phyric basalt
235
basaltic hyaloclastite
236
moderately-to-highly oliv-phyric basalt
237
basaltic hyaloclastite
SR0655
238
basaltic hyaloclastite
moderately oliv-phyric basalt
moderately sorted intervals
sandstone with silty interbeds
239
240
basaltic hyaloclastite
241
sandstone with silty and pebbly interbeds
242
basaltic hyaloclastite
243
basaltic hyaloclastite
moderately sorted intervals
244
basaltic hyaloclastite
SR0683
highly oliv-phyric basalt
basaltic hyaloclastite
247
highly oliv-phyric basalt
moderately sorted interval
248
basaltic hyaloclastite
249
moderately oliv-phyric basalt
250
basaltic hyaloclastite
251
moderately oliv-phyric basalt
252
basaltic hyaloclastite
253
moderately oliv-phyric basalt
moderately-sorted, finer-grained intervals
254
basaltic hyaloclastite
255
basaltic hyaloclastite (with silty interbeds)
256
basaltic hyaloclastite
257
sandstone with silty intervals
258
basaltic hyaloclastite
259
sandstone with silty intervals
moderately-sorted, finer-grained intervals
260
basaltic hyaloclastite
(polymict, aphyric to highly oliv-phyric basalt clasts)
SR0709
261
basaltic hyaloclastite
(dominantly highly oliv-phyric basalt clasts)

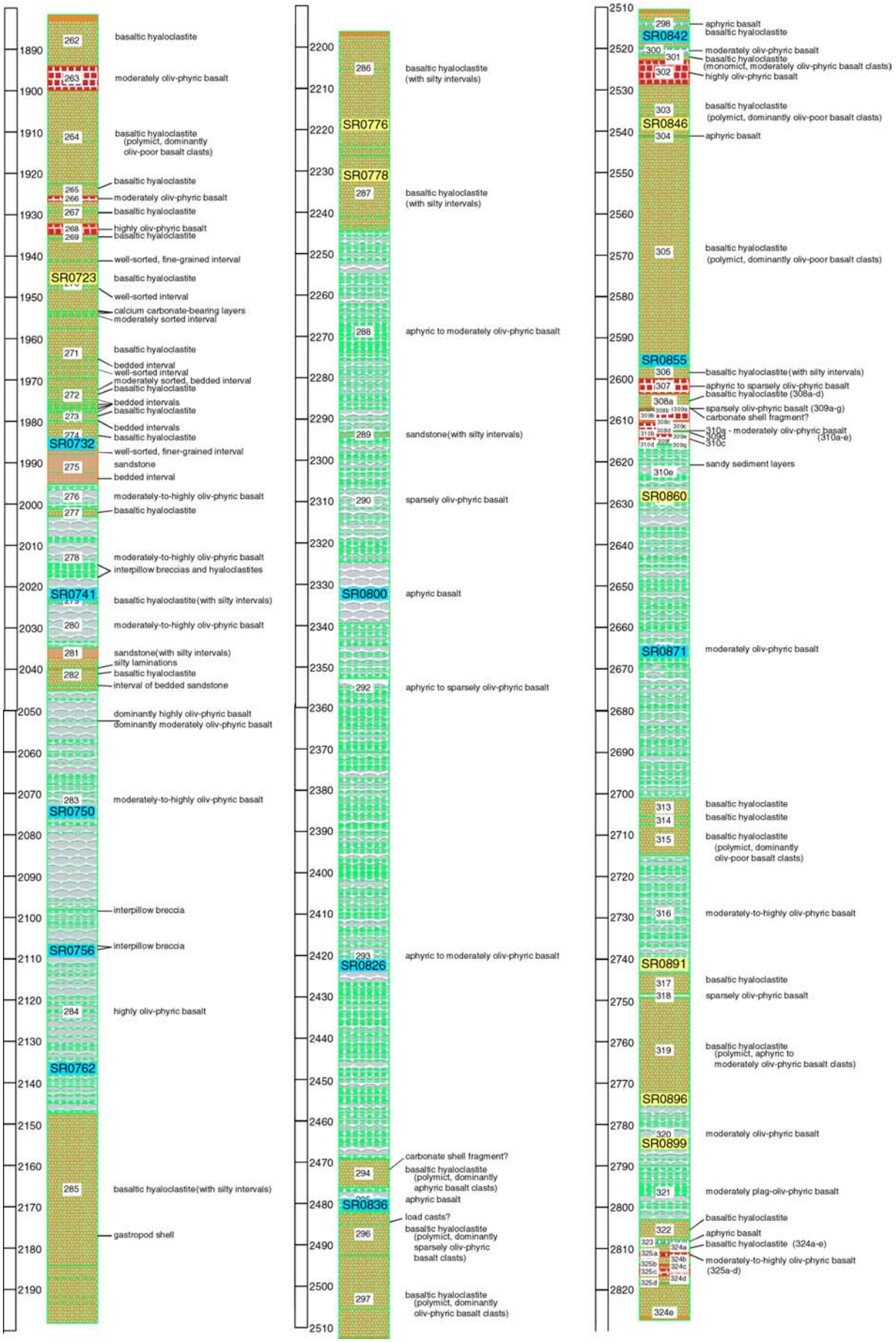
1890
1900
1910
1920
1930
1940
1950
1960
1970
1980
1990
2000
2010
2020
2030
2040
2050
2060
2070
2080
2090
2100
2110
2120
2130
2140
2150
2160
2170
2180
2190
262
basaltic hyaloclastite
263
moderately oliv-phyric basalt
264
basaltic hyaloclastite (polymict, dominantly oliv-poor basalt clasts)
265
basaltic hyaloclastite
266
moderately oliv-phyric basalt
267
basaltic hyaloclastite
268
highly oliv-phyric basalt
269
basaltic hyaloclastite
well-sorted, fine-grained interval
SR0723
basaltic hyaloclastite
well-sorted interval
calcium carbonate-bearing layers
moderately sorted interval
271
basaltic hyaloclastite
bedded interval
well-sorted interval
moderately sorted, bedded interval
272
basaltic hyaloclastite
bedded intervals
273
basaltic hyaloclastite
bedded intervals
274
basaltic hyaloclastite
SR0732
well-sorted, finer-grained interval
275
sandstone
bedded interval
276
moderately-to-highly oliv-phyric basalt
277
basaltic hyaloclastite
278
moderately-to-highly oliv-phyric basalt
interpillow breccias and hyaloclastites
SR0741
basaltic hyaloclastite (with silty intervals)
280
moderately-to-highly oliv-phyric basalt
281
sandstone (with silty intervals)
silty laminations
282
basaltic hyaloclastite
interval of bedded sandstone
dominantly highly oliv-phyric basalt
dominantly moderately oliv-phyric basalt
283
moderately-to-highly oliv-phyric basalt
SR0750
interpillow breccia
SR0756
interpillow breccia
284
highly oliv-phyric basalt
SR0762
285
basaltic hyaloclastite (with silty intervals)
gastropod shell
2200
2210
2220
2230
2240
2250
2260
2270
2280
2290
2300
2310
2320
2330
2340
2350
2360
2370
2380
2390
2400
2410
2420
2430
2440
2450
2460
2470
2480
2490
2500
2510
286
basaltic hyaloclastite (with silty intervals)
SR0776
SR0778
287
basaltic hyaloclastite (with silty intervals)
288
aphyric to moderately oliv-phyric basalt
289
sandstone (with silty intervals)
290
sparsely oliv-phyric basalt
SR0800
aphyric basalt
292
aphyric to sparsely oliv-phyric basalt
293
SR0826
aphyric to moderately oliv-phyric basalt
carbonate shell fragment?
294
basaltic hyaloclastite (polymict, dominantly aphyric basalt clasts)
aphyric basalt
SR0836
load casts?
296
basaltic hyaloclastite (polymict, dominantly sparsely oliv-phyric basalt clasts)
297
basaltic hyaloclastite (polymict, dominantly oliv-phyric basalt clasts)
2510
2520
2530
2540
2550
2560
2570
2580
2590
2600
2610
2620
2630
2640
2650
2660
2670
2680
2690
2700
2710
2720
2730
2740
2750
2760
2770
2780
2790
2800
2810
2820
298
aphyric basalt
basaltic hyaloclastite
SR0842
300
moderately oliv-phyric basalt
301
basaltic hyaloclastite (monomict, moderately oliv-phyric basalt clasts)
302
highly oliv-phyric basalt
303
basaltic hyaloclastite (polymict, dominantly oliv-poor basalt clasts)
SR0846
304
aphyric basalt
305
basaltic hyaloclastite (polymict, dominantly oliv-poor basalt clasts)
SR0855
306
basaltic hyaloclastite (with silty intervals)
307
aphyric to sparsely oliv-phyric basalt
basaltic hyaloclastite (308a-d)
308a
sparsely oliv-phyric basalt (309a-g)
carbonate shell fragment?
310a - moderately oliv-phyric basalt (310a-e)
310c
sandy sediment layers
310e
SR0860
SR0871
moderately oliv-phyric basalt
313
basaltic hyaloclastite
314
basaltic hyaloclastite
315
basaltic hyaloclastite (polymict, dominantly oliv-poor basalt clasts)
316
moderately-to-highly oliv-phyric basalt
SR0891
317
basaltic hyaloclastite
318
sparsely oliv-phyric basalt
319
basaltic hyaloclastite (polymict, aphyric to moderately oliv-phyric basalt clasts)
SR0896
320
moderately oliv-phyric basalt
SR0899
321
moderately plag-oliv-phyric basalt
322
basaltic hyaloclastite
aphyric basalt
basaltic hyaloclastite (324a-e)
moderately-to-highly oliv-phyric basalt (325a-d)
324e

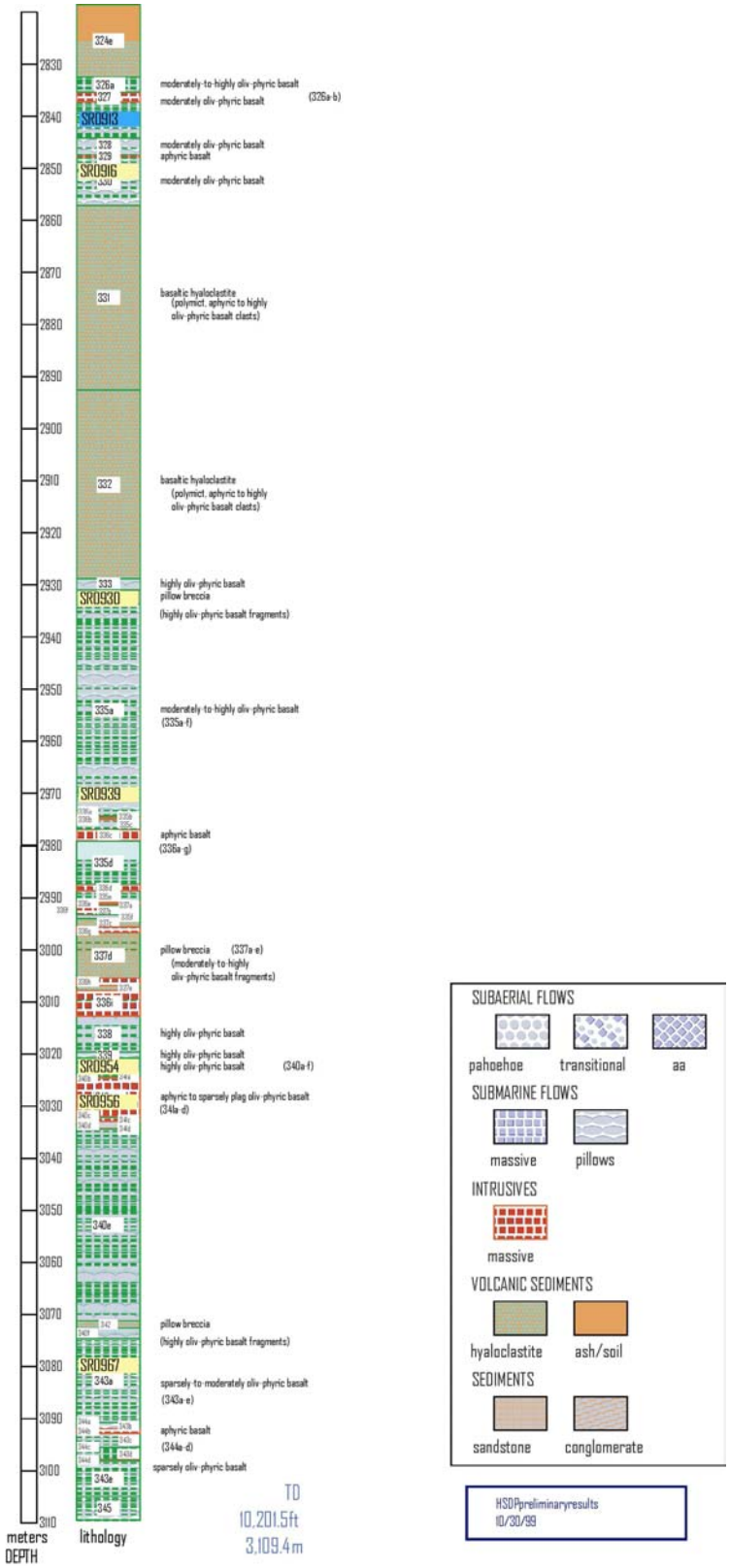

Fig. 5.2: Lithologic core log of the HSDP-2 drill hole with the position of samples measured for Pb isotopes (Chapter 3). Sample numbers are in the format SR0XXX where the triple X denominate the number of the core run. Samples belonging to the Kea-lo8 Pb isotope array have a red background, samples of the Kea-mid8 Pb isotope array are shown with a yellow background, while Kea-hi8 samples are in blue.

Appendix 5.B: Analytical methods

5.B.1 Os and Re chemistry and mass spectrometry

5.B.1.1 Optimal spiking

Osmium isotopic compositions, together with Re and Os concentrations, were determined on dissolutions of 0.5 to 3 g of whole-rock powder to which a mixed ^{190}Os-^{185}Re spike was added. The Re and Os isotopic compositions and concentrations of the spike are shown in Table 5.1, which also displays the isotopic compositions of natural samples. The amount of spike to be added to a sample was estimated using the rule of thumb that Os concentration in OIB correlates with MgO concentration. The literature data of Fig. 5.3 for Os and MgO concentration were compiled using the MPI GEOROC database (http://georoc.mpch-mainz.gwdg.de/). The range of Os concentrations in whole rock OIB samples at a given MgO content varies by more than an order of magnitude, but the Pitcairn samples were relatively well behaved and a sample with e.g. MgO of 10 wt. % could be expected to contain ~50 pg/g Os (see Fig. 5.3).

The most favorable amount of spike added to a sample was intended to minimize the error magnification factors on the measured Os isotopic ratios. Figure 5.4 shows the error magnification factors for the measured ratios of ^{190}Os/^{188}Os (Figure courtesy of G. Brügmann). The error magnification factors for both the Os concentration measurement and the determination of ^{187}Os/^{188}Os ratios are optimal for samples spiked so that the ^{190}Os/^{188}Os ratios range between 4 and 8.

5.B.1.2 Os and Re extraction

The rock samples were dissolved using the Carius tube method (Shirey and Walker, 1995). Osmium was extracted into liquid bromine and purified using microdistillation (Birck et al., 1997). The Os and Re concentrations were calculated using the isotope dilution equation. For e.g. Re this equation is expressed as

Table 5.1: Isotopic composition of Os and Re for natural material and spike

Os

isotopes	abundance	isotope ratios	
Natural composition			
^{184}Os	0.0005	$^{184}Os/^{188}Os$	0.002
^{186}Os	[0.0159]	$^{186}Os/^{188}Os$	[0.120]
^{187}Os	[0.0142]	$^{187}Os/^{188}Os$	[0.107]
^{188}Os	0.1331		
^{189}Os	0.1624	$^{189}Os/^{188}Os$	1.220
^{190}Os	0.2638	$^{190}Os/^{188}Os$	1.981
^{192}Os	0.4104	$^{192}Os/^{188}Os$	3.083
MPI Tracer			
^{184}Os	0.0001	$^{184}Os/^{188}Os$	0.020
^{186}Os	0.0002	$^{186}Os/^{188}Os$	0.039
^{187}Os	0.0002	$^{187}Os/^{188}Os$	0.039
^{188}Os	0.0045		
^{189}Os	0.0062	$^{189}Os/^{188}Os$	1.369
^{190}Os	0.9790	$^{190}Os/^{188}Os$	217.814
^{192}Os	0.0100	$^{192}Os/^{188}Os$	2.215

Re

isotopes	abundance	isotope ratios	
Natural composition			
^{185}Re	0.3740	$^{185}Re/^{187}Re$	0.59738
^{187}Re	0.6260		
MPI Tracer			
^{185}Re	0.9741	$^{185}Re/^{187}Re$	37.572
^{187}Re	0.0259		

Numbers in brackets denominate isotope abundances of radiogenic isotopes that are variable in nature.

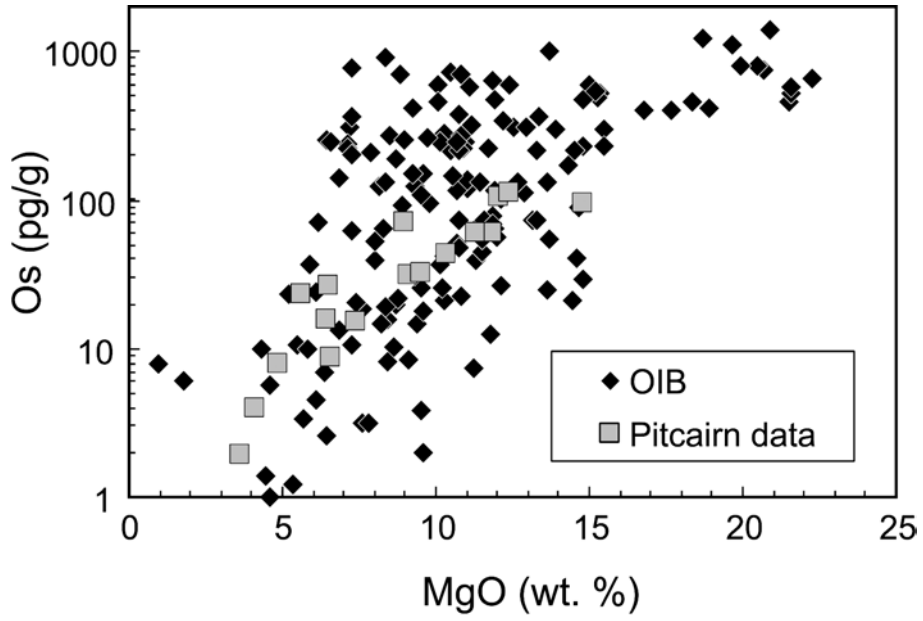

Fig. 5.3: Os versus MgO concentration of ocean island basalt and Pitcairn lavas. Os concentration is on a log scale, while MgO is on a linear scale.

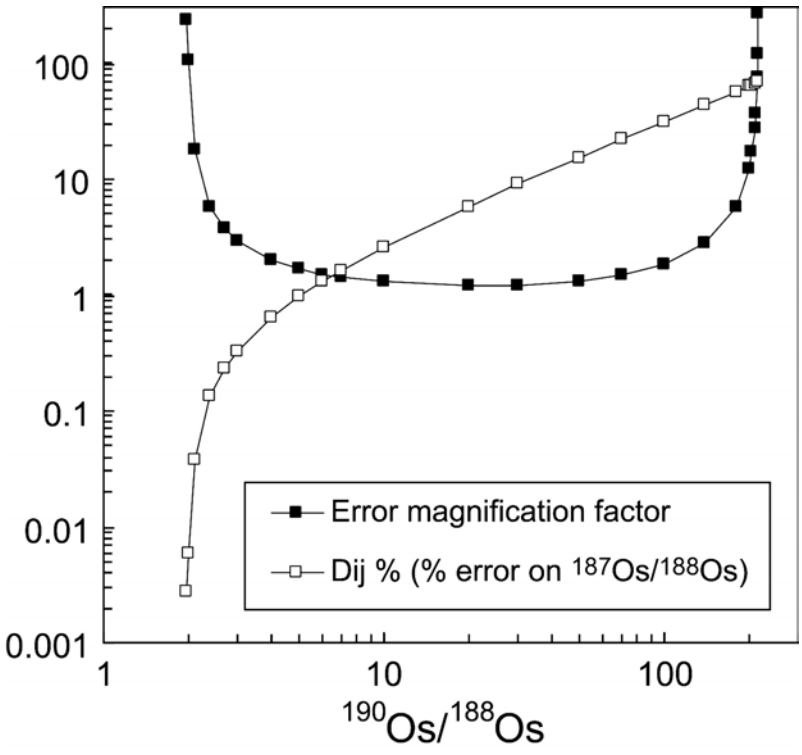

Fig. 5.4: Error magnification factors for the $^{190}Os/^{188}Os$ and $^{187}Os/^{188}Os$ depending on the amount of Os spike added to a sample.

$$^{187}\mathrm{Re}_{sample} = {}^{185}\mathrm{Re}_{spike}\frac{(\frac{^{187}\mathrm{Re}}{^{185}\mathrm{Re}})_{measured} - (\frac{^{187}\mathrm{Re}}{^{185}\mathrm{Re}})_{spike}}{1-(\frac{^{187}\mathrm{Re}}{^{185}\mathrm{Re}})_{measured}\times(\frac{^{185}\mathrm{Re}}{^{187}\mathrm{Re}})_{normal}}$$

where Re isotopic composition of the spike, the natural isotopic composition (see Table 5.1), the spike weight and its ^{185}Re concentration have to be known.

5.B.1.3 Os and Re blanks

For Os separation chemistry, blanks of reagents, loading blanks and total procedural blanks were consistently monitored. Osmium blank concentrations and ^{187}Os/^{188}Os ratios of the blanks are shown in Table 5.2. Seven procedural blanks for Os analyzed alongside with the samples ranged from 23 fg to 178 fg (^{187}Os/^{188}Os between 0.30 and 0.58), with one outlier of 892 fg (^{187}Os/^{188}Os = 0.22). Table 5.2 shows that a new batch of HNO_3 (blank IV, V) treated with the cleaning procedure for 6 hrs had a considerable Os blank of at least ~0.3 pg/ml. Very little blank contribution came from HBr, Br_2 or the loading procedure (blanks VI, VII, IX). The Os blank of the HNO_3 was lowered by repetitive aeration of the acid until Os concentrations in the HNO_3 of <0.04 pg/ml were achieved (Blank X). Using the procedural blanks that were run alongside with a batch of samples, blank corrections on ^{187}Os/^{188}Os ratios for the samples were smaller than 1% in most cases, between 1 and 2% for six analyses, and 5% for Pit89-21. Blank corrections to Os concentrations were smaller than 1%, except in four cases where corrections ranged from 2% to 8% (Table 5.3). Measured Re procedural blanks contained 1.5 pg, 5 pg and 37 pg Re, resulting in corrections to Re concentrations between 1% and 28% (Table 5.3). Because of the large uncertainty associated with the large and variable Re blanks, Re concentration measurements were only used to show that radiogenic ingrowth of Os since eruption was negligible for the Pitcairn samples (Chapter 2).

Table 5.2: Os concentrations and isotopic compositions of blanks

blank #	type	[Os] (pg)	$^{187}Os/^{188}Os$	2σ
blank I	procedural blank	0.178	0.583	0.390
blank II	procedural blank	0.156	0.453	0.024
blank III	procedural blank	0.892	0.215	0.004
blank IV	1ml HCl, 5ml HNO_3 (new acid, aerated 6 hrs)	2.208	0.186	0.024
blank V	3ml HCl, 5ml HNO_3 (new acid, aerated 6 hrs)	1.690	0.198	0.007
blank VI	2,5 ml HBr	0.133	0.348	0.024
blank VII	2 ml HBr + 3 ml Br_2	0.034	0.695	0.016
blank VIII	2 ml HNO_3	0.357	0.217	0.003
blank IX	loading blank, unleached filament	0.022	0.206	0.007
blank X	5 ml HNO_3 (acid aerated twice)	0.207	0.477	0.068
blank XI	3 ml HCl (new acid) + 5ml HNO3 (acid aerated twice)	0.138	0.446	0.063
blank XII	3 ml HCl (old) + 5ml HNO3 (acid aerated twice)	0.143	0.650	0.083
blank XIII	procedural blank	0.103	0.492	0.016
blank XV	procedural blank	0.030	0.391	0.018
blank XVI	procedural blank	0.023	0.482	0.027
blank XVII	procedural blank	0.024	0.299	0.002

Table 5.3: blank correction and reproducibility of Pitcairn samples

	corrected	blank			blank correction (%)			deviation of duplicates (%)	
sample	with	[Os] (pg)	$^{187}Os/^{188}Os$	[Re] (pg)	$^{187}Os/^{188}Os$	[Os]	[Re]	$^{187}Os/^{188}Os$	[Os]
Pit89-1	blankII	0.156	0.453	5.1	-0.77	-0.39	-25		
Pit89-2	blankII	0.156	0.453	5.1	-1.16	-0.49	-28		
Pit89-4	blankXIII	0.103	0.492	1.5	-0.47	-0.27	-2	-1.2	11.2
duplicate	blankIII	0.892	0.215	37.1	-1.47	-7.16		1.2	-11.2
Pit89-5	blankXIII	0.103	0.492	1.5	-0.83	-0.38			
Pit89-8	blankIII	0.892	0.215	37.1	1.11	-7.56	-27		
Pit89-10	blankXIII	0.103	0.492	1.5	-0.79	-0.42	-2		
Pit89-19	blankXIII	0.103	0.492	1.5	-0.15		-1	-3.1	underspiked
duplicate	blankXIII	0.103	0.492	1.5	-0.53	-0.24		1.5	5.3
duplicate2	blankXV	0.030	0.391		-0.09	-0.04		1.6	-5.3
Pit89-20	blankIII	0.892	0.215	37.1	-0.62	-2.36	-9		
Pit89-21	blankII	0.156	0.453	5.1	-5.25	-4.71	-1		
46DS-2	blankXIII	0.103	0.492	1.5	-1.87	-0.82		-1.7	
duplicate	blankXIII	0.103	0.492	1.5	-0.48			1.7	underspiked
47DS-2	blankXVII	0.024	0.299		-0.01	-0.01			
47DS-4	blankXVII	0.024	0.299		-0.02	-0.02			
47DS-8	blankXIII	0.103	0.492	1.5	-0.18	-0.07			
47DS-11	blankXVII	0.024	0.299		-0.02	-0.02			
49DS-1	blankXIII	0.103	0.492	1.5	-0.28	-0.11			
51DS-1	blankXIII	0.103	0.492	1.5	-0.06			-0.5	underspiked
duplicate	blankXIII	0.103	0.492	1.5	-1.11	-0.49		0.5	
51DS-2	blankXVII	0.024	0.299		-0.03	-0.02			
55SLS-6	blankXIII	0.103	0.492	1.5	-1.55	-0.67			

5.B.1.4 Os and Re mass spectrometry

Isotopic compositions of Os were measured at MPI in Mainz using a Finnigan MAT-262 operating in negative ion mode (N-TIMS). Osmium was loaded onto Pt filaments as hexabromoosmate, dried and then mixed with a NaOH - $Ba(OH)_2$ emitter, while Re was loaded on Ni filaments with a $BaSO_4$ emitter. Figure 5.5 shows the Os isotope mass spectrum of a standard resolved by the N-TIMS (isotopic composition see Table 5.1). The Os species that are measured are shown in Table 5.4. On mass 235 there may be an interference of $^{187}Os^{16}O_3^-$ with $^{187}Re^{16}O_3^-$. Therefore, a good separation of Re from Os is necessary and the Re blank contribution from the Pt filament must be monitored. This is achieved by monitoring $^{187}Re^{16}O_4^-$ at mass 251 during the Os measurement and assuming a ratio of $\sim 1 \cdot 10^4$ for the Re species $^{187}Re^{16}O_4^-/^{187}Re^{16}O_3^-$. The contribution of Re to the peak at mass 235 can then be determined. Alternatively, the peak at mass 233, which is $^{185}Re^{16}O_3^-$, can be monitored to calculate the Re interference at mass 235. The contribution of Re to the Os peak at mass 235 should be less than ~2‰.

The ionization efficiency of a known amount of standard loaded on the filament can be estimated by calculating the number of atoms loaded and then comparing this number to the time-integrated count-rate of the ion counter. The number of atoms of the Os standard load is calculated with

$$n = \frac{m_{standard}}{w_m} \times N_a$$

where n is the number of atoms, m is the mass of the standard, w_m = 190.3 g/mol is the molecular weight of Os and $N_a = 6.022 \cdot 10^{23}$ is the Avogadro constant. Typical amounts of standard loaded are 35 pg Os, which contain $\sim 1.1 \cdot 10^{11}$ atoms. If such a standard runs at 100000 counts per second (cps) of ^{192}Os for three hours, then the number of atoms of ^{192}Os detected by the ion counter is 100000 cps · 60 s · 180 min = $1.08 \cdot 10^9$. The number of ionized Os atoms is therefore $2.6 \cdot 10^9$ and the ionization efficiency in these three hours is ~2.4 %.

Table 5.4: Os and Re species

mass (amu)	species
	Os
234	$^{186}Os^{16}O_3^-$
235	$^{187}Os^{16}O_3^-$
236	$^{188}Os^{16}O_3^-$
237	$^{189}Os^{16}O_3^-$
238	$^{190}Os^{16}O_3^-$
240	$^{192}Os^{16}O_3^-$
	Re
249	$^{185}Re^{16}O_4^-$
251	$^{187}Re^{16}O_4^-$

Table 5.5: Pb triple spike composition - Measurement 1997 (Galer & Abouchami)

	$^{204}Pb/^{206}Pb$	$^{207}Pb/^{206}Pb$	$^{208}Pb/^{206}Pb$
	4.330424	4.342171	0.222121
2σ	0.000171	0.000109	0.000015

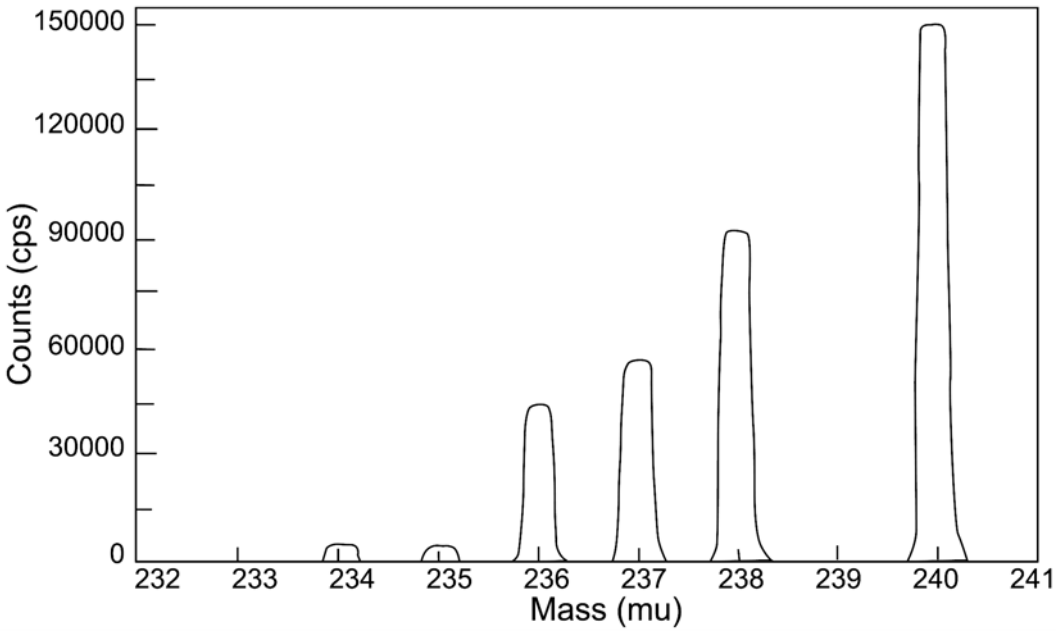

Fig 5.5: Mass spectrum of an Os standard as resolved by the mass spectrometer. The Os species relating to the peaks at 234 to 240 amu are listed in Table 5.4.

The Mainz in-house Os standard yielded $^{187}Os/^{188}Os$ of 0.10693 ± 18 (N = 7, 2σ error). The reproducibility of $^{187}Os/^{188}Os$ ratios, on the basis of four duplicate dissolutions, ranged from 0.5 % to 3.1%, while that of Os concentrations is 5 % and 11% for two duplicates, respectively (Table 5.3). The reproducibility of Os isotopic compositions of the samples is therefore more than ten times that of the standard. This may be explained by sample contamination, because the rock powder used for Os isotope analyses are unleached. The large uncertainty on the Os concentration measurement of the duplicates could also be explained by an inhomogeneous distribution of Os in the rock powder (see Appendix 5.C.1).

Re isotopes were measured on the same Finnigan MAT-262 N-TIMS at masses 249 and 251, which are the isotopes of ReO_4^- (see Table 5.4). The ionization efficiency of a 16 pg Re standard, that runs at 100000 cps for three hours is about 5.2 %. The Re in-house standard yielded $^{185}Re/^{187}Re$ = 0.5981±25 (N = 4, 2σ error).

5.B.2 Pb separation and mass spectrometry

5.B.2.1 Pb extraction and blanks

Rock chips (~100-200 mg) were used for Pb isotope analysis. The chips were thoroughly cleaned in H_2O, leached with hot 6N HCl for one hour, and then rinsed with water prior to dissolution. Following dissolution, lead was separated by anion exchange in mixed HBr-HNO_3 media (Abouchami et al., 2000). Ten procedural Pb blanks analyzed alongside the samples for the duration of the thesis varied between 5 and 65 pg Pb and are negligible.

5.B.2.2 Correction for instrumental mass fractionation using the triple spike technique

The Pb isotopic composition was corrected for instrumental mass fractionation using a triple-spike technique (Galer, 1999). For this purpose, an aliquot of the sample Pb was taken after separation, and mixed with the triple spike. The isotopic composition of the triple spike is shown in Table 5.5. The Pb isotopic compositions of spiked and unspiked aliqouts were

determined in two mass spectrometer runs. The Pb isotope ratios of the sample were corrected for instrumental mass fractionation using the equations as described by Galer (1999). A graphical representation of the compositions in 3D isotope space from Galer (1999) is shown in Fig. 5.6. The isotopic composition of a sample in a mass spectrometer measurement can be described by

$$N_i = n_i \times (1 + \varepsilon \Delta_i)$$

this equation applies to the "normal" run, where the sample composition is determined, where N_i is the "true" isotopic ratio, n_i the measured isotope ratio, ε the fractionation factor and Δ_i is the mass difference. For the Pb isotopic composition, three of the above equations can be found for the $^{204}Pb/^{206}Pb$, $^{207}Pb/^{206}Pb$ and $^{208}Pb/^{206}Pb$ ratios. To minimize the propagated errors in the calculations of the fractionation correction, ^{206}Pb is used as the denominator isotope (for details, see Galer, 1999). For the "mixture" run, where the composition of the spike-sample mixture is determined, the equation is

$$M_i = m_i \times (1 + \zeta \Delta_i)$$

where M_i is the true isotopic composition of the mixture, m_i the measured isotopic composition and ζ the fractionation factor. A third equation states that the vectors N-S and M-S are parallel (see Fig. 5.6)

$$N_i - S_i = q \times (M_i - S_i)$$

where S_i are the isotopic compositions of the spike and q is a scalar that is related to the mixing proportions of sample and spike. Substituting $z = \zeta \cdot q$ and combining the three equations one arrives at

$$q \cdot (S_i - m_i) - z \cdot (\Delta_i \cdot m_i) + \varepsilon \cdot (\Delta_i \cdot n_i) = S_i - n_i$$

This equation can be solved by matrix multiplication

$$\begin{pmatrix} S_1 - m_1 & -\Delta_1 \cdot m_1 & +\Delta_1 \cdot n_1 \\ S_2 - m_2 & -\Delta_2 \cdot m_2 & +\Delta_2 \cdot n_2 \\ S_3 - m_3 & -\Delta_2 \cdot m_2 & +\Delta_3 \cdot n_3 \end{pmatrix} \cdot \begin{pmatrix} q \\ z \\ \varepsilon \end{pmatrix} = \begin{pmatrix} S_1 - n_1 \\ S_2 - n_2 \\ S_3 - n_3 \end{pmatrix}$$

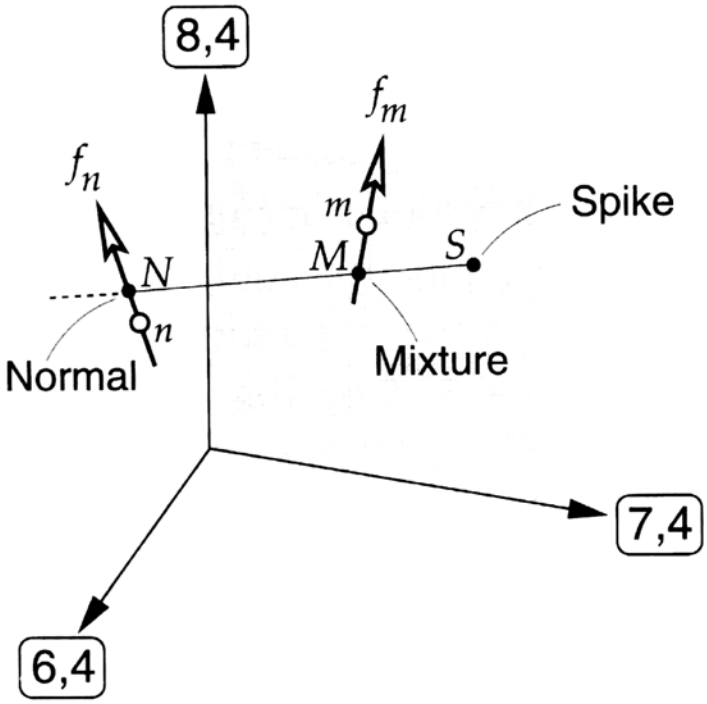

Fig. 5.6: Graphical representation of the compositions of a natural sample, a Pb isotope triple spike and a mixed composition in 3D Pb isotope space (from Galer, 1999).

If this matrix multiplication is expressed as

$$A \cdot \begin{pmatrix} q \\ z \\ \varepsilon \end{pmatrix} = B$$

then a solution for the fractionation factors can be found with

$$\begin{pmatrix} q \\ z \\ \varepsilon \end{pmatrix} = A^{-1} \cdot B$$

A computer program to calculate the correction for instrumental mass fractionation as well as the propagated errors on the Pb isotopic ratios used during this thesis was developed by Stephen Galer and the calculations are described in Galer (1999). The NIST NBS-981 standard measured during this thesis and corrected by the triple spike method yielded $^{206}Pb/^{204}Pb$ = 16.9409 ± 19, $^{207}Pb/^{204}Pb$ = 15.4976 ± 24 and $^{208}Pb/^{204}Pb$ = 36.7262 ± 86 (2σ errors) based on 60 runs.

5.B.3 Other analytical methods

Thorium, Uranium, Hafnium and Tantalum concentrations on samples from Pitcairn (Chapter 2) were measured at the MPI, by spark-source mass spectrometry (SSMS) equipped with a multi-ion counting system (Jochum et al., 1997). About 60 mg of rock powder were mixed with a multi-element tracer containing ^{179}Hf and ^{235}U as spike isotopes. The accuracy of the SSMS measurement of the elements Th, U, Hf, Ta is <4 % and standard reference material BHVO-1 yielded concentrations of Hf = 4.3 ± 0.1 µg/g, Ta = 1.18 ± 0.04 µg/g, Th = 1.22 ± 0.05 µg/g, U = 0.410 ± 0.006 µg/g (Jochum et al., 1997). For further details on analytical methods and standard values see Jochum et al. (1997, 2001).

Major elements and some trace elements (Sc, V, Cr, Co, Ni, Cu, Zn, Ga and Nb) on Pitcairn samples were determined by XRF methods using a Philips PW 1404 at the Institut für Geowissenschaften, Universität Mainz. Fused pellets for major element determination were

produced by melting ~1 g of sample powder with ~5g flux (Lithium-tetraborate). Trace element concentrations were determined on pressed powder pellets consisting of ~6g of sample powder and a small amount of resin. The 2σ reproducibility of major element concentrations is given as <2 % (http://www.uni-mainz.de/FB/Geo/Geologie/EMSRFA/RFA.html), while reproducibility of trace elements is ~2 % for Sc, V, Cr, Ni and Nb and ~8 % for Co, Cu, Ga. Commercial analyses of trace element concentrations were performed on some samples from Pitcairn (see Chapter 2) at the Department of Earth Science, Memorial University of Newfoundland, St. John's, Canada, by inductively coupled plasma mass spectrometry (ICP-MS). Sr and Nd isotopic compositions of Pitcairn samples were determined at the MPI and analytical methods and standard values are given in the Background Dataset of Chapter 2.

Appendix 5.C: Data analysis and evaluation methods

5.C.1 The "distribution error" in an Os concentration measurement

Osmium is a strongly chalcophile element and the Os budget in a sample is dominated by Os contained in small sulfide globules (Roy-Barman et al., 1998). Using statistical methods, one can calculate the 95% confidence interval of sampling a number of sulfide grains in a total population of rock particles in a sample of rock powder. The 95% confidence interval in a binomial experiment is:

$$\frac{x}{n} \pm 1.96 \sqrt{\frac{\frac{x}{n}(1-\frac{x}{n})}{n}}$$

where x is the number of successes in n trials (Rees, 1995). For a sample of rock powder one would have x sulfide grains in n particles of rock powder. One can estimate the number n of sulfide grains expected for a certain Os concentration in a rock and calculate the 95% confidence interval. From this calculation one can estimate the 95% confidence interval for a Os concentration measurement on several aliquots of powder from the same rock sample. This calculation will not take into account heterogeneities in the rock but give the uncertainty of the measurement for a random distribution of the sulfide grains. The calculation therefore gives a minimum of uncertainty.

First, one can estimate the amount of sulfide in the rock assuming that half of the Os budget resides in the sulfide with

$$C_{sulfide}^{wholerock} = \frac{\frac{1}{2} C_{Os}^{wholerock}}{C_{Os}^{sulfide}}$$

where C_i^j denominates the concentration of species i in j. The concentration of Os in the sulfide is quite variable (Roy-Barman et al., 1998), and I use a value of 500 ng/g as an average for the calculations below. The number of sulfide grains in a sample of rock powder are calculated using

$$x = \frac{C_{sulfide}^{wholerock} \times m_{sample}}{\rho \frac{4}{3} \pi r^3}$$

where m is the mass of the sample, ρ = 5 g/cm³, the approximate density of the sulfide grains and r the radius of the particles in the rock powder. The expected particle size after pulverization in the MPI agate mill is ~100 µm diameter (manual, Pulverisette 6, Fa. Fritsch). The total number of particles in a sample can be calculated as

$$n = \frac{m_{sample}}{\rho \frac{4}{3} \pi r^3}$$

assuming an average density of 3.5 g/cm³, which is that of olivine. Then, one can calculate the ratio x/n of sulfide grains in the sample and the 95% confidence intervals for this number. The confidence interval can be expressed in percent and when halved represents the "distribution error" of $C_{Os}^{wholerock}$. Figure 5.7 shows the dependance of this distribution error on the Os concentration in a sample and how this error will influence linear arrays in $^{187}Os/^{188}Os$ versus 1/Os concentration plots.

The calculations of the distribution error shown in Fig. 5.7 assume 500 ng/g Os concentration in sulfide, 2 g as sample weight, 50% of the Os budget residing in sulfide and 50 µm radius for the rock particles. The uncertainty on the Os concentration that is shown in Fig. 5.7 is relatively large compared to the error of the mass spectrometer measurement and the uncertainty introduced by laboratory blanks. This distribution error will limit our ability to accurately determine Os concentrations, especially in low concentration samples.

5.C.2 Error propagation on the Nb/Nb parameter*

For the parameter Nb/Nb* used for the Pitcairn dataset (Chapter 2), the error on the measured concentrations of Nb, Th and La must be propagated to determine the error on this parameter. Nb/Nb* was calculated as

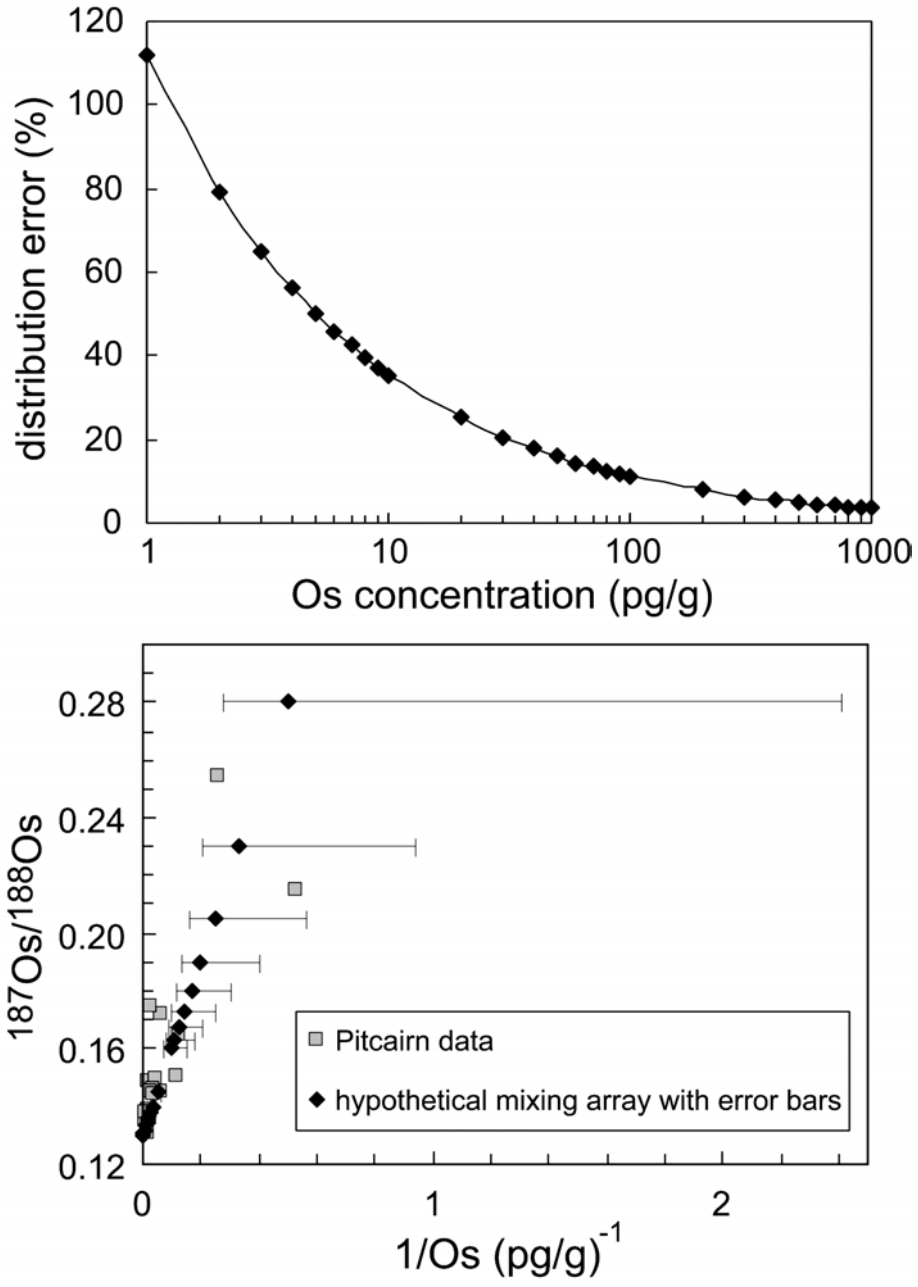

Fig. 5.7: The estimated distribution error for an Os concentration measurement, assuming that 50% of the Os is concentrated in small sulfide grains which are statistically distributed in a sample of rock powder (see text for details).

$$\frac{Nb}{Nb*} = \frac{\frac{[Nb]}{0.6175}}{\sqrt{\frac{[Th]}{0.0813} \cdot \frac{[La]}{0.6139}}}$$

where the normalizing values are from Hofmann (1988). To estimate the error on Nb/Nb* and therefore estimate the significance of the variation of this value, I have used the Gaussian error propagation law (Kuchling, 1995)

$$\Delta\overline{F} = \sqrt{\left(\frac{\partial F}{\partial x}\Delta\bar{x}\right)^2 + \left(\frac{\partial F}{\partial y}\Delta\bar{y}\right)^2 + \left(\frac{\partial F}{\partial z}\Delta\bar{z}\right)^2}$$

where $\Delta\overline{F}$ is the mean error on the function value Nb/Nb*, $\Delta\bar{x}$, $\Delta\bar{y}$ and $\Delta\bar{z}$ are the errors on the measured elements, where x stands for Nb, y for Th and z for La. The partial derivatives were substituted into the equation and the error calculated as

$$\Delta\overline{F} = \sqrt{\left(\frac{1}{0.6175 \cdot \sqrt{\frac{y}{0.0813} \cdot \frac{z}{0.6136}}}\Delta\bar{x}\right)^2 + \left(\frac{\frac{x}{0.6175}}{\left(\frac{z}{0.6139}\right)^{\frac{1}{2}}} \cdot -\frac{\frac{1}{2}}{\left(\frac{y}{0.0813}\right)^{\frac{3}{2}}}\Delta\bar{y}\right)^2 + \left(\frac{\frac{x}{0.6175}}{\left(\frac{y}{0.0813}\right)^{\frac{1}{2}}} \cdot -\frac{\frac{1}{2}}{\left(\frac{z}{0.6139}\right)^{\frac{3}{2}}}\Delta\bar{z}\right)^2}$$

Assuming an error of 5% on the Nb concentration measurement and 3 % on the Th and La concentration measurement, the error on Nb/Nb* e.g. for Pit89-1 was 5.1 %. This error is mainly dependent on the precision of the Nb measurement.

5.C.3 Mixing calculations

The isotope ratios for two component mixing lines in Chapter 2 were calculated using the mass-balance equation (e. g. Albarède, 1995)

$$\alpha = \frac{\alpha_{endmember1} \cdot C^i_{endmember1} \cdot (1-f) + \alpha_{endmember2} \cdot C^i_{endmember2} \cdot f}{C^i_{endmember1} \cdot (1-f) + C^i_{endmember2} \cdot f}$$

where α is an isotope ratio, C^i_j is the concentration of element i in j and f is the mass fraction of endmember two. The trace element ratios of a mixture were determined with

$$\left(\frac{C^a_{mix}}{C^b_{mix}}\right) = \frac{C^a_{endmember1} \cdot (1-f) + C^a_{endmember2} \cdot f}{C^b_{endmember1} \cdot (1-f) + C^b_{endmember2} \cdot f}$$

Multi-component mixing in trace element space can be described by

$$C^i_{mix} = \sum_{j=1}^{n} C^i_j f$$

while in isotope space, the equation is

$$\alpha_{mix} = \frac{\sum_{j=1}^{n} \alpha_j C^i_j f_j}{\sum_{j=1}^{n} C^i_j f_j}$$

To perform mixing calculations for multiple components, these equations were solved using a C++ computer program. In the program the fractions of different materials are varied systematically to find solutions for a specific trace element or isotopic composition (see description in Chapter 2).

The header file for the Os and Pb isotope mixing model "ospbmix.h" is

```
#ifndef osmix_h
#define ospbmix_h

class ospbmix {

 public:
  ospbmix();
  //Parameterdeklaration
  float Os_konz[6];
  float Os_iso[6];
  float Pb_konz[6];
  float Pb_iso[6];
  float mix_konz;
  float mix_Pb_iso;
  float mix_Os_iso;

  //Funktionendeklaration
  void mische_konz(float frak1, float frak2, float frak3, float frak4,
  float frak5);
  void mische_Os_iso(float frak1, float frak2, float frak3, float frak4,
  float frak5);
  void mische_Pb_iso(float frak1, float frak2, float frak3, float frak4,
  float frak5);
  int pruefe_Os_iso(float *mix_zus);
  int pruefe_Pb_iso(float *mix_zus);
  int pruefe_konz(float *mix_zus);

  //Uebergabefunktionen
  double gib_konz() {return mix_konz;};
  double gib_Pb_iso() {return mix_Pb_iso;};
  double gib_Os_iso() {return mix_Os_iso;};

};
#endif
```

The code performing the calculations "ospbmix.cc" is

```
#include "ospbmix.h"
#include <stdio.h>

ospbmix::ospbmix() {

  //Initialisierung der Zusammensetzungen

  Os_konz[1]   =  200;   //pelsed
  Os_konz[2]   =  20;    //tersed
  Os_konz[3]   =  10;   //okru
  Os_konz[4]   =  1000;  //cont lith
  Os_konz[5]   =  3000;  //Mantel

  Os_iso[1]    =  0.78;  //pelsed
  Os_iso[2]    =  2;     //tersed
  Os_iso[3]    =  1.78;  //okru
  Os_iso[4]    =  0.11;  //cont lith
  Os_iso[5]    =  0.127; //Mantel

  Pb_iso[1]    =  17.1;  //pelsed
  Pb_iso[2]    =  18.9;  //tersed
  Pb_iso[3]    =  22.5;  //okru
  Pb_iso[4]    =  18.5;  //cont lith
  Pb_iso[5]    =  18.5;  //Mantel

  Pb_konz[1]   =  11.6;  //pelsed
  Pb_konz[2]   =  3.03;  //tersed
  Pb_konz[3]   =  0.073; //okru
  Pb_konz[4]   =  0.1;   //cont lith
  Pb_konz[5]   =  0.0489;//Mantel

}

void ospbmix::mische_konz(float frak1, float frak2, float frak3, float
frak4, float frak5) {

  mix_konz = Os_konz[1] * frak1 + Os_konz[2] * frak2 + Os_konz[3] * frak3 +
             Os_konz[4] * frak4 + Os_konz[5] * frak5;

}

void ospbmix::mische_Os_iso(float frak1, float frak2, float frak3, float
frak4, float frak5) {

  mix_Os_iso = (Os_iso[1] * frak1 * Os_konz[1] +
                Os_iso[2] * frak2 * Os_konz[2] +
                Os_iso[3] * frak3 * Os_konz[3] +
                Os_iso[4] * frak4 * Os_konz[4] +
                Os_iso[5] * frak5 * Os_konz[5])
             / (Os_konz[1] * frak1 + Os_konz[2] * frak2 +
                Os_konz[3] * frak3 + Os_konz[4] * frak4 +
                Os_konz[5] * frak5);

}

void ospbmix::mische_Pb_iso(float frak1, float frak2, float frak3, float
frak4, float frak5) {

  mix_Pb_iso = (Pb_iso[1] * frak1 * Pb_konz[1] +
                Pb_iso[2] * frak2 * Pb_konz[2] +
```

```
                Pb_iso[3] * frak3 * Pb_konz[3] +
                Pb_iso[4] * frak4 * Pb_konz[4] +
                Pb_iso[5] * frak5 * Pb_konz[5])
             / (Pb_konz[1] * frak1 + Pb_konz[2] * frak2 +
                Pb_konz[3] * frak3 + Pb_konz[4] * frak4 +
                Pb_konz[5] * frak5);

}

int ospbmix::pruefe_konz(float *mix_zus) {

  if ((mix_konz > mix_zus[1]) || (mix_konz <  mix_zus[2])) return 0;
  else return 1;

}

int ospbmix::pruefe_Os_iso(float *mix_zus) {

  if ((mix_Os_iso > mix_zus[3]) || (mix_Os_iso <  mix_zus[4])) return 0;
  else return 1;

}

int ospbmix::pruefe_Pb_iso(float *mix_zus) {

  if ((mix_Pb_iso > mix_zus[5]) || (mix_Pb_iso <  mix_zus[6])) return 0;
  else return 1;

}
```

The input-output program for the Pitcairn model "ospbpitmix.cc" was programmed as

```
#include <stdio.h>
#include "ospbmix.h"
#include <iostream.h>

main() {

  FILE *dateizeiger;
  int ratio = 1;
  float frak1, frak2, frak3, frak4, frak5;

  int nummer;

  //Grenzen der Elementkonzentrationen oder -verhältnisse
  float mix_zus[7];

  printf("Geben Sie die gewünschten Mischung ein\n");
  printf("obere Grenze Os konzentration: ");
  cin >> mix_zus[ratio]; //1
  printf("untere Grenze Os konzentration: ");
  ratio++;
  cin >> mix_zus[ratio]; //2
  printf("obere Grenze Os Isotopie: ");
  ratio++;
  cin >> mix_zus[ratio]; //3
  printf("untere Grenze Os Isotopie: ");
  ratio++;
  cin >> mix_zus[ratio]; //4
  printf("obere Grenze 6/4Pb Isotopie: ");
  ratio++;
```

```
  cin >> mix_zus[ratio]; //5
  printf("untere Grenze 6/4Pb Isotopie: ");
  ratio++;
  cin >> mix_zus[ratio]; //6

  //Konstruktoraufruf
  ospbmix ospbpitmix;

  dateizeiger = fopen("ospbpitmixv2_out", "a");
  fprintf(dateizeiger, "nummer2, pelsed, tersed, okru, cont lith, DMM, Os,
  187/188, 6/4Pb,\n");
  nummer = 0;
  //0-5% sediment jeweils in 0.5% schritten
  for (int a = 0; a <= 10; a++) {
    frak1 = a * 0.005;
    for (int b = 0; b <= 10; b++) {
      frak2 = b * 0.005;
      //0-90% Ozeankruste
      for (int c = 0; c <= 9; c++) {
      frak3 = c * 0.1;
      for (int d = 0; d <= 4; d++) {
        //in 4 schritten mit cont lithosphäre auffüllen
        frak4 = (1-(frak1+frak2+frak3))* d * 0.25;
        //Rest mit Mantel auffüllen
        frak5 = 1-(frak1+frak2+frak3+frak4);
        if ((frak5) < 1) {

          ospbpitmix.mische_Os_iso(frak1, frak2, frak3, frak4, frak5);
          if(ospbpitmix.pruefe_Os_iso(mix_zus)) {
            ospbpitmix.mische_konz(frak1, frak2, frak3, frak4, frak5);
            if(ospbpitmix.pruefe_konz(mix_zus)) {
            ospbpitmix.mische_Pb_iso(frak1, frak2, frak3, frak4, frak5);
            if(ospbpitmix.pruefe_Pb_iso(mix_zus)) {
                nummer++;
                fprintf(dateizeiger, "%d, %.3f, %.3f, %.1f, %.2f, %.2f,",
                nummer, frak1, frak2, frak3, frak4, frak5);
                fprintf(dateizeiger, "%.1f,  ", ospbpitmix.gib_konz());
                fprintf(dateizeiger, "%.4f, ", ospbpitmix.gib_Os_iso());
                fprintf(dateizeiger, "%.4f,\n", ospbpitmix.gib_Pb_iso());
                }
              }
            }
          }
        }
      }
    }
  }
}
```

The trace element modeling was performed using "tracemix3.h" as header

```
#ifndef tracemix3_h
#define tracemix3_h

class tracemix3 {

 public:
  tracemix3();

  //Parameterdeklaration
```

```
  float element[12][7];
  float mix[12];

  //Funktionendeklaration

  void mische(int i, float frak1, float frak2, float frak3, float frak4,
  float frak5, float frak6);
  int pruefe_ratio(int i1, int i2, int ratio, float *mix_zus, float bound);
  int pruefe_abs(int i1, int ratio, float *mix_zus);
  double gib_mix(int i) {return mix[i];};

};

#endif
```

Trace element concentrations were calculated and tested using "tracemix3.cc"

```
#include "tracemix3.h"
#include <stdio.h>

tracemix3::tracemix3() {

 //Initialisierung der Zusammensetzungen

  // Reihenfolge:       Rb  Sr  Nb   Ba   La  Ce   Nd  Sm   Pb   Th   U
  //float pelsed[11]={51.2,340,17.3,737, 255,345, 313,68.3,68.6, 8.2,2.07};
  //Johnson&Plank av

  //float pelsed[11]={98.7,204,12.8,821,75.7,140,82.2,18.4,38.6,11.6,1.43};
  //Plank&Langmuir av

  float pelsed[11] = {69.1,139,11.5,616,75.7,126,75.6,17.5,11.6,9.28,1.07};
  //PL sed residue

  //float tersed[11]={43.9,246,11.9,353, 20,41.4,19.9, 4.2,10.1,4.48,1.29};
  //Plank&Langmuir av

  //float tersed[11]={57.2,327, 8.9,776,28.8,57.3, 27,5.78,19.9, 6.9,1.68};
  //GLOSS

  //float tersed[11]={ 40.,222, 8.,582,28.8,51.6,24.8,5.49,9.95,5.52,0.97};
  //GLOSS residue

  float tersed[11] = {30.7,167,10.7,265, 20,37.3,18.3,3.99,3.03,3.58,0.97};
  //PL sed residue

  //float okru[11]={1.26,113,3.51,13.9,3.9,12,11.2,3.75,0.489,0.187,0.071};

  float okru[11] =
  {0.544,66.7,3.37,6.67,1.72,5.88,7.73,3.23,0.073,0.116,0.05};
  //okru residue

  //float
  gabbro[11]={4.37,453,2.89,50.8,1.43,4.09,2.75,0.77,0.31,0.046,0.027};


  float
  gabbro[11]={1.49,267,2.77,24.4,0.63,2.,1.9,0.66,0.0465,0.029,0.019};
  //gabbro residue

  float
```

```
  DMM[11]={0.126,11.3,0.351,1.39,0.39,1.2,1.12,0.375,0.0489,0.019,0.007};

  float
PRIMA[11]={0.535,18.2,0.618,6.05,0.614,1.6,1.19,0.387,0.175,0.0813,0.0203};

  //Verarmungsfaktoren
  //Reihenfolge:           Rb   Sr   Nb  Ba  La  Ce  Nd   Sm   Pb  Th  U
  float fak_pelsed[11] ={0.7, 0.68,0.9,0.75, 1,0.9,0.92,0.95,0.3,0.8,0.75};
  float fak_tersed[11] ={0.7,0.68,0.9,0.75, 1,0.9,0.92, 0.95,0.3,0.8,0.75};
  float
     fak_okru[11]={0.34,0.59,0.96,0.48,0.44,0.49,0.69,0.86,0.15,0.62,0.71};
  float
  fak_gabbro[11] ={0.34,0.59,0.96,0.48,0.44,0.49,0.69,0.86,0.15,0.62,0.71};

  for (int i = 1; i <11 ; i++) {
    element[i][1] = pelsed[i-1];
    element[i][2] = tersed[i-1];
    element[i][3] = okru[i-1];
    element[i][4] = gabbro[i-1];
    element[i][5] = DMM[i-1];
    element[i][6] = PRIMA[i-1];
  }
}

void tracemix3::mische(int i, float frak1, float frak2, float frak3, float
frak4, float frak5, float frak6) {

  mix[i] = element[i][1] * frak1 + element[i][2] * frak2 +
           element[i][3] * frak3 + element[i][4] * frak4 +
           element[i][5] * frak5 + element[i][6] * frak6;

}


int tracemix3::pruefe_ratio(int i1, int i2, int ratio, float *mix_zus,
float bound) {

  if ((mix[i1] / mix[i2] > mix_zus[ratio] + mix_zus[ratio] * bound)
   || (mix[i1] / mix[i2] < mix_zus[ratio] - mix_zus[ratio] * bound))
   return 0;

  else return 1;

}

int tracemix3::pruefe_abs(int i1, int ratio, float *mix_zus) {

  if (mix[i1] > mix_zus[ratio]) return 0;

 else return 1;

}
```

And the input-output and function calls were programmed in "Pitmix3.cc" as follows

```
#include <stdio.h>
#include "tracemix3.h"
#include <iostream.h>

main() {

  FILE *dateizeiger2;
```

```
int ratio = 1;
float frak1, frak2, frak3, frak4, frak5, frak6;

int nummer;

//Grenzen der Elementkonzentrationen oder -verhältnisse
float mix_zus[13];

printf("Geben Sie die Elementverhältnisse der gewünschten Mischung
ein\n");
printf("Th/Nb: ");
cin >> mix_zus[ratio]; //1
printf("Th/U: ");
ratio++;
cin >> mix_zus[ratio]; //2
printf("Ba/Nb: ");
ratio++;
cin >> mix_zus[ratio]; //3
printf("Ba/Rb: ");
ratio++;
cin >> mix_zus[ratio]; //4
printf("Sr/Nd: ");
ratio++;
cin >> mix_zus[ratio]; //5
printf("Ce/Pb: ");
ratio++;
cin >> mix_zus[ratio]; //6
printf("Ba/La: ");
ratio++;
cin >> mix_zus[ratio]; //7
printf("Sm/Nd: ");
ratio++;
cin >> mix_zus[ratio]; //8
printf("Geben Sie die maximale Konzentration von Pb, Nb, Sr und Nd ein
(ppm)\n");
for (ratio = 9; ratio <= 12; ratio++) cin >> mix_zus[ratio];

//Konstruktoraufruf
tracemix3 Pitmix;

dateizeiger2 = fopen("Pitfraks3v3_out", "a");
fprintf
(dateizeiger2, "Nummer, pelsed, tersed, okru, gabbro, DMM, PRIMA, " );
fprintf(dateizeiger2, "Rb, Sr, Nb, Ba, La, Ce, Nd, Sm, Pb, Th, U,\n" );

nummer = 0;

//0-5% sediment jeweils in 0.5% schritten
for (int a = 0; a <= 10; a++) {
  frak1 = a * 0.005;
  for (int b = 0; b <= 10; b++) {
    frak2 = b * 0.005;

    //0-90% Ozeankruste in 5% steps
    for (int c = 0; c <= 18; c++) {
    frak3 = c * 0.05;
    for (int d = 0; d <= 10; d++) {

      //in 10 schritten mit gabbro auffüllen
      frak4 = (1-(frak1+frak2+frak3)) * d * 0.1;

      //Rest mit DMM und PRIMA auffüllen
      for (int e = 0; e <= 5; e++) {
```

```
          frak5 = (1-(frak1+frak2+frak3+frak4)) * e * 0.2;
          frak6 = 1-(frak1+frak2+frak3+frak4+frak5);
          if ((frak5 + frak6) < 1) {

            Pitmix.mische(1, frak1, frak2, frak3, frak4, frak5, frak6);

            Pitmix.mische(2, frak1, frak2, frak3, frak4, frak5, frak6);
            if(Pitmix.pruefe_abs(2, 11, mix_zus)) {

            Pitmix.mische(3, frak1, frak2, frak3, frak4, frak5, frak6);
            if(Pitmix.pruefe_abs(3, 10, mix_zus)) {

              Pitmix.mische(4, frak1, frak2, frak3, frak4, frak5, frak6);
              if(Pitmix.pruefe_ratio(4,3, 3, mix_zus, 0.2)) {
                if(Pitmix.pruefe_ratio(4,1, 4, mix_zus, 0.6)) {

                  Pitmix.mische
                  (5, frak1, frak2, frak3, frak4, frak5, frak6);
                  if(Pitmix.pruefe_ratio(4,5, 7, mix_zus, 0.2)) {

Pitmix.mische(6, frak1, frak2, frak3, frak4, frak5, frak6);

 Pitmix.mische(7, frak1, frak2, frak3, frak4, frak5, frak6);
 if(Pitmix.pruefe_abs(7, 12, mix_zus)) {
   if(Pitmix.pruefe_ratio(2,7, 5, mix_zus, 0.2)) {

     Pitmix.mische(8, frak1, frak2, frak3, frak4, frak5, frak6);
     if(Pitmix.pruefe_ratio(8,7, 8, mix_zus, 0.8)) {

       Pitmix.mische(9, frak1, frak2, frak3, frak4, frak5, frak6);
       if(Pitmix.pruefe_abs(9, 9, mix_zus)) {
       if(Pitmix.pruefe_ratio(6,9, 6, mix_zus, 0.2)) {

         Pitmix.mische(10, frak1, frak2, frak3, frak4, frak5, frak6);
         if(Pitmix.pruefe_ratio(10,3, 1, mix_zus, 0.2)) {

           Pitmix.mische(11, frak1, frak2, frak3, frak4, frak5, frak6);
           if(Pitmix.pruefe_ratio(10,11, 2, mix_zus, 0.2)) {

             nummer++;

             if (nummer == 1000) exit(0);

             fprintf(dateizeiger2, "%d,%.3f,%.3f,%.2f,%.2f,%.2f,%.2f,",
                   nummer, frak1, frak2, frak3, frak4, frak5, frak6);
             fprintf(dateizeiger2, "
             %.2f,%.2f,%.2f,%.2f,%.2f,%.2f,%.2f,%.2f,%.2f,%.2f,%.2f,\n",
             Pitmix.gib_mix(1),Pitmix.gib_mix(2),Pitmix.gib_mix(3),
             Pitmix.gib_mix(4),Pitmix.gib_mix(5),Pitmix.gib_mix(6),
             Pitmix.gib_mix(7),Pitmix.gib_mix(8),Pitmix.gib_mix(9),
             Pitmix.gib_mix(10),Pitmix.gib_mix(11));

           }
         }
       }
     }
   }
 }
                    }
                  }
                }
              }
```

```
                }
            }
        }
    }
}
}
}
}
```

5.C.4 Data analysis methods for Pb isotopic compositions

5.C.4.1 Regression lines in Pb isotope space

Regression lines and parameters for Pb isotope data of Pitcairn, HSDP-2 and Rurutu lavas were determined using Microsoft Excel and the XLSTAT software tool. The y-axis residual from a the regression line for a given sample is

$$r = y_{sample} - y_{predicted}$$

From the residuals the goodness of the regression can be assessed with the χ^2 parameter (Taylor, 1982) which is

$$\chi^2 = \sum_{1}^{N} \left(\frac{y_{sample} - f(x_i)}{\sigma_i} \right)^2$$

where N is the number of samples, $f(x_i)$ the function value predicted by the regression and σ_i the standard deviation. The reduced chi-square is then calculated as

$$\chi^2_{red.} = \frac{\chi^2}{N-1}$$

5.C.4.2 Pb isotope evolution model

To evaluate the evolution and meaning of the Pb isotopic signatures of the ocean island basalts measured during this thesis, I developed a computer program to simulate the possible Pb isotope evolution of of the sources of the hotspot volcanoes.

The simulations use the equations for a three-stage Pb isotope evolution (see Chapters 2, 3 and 4). To model the Pb isotopic evolution with this program, a field in $^{207}Pb/^{204}Pb$-

$^{206}Pb/^{204}Pb$ and $^{208}Pb/^{204}Pb$-$^{206}Pb/^{204}Pb$ space, for which solutions are sought is defined by the user. Additionally, limits can be entered on the parameters μ_2, μ_3, κ_2 and κ_3, denominating the $(^{238}U/^{204}Pb)_{today}$ and $(^{232}Th/^{238}U)_{today}$ ratios of the source during the second and third evolution stage. In the model, the Pb isotopic composition during Earth's evolution from 4.6 Ga to 3.7 Ga is not simulated by radiogenic ingrowth of Pb. Either the composition at 3.7 Ga was kept constant, using the values of Stacey and Kramers (1975), or an intial composition at 3.7 Ga was generated randomly. For this purpose, the computer program defines a random intial Pb isotopic composition ranging between $^{206}Pb/^{204}Pb$ = 11.151 and 11.434, $^{207}Pb/^{204}Pb$ = 12.998 and 13.345, $^{208}Pb/^{204}Pb$ = 30.978 and 31.424. This initial isotopic composition is constrained by Pb isotope evolution models for the bulk silicate Earth (Galer and Goldstein, 1996; Kramers and Tolstikhin, 1997) and by the composition of galenas from the oldest terrestrial rocks, the Isua volcanics (Galer and Goldstein, 1996). Then, the computer program generates random values for μ_2, μ_3, κ_2, κ_3 and t_2 and calculates a Pb isotopic evolution to the present. This calculated Pb isotopic composition is compared with the Pb isotopic field defined by the user. If the simulation matches this Pb isotope field, the solution is saved to a file. If it does not match, a new simulation is initiated. The efficiency of finding solutions with this program depends on the range of the evolution parameters μ and κ and the size of the Pb isotope field. In most cases, several million trial models are involved to find several hundreds of solutions, so in most cases only about 1 in 10000 simulation is successful.

Below is the C++ source code for the modeling program. The header "Bleimodell.h" is:

```
#ifndef Bleimodell_h
#define Bleimodell_h

class Bleimodell {

  /* Parameter des Objekts: initiale Isotopenverhältnisse,
     Jetzt-Zeit-Isotopenverhältnisse der Probe, mu1,2, k1,2, t2*/

  double i_64, i_74, i_84, s_64, s_74, s_84, mu1, mu2, k1, k2, t2;

 public:
```

```
  Bleimodell();
  void berechne(double *Grenzen_7_6, double *Grenzen_8_6, double
  *Ev_param);

  double gib_i_64() {return i_64;};
  double gib_i_74() {return i_74;};
  double gib_i_84() {return i_84;};
  double gib_s_64() {return s_64;};
  double gib_s_74() {return s_74;};
  double gib_s_84() {return s_84;};
  double gib_mu1()  {return mu1;};
  double gib_mu2()  {return mu2;};
  double gib_k1()   {return k1;};
  double gib_k2()   {return k2;};
  double gib_t2()   {return t2;};
};

#endif
```

The algorithm of the simulations is implemented in "Bleimodell.cc" and is as follows:

```
#include "Bleimodell.h"
#include <stdio.h>
#include <math.h>
#include <stdlib.h>
#include <unistd.h>

Bleimodell::Bleimodell() {
  srand(getpid());
}

void Bleimodell::berechne(double *Grenzen_7_6, double *Grenzen_8_6, double
*Ev_param) {

  double max = RAND_MAX + 1.;
  double t1 = 3.7;
  double l238U = 0.155125;
  double l235U = 0.98485;
  double l232Th = 0.049475 ;
  double w = 0;
  int i = 1;
  double upper_bound_76;
  double lower_bound_76;
  double left_bound_76;
  double right_bound_76;
  double upper_bound_86;
  double lower_bound_86;
  double left_bound_86;
  double right_bound_86;

  //Algorithmus rechnet w Versuche
    while (i) {

    //Randomwerte der initialen Pb zusammensetzung erzeugen
    i_64 = 11.151 + 0.283 * rand()/max;
    i_74 = 12.998 + .347 * rand()/max;
    i_84 = 30.978 + 0.446 * rand()/max;

    //Randomwerte für mu, k, t2 erzeugen
    mu1 =  Ev_param[2] + (Ev_param[1]-Ev_param[2]) * rand()/max;
    mu2 =  Ev_param[4] + (Ev_param[3]-Ev_param[4]) * rand()/max;
```

```
    k1 =   Ev_param[6] + (Ev_param[5]-Ev_param[6]) * rand()/max;
    k2 =   Ev_param[8] + (Ev_param[7]-Ev_param[8]) * rand()/max;
    t2 =   Ev_param[10] + (Ev_param[9]-Ev_param[10]) * rand()/max;

    //Pb isotopie berechnen
    s_64 = i_64 + mu1 * (exp(l238U*t1) - exp(l238U*t2))
                + mu2 * (exp(l238U*t2)-1);

    upper_bound_76 = Grenzen_7_6[1] * s_64 + Grenzen_7_6[2];
    lower_bound_76 = Grenzen_7_6[3] * s_64 + Grenzen_7_6[4];
    left_bound_76  = Grenzen_7_6[5] * s_64 + Grenzen_7_6[6];
    right_bound_76 = Grenzen_7_6[7] * s_64 + Grenzen_7_6[8];

    s_74 = i_74 + mu1/137.88 * (exp(l235U*t1) - exp(l235U*t2)) +
      mu2/137.88 * (exp(l235U*t2) - 1);

    if (s_74 < upper_bound_76 && s_74 > lower_bound_76 &&
      s_74 > right_bound_76 && s_74 < left_bound_76) {
      upper_bound_86 = Grenzen_8_6[1]  * s_64 + Grenzen_8_6[2];
      lower_bound_86 = Grenzen_8_6[3]  * s_64 + Grenzen_8_6[4];
      left_bound_86 = Grenzen_8_6[5] * s_64 + Grenzen_7_6[6];
      right_bound_86 = Grenzen_7_6[7] * s_64 + Grenzen_7_6[8];

      s_84 = i_84 + k1*mu1 * (exp(l232Th*t1) - exp(l232Th*t2))
                  + k2*mu2 *(exp(l232Th*t2) - 1);

      if (s_84 < upper_bound_86 && s_84 > lower_bound_86 &&
        s_84 > right_bound_86 && s_84 < left_bound_86)
      {
        i = 0;
      }
    }

    //Abbruch nach 1E6 Versuchen
      w++;
      if (w == 1e6) {i = 0; s_64 = 0;}
  }
}
```

The program that produces the instance (e.g. HSDP-2) of the object Bleimodell and regulates the input-output is:

```
#include <stdio.h>
#include "Bleimodell.h"
#include <istream.h>
#include <stdlib.h>

main() {

  Bleimodell HSDP2;
  FILE *dateizeiger;

  /*Grenzen des zu modellierenden Bleiisotopenfelds
    als double-Vektoren: Grenzen_7_6[n].
    [1]: Steigung der oberen Grenze (m oben),
    [2] y-Achsen-abschnitt der oberen Grenze (b oben),
    [3]: m unten, [4] b unten,
    [5] m links, [6] b links,
    [7] m rechts, [8] b rechts.
```

```
    Analog in Grenzen_8_6 */

  double Grenzen_7_6[9];
  double Grenzen_8_6[9];

  /*Eingabeparameter für die Evolutionsparamter, obere und untere Grenzen
    für mu1,2, k1,2 und t2 als double-vektoren: Ev_param[n].
    [1]:mu1 oben,[2] mu1 unten, [3-4] mu2,[5-6] k1, [7-8] k2, [9-10] t2. */

  double Ev_param[11];

  double ergebnisanzahl;

  printf("Geben Sie 8 Grenzparameter des zu modellierenden
  Bleiisotopenfeldes");
  printf(" in 7-6 ein: jeweils Steigung und y-Achsen Abschnitt für ");
  printf("die obere Grenze, die untere Grenze, die linke Grenze, die rechte
  Grenze.\n");
  for (int i = 1; i<=8; i++) cin >> Grenzen_7_6[i];

  printf("Geben Sie 8 Grenzparameter des zu modellierenden
  Bleiisotopenfeldes");
  printf(" in 8-6 ein: jeweils Steigung und y-Achsen Abschnitt für ");
  printf("die obere Grenze, die untere Grenze, die linke Grenze, die rechte
  Grenze.\n");

  for (int i = 1; i<=8; i++) cin >> Grenzen_8_6[i];

  printf("Geben Sie 10 Grenzen der Evolutionsparameter ein: ");
  printf("jeweils obere Grenze und untere Grenze für mu1, mu2, k1, k2 und
  t2 (in Ga).\n");

  for (int i = 1; i<=10; i++) cin >> Ev_param[i];

  printf("Geben Sie die gewünschte Anzahl von Ergebnissen an.\n");

 cin >> ergebnisanzahl;

  //Ausgabe in Datei
  dateizeiger = fopen("HSDP2_out", "a");
  fprintf(dateizeiger,
  "\n#,i_64,i_74,i_84,s_64,s_74,s_84,mu1,mu2,k1,k2,t2\n");
  for (int i = 1; i <= ergebnisanzahl; i++) {
    HSDP2.berechne(Grenzen_7_6,  Grenzen_8_6,  Ev_param);
    if (!HSDP2.gib_s_64()) fprintf(dateizeiger, "%i, keine Lösung nach 1e6
    Versuchen\n", i);
    else
    fprintf(dateizeiger,
    "%i,%.4f,%.4f,%.4f,%.4f,%.4f,%.4f,%.2f,%.2f,%.2f,%.2f,%.2f\n", i,
    HSDP2.gib_i_64(), HSDP2.gib_i_74(), HSDP2.gib_i_84(),
    HSDP2.gib_s_64(), HSDP2.gib_s_74(), HSDP2.gib_s_84(),
    HSDP2.gib_mu1(), HSDP2.gib_mu2(),HSDP2.gib_k1(),
    HSDP2.gib_k2(), HSDP2.gib_t2());
  }
  fprintf(dateizeiger, "\nEingabeparameter, Kommentar:\n");
  fprintf(dateizeiger,
  "mu1_oben,mu1_unten,mu2_oben,mu2_unten,k1_oben,k1_unten,");
  fprintf(dateizeiger, "k2_oben,k2_unten,t2_oben,t2_unten\n");
  fprintf(dateizeiger,
  "%.2f,%.2f,%.2f,%.2f,%.2f,%.2f,%.2f,%.2f,%.2f,%.2f\n\n",
  Ev_param[1], Ev_param[2], Ev_param[3], Ev_param[4], Ev_param[5],
  Ev_param[6], Ev_param[7], Ev_param[8], Ev_param[9], Ev_param[10]);
}
```

References:

Abouchami, W., Galer, S. J. G. and Hofmann, A. W. (2000): High precision lead isotope systematics of lavas from the Hawaiian Scientific Drilling Project, Chemical Geology 169, 187-209

Albarède, F. (1995): Introduction to geochemical modeling, Cambridge University Press, Cambridge, U.K., 543 pp.

Birck, J. L., Roy-Barman, M. and Capmas, F. (1997): Re-Os isotopic measurements at the femtomole level in natural samples, Geostandard Newsletters 20, 19-27

Galer, S. J. G. and Goldstein, S. L. (1996): Influence of accretion on lead in the Earth, in: Earth Processes: Reading the Isotopic Code (eds Basu, A. and Hart, S. R.), American Geophysical Union, Washington DC 95, 75-98

Galer, S. J. G. (1999): Optimal double and triple spiking for high precision lead isotopic measurement, Chemical Geology 157, 255-274

Hofmann, A. W. (1988): Chemical differentiation of the Earth: the relationship between mantle, continental crust and oceanic crust, Earth and Planetary Science Letters 90, 297-314

Jochum, K. P., Laue, H.-J., Seufert, H. M., Dienemann, C., Stoll, B., Pfänder, J., Flanz, M., Achtermann, H. and Hofmann, A. W. (1997): Multi-ion counting spark-source mass spectrometry (MIC-SSMS): A new multielement technique in geo- and cosmochemistry, Fresenius Journal of Analytical Chemistry 359, 385-389

Jochum, K. P., Stoll, B., Pfänder, J. A., Seufert, M., Flanz, M., Maissenbacher, P., Hofmann, M. and Hofmann, A. W. (2001): Progress in multi-ion counting spark-source mass spectrometry (MIC-SSMS) for the analysis of geological samples, Fresenius Journal of Analytical Chemistry 370, 647-653

Kramers, J. D. and Tolstikhin, I. N. (1997): Two terrestrial lead isotope paradoxes, forward transport modelling, core formation and the history of the continental crust, Chemical Geology 139, 75-110

Kuchling, H. (1995): Taschenbuch der Physik, Fachbuchverlag Leipzig-Köln, 711 pp.

Rees, D. G. (1995): Essential Statistics, Chapman and Hall, London, 265 pp.

Rhodes, J. M. (1996): Geochemical stratigraphy of lava flows sampled by the Hawaii Scientific Drilling Project, Journal of Geophysical Research 101, 11729-11746

Roy-Barman, M., Wasserburg, G. J., Papanastassiou, D. A. and Chaussidon, M. (1998): Osmium isotopic composition and Re-Os concentration on sulfide globules from basaltic glasses, Earth and Planetary Science Letters 154, 331-347

Shirey, S. B. and Walker, R. J. (1995): Carius Tube digestion for low-blank Rhenium-Osmium analysis, Analytical Chemistry 67, 2136-2141

Stacey, J. S. and Kramers, J. D. (1975): Approximation of terrestrial lead isotope evolution by a two-stage model, Earth and Planetary Science Letters 26, 207-221

Taylor, J. R. (1982): An introduction to error analysis, University Science Books, Mill Valley, USA, 270 pp.